

**WASTE DERIVED CARBONS FOR  
NO<sub>x</sub> CONTROL OR SYNGAS TAR  
REMOVAL**

By

Amal Salim Said Al-Rahbi

Submitted in accordance with the requirements for the degree of  
Doctor of Philosophy

School of Chemical and Process Engineering  
The University of Leeds

March 2017

The candidate confirms that the work submitted is her own, except where work which has formed part of jointly-authored publications has been included. The contribution of the candidate and the authors to this work has been explicitly indicated below. The candidate confirms that appropriate credit has been given within the thesis where reference has been made to the work of others.

This copy has been supplied on the understanding that it is copyright material and that no quotation from the thesis may be published without proper acknowledgment.

### **Journal Papers**

Chapter 4 was based on the following published papers;

1. Al-Rahbi, A.S.S., Nahil, M.A., Wu, C., and Williams, P.T. (2016) Waste derived activated carbons for control of nitrogen oxides. Proceedings of the Institution of Civil Engineers-Waste and Resource Management, 169 (1), 30-41.
2. Al-Rahbi, A.S. and Williams, P.T. (2016) Production of activated carbons from waste tyres for low temperature NO<sub>x</sub> control. Waste Management, 49, 188-195.

Chapter 5 was based on the following published papers;

1. Al-Rahbi, A.S., Onwudili, J.A., and Williams, P.T. (2016) Thermal decomposition and gasification of biomass pyrolysis gases using a hot bed of waste derived pyrolysis char. Bioresource Technology, 204, 71-79.
2. Al-Rahbi, A.S. and Williams, P.T. (2016) Catalytic decomposition/steam reforming of biomass tar over sacrificial tyre pyrolysis char for H<sub>2</sub> rich syngas production. Applied Energy, 190, 501-509.

## Conference Papers

1. Al-Rahbi, A.S., and Williams P.T. Activated carbons from chemical activation of waste tyres for low temperature NO<sub>x</sub> control, In The 18<sup>th</sup> International Flame Research Foundation Conference: Flexible and clean fuel conversion in industry, Freising, Germany, 2015.
2. Al-Rahbi, A.S., Onwudili, J.A., and Williams P.T. Tar reduction from biomass gasification using waste derived pyrolysis chars, In the 8<sup>th</sup> International Symposium of Feedstock Recycling and Polymeric Materials, Leoben, Austria, 2015.
3. Al-Rahbi, A.S., and Williams P.T. (2016) Steam reforming of biomass tar over tyre char for hydrogen production, In the 21<sup>th</sup> World Hydrogen Energy Conference, Zaragoza, Spain, 2016.

The candidate Amal Salim Said Al-Rahbi performed the experimental and analytical work, wrote the initial drafts of the papers along with supporting material, and carried out the calculation and summarization of the results and developed the discussion part.

The co-author, Prof. P. T. Williams supervised and supported the entire research work, proofread the drafts and made suggestions and corrections to the draft papers. Co-authors Nahil, Wu and Onwudili, helped with the development of the analytical work.

The right of Amal Salim Said Al-Rahbi to be identified as Author of this work has been asserted by her in accordance with the Copyright, Designs and Patents Act 1988.

© 2017 The University of Leeds and Amal Salim Said Al-Rahbi

# Acknowledgements

In the name of Allah, most Gracious, most Merciful

I would like to convey my heartfelt thanks to all the people who have helped me and stood beside me during my doctoral study.

First and foremost, I would like to express my sincere gratitude and appreciation to my supervisor Prof. Paul T. Williams for his endless support, guidance, help and encouragement throughout my PhD. Thanks for being always accessible, for many hours of discussions and for trusting me and letting me undertake this project. This thesis would not have been possible without his valuable assistance.

I am grateful to the support of the Oman government for awarding me a scholarship to pursue my PhD. I would also like to thank the Royal Society of Chemistry for the funding to present my research in an international conference in Germany. Additionally, I want to acknowledge the Transnational Access granted from the Biofuels Research Infrastructure for Sharing Knowledge programme (BRISK), to carry out experiments in a pilot plant at the Italian National Agency for New Technologies, Energy and Sustainable Economic Development (ENEA). Also, I would like to acknowledge the support from the European Union Horizon 2020 research and innovation programme (Flexi-pyrocat, No.:643322), for providing funding for a one month research stay at the State Key Laboratory of Coal Combustion, Huazhong University of Science and Technology, Wuhan, China.

Special thanks are also extended to Dr. Jude Onwudilli and Dr. Mohammed Anas Nahil for their support and encouragement throughout the past four years. Many thanks also to Ed Woodhouse for his help with technical support in the modification of reactors. Additionally, I am thankful for the opportunity to meet and work with many friendly researchers in our lab for which special thanks go to Dr. Chika, Dr. Eyup, Dr. Jonathon, Dr. Juniza, Dr. Paula, Yeshui, Kenneth, Devi, Andrew, Japhet, Peace, Devy, Ella and Julius. Also, my sincere thanks goes to the rest of my friends both in Oman and U.K who supported me during the completion of this work.

My deepest gratitude goes to my beloved family; words can never describe my heartfelt sentiments to you. I am forever indebted to my dear mother for her deep faith, prayers, unconditional love and supreme trust. Warm thanks also goes to my brother Hussein and his lovely family. Thanks are also given to my grand moms, uncles, aunts and cousins for their continuous love and unwavering support in spite of the long distance. Moreover, I am profoundly grateful to my best friend Wafa for all the great years we spent together and the sincere friendship we share.

# Dedication

*This thesis is dedicated to the memory of my father and grandfather.*

# Abstract

The utilization of waste materials as precursors for generating low-cost and effective carbonaceous materials, which can be used on a large scale, is very attractive and would help to solve the issues associated with waste disposal. In this work, scrap tyre, municipal solid waste in the form of refuse derived fuel (RDF) and date stones were selected for char and activated carbon production. The produced carbons were investigated as valuable adsorbent materials for control of (i) a problematic industrial nitric oxide (NO) gaseous pollutant or alternatively (ii) as a low-cost catalyst for tar cracking in relation to cleaning up the syngas produced from the gasification of biomass. The investigated carbonaceous materials were prepared using a fixed bed reactor.

(i) The use of waste derived activated carbons as an adsorbent for NO removal under different test conditions at a low temperature of 50 °C was investigated using a fixed bed reactor. The activated carbons were synthesized through carbonisation of the precursor at a temperature of 600 °C, followed by subsequent physical activation with steam at 900 °C. The NO removal efficiency of the waste-derived activated carbons was compared with different commercial carbons with varied porous texture and surface chemistry. Date stones activated carbon exhibited the highest NO removal efficiency of 40%, whereas a lower NO removal efficiency of 23% and 21% was obtained with RDF and tyre activated carbons respectively at 120 minutes time on stream. Commercially produced activated carbons had NO removal efficiencies of between 40% and 60%. The lower NO sorption of waste tyre and RDF activated carbons compared to those of commercial activated carbons or date stones was because of the difference in porous texture. Considering the Kinetic diameter of NO is 0.317 nm, effective adsorbents should exhibit a large volume of micropores. It was shown that the pores of the commercial activated carbons and date stones are mostly located in the micropore range of 1-2 nm (micropores), whereas RDF and waste tyre derived activated carbons have a much greater number of pores with diameters in the range of 2-10 nm (mesopores). Chemical activation can greatly alter the pore size and characteristics of the produced carbon. Therefore, surface modification of waste tyre was investigated via chemical activation to develop the porous texture and thereby enhance the NO adsorption capacity of tyre derived activated carbon. Thus, the influence of chemical activation of the waste tyre with KOH, K<sub>2</sub>CO<sub>3</sub>, NaOH and Na<sub>2</sub>CO<sub>3</sub> on porosity development and the corresponding NO adsorption was investigated. It was shown that the activation of waste tyre with KOH favored the production of activated carbon with high micropore volume, which has been considered a key feature affecting NO adsorption at low temperature. Therefore, waste tyre activated with KOH at a char: KOH ratio of 1:3, with a total micropore volume of 0.437 cm<sup>3</sup> g<sup>-1</sup> and surface area of 621 m<sup>2</sup> g<sup>-1</sup> gave the highest NO adsorption capacity

(17.23 mg g<sup>-1</sup>), which was double that of the physically activated tyre derived activated carbon. The results obtained in this study have shown that the adsorption capacity of carbonaceous sorbents relies greatly on the porous texture, in particular, the micropore structure of the carbon, as well as on the method of activation, but to a lesser extent on the BET surface area and acid-base surface groups on the carbon surface.

(ii) Char materials derived from the pyrolysis of scrap tyre, RDF and date stones were also investigated in term of their use as a catalyst for the catalytic cracking of biomass pyrolysis gases during the two-stage pyrolysis/gasification of biomass. Biomass was used to generate a range of hydrocarbon gases typically found in biomass gasification tars through the pyrolysis of biomass. Among the investigated chars for bio-oil/tar decomposition, at a char cracking temperature of 800 °C, tyre-derived pyrolysis char presented the highest activity resulting in a 70% reduction in bio-oil/tar yield compared to the non-char catalytic experiments. The results suggest that tar decomposition by char materials is mainly ascribed to the catalytic conversion of tar species, as the decrease of the hydrocarbon tar yields was accompanied with a consequent increase in total gas yield. Analysis of the tar composition showed the presence of naphthalene, fluorene and phenanthrene as the major polyaromatic hydrocarbon (PAH) components at the higher cracking temperature. To understand the tar decomposition mechanism and to further investigate the influence of porous texture and oxygen functional groups of char on tar decomposition process, the catalytic cracking of tar model (furfural, phenol, toluene, methylnaphthalene) over tyre char was investigated. The most reactive compound was furfural, followed by phenol and toluene, whereas methylnaphthalene presented the lowest reactivity. The results also indicated that both the porous texture and the oxygen functional groups of the carbonaceous materials had a marginal effect on tar decomposition. Additionally, tyre char was used as a sacrificial catalyst for the reforming/gasification of tars from the gasification of biomass to produce a hydrogen-rich syngas and also to contribute to the yield of biomass syngas through tyre char gasification reactions. The influence of tyre ash metals, catalyst bed temperature, steam to biomass ratio and reaction time were investigated. The metallic mineral content of tyre char has been shown to contribute significantly to the tar degradation. The maximum H<sub>2</sub> content of the product syngas of 56 vol.% was obtained at a reforming temperature of 900 °C and with steam to biomass ratio of 6 g g<sup>-1</sup>. Tyre char was also subjected to steam gasification during the process, whereby the tyre pyrolysis char catalyst is sacrificed to produce hydrogen and carbon monoxide to enhance the yield of the syngas.

Overall, this research work shows that waste derived carbonaceous materials are low-cost promising adsorbents for NO control and tar removal from the syngas produced from biomass gasification.

# Table of Contents

|   |           |
|---|-----------|
| Acknowledgments.....  | iii       |
| Dedication.....   | iv        |
| Abstract.....   | v         |
| Table of Contents.....  | vii       |
| List of Tables.....   | xii       |
| List of Figures.....  | xiv       |
| Abbreviations.....  | xix       |
| <br>  |           |
| <b>CHAPTER 1. INTRODUCTION .....</b>                          | <b>1</b>  |
| 1.1. WORLD ENERGY CONSUMPTION AND WASTE GENERATION .....      | 1         |
| 1.2. ENERGY RECOVERY FROM WASTE.....                          | 3         |
| 1.3. THERMOCHEMICAL CONVERSION PROCESS.....                   | 3         |
| 1.3.1 Incineration.....                                       | 4         |
| 1.3.2 Pyrolysis .....   | 6         |
| 1.3.3 Gasification.....                                       | 7         |
| 1.4. WASTES AS SOURCES FOR HIGHER VALUE CARBON PRODUCTS.....  | 9         |
| 1.4.1 Refuse Derived Fuel (RDF).....                          | 10        |
| 1.4.2 Waste tyre.....   | 10        |
| 1.4.3 Biomass .....   | 11        |
| 1.5. OBJECTIVES OF THIS RESEARCH .....                        | 12        |
| <br>  |           |
| <b>CHAPTER 2. LITERATURE REVIEW .....</b>                     | <b>21</b> |
| 2.1. WASTE DERIVED CARBONACEOUS MATERIALS .....               | 21        |
| 2.1.1 Carbonisation.....                                      | 21        |
| 2.1.2 Activation .....  | 23        |
| 2.1.2.1 Physical activation.....                              | 24        |
| 2.1.2.2 Chemical activation.....                              | 27        |
| 2.2. WASTE DERIVED MATERIALS APPLICATIONS .....               | 29        |
| 2.2.1 Tar reduction.....                                      | 29        |
| 2.2.1.1 Tar definition and classification.....                | 29        |
| 2.2.1.2 Tar formation.....                                    | 31        |
| 2.2.1.3 Decomposition mechanism .....                         | 34        |
| 2.2.1.4 Tar removal cracking methods .....                    | 37        |
| 2.2.1.5 Catalytic tar cracking.....                           | 37        |
| 2.2.1.5.1 Char for catalytic tar conversion.....              | 40        |
| 2.2.1.5.2 Syngas production from biomass steam reforming .... | 43        |
| 2.2.1.5.3 Tar model compounds .....                           | 44        |
| 2.2.1.6 Mechanism of tar cracking over char surface .....     | 46        |
| 2.2.2 NO <sub>x</sub> adsorption .....                        | 49        |
| 2.2.2.1 The NO <sub>x</sub> problem .....                     | 49        |

|           |  |    |
|-----------|--|----|
| 2.2.2.2   | Environmental Impacts.....   | 49 |
| 2.2.2.3   | Abatement of NO <sub>x</sub> .....   | 50 |
| 2.2.2.3.1 | NO removal by activated carbon .....   | 50 |
| 2.2.2.3.2 | The role of porous texture on NO removal.....                                | 52 |
| 2.2.2.3.3 | Effects of oxygen on adsorption .....  | 53 |
| 2.2.2.4   | Activated carbon modification methods of enhancement of gas adsorption ..... | 54 |
| 2.2.2.5   | NO reaction mechanism with activated carbon.....                             | 55 |
| 2.3.      | SUMMARY .....  | 57 |

**CHAPTER 3. METHODOLOGY .....77**

|           |   |     |
|-----------|---|-----|
| 3.1.      | NO ADSORPTION PERFORMANCE ON THE ACTIVATED CARBONS .....                                | 79  |
| 3.1.1     | Materials .....   | 79  |
| 3.1.1.1   | Refuse derived fuel (RDF) .....   | 79  |
| 3.1.1.2   | Waste tyre.....   | 80  |
| 3.1.1.3   | Date stones .....   | 80  |
| 3.1.1.4   | Commercial activated carbons .....  | 81  |
| 3.1.2     | Acid Demineralization.....  | 81  |
| 3.1.3     | Production of chars .....   | 82  |
| 3.1.3.1   | Repeatability of the pyrolysis procedure.....   | 83  |
| 3.1.4     | Production of activated carbons .....   | 85  |
| 3.1.4.1   | Physical activation.....  | 85  |
| 3.1.4.2   | Chemical activation.....  | 88  |
| 3.1.5     | Analysis of the raw materials, chars and activated carbons .....                        | 89  |
| 3.1.5.1   | Ultimate analysis .....   | 89  |
| 3.1.5.2   | Proximate analysis.....   | 90  |
| 3.1.5.3   | Scanning Electron Microscope (SEM) and Energy-Dispersive X-ray spectroscopy (EDXS)..... | 91  |
| 3.1.5.4   | Boehm titration.....  | 92  |
| 3.1.5.5   | Fourier Transform Infrared spectrometry (FTIR) .....                                    | 93  |
| 3.1.5.6   | Metal analysis.....   | 93  |
| 3.1.5.7   | Pore structure characterization .....   | 94  |
| 3.1.5.7.1 | Determination of BET surface area by Brunauer-Emmer-Teller (BET) method.....            | 96  |
| 3.1.5.7.2 | Determination of mesopore volume (BJH) method....                                       | 98  |
| 3.1.5.7.3 | Determination of micropore volume – Dubinin-Radushkevich (DR) method.....               | 98  |
| 3.1.5.7.4 | Pore size distribution by Density Functional Theory (DFT).....                          | 99  |
| 3.1.6     | Analysis of Gaseous Products .....  | 100 |
| 3.1.6.1   | Calibration of the Gas Chromatograph Instruments.....                                   | 101 |
| 3.1.6.2   | Permanent gases analyses.....   | 102 |

|           |   |     |
|-----------|---|-----|
| 3.1.6.3   | Hydrocarbon gases analyses.....   | 103 |
| 3.1.6.4   | Calculation of gas concentration .....  | 103 |
| 3.1.6.5   | Repeatability of the gas analysis .....   | 104 |
| 3.1.7     | NO adsorption experiments .....   | 107 |
| 3.1.7.1   | Chemiluminescent NO <sub>x</sub> Analyser .....                                 | 109 |
| 3.1.7.2   | The precision assessment of the used gas analyser .....                         | 112 |
| 3.1.7.3   | Estimation of Errors in NO measurements.....                                    | 113 |
| 3.1.7.4   | Repeatability of the NO adsorption performance of the activated<br>carbons..... | 114 |
| 3.2.      | TAR CONVERSION OVER A HOT BED OF CHAR.....                                      | 115 |
| 3.2.1     | Materials .....   | 115 |
| 3.2.1.1   | Biomass feedstock.....  | 115 |
| 3.2.1.2   | Chars.....  | 116 |
| 3.2.1.3   | Tar model compounds .....   | 116 |
| 3.2.2     | Acid treatment .....  | 117 |
| 3.2.3     | Two stage-Fixed bed pyrolysis/cracking reactor.....                             | 118 |
| 3.2.3.1   | Reactor set-up.....   | 118 |
| 3.2.3.2   | Experimental procedure .....  | 119 |
| 3.2.3.2.1 | Tar cracking using waste derived chars .....                                    | 120 |
| 3.2.3.2.2 | Char catalytic performance for tar model compounds<br>cracking.....             | 121 |
| 3.2.3.2.3 | Steam reforming reaction system .....   | 122 |
| 3.2.3.3   | Experiment repeatability and validation of the reactor .....                    | 123 |
| 3.2.4     | Products analyses.....  | 126 |
| 3.2.4.1   | Liquid Effluent analyses.....   | 126 |
| 3.2.4.1.1 | Karl-Fischer Titration (KFT) .....  | 126 |
| 3.2.4.1.2 | Gas Chromatography/Mass Spectrometry .....                                      | 128 |
| 3.2.4.1.3 | Size Exclusion Chromatography .....   | 131 |
| 3.2.4.2   | Effluent Gas Analyses .....   | 132 |
| 3.2.4.3   | Char characterization.....  | 132 |

**CHAPTER 4. NO REMOVAL USING WASTE DERIVED ACTIVATED CARBONS .....137**

|         |   |     |
|---------|---|-----|
| 4.1.    | NITROGEN OXIDE REMOVAL USING COMMERCIAL AND WASTE-DERIVED<br>PHYSICALLY ACTIVATED CARBONS ..... | 138 |
| 4.1.1   | Properties of the raw precursors .....  | 138 |
| 4.1.2   | Product Yield from the Fixed Bed Pyrolysis of the Waste Materials .....                         | 139 |
| 4.1.3   | Properties of the commercial and waste-derived activated carbons.....                           | 141 |
| 4.1.4   | NO removal using commercial and waste derived activated carbons.....                            | 144 |
| 4.1.5   | Surface Area and Pore Characteristics of the Activated Carbons .....                            | 147 |
| 4.1.5.1 | Acid-base properties.....   | 153 |

|   |            |
|---|------------|
| 4.1.6 Influence of Temperature, NO Concentration and Oxygen on NO Adsorption.....   | 154        |
| 4.1.7 Reaction mechanism of NO adsorption.....  | 158        |
| 4.1.8 Summary of section 4.1 .....  | 162        |
| 4.2. ACTIVATED CARBONS FROM CHEMICAL ACTIVATION OF WASTE TYRES FOR LOW TEMPERATURE NO CONTROL .....                         | 163        |
| 4.2.1 Activated carbon preparation and characterization .....   | 163        |
| 4.2.2 Nitrogen Oxide adsorption .....   | 172        |
| 4.2.3 Summary of section 4.2 .....  | 181        |
| <br>  |            |
| <b>CHAPTER 5. TAR REDUCTION USING WASTE DERIVED PYROLYSIS CHAR.....</b>   | <b>188</b> |
| 5.1. THERMAL DECOMPOSITION AND GASIFICATION OF BIOMASS PYROLYSIS GASES USING A HOT BED OF WASTE DERIVED PYROLYSIS CHAR..... | 189        |
| 5.1.1 Biomass pyrolysis gas conversion using waste derived pyrolysis chars .  | 189        |
| 5.1.2 Tar analysis.....   | 195        |
| 5.1.3 GC-MS analysis of the tar composition .....   | 195        |
| 5.1.4 Size Exclusion Chromatography .....   | 204        |
| 5.1.5 Char characterization.....  | 205        |
| 5.1.6 Influence of the biomass to char ratio .....  | 209        |
| 5.1.7 Summary of section 5.1 .....  | 211        |
| 5.2. TAR MODEL COMPOUNDS CRACKING USING TYRE CHAR.....  | 212        |
| 5.2.1 Catalytic activity of tyre char for cracking of tar model compounds.....  | 212        |
| 5.2.2 Parametric study .....  | 219        |
| 5.2.3 The influence of porosity on methylnaphthalene conversion.....  | 222        |
| 5.2.4 The influence of Acidity on methylnaphthalene conversion.....   | 225        |
| 5.2.5 Summary of section 5.2 .....  | 226        |
| 5.3. STEAM REFORMING OF BIOMASS TAR OVER SACRIFICIAL TYRE PYROLYSIS CHAR FOR H <sub>2</sub> -RICH SYNGAS PRODUCTION .....   | 228        |
| 5.3.1 Effects of char ash on tar decomposition and hydrogen production .....  | 228        |
| 5.3.2 Effect of steam to biomass ratio .....  | 237        |
| 5.3.3 Effect of reaction time .....   | 240        |
| 5.3.4 Summary of section 5.3 .....  | 245        |
| <br>  |            |
| <b>CHAPTER 6. CONCLUSIONS AND FUTURE WORK.....</b>  | <b>255</b> |
| 6.1. WASTE DERIVED ACTIVATED CARBONS FOR NO REMOVAL .....   | 256        |
| 6.1.1 Nitrogen oxide removal using commercial and waste-derived physically activated carbons.....                           | 256        |
| 6.1.2 Activated carbons from chemical activation of waste tyres for low temperature NO control.....                         | 257        |
| 6.2. TAR DECOMPOSITION USING WASTE DERIVED PYROLYSIS CHARs .....  | 258        |

|  |     |
|--|-----|
| 6.2.1 Thermal decomposition and cracking of biomass pyrolysis gases using a hot bed of waste derived pyrolysis chars ..... | 258 |
| 6.2.2 Catalytic activity of tyre char for cracking of tar model compounds .....  | 259 |
| 6.2.3 Steam reforming of biomass tar over sacrificial tyre pyrolysis char for H <sub>2</sub> -rich syngas production ..... | 260 |
| 6.3. FUTURE WORK.....  | 261 |
| 6.3.1 Waste derived activated carbons for NO removal.....  | 261 |
| 6.3.2 Tar decomposition using waste derived pyrolysis chars .....  | 262 |

## List of Tables

|  |     |
|--|-----|
| Table 1.3-1. The concentration of pollutants in MSW incineration flue gas and Emission limits set by the European Commission.....                                | 5   |
| Table 1.3-2. Pyrolysis products from different waste material.....   | 6   |
| Table 1.3-3. Composition of gaseous species from biomass gasification.....   | 7   |
| Table 2.2-1. Tar classification based on molecular weight of tar compounds.....  | 30  |
| Table 3.1-1. Repeatability of pyrolysis products .....   | 84  |
| Table 3.1-2. Repeatability of the physical activation procedure.....   | 88  |
| Table 3.1-3. Metals composition of tyre and RDF waste raw materials.....   | 94  |
| Table 3.1-4. Repeatability of GC analysis .....  | 106 |
| Table 3.1-5. Test the reliability of the instrument with multipoint calibration.....   | 113 |
| Table 3.2-1. Aromatic model compounds studied in this study.....   | 117 |
| Table 3.2-2. Validation of the two stage fixed bed reactor.....  | 124 |
| Table 3.2-3. Validation of the two stage fixed bed reactor.....  | 125 |
| Table 4.1-1. Composition of the raw waste materials.....   | 139 |
| Table 4.1-2. Product yield from the pyrolysis of waste materials .....   | 140 |
| Table 4.1-3. Proximate and ultimate analysis of the activated carbons.....   | 141 |
| Table 4.1-4. Mineral composition of the commercial activated carbons.....  | 142 |
| Table 4.1-5. Adsorption amount of NO (mg g <sup>-1</sup> ) and as NO per mass of carbon...   | 146 |
| Table 4.1-6. Surface area and pore size characteristics of the commercial and waste derived activated carbons.....   | 150 |
| Table 4.1-7. Influence of surface area, mesopore volume and micropore volume of the tyre derived activated carbons on NO removal efficiency at 120 minutes. .... | 153 |
| Table 4.1-8. Acid and base properties of the activated carbons.....  | 154 |
| Table 4.1-9. Proposed reaction mechanisms of NO oxidation to NO <sub>2</sub> on carbon ..  | 161 |
| Table 4.2-1. Preparation conditions of the activated carbons .....   | 163 |
| Table 4.2-2. Elemental analysis of the waste derived activated carbons.....  | 164 |
| Table 4.2-3. Porous properties of the waste derived activated carbons .....  | 165 |
| Table 4.2-4. NO adsorption capacity of the activated carbons obtained (mg g <sup>-1</sup> ads) .....   | 173 |
| Table 5.1-1. Composition of the biomass waste wood and the waste derived char samples.....   | 189 |

|   |     |
|---|-----|
| Table 5.1-2. Influence of waste derived pyrolysis char on the product yield from the pyrolysis-gasification of biomass..... | 191 |
| Table 5.1-3. Tar decomposition reactions.....   | 195 |
| Table 5.1-4. Porous properties of the samples .....   | 206 |
| Table 5.2-1. Influence of carbon porosity on methylnaphthalene conversion, gas yield and hydrogen production.....           | 223 |
| Table 5.2-2. Influence of carbon acidity on methylnaphthalene conversion and hydrogen production. ....                      | 225 |
| Table 5.3-1. Ultimate and mineral content of char .....   | 229 |
| Table 5.3-2. Influence of char minerals on product distribution and gas characterization .....                              | 230 |
| Table 5.3-3. Reactions involve during the gasification process.....   | 231 |

# List of Figures

|  |    |
|--|----|
| Figure 1.1-1. (a) World energy demand and (b) energy sources .....   | 2  |
| Figure 1.3-1. Thermochemical conversion processes .....  | 4  |
| Figure 1.3-2. The difference between the incineration, gasification and pyrolysis conversion processes.....  | 4  |
| Figure 1.3-3. Main processes during biomass gasification .....   | 8  |
| Figure 1.3-4. Production of fuels and chemicals from syngas .....  | 9  |
| Figure 1.4-1. Global municipal solid waste composition .....   | 10 |
| Figure 2.1-1. Carbonisation reaction of carbonaceous material .....  | 21 |
| Figure 2.1-2. The dimension of water (a) and carbon dioxide (b) molecules.....   | 25 |
| Figure 2.2-1. Biomass tar composition .....  | 30 |
| Figure 2.2-2. Tar classes .....  | 31 |
| Figure 2.2-3. Chemical tar components formation with temperature .....   | 32 |
| Figure 2.2-4. Biomass components (a) cellulose, (b) hemicellulose and (c) lignin...33  |    |
| Figure 2.2-5. Lignin decomposition mechanism . .....   | 34 |
| Figure 2.2-6. Cracking and polymerization products formed during tar conversion process.....   | 35 |
| Figure 2.2-7. Simplified reaction scheme of tar conversion in the presence of hydrogen and steam .....   | 35 |
| Figure 2.2-8. Naphthalene cracking mechanism .....   | 36 |
| Figure 2.2-9. Naphthalene decomposition mechanism .....  | 36 |
| Figure 2.2-10. The role of carbon porous texture in tar cracking . .....   | 46 |
| Figure 2.2-11. Mechanism of tar conversion over char .....   | 47 |
| Figure 2.2-12. Tar cracking mechanism over activated carbon via reactions with gas components .....  | 48 |
| Figure 2.2-13. Reaction scheme of NO adsorption on activated carbon in the presence of oxygen .....  | 56 |
| Figure 2.2-14. Temperature-programmed desorption pattern of NO after adsorption on activated carbon- NO desorption peaks showing the multiple adsorption sites on the activated carbon surface. .... | 56 |
| Figure 3.1. A synopsis of the sequence of the experimental system.....   | 78 |

|   |     |
|---|-----|
| Figure 3.1-1. RDF sample (a) original pellets (b) shredded samples.....   | 80  |
| Figure 3.1-2. Date stones sample (a) original pellets (b) shredded samples.....   | 81  |
| Figure 3.1-3. Schematic diagram of the waste pyrolysis reactor. ....  | 83  |
| Figure 3.1-4. Photograph of the activation reactor. ....  | 86  |
| Figure 3.1-5. Schematic diagram of the char activation reactor .....  | 87  |
| Figure 3.1-6. Schematic diagram of the Flash EA2000 Elemental analyser. ....  | 90  |
| Figure 3.1-7. A TGA Thermogram for the proximate analysis of RDF. ....  | 91  |
| Figure 3.1-8. SEM-EDXS results for tyre char activated carbon. ....   | 92  |
| Figure 3.1-9. Quanatachrome NOVA 2200e. ....  | 95  |
| Figure 3.1-10. Sample BET Plots for tyre char.....  | 97  |
| Figure 3.1-11. GC Chromatography equipment and general layout of a typical GC.<br>.....   | 100 |
| Figure 3.1-12. GC response peaks for a standard gas mixture of permanent gases (H <sub>2</sub> ,<br>O <sub>2</sub> , N <sub>2</sub> , CO). ....   | 101 |
| Figure 3.1-13. GC response peaks for standard gas mixture of hydrocarbons (C <sub>1</sub> -C <sub>4</sub> ).<br>.....   | 102 |
| Figure 3.1-14. Overlaying Chromatograms indicating repeatability of GC analysis<br>results .....  | 105 |
| Figure 3.1-15. A Schematic diagram of the gas adsorption reactor.....   | 108 |
| Figure 3.1-16. Horiba VS3000/VA3000 multi gas analyser; (a) Analyser pump,(b)<br>Sample pump, (c) Mist catcher, (d) Selector valve, (e) Filter, (f) Sample flowmeter,<br>(g) Calibration gas flow meter, (h) VS-3000 Gas sampling unit, (i) VA-3000 Multi –<br>gas analyser unit..... | 110 |
| Figure 3.1-17.The principle of operation of the gas analyser. ....  | 111 |
| Figure 3.1-18. Calibration mixtures to test the uncertainty of the gas analyser.....  | 113 |
| Figure 3.1-19. Repeatability of NO adsorption experiments .....   | 114 |
| Figure 3.2-1. Wood pellets.....   | 115 |
| Figure 3.2-2. Assembled and main parts of the pyrolysis-gasification reactor; (a)<br>Syringe pump, (b) Thermocouple, (c) 1 <sup>st</sup> stage pyrolysis reactor, (d) 2 <sup>nd</sup> stage<br>catalytic reactor, (e) Furnace controller, and (f) Mass flow controller. ....          | 119 |
| Figure 3.2-3. Schematic two-stage pyrolysis-gasification reaction system .....  | 121 |
| Figure 3.2-4. Flowchart of liquid analysis route. ....  | 126 |
| Figure 3.2-5. General diagram of GC-MS. ....  | 129 |

|   |     |
|---|-----|
| Figure 3.2-6. Calibration curves for dibenzofuran and phenol. ....  | 130 |
| Figure 3.2-7. An example of a GC-MS chromatogram. ....  | 131 |
| Figure 3.2-8. Size exclusion chromatogram of tar/oil sample. ....   | 132 |
| Figure 4.1-1. SEM-EDXS results of the waste-derived activated carbons: (a) activated carbon from RDF (AC-R); (b) activated carbon from waste tyre (AC-T); and (c) activated carbon from date stones (AC-D) .....                            | 143 |
| Figure 4.1-2. The NO removal efficiency curves for (a) the commercial activated carbons and (b) the waste derived activated carbons at 50 °C adsorption temperature .....   | 145 |
| Figure 4.1-3. Comparison of NO breakthrough curve obtained for AC-T sample before and after demineralization.....   | 147 |
| Figure 4.1-4. Nitrogen adsorption desorption isotherms for the (a) waste derived activated carbons and (b) commercial activated carbons.....  | 149 |
| Figure 4.1-5. Pore size distribution for (a) the waste-derived activated carbons and (b) the commercial activated carbons .....   | 152 |
| Figure 4.1-6. Influence of temperature on NO removal efficiency at 120 minutes for (a) date stones (AC-D) and (b) tyre (AC-T) derived activated carbons.....  | 155 |
| Figure 4.1-7. Influence of NO concentration (ppm) on NO removal efficiency at 120 minutes for (a) date stones (AC-D) and (b) tyre (AC-T) derived activated carbons. ....  | 156 |
| Figure 4.1-8. Influence of oxygen concentration on NO removal efficiency at 120 minutes for (a) date stones (AC-D) and (b) tyre (AC-T) derived activated carbons. ....  | 157 |
| Figure 4.1-9. FTIR spectra for the waste derived activated carbons before and after NO removal at 50 °C.....  | 159 |
| Figure 4.1-10. The nature of NO adsorbed species formed on carbon (adapted from. ....   | 160 |
| Figure 4.2-1. Adsorption and desorption isotherms of the waste tyre derived activated carbons in relation to (a) char:KOH impregnation ratio (b) activation temperature with KOH char impregnation (c) type of alkali activating agent..... | 168 |
| Figure 4.2-2. Pore size distribution (DFT) of the waste derived activated carbons in relation to (a) activation temperature with KOH char impregnation (b) char:KOH impregnation ratio (c) type of alkali activating agent .....            | 169 |

|   |     |
|---|-----|
| Figure 4.2-3. SEM images for (a) TAKOH, (b)TANaOH, (c)TANa <sub>2</sub> CO <sub>3</sub> , (d) TAK <sub>2</sub> CO <sub>3</sub> .....                                      | 170 |
| Figure 4.2-4. KOH activation mechanism at a temperature above 700 °C and the expansion of carbon lattice due to the intercalation of potassium [12].....                  | 172 |
| Figure 4.2-5. (a) NO breakthrough curves and (b) removal efficiency of the waste tyre derived activated carbons in relation to char: KOH ratio .....                      | 174 |
| Figure 4.2-6. (a) NO breakthrough curves and (b) removal efficiency of the waste tyre derived activated carbons in relation to activation temperature .....               | 176 |
| Figure 4.2-7. (a) NO breakthrough curves and (b) removal efficiency of the waste tyre derived activated carbons in relation to char: activating agent.....                | 178 |
| Figure 4.2-8. Expected reaction mechanism of NO with TA-KOH .....   | 179 |
| Figure 4.2-9. SEM-EDX of TA-KOH900 .....  | 180 |
| Figure 5.1-1. Photographs of bio-oil/tar samples during the pyrolysis-gasification of biomass with and without char.....  | 193 |
| Figure 5.1-2. Effect of char type over tar composition at a cracking temperature of 800 °C. ....  | 196 |
| Figure 5.1-3. Tar composition with different carbon samples at a cracking temperature of 800 °C. ....   | 197 |
| Figure 5.1-4. Distribution of tar compounds with respect to cracking temperature at (a) 600 °C; (b) 700 °C; and (c) 800 °C. ....  | 200 |
| Figure 5.1-5. Tar composition at different char cracking temperatures for (a) without char; (b) with tyre char .....  | 202 |
| Figure 5.1-6. (a) Pyrolysis of phenol and (b) reaction pathway for the formation of naphthalene and methylindenes .....   | 203 |
| Figure 5.1-7. H <sub>2</sub> abstraction-C <sub>2</sub> H <sub>2</sub> -addition (HACA) .....   | 203 |
| Figure 5.1-8. Size exclusion chromatograms of tar samples .....   | 205 |
| Figure 5.1-9. Scanning electron microscopy (SEM) images of fresh and used char samples.....   | 208 |
| Figure 5.1-10. Tar cracking paths over char materials.....  | 209 |
| Figure 5.1-11. (a) Product yields and (b) gas composition in relation to biomass: char ratio for the tyre derived pyrolysis char at 700 °C hot char bed temperature. .... | 210 |
| Figure 5.2-1. (a) Carbon conversion; and (b) hydrogen potential of tar model compounds with sand and tyre char. ....  | 213 |

|   |     |
|---|-----|
| Figure 5.2-2. Influence of tyre char (a); and sand (b) on the gaseous yield (%) from the cracking of tar model compounds. ....  | 215 |
| Figure 5.2-3. Oxygen functional groups on activated carbon surface and their decomposition with temperature. ....   | 216 |
| Figure 5.2-4. Reaction pathways of Toluene catalytic cracking .....   | 217 |
| Figure 5.2-5. TGA-FTIR curves of fresh and spent tyre char.....   | 218 |
| Figure 5.2-6. Products yields of methylnaphthalene cracking over tyre char at different cracking temperatures.....  | 220 |
| Figure 5.2-7. Influence of reaction time on gaseous compounds and carbon conversion .....   | 222 |
| Figure 5.2-8. Influence of carbon porosity on gaseous compounds .....   | 224 |
| Figure 5.3-1. Gas compositions and hydrogen yield with original and acid treated tyre chars. ....   | 232 |
| Figure 5.3-2. Concentration of the classified tar compounds in the tar collected from the pyrolysis-reforming/gasification of biomass with tyre char catalyst at 800 °C (Class 2 = heterocyclic compounds e.g. phenols and cresols; class 3 = 1-ring aromatic compounds e.g. ethylbenzene and xylene; Class 4 = 2-3 ring aromatic compounds e.g. naphthalene and phenanthrene; Class 5 = 4-7 ring aromatic compounds e.g. fluoranthene and pyrene)..... | 236 |
| Figure 5.3-3. The influence of steam to biomass (S/B) ratio on gas composition and total gas yield .....  | 238 |
| Figure 5.3-4. Effect of steam to biomass ratio on H <sub>2</sub> yield, HHV, H <sub>2</sub> /CO and CO/CO <sub>2</sub> . ....   | 239 |
| Figure 5.3-5. The influence of reaction time on the product gas compositions.....   | 241 |
| Figure 5.3-6. The influence of reaction time on tyre char conversion and total gas yield.....   | 242 |
| Figure 5.3-7. Carbon and ash content of tyre char from catalytic gasification of biomass at different reaction times .....  | 243 |

# Abbreviations

|       |  |
|-------|--|
| AC    | Activated carbon   |
| AC-T  | Activated carbon produced from waste tyres   |
| AC-R  | Activated carbon produced from refuse derived fuel                                     |
| AC-D  | Activated carbon produced from date stones   |
| APC   | Air pollution control  |
| BTU   | British Thermal Unit   |
| BET   | Brunauer-Emmet-Teller method for surface area and porous determination                 |
| BJH   | Barrett, Joyner & Halenda method for total pore volume and pore diameter determination |
| DR    | Dubinin-Radushkevich method for micropore volume determination                         |
| DFT   | Density Functional Theory for pore size distribution determination                     |
| DCM   | Dichloromethane  |
| EDXS  | Energy Dispersive X-Ray Spectrometer   |
| EC    | European Commission  |
| FID   | Flame Ionisation Detector  |
| FTIR  | Fourier Transform Infrared Spectrometry  |
| GC-MS | Gas Chromatograph coupled to a Mass Spectrometer                                       |
| GC    | Gas Chromatograph  |
| HHV   | Higher Heating Value   |
| KFT   | Karl-Fisher Titration  |
| MSW   | Municipal solid waste  |

|      |                                   |
|------|-----------------------------------|
| ND   | Not detected                      |
| PAH  | Polyaromatic Hydrocarbons         |
| RDF  | Refuse Derived Fuel               |
| RSD  | Relative Standard Deviation       |
| RF   | Response factor                   |
| SCR  | Selective catalytic reduction     |
| SD   | Standard deviation                |
| SNCR | Selective non catalytic reduction |
| SEM  | Scanning Electron Microscopy      |
| TCD  | Thermal Conductivity Detector     |
| THF  | Tetrahydrofuran                   |
| XPS  | X-Ray Photoelectron Spectroscopy  |
| XRD  | X-Ray Diffraction                 |
| XRF  | X-Ray Fluorescence                |

# CHAPTER 1. INTRODUCTION

---

## 1.1 World Energy Consumption and Waste Generation

Energy consumption and waste generation are expected to increase worldwide as a result of growths in population and industrialization [1]. As can be seen in Figure 1.1-1 (a), total worldwide energy demand is expected to be about 25% higher in 2040 compared to the energy consumption in 2014, and fossil fuels will still continue to dominate the global energy use. The major source of energy comes from fossil fuels and accounts for 85% of total energy use and where oil remains the world's largest source of energy [2]. However, to mitigate environmental issues associated with fossil fuel use, another sustainable source of energy is needed. As presented in Figure 1.1-1 (b), a marginal change (0.3%) is expected with the energy provided by biomass/wastes [2]. In addition, global municipal solid waste generation is estimated to double by 2025. The current global generation rate is 1.3 billion tonnes per year and is likely to be around 2.2 billion tonnes in 2025, with landfills remaining the most widely used disposal option [3].

Developing value-added products derived from waste materials is a promising route to solve the environmental issues associated with increasing amounts of waste being landfilled [4]. Furthermore, energy and waste management issues have become a matter of global concern. Therefore, managing the waste in a sustainable way and developing waste to energy facilities would help to solve both issues. Recovering energy from waste is performed through thermal treatment processes such as gasification, incineration and pyrolysis.

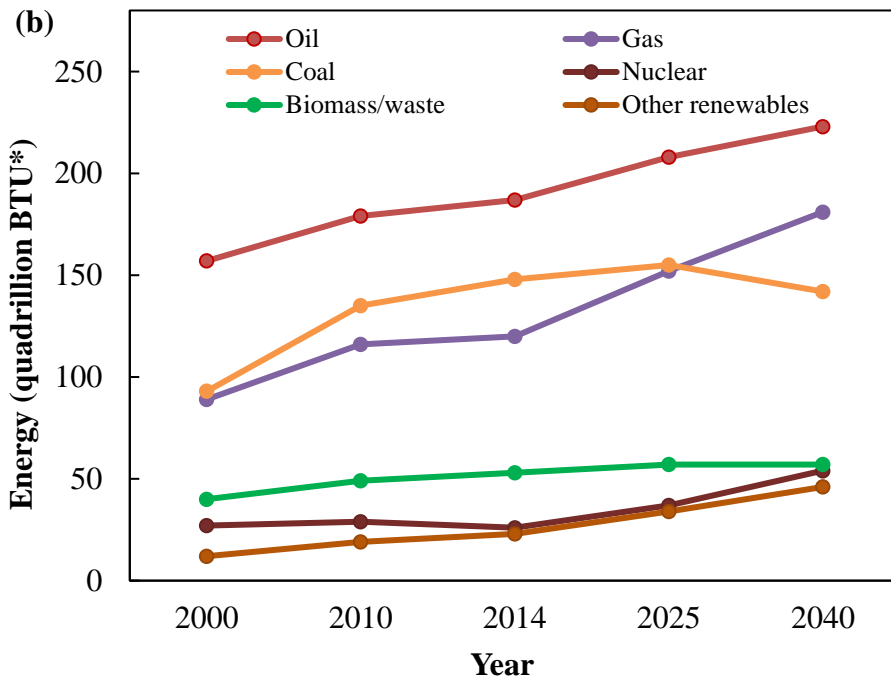
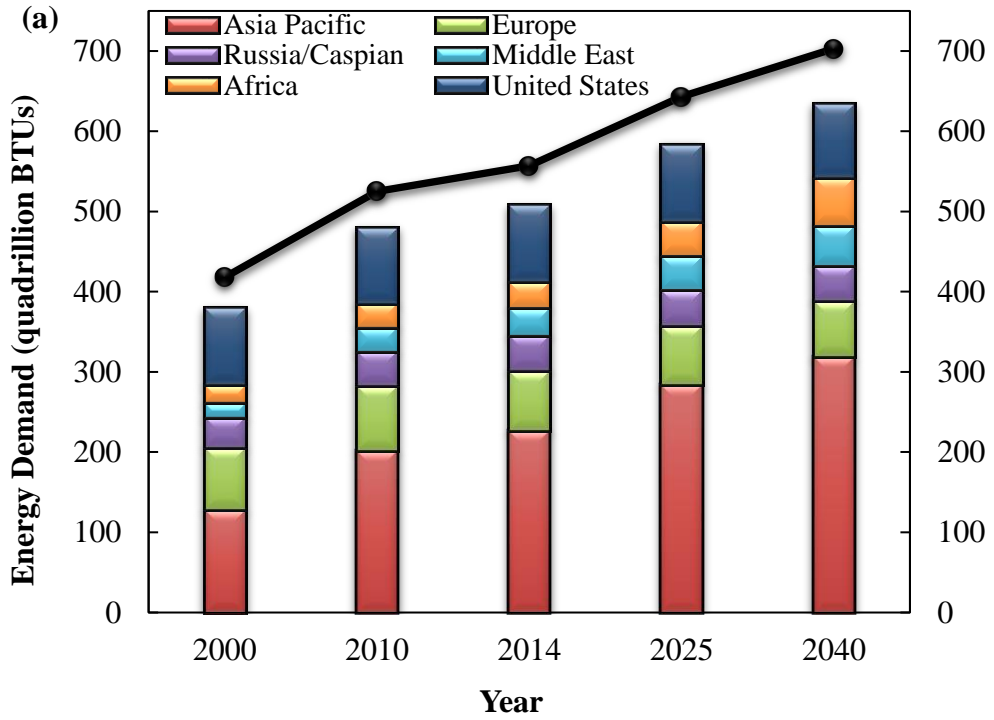


Figure 1.1-1. (a) World energy demand and (b) energy sources [2].  
 \*1 quadrillion BTUs =  $1.05 \times 10^{18}$ .

## **1.2 Energy Recovery from Waste**

Waste is considered as an unavoidable by-product of human activity [5], however, it can be regarded as a resource of valuable products [6]. Waste could have an important role in both meeting the rising demand for energy and in mitigating the environmental pollution caused by waste management practices such as landfills. Therefore, waste to energy technologies offer various environmental benefits such as; offsetting the use of fossil fuels for energy production thereby reducing CO<sub>2</sub> emissions, reducing the overall waste quantities requiring final disposal in landfills, providing a safe and economical option for wastes that have significant disposal issues and avoiding methane emissions from landfill [7]. The main available technologies for converting waste to energy are thermochemical, biochemical and physicochemical.

In thermochemical conversion processes, the organic matter is decomposed thermally to produce fuel oil, syngas or heat energy, through pyrolysis, gasification or incineration respectively.

## **1.3 Thermochemical Conversion Process**

The possible options for converting waste into useful products are displayed in Figure 1.3-1 [8]. Different ranges of products are generated depending on the process. For example, both gasification and pyrolysis are used to convert the waste to secondary products (liquid, gas and solid) that undergo further processing to generate energy in the form of heat and/or electricity, while in incineration the energetic value of waste is recovered directly [9-10].

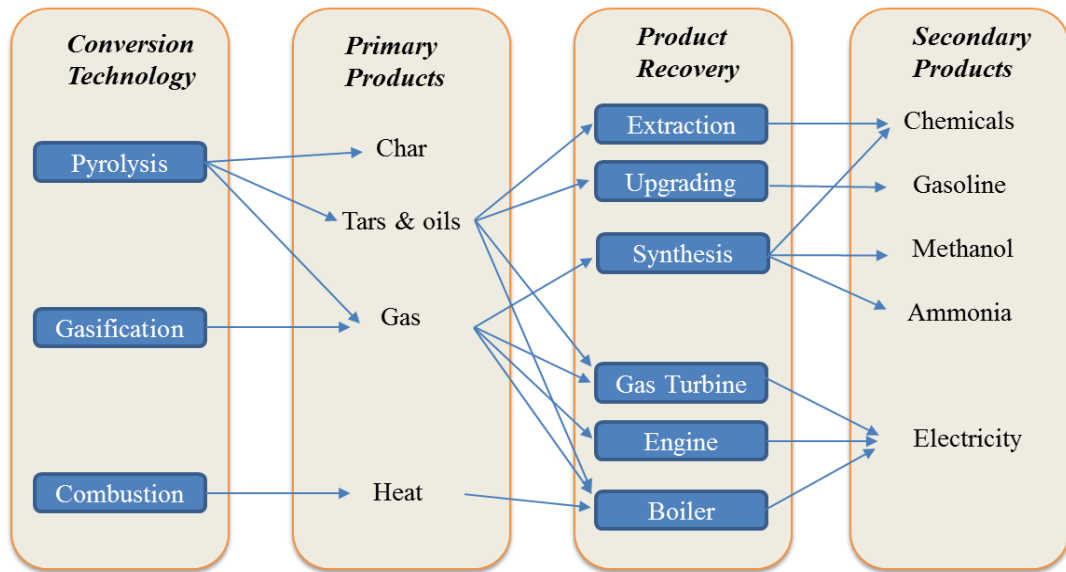


Figure 1.3-1. Thermochemical conversion processes [8].

The main difference between the incineration, gasification and pyrolysis, is the amount of air that is supplied to thermal reactors as presented in Figure 1.3-2 [11].

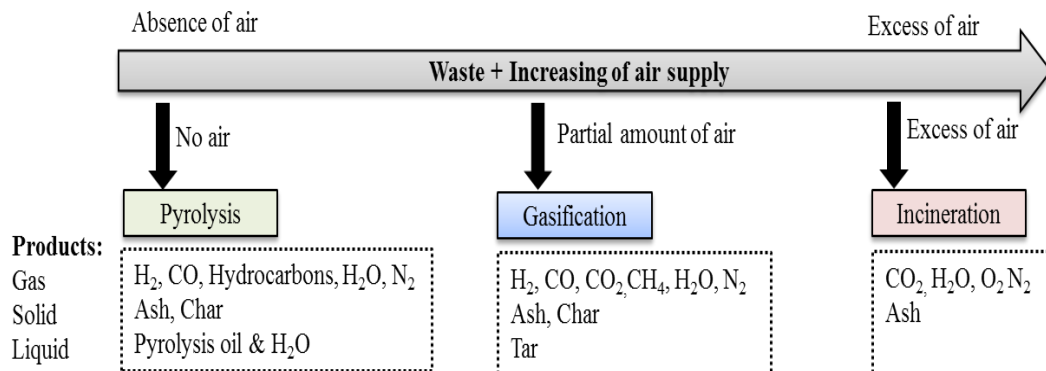


Figure 1.3-2. The difference between the incineration, gasification and pyrolysis conversion processes.

### 1.3.1 Incineration

Incineration is the oxidation of the combustible materials contained in the waste [9]. Incineration is used as a waste treatment option to reduce the volume and the hazard of waste [12]. Incineration allows the reduction of about 90 wt.% of the total volume

of waste to generate heat, water vapour, CO<sub>2</sub>, N<sub>2</sub> and O<sub>2</sub>, and depending on the waste composition, other emissions may be formed such as CO, HF, HCl, NO<sub>x</sub>, SO<sub>2</sub>, dioxins and furans, heavy metals and others [9, 13]. Incineration can be applied to a wide range of wastes such as municipal solid wastes (MSW) (not-pre-treated), refuse derived fuels (RDF), hazardous wastes, clinical wastes and sewage sludge [12]. Additionally, incineration allows the recovery of much of the energy bound in the waste in the form of electricity or heat [14]. Generally, 1 tonne of waste generates about 400-700 kWh of electricity and about 1205 kWh as heat. One tonne of MSW requires about 4000-4500 m<sup>3</sup> of air to be fully oxidized. The main products are 300 kg bottom ash (25-30 % of the solid waste input), 30 kg air pollution control (APC) residues and flue gas volumes of about 4500-6000 Nm<sup>3</sup> are generated [11]. The flue gas should contain low level of pollutants as stated by the EC Industrial Emissions Directive (2010) as also set out in the EC Waste Incineration Directive (2000). The concentration of MSW incineration flue gas components and final emission limits set by the European Commission in the Industrial Emissions Directive 2010, Waste Incineration Directive 2000 [15], are displayed in Table 1.3-1;

Table 1.3-1. The concentration of pollutants in MSW incineration flue gas and Emission limits set by the European Commission.

| <b>Pollutant</b>                   | <b>Concentration in raw gas (mg m<sup>-3</sup>)</b><br>(Basis: 6500 m <sup>3</sup> /t waste, 11% O <sub>2</sub> )[16] | <b>Emission limit (mg m<sup>-3</sup>)</b><br>(dry, 273K, 101.3 KPa)<br>[14] |
|------------------------------------|---|---|
| Dust                               | 1000-5000   | 10  |
| HCl                                | 500-2000  | 10  |
| SO <sub>2</sub>                    | 150-400   | 50  |
| NO <sub>x</sub> as NO <sub>2</sub> | 250-450   | 200   |
| CO                                 | 10-30   | 50  |
| Hg                                 | 0.1-0.5   | 0.05  |
| PCDD/F                             | 0.5-5.0   | 0.1   |

### 1.3.2 Pyrolysis

Pyrolysis is the thermal degradation of waste in the absence of oxygen to produce gas, liquid (tars and oils) and char consisting of carbon [17]. Yields of pyrolysis products depend on the pyrolysis operating conditions such as heating rates, residence time and pyrolysis temperature. These conditions can be optimised to obtain the required final product. Based on the heating rate and pyrolysis temperature, pyrolysis is categorised into slow, fast and flash processes. Slow pyrolysis is conducted at temperatures of 400-800 °C with heating rates of 10-80 °C min<sup>-1</sup>, while fast pyrolysis is carried out at temperatures of about 500 °C with relatively high heating rates of > 100 °C s<sup>-1</sup> [18]. Various feedstocks have been investigated including biomass, RDF, plastics and tyres. Products yields obtained from the conventional pyrolysis of these materials are summarized in Table 1.3-2

Table 1.3-2. Pyrolysis products from different waste material

| Raw material   | Temperature (°C) | Pyrolysis type | Gas (wt.%) | Oil (wt.%) | Char (wt.%) | Ref  |
|----------------|------------------|----------------|------------|------------|-------------|------|
| RDF            | 600              | Moderate       | 20.0       | 49.0       | 35.0        | [19] |
| Tyres          | 600              | Moderate       | 5.8        | 54.0       | 40.2        | [20] |
| Biomass (wood) | 600              | Moderate       | 27.0       | 50.4       | 22.6        | [21] |

Char product yields depends on the pyrolysis conditions. For example, slow pyrolysis of tyre produces a char of about 40-50 wt.%, while the pyrolysis of MSW produces about 33-50 wt.% [22]. Char can be recovered and used as low-value adsorbent or upgraded to activated carbon [22]. The pyrolysis gas composition depends on the type of waste material. Both MSW and biomass waste have a high oxygen content, thus the main pyrolysis gases are carbon monoxide and carbon dioxide. In contrast, as tyres have low content of oxygenated compounds, pyrolysis of tyres yields high concentrations of hydrogen, methane and hydrocarbon gases [22]. Pyrolysis gas could be used to power turbines and engines for electricity generation.

### 1.3.3 Gasification

Gasification is a process that converts the carbonaceous materials into combustible gas called synthesis gas at a quite high temperature ( $>600\text{ }^{\circ}\text{C}$ ) and with the presence of steam, oxygen, air or mixtures of these [23]. Oxygen or steam gasification leads to a gas product with a medium heating value ( $10\text{-}18\text{ MJ m}^{-3}$ ), while gasification with air produces a gas with a low heating value ( $4\text{-}7\text{ MJ m}^{-3}$ ) [9, 22]. Steam is the most commonly used gasification agent and can produce a combustible gas with high hydrogen content [17]. The gas composition produced from biomass gasification as a function of the type of gasifying agent is presented in Table 1.3-3 [24]. As shown in Table 1.3-3, the synthesis gas obtained with the use of steam has a higher hydrogen content, compared to the other gasifying agents.

Table 1.3-3. Composition of gaseous species from biomass gasification.

| Gasifying agent       | Temperature range ( $^{\circ}\text{C}$ ) | Gas product (vol.%) |                 |       |                 |                                |                  |
|-----------------------|--|---------------------|-----------------|-------|-----------------|--------------------------------|------------------|
|                       |  | H <sub>2</sub>      | CO <sub>2</sub> | CO    | CH <sub>4</sub> | C <sub>2</sub> -C <sub>6</sub> | H <sub>2</sub> O |
| Steam+ O <sub>2</sub> | 785-830                                  | 14-32               | 14-36           | 43-52 | 6-8             | 3-4                            | 38-61            |
| Steam                 | 750-780                                  | 38-56               | 13-17           | 17-32 | 7-12            | 2                              | 52-60            |
| Air                   | 780-830                                  | 5-16                | 9-19            | 10-22 | 2-6             | 0-3                            | 11-34            |

Various raw materials can be used in the gasification process such as biomass, agricultural waste, sewage sludge, petroleum based materials and coal [25]. However, for an efficient gasification process and with a high conversion efficiency and minimal tar formation, a pre-treatment step is required for certain types of waste in order to obtain a homogenous carbon-based material. A gasification system consists mainly of a gasifier, which is used to produce the combustible gas, a gas cleaning system to clean the syngas and remove the harmful components before the application of the gas and an energy recovery system [9, 17].

The most frequently used gasification reactors are fixed bed, fluidized bed and entrained flow gasifiers [9, 26]. Fixed bed gasifiers can be classified as downdraft, cross-flow or updraft. Depending on the fluidization pattern, fluidized beds can also

be further classified into bubbling and circulating fluidized bed gasifiers. During gasification, the feedstock undergoes several stages (Figure 1.3-3) and these begin with drying to evaporate the moisture contents of the feedstock at a temperature of about 150 °C, followed by pyrolysis where light hydrocarbons, CO, CO<sub>2</sub>, char and tar are produced in the absence of oxygen. Evaporation is followed by an oxidation stage in which carbon content of the feedstock are reacted with oxygen, and finally, a reduction stage in which syngas is produced through several endothermic reactions [22, 26].

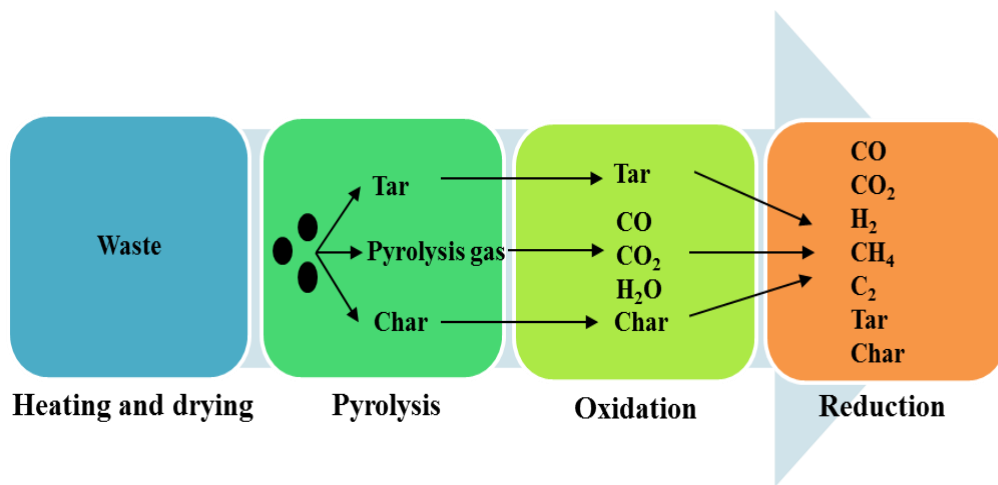


Figure 1.3-3. Main processes during biomass gasification [27].

The main product of gasification is syngas which consists mainly of carbon monoxide and hydrogen (about 85 volume percent) and smaller quantities of methane and carbon dioxide [28]. The most common syngas applications are shown in Figure 1.3-4. Syngas can be used to generate electricity or to produce heat or it can be further processed to produce hydrogen by the water gas-shift reaction, synthesis fuels by the Fisher-Tropsch process, ethanol by fermentation and methanol by methanol synthesis which can be further processed to produce other chemicals and fuels such as olefins, gasoline, formaldehyde and dimethyl ether [29].

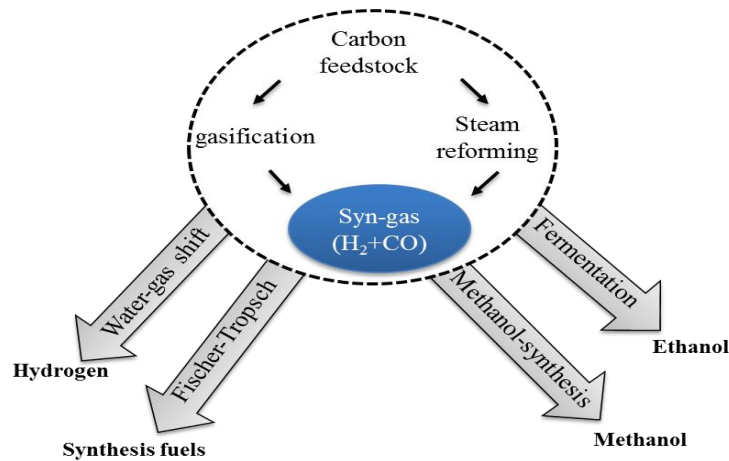


Figure 1.3-4. Production of fuels and chemicals from syngas [29].

Gasification is a promising process, which could play a significant role in solving the issues associated with waste accumulation and greenhouse gas emissions. However, one of the main issues associated with gasification is tar formation in the syngas. Tars can condense in the process equipment-causing blockage of pipelines and downstream syngas utilisation systems such as engine and turbine fuel lines and injector nozzles.

#### 1.4 Wastes as sources for higher value carbon products

An increasing degree of importance is currently given to the conversion of wastes to useful products. Pyrolysis and gasification both have the potential to yield valuable products which can be used in various applications. For instance, carbonaceous materials (including char and activated carbon materials) can play a vital role in addressing several environmental issues [30]. The use of wastes as raw materials for production of low-cost adsorbents is an attractive pathway to minimize the amount of wastes. It will also decrease costs of waste disposal. Waste-derived carbons offer low cost alternatives to commercial activated carbons and have been used in wide applications such as adsorption of heavy metals and organic pollutants [31-32], tar cracking [33-34] and gas pollutants removal [35-36].

In this project, three different waste materials were selected for char and activated carbon production to be investigated as valuable adsorbent materials for control of a

NO<sub>x</sub>, a problematic gaseous pollutant from industries, or alternatively as a low-cost catalyst for the removal of tar during biomass gasification process.

#### 1.4.1 Refuse Derived Fuel (RDF)

Recently, the global MSW generation level has increased significantly, and it is expected to be 2.2 billion tonnes by 2025 [37]. Typically, municipal solid wastes (MSW) are composed of paper, food, wood, cotton, plastic, glass, and various inorganic wastes from industrial, commercial and residential sources. According to the data reported by the World Bank, worldwide composition of MSW is presented in Figure 1.4-1 [37].

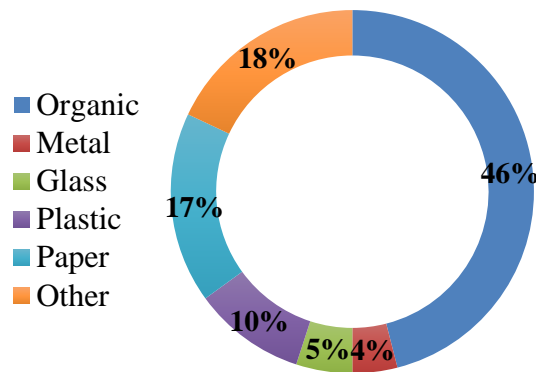


Figure 1.4-1. Global municipal solid waste composition [37].

While MSW is a heterogeneous waste, which has not been sorted and shredded, RDF represents the municipal solid waste with the elimination of recyclable materials such as metals and glass. As such, RDF is a more homogenous fraction of MSW. The main steps involved in the production of RDF are bag splitting, size screening, magnetic separation and coarse shredding and finally a refining separation stage [38].

#### 1.4.2 Waste tyre

Another attractive waste raw material for the production of valuable products is waste tyres. It is projected that about 1 billion waste tyres are generated annually worldwide [39]. Increasing amounts of waste tyre represent a serious environmental issue as tyres can neither self-decompose at normal atmospheric conditions nor even respond to

biological degradation processes [30]. In addition, most developed countries prohibit the disposal of waste tyres in landfills [40].

Therefore, there is a need to find another treatment option that could transform waste tyres to valuable materials without causing environmental problems. Pyrolysis has been shown by several researchers to be an effective method that converts waste tyres to useful products [20, 41-42]. Tyre rubber has been found to decompose at 450 °C and the process reaches completion at 500-600 °C [43-45]. The main products obtained from the pyrolysis of waste tyres are 33-38% char, 38-58% oil and 10-30% gas [20].

Typical tyre chars have a BET surface area of about 100 m<sup>2</sup> g<sup>-1</sup>, which make tyre-derived chars good precursors for production of activated carbon adsorbents [46]. The carbon char can be used for many applications depending on its pore size, porosity and surface area. Tyre char has also been reported to have a high aqueous adsorption capacity of large molecular weight species [47]. Moreover, tyre-derived activated carbon has been used to adsorb SO<sub>2</sub> from flue gas [48], butane [49], phenol from water [50] methylene blue and phenol [51]. Therefore, production of adsorbent from waste tyres represents a doubly useful solution to address the environmental pollution associated with tyres as it can transform a hard-to-dispose waste material to a pollution-cleaning adsorbent [52].

### **1.4.3 Biomass**

Materials with a biological origin that are derived from plant and animal matter are called biomass [53]. Biomass is a source of various valuable products such as bio-oil, biochar, syngas and chemicals. In this research, date stones are used as a source of biomass material to produce char and activated carbon. Worldwide production of dates was about 7.9 million in 2010 [54]. Gulf Cooperation Council (GCC) countries are one of the world's major producers of dates. Large quantities of agricultural waste are produced from date trees [55]. These wastes consist mainly of cellulose (57%), lignin (15%), hemicellulose (23%) and other components that can be used in several applications [55-56]. However, these wastes are normally combusted in farms causing serious environmental issues. Therefore, there is a need to find a suitable application

of this waste. Date stones represent about 10% in weight of the fruit [55]. It has been reported by other researchers that date stones have excellent natural structure and they are suitable for preparing activated carbons [56-57].

## **1.5 Objectives of this research**

From the aforementioned information, it can be deduced that the use of waste materials as sources of higher value carbon materials offers a unique solution of utilization of waste materials and slowly biodegrading materials such as tyres. The utilization of these raw materials as precursors for generating low-cost and effective carbonaceous materials is very attractive and would help to solve the issues associated with waste disposal [58]. In addition, this would also contribute to diverting the waste away from landfills; thereby protecting the environment by reducing volumes of wastes deposited in landfills and consequently reducing the adverse impacts of landfills. Limited attention has been devoted to the use of carbonaceous materials derived from waste materials for NO adsorption or tar decomposition. To the author's best knowledge, no reports related to the use of carbonaceous materials derived from RDF, waste tyres, and date stones for either the removal of nitric oxide at low temperatures or tar decomposition can be found in the literature. It is thus important to assess and develop applications of these carbonaceous materials, thereby making them ready for commercial use.

Therefore, in light of these, the aim of this project is to use the carbon derived from these waste materials as a low-cost route to develop two different novel processes;

(i) As an adsorbent for the removal of  $\text{NO}_x$  from a combustion plant. The combustion of solid fuels such as coal, biomass and wastes generates nitrogen oxides ( $\text{NO}_x$ ), which cause environmental problems such as acid rain and smog. This research is aimed to produce activated carbons from RDF, waste tyres and waste biomass to be used as adsorbents to trap NO at low temperatures.

(ii) Using the waste derived pyrolysis chars to catalyse the cracking of tar compounds in the product syngas from the gasification of biomass. The aim is to further convert

tars contained in syngas to produce a hydrogen rich-syngas. There is increasing worldwide concern in relation to the use of fossil fuels and the associated emissions of greenhouse gases. The thermochemical conversion of biomass, as a renewable source of energy, have received increased interest since it is considered as a viable and sustainable alternative source of energy supply [59]. However, tar formation during biomass gasification is one of the main problems, which can prevent the direct use of the producer gas in gas turbines and gas engines. Tar is a chemically complex mixture of aromatic hydrocarbons and oxygenated hydrocarbons and is normally defined as hydrocarbons with molecular weight higher than benzene ( $MW > 78$ ) [60]. This research is aimed to develop a novel low-cost char to crack the tar, thereby producing a clean synthesis gas. There have been a few studies published on the use of char for tar decomposition during the gasification of biomass waste. However, chars from date stones, RDF and waste tyre are used for the first time in this project for tar cracking.

To achieve these aims, various phases of the research were mapped out, with each phase having set objectives. These were:

Phase 1: Preparation of char and activated carbons from waste tyres, RDF and date stones. This phase of the project involves:

- Carbonisation of waste materials to produce char
- Physical and chemical activation of chars using a fixed bed reactor

Phase 2: NO removal using waste derived activated carbons. This phase involves:

- Characterization of the waste derived activated carbons in terms of porous texture, BET surface area, surface chemistry and morphology.
- Evaluation of NO removal performance of waste derived activated carbons at a temperature of 50 °C.
- Comparison with commercial activated carbons with various porous texture and surface chemistry
- Assessment of the effects of porous texture and surface chemistry of carbons on NO removal.

- Investigation of the influence of adsorption temperature, NO and O<sub>2</sub> concentrations on NO adsorption.
- Comparison of the effect of physical and chemical activation on the porosity development of waste tyre activated carbon and consequently on NO removal at low temperatures
- Assessment of the influence of various chemical activation agents on altering the porous texture of waste tyre-derived activated carbon.

Phase 3: Tar removal using waste derived pyrolysis chars. This phase involves:

- Gasification of Biomass in a two-stage fixed bed reactor.
- Investigation of the effectiveness of waste-derived chars for tar cracking during the pyrolysis-gasification of biomass.
- Investigation of the influence of operating conditions on tar species and gas composition. Analysis of the tar composition obtained with the three different char materials.
- A comparison of the above results with the performance of tyre char for cracking of tar model compounds.
- Assessment of the influence of porous texture and oxygen functional groups on contributing to the catalytic activity of carbonaceous materials.
- Steam reforming of biomass tar over tyre char for hydrogen-rich syngas production.
- Investigation of the effect of ash minerals, steam rate, reforming temperature and reaction time on hydrogen production.

## References

1. OUDA, O.K.M., S.A. RAZA, R. AL-WAKED, J.F. AL-ASAD and A.-S. NIZAMI. Waste-to-energy potential in the Western Province of Saudi Arabia. *Journal of King Saud University - Engineering Sciences*.
2. EXXON MOBIL. The Outlook for Energy: A View to 2040. [online], 2016, [Accessed 23.07.2016]. Available from: <http://cdn.exxonmobil.com/~media/global/files/outlook-for-energy/2016/2016-outlook-for-energy.pdf>.
3. HOORNWEG, D. and P. BHADA-TATA. What a Waste: A Global Review of Solid Waste Management. [online], 2012, [Accessed 23.07.2016]. Available from: [http://siteresources.worldbank.org/INTURBANDEVELOPMENT/Resources/336387-1334852610766/What\\_a\\_Waste2012\\_Final.pdf](http://siteresources.worldbank.org/INTURBANDEVELOPMENT/Resources/336387-1334852610766/What_a_Waste2012_Final.pdf).
4. OLIVARES-MARÍN, M. and M.M. MAROTO-VALER. Development of adsorbents for CO<sub>2</sub> capture from waste materials: a review. *Greenhouse Gases: Science and Technology*, 2012, **2**(1), pp.20-35.
5. ASHOK K. RATHOURE and V.K. DHATWALIA. *Toxicity and Waste Management Using Bioremediation (Advances in Environmental Engineering and Green Technologies)*. first ed. USA: IGI Global, 2015.
6. ATIQ UZ ZAMAN. *Technical Development of Waste Sector in Sweden: Survey and Life Cycle Environmental Assessment of Emerging Technologies*. Master thesis, KTH, 2009.
7. BEGUM, S., M.G. RASUL and D. AKBAR. An Investigation on Thermo Chemical Conversions of SolidWaste for Energy Recovery. *World Academy of Science. Engineering and Technology*, 2012, **62**, pp.624-630.
8. BRIDGWATER, A.V. Catalysis in thermal biomass conversion. *Applied Catalysis A: General*, 1994, **116**(1), pp.5-47.
9. BOSMANS, A., I. VANDERREYDT, D. GEYSEN and L. HELSEN. The crucial role of Waste-to-Energy technologies in enhanced landfill mining: a technology review. *Journal of Cleaner Production*, 2013, **55**, pp.10-23.
10. DEFRA. Incineration of Municipal Solid Waste. [online], 2013, [Accessed 14.08.2016]. Available from: [https://www.gov.uk/government/uploads/system/uploads/attachment\\_data/file/221036/pb13889-incineration-municipal-waste.pdf](https://www.gov.uk/government/uploads/system/uploads/attachment_data/file/221036/pb13889-incineration-municipal-waste.pdf).

11. MARGARIDA J. QUINA, JOÃO C.M. BORDADO and R.M. QUINTA-FERREIRA. Air pollution control in municipal solid waste incinerators. *In: M. KHALLAF, ed. The Impact of Air Pollution Health, Economy, Environment and Agricultural Sources.* InTech, 2011, pp.331-358.
12. EUROPEAN COMMISSION. *Integrated pollution prevention and control. Draft reference document on the best available techniques for waste incineration,* 2006. [Accessed 19.08.2016]. Available from: [http://eippcb.jrc.ec.europa.eu/reference/BREF/wi\\_bref\\_0806.pdf](http://eippcb.jrc.ec.europa.eu/reference/BREF/wi_bref_0806.pdf).
13. CHENG, H. and Y. HU. Municipal solid waste (MSW) as a renewable source of energy: Current and future practices in China. *Bioresource Technology*, 2010, **101**(11), pp.3816-3824.
14. WILLIAMS, P.T. Waste Incineration. *In: Waste Treatment and Disposal.* John Wiley & Sons, Ltd, 2005, pp.245-323.
15. EUROPEAN COMMISSION. *The Waste Incineration Directive*, 2008, [Accessed 09/01/2017]. Available from: <http://eur-lex.europa.eu/LexUriServ/LexUriServ.do?uri=CONSLEG:2000L0076:20081211:EN:PDF>.
16. JURGEN, V and S. DALAGER. Incineration:Flue Gas Cleaning and Emissions. *In: THOMAS H. CHRISTENSEN, ed. Solid Waste Technology and Management.* John Wiley & Sons INC, 2011, pp.393-420.
17. BELGIORNO, V., G. DE FEO, C. DELLA ROCCA and R.M.A. NAPOLI. Energy from gasification of solid wastes. *Waste Management*, 2003, **23**(1), pp.1-15.
18. RYU, C., V.N. SHARIFI and J. SWITHENBANK. Thermal waste treatment for sustainable energy. *Proceedings of the Institution of Civil Engineers - Engineering Sustainability*, 2007, **160**(3), pp.133-140.
19. BUAH, W.K., A.M. CUNLIFFE and P.T. WILLIAMS. Characterization of Products from the Pyrolysis of Municipal Solid Waste. *Process Safety and Environmental Protection*, 2007, **85**(5), pp.450-457.
20. WILLIAMS, P.T., S. BESLER and D.T. TAYLOR. The pyrolysis of scrap automotive tyres: The influence of temperature and heating rate on product composition. *Fuel*, 1990, **69**(12), pp.1474-1482.

21. WILLIAMS, P.T. and S. BESLER. The influence of temperature and heating rate on the slow pyrolysis of biomass. *Renewable Energy*, 1996, **7**(3), pp.233-250.
22. WU, C. and P.T. WILLIAMS. Advanced Thermal Treatment of Wastes for Fuels, Chemicals and Materials Recovery. *In: Waste as a Resource*. The Royal Society of Chemistry, 2013, pp.1-43.
23. LOMBARDI, L., E. CARNEVALE and A. CORTI. A review of technologies and performances of thermal treatment systems for energy recovery from waste. *Waste Management*, 2015, **37**, pp.26-44.
24. GIL, J., J. CORELLA, M.A.P. AZNAR and M.A. CABALLERO. Biomass gasification in atmospheric and bubbling fluidized bed: Effect of the type of gasifying agent on the product distribution. *Biomass and Bioenergy*, 1999, **17**(5), pp.389-403.
25. STIEGEL, G.J. and R.C. MAXWELL. Gasification technologies: the path to clean, affordable energy in the 21st century. *Fuel Processing Technology*, 2001, **71**(1-3), pp.79-97.
26. DAMARTZIS, T. and A. ZABANIOTOU. Thermochemical conversion of biomass to second generation biofuels through integrated process design—A review. *Renewable and Sustainable Energy Reviews*, 2011, **15**(1), pp.366-378.
27. GUAN, G., M. KAEWPANHA, X. HAO and A. ABUDULA. Catalytic steam reforming of biomass tar: Prospects and challenges. *Renewable and Sustainable Energy Reviews*, 2016, **58**, pp.450-461.
28. ROGOFF, M.J. and F. SCREVE. Chapter 3 - WTE technology. *In: Waste-to-Energy (Second Edition)*. Oxford: William Andrew Publishing, 2011, pp.21-43.
29. HUBER, G.W., S. IBORRA and A. CORMA. Synthesis of Transportation Fuels from Biomass: Chemistry, Catalysts, and Engineering. *Chemical Reviews*, 2006, **106**(9), pp.4044-4098.
30. HADI, P., K.Y. YEUNG, J. GUO, H. WANG and G. MCKAY. Sustainable development of tyre char-based activated carbons with different textural properties for value-added applications. *Journal of Environmental Management*, 2016, **170**, pp.1-7.

31. CHUN, Y., G. SHENG, C.T. CHIOU and B. XING. Compositions and Sorptive Properties of Crop Residue-Derived Chars. *Environmental Science & Technology*, 2004, **38**(17), pp.4649-4655.
32. QIU, Y., H. CHENG, C. XU and G.D. SHENG. Surface characteristics of crop-residue-derived black carbon and lead(II) adsorption. *Water Research*, 2008, **42**(3), pp.567-574.
33. ABU EL-RUB, Z., E.A. BRAMER and G. BREM. Experimental comparison of biomass chars with other catalysts for tar reduction. *Fuel*, 2008, **87**(10–11), pp.2243-2252.
34. GILBERT, P., C. RYU, V. SHARIFI and J. SWITHENBANK. Tar reduction in pyrolysis vapours from biomass over a hot char bed. *Bioresource Technology*, 2009, **100**(23), pp.6045-6051.
35. YAN, R., T. CHIN, Y.L. NG, H. DUAN, D.T. LIANG and J.H. TAY. Influence of Surface Properties on the Mechanism of H<sub>2</sub>S Removal by Alkaline Activated Carbons. *Environmental Science & Technology*, 2004, **38**(1), pp.316-323.
36. BANDOSZ, T.J. On the Adsorption/Oxidation of Hydrogen Sulfide on Activated Carbons at Ambient Temperatures. *Journal of Colloid and Interface Science*, 2002, **246**(1), pp.1-20.
37. HOORNWEG, D. and P. BHADA-TATA. What a waste: a global review of solid waste management. 2012.
38. BUAH, W.K. and P.T. WILLIAMS. Activated carbons prepared from refuse derived fuel and their gold adsorption characteristics. *Environmental Technology*, 2010, **31**(2), pp.125-137.
39. MARTÍNEZ, J.D., N. PUY, R. MURILLO, T. GARCÍA, M.V. NAVARRO and A.M. MASTRAL. Waste tyre pyrolysis – A review. *Renewable and Sustainable Energy Reviews*, 2013, **23**, pp.179-213.
40. WILLIAMS, P.T. Pyrolysis of waste tyres: A review. *Waste Management*, 2013, **33**(8), pp.1714-1728.
41. TENG, H., M.A. SERIO, M.A. WOJTOWICZ, R. BASSILAKIS and P.R. SOLOMON. Reprocessing of used tires into activated carbon and other products. *Industrial & Engineering Chemistry Research*, 1995, **34**(9), pp.3102-3111.

42. CUNLIFFE, A.M. and P.T. WILLIAMS. Influence of Process Conditions on the Rate of Activation of Chars Derived from Pyrolysis of Used Tires. *Energy & Fuels*, 1999, **13**(1), pp.166-175.
43. MUI, E.L.K., D.C.K. KO and G. MCKAY. Production of active carbons from waste tyres—a review. *Carbon*, 2004, **42**(14), pp.2789-2805.
44. CUNLIFFE, A.M. and P.T. WILLIAMS. Influence of process conditions on the rate of activation of chars derived from pyrolysis of used tires. *Energy and Fuels*, 1999, **13**(1), pp.166-175.
45. MERCHANT, A.A. and M.A. PETRICH. Preparation and characterization of activated carbons from scrap tires, almond shells, and Illinois coal. *Chemical Engineering Communications*, 1992, **118**, pp.251-263.
46. LEHMANN, C.M.B., M. ROSTAM-ABADI, M.J. ROOD and J. SUN. Reprocessing and Reuse of Waste Tire Rubber to Solve Air-Quality Related Problems. *Energy & Fuels*, 1998, **12**(6), pp.1095-1099.
47. MIGUEL, G.S., G.D. FOWLER and C.J. SOLLARS. Pyrolysis of Tire Rubber: Porosity and Adsorption Characteristics of the Pyrolytic Chars. *Industrial & Engineering Chemistry Research*, 1998, **37**(6), pp.2430-2435.
48. BRADY, T.A., M. ROSTAM-ABADI and M.J. ROOD. Applications for activated carbons from waste tires: natural gas storage and air pollution control. *Gas Separation & Purification*, 1996, **10**(2), pp.97-102.
49. ALLEN, J.L., J.L. GATZ and P.C. EKLUND. Applications for activated carbons from used tires: Butane working capacity. *Carbon*, 1999, **37**(9), pp.1485-1489.
50. STREAT, M., J.W. PATRICK and M.J.C. PEREZ. Sorption of phenol and para-chlorophenol from water using conventional and novel activated carbons. *Water Research*, 1995, **29**(2), pp.467-472.
51. HELLEUR, R., N. POPOVIC, M. IKURA, M. STANCIULESCU and D. LIU. Characterization and potential applications of pyrolytic char from ablative pyrolysis of used tires. *Journal of Analytical and Applied Pyrolysis*, 2001, **58–59**(0), pp.813-824.
52. ARIYADEJWANICH, P., W. TANTHAPANICHAKOON, K. NAKAGAWA, S.R. MUKAI and H. TAMON. Preparation and characterization of mesoporous activated carbon from waste tires. *Carbon*, 2003, **41**(1), pp.157-164.

53. SUNGGYU LEE and Y.T. SHAH. *Biofuels and Bioenergy: Processes and Technologies*. New York: CRC Press, 2012.
54. JAIN, S.M. In vitro mutagenesis for improving date palm (*Phoenix dactylifera* L.). *Emir. J. Food Agric*, 2012, **24**(5), pp.400-407.
55. CHANDRASEKARAN, M. and A.H. BAHKALI. Valorization of date palm (*Phoenix dactylifera*) fruit processing by-products and wastes using bioprocess technology – Review. *Saudi Journal of Biological Sciences*, 2013, **20**(2), pp.105-120.
56. SEKIRIFA, M.L., M. HADJ-MAHAMMED, S. PALLIER, L. BAAMEUR, D. RICHARD and A.H. AL-DUJAILI. Preparation and characterization of an activated carbon from a date stones variety by physical activation with carbon dioxide. *Journal of Analytical and Applied Pyrolysis*, 2013, **99**, pp.155-160.
57. BOUCHELTA, C., M.S. MEDJRAM, O. BERTRAND and J.-P. BELLAT. Preparation and characterization of activated carbon from date stones by physical activation with steam. *Journal of Analytical and Applied Pyrolysis*, 2008, **82**(1), pp.70-77.
58. EL-SAYED, G.O., M.M. YEHIA and A.A. ASAAD. Assessment of activated carbon prepared from corncob by chemical activation with phosphoric acid. *Water Resources and Industry*, 2014, **7–8**, pp.66-75.
59. SUN, Q., S. YU, F. WANG and J. WANG. Decomposition and gasification of pyrolysis volatiles from pine wood through a bed of hot char. *Fuel*, 2011, **90**(3), pp.1041-1048.
60. DEVI, L., K.J. PTASINSKI and F.J.J.G. JANSSEN. A review of the primary measures for tar elimination in biomass gasification processes. *Biomass and Bioenergy*, 2003, **24**(2), pp.125-140.

# CHAPTER 2. LITERATURE REVIEW

---

## 2.1 Waste derived carbonaceous materials

### 2.1.1 Carbonisation

Carbonisation is the process to convert organic material to a solid residue richer in carbon content by pyrolysis in the absence of oxygen [1]. A schematic representation of the carbonisation process is shown in Figure 2.1-1.

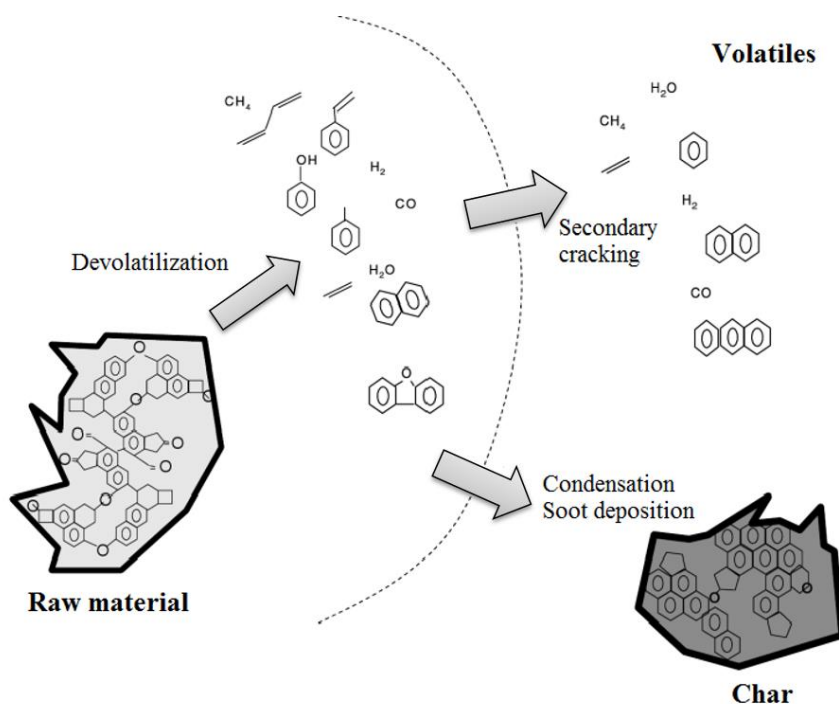


Figure 2.1-1. Carbonisation reaction of carbonaceous material [2].

Decomposition of the feedstock precursor occurs during carbonisation, usually at temperatures below 800 °C and in the absence of oxygen [3]. During this process the non-carbon species are eliminated, volatiles, aromatic and hydrogen are released and, a solid rich in carbon, called char is produced [2]. The char can be used directly as an adsorbent or upgraded to activated carbon [4]. Compared to the starting precursor, the formed char has a higher carbon content. The char consists of disordered short graphitic crystals, with the presence of micropores which are not accessible because of the blockage of micropores and mesopores due to soot deposition that could be

formed at high temperatures and high heating rates. Generally, low heating rates generate chars with a well-developed mesopore and macropore structure [2].

Process conditions, such as heating rates and pyrolysis temperatures, greatly influence the characteristics of pyrolysis chars. Generally, low heating rates maximize yields of char. Yields of char have been reported to decrease with the increase in pyrolysis temperatures. For example, Dai et al. [5] pyrolysed waste tyre in a circulating fluidized bed reactor. They found that the char yield decreased from 40 to 27 wt.% as the temperature of pyrolysis increased from 450 to 800 °C. Using a fixed bed reactor, Kar [6] pyrolysed 10 g of waste tyre at temperatures ranging from 375 to 500 °C at a heating rate of 10 °C min<sup>-1</sup>. The char yield was found to decrease with increasing temperature from 50.7 wt.% (375 °C) to 26.4 wt.% (500 °C). The char yields attained from pyrolysis of tyre ranged from 22 to 49 wt.%. Buah et al. [7] also showed during their pyrolysis of RDF in a fixed bed reactor that as pyrolysis temperature was raised from 400 to 700 °C, yields of char fell from 49.8 to about 32 wt.%, with a BET surface area of 82.06 m<sup>2</sup> g<sup>-1</sup>. They reported that the complete pyrolysis of RDF was achieved at a temperature of 600 °C. Tippayawong et al. [8] indicated that the most significant reduction in the yield of RDF char occurred at temperatures up to around 600 °C.

Regarding the influence of pyrolysis temperature on characteristics of the product char, Guo and Lua [9] reported that the volatile content of the produced RDF char decreased from 63.6 wt.% at 400 °C to 2.2 wt.% at 900 °C. They also reported that both fixed carbon and the ash contents increased with the increase in pyrolysis temperature. This was attributed to an increase of devolatilization of the sample during pyrolysis, which increased the fixed carbon content of char. Buah et al. [7] also investigated the characteristics of chars produced from the fixed bed pyrolysis of RDF over a temperature range of 400-700 °C and reported a decrease in volatile content from 41.5 to 13.7 wt.% with increasing pyrolysis temperature. They also reported that hydrogen, sulphur and nitrogen contents of the product chars were reduced as the pyrolysis temperature was increased, which is also ascribed to the increasing devolatilization of the chars with temperature.

### 2.1.2 Activation

Activated carbon is a solid black carbonaceous material, which has a well-developed porous structure and high surface area. It can be prepared from various carbon containing materials by physical or chemical activation of pyrolysed char. Activation of the char is required to develop the pores, as pores formed during carbonisation are filled with tarry pyrolysis products [3, 10]. Carbonisation temperature, heating rate and the activation conditions all affect the pore structure and the surface area of the resultant product. Typical surface areas of the commercial carbons are in the range of 400-1600 m<sup>2</sup> g<sup>-1</sup> [3]. Regarding the pore dimensions, activated carbon has a wide range of pores which can be classified according to their widths as: micropores with pore widths < 2 nm, mesopores with pore widths of 2-50 nm and macropores with pore widths of > 50 nm. To increase the adsorption capacity of activated carbon, the pore network should be developed during the preparation of activated carbon by physical or chemical treatments.

The main existing feedstocks for commercial production of active carbons are peat, anthracite, bituminous coal, coconut shell and wood. Carbon contents of these materials are in the range of 40 to 90% [3]. Activated carbon has a high adsorption capacity and it has been found to be effectively used in pollution control processes for removal of gaseous pollutants such as heavy metals, nitric oxides and sulphur dioxide [11]. The following properties make the activated carbon suitable for adsorption applications: surface structure can be easily modified; they can be used in both acidic and basic conditions; their pore structure can be modified to be used for different purposes [12-13]. Generally, activated carbon has a highly-developed surface area and a porous structure consisting of pores with different sizes in which the adsorbate molecules are captured during the adsorption process. Moreover, activated carbon has a chemical structure with associated heteroatoms (hydrogen, oxygen, nitrogen, sulphur), which are bonded at the edges of aromatic sheets or to carbon atoms within the carbon matrix forming various surface functional groups which can be acidic, basic or neutral [14]. The main functional groups present in activated carbon are carboxyl, carbonyl, lactones and phenols. These functional groups are responsible for the uptake of pollutants. The nature of these functional groups may be modified by chemical or

thermal treatments to enhance the uptake of different pollutants [15]. Mainly the type of the precursor and the activation method affects the surface functional groups and pore structure of activated carbons. The activated carbon surface has various proportions of active sites distributed mainly at the edges and defects within the carbon layers. These active sites are made of unsaturated valences. An increase in the surface area and porosity result in an increase in the proportion of these active sites [16].

Development of low cost activated carbon adsorbents using waste materials has attracted the attention of many researchers, as a route for producing valuable materials from wastes and as an alternative to waste disposal. A variety of solid wastes and biomass wastes have been used as feedstock to produce activated carbon [10, 17-25]. For example, activated carbons have been produced from municipal solid waste and used in the metals extraction industry [25]; from waste tyres and used for dioxin adsorption from flue gases [19]; also from waste tyres for use in adsorption of phenolic compounds [21]; from waste fibreboard for use for copper (II) adsorption [22]; from tannery wastes for use in the removal of dyes [10] and from agricultural wastes for the removal of pesticides from water [23].

Activated carbons can be prepared either by physical or chemical activation.

#### 2.1.2.1 Physical activation

The physical activation consists of: the pyrolysis of the precursor followed by the activation of the resultant char at higher temperatures (800 – 1000 °C) with the use of steam or CO<sub>2</sub> as the activating agents [21-23]. In this method, the reaction occurs between the carbon atom and the oxidizing gas. Reactions involved during the physical activation of char in the presence of steam and CO<sub>2</sub> are reported as follows [26]:



Both reactions are endothermic, implying that heat has to be supplied to perform the activation [26]. However, a higher activation temperature is required with carbon

dioxide activation of carbon, as the carbon-steam reaction showed a lower reaction enthalpy (Eq. 2.1). During the steam activation of char, the carbon fraction of char is combusted or 'burned off' producing carbon monoxide and hydrogen, thus creating porous sites [27].

Regarding the effect of activating agent, recent studies found that the activation kinetic with steam is higher than that with CO<sub>2</sub> [28-29]. The BET surface areas of the CO<sub>2</sub>-activated carbons were found to be in the range of 70-980 m<sup>2</sup> g<sup>-1</sup> [30-32], whereas steam-activated carbons revealed surface areas of higher than 1000 m<sup>2</sup> g<sup>-1</sup> [33-35]. This was attributed to the molecular dimension of steam, as the water molecule is smaller than the CO<sub>2</sub> molecule (Figure 2.1-2), which allows faster diffusion into the carbon porous structure [26]. It was found that using steam as an activating agent increased the pores in tyre carbons [33].

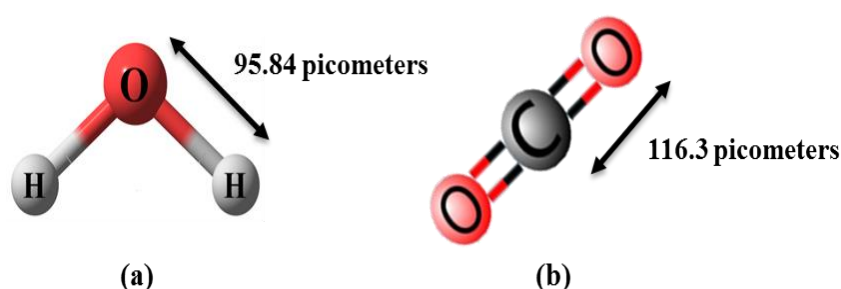


Figure 2.1-2. The dimension of water (a) and carbon dioxide (b) molecules.

In contrast, Rodriguez-Reinoso et al. [28] concluded that CO<sub>2</sub>, as activating agent, produced activated carbon with a higher micropore volume than the one activated with steam. In addition, the use of CO<sub>2</sub> caused an opening of ultramicropores, followed by widening to form supermicropores, while in the case with steam, the entire fraction of microporosity was widened from the beginning of the process.

Apart from the influence of the nature of an activating agent, activation temperature and degree of activation are also essential factors affecting characteristics of carbons. A number of studies reported an increase in pore volume and BET surface area with

activation temperature and time [36-37]. For example, in a study conducted by Fung et al. [38], it was shown that BET surface area of tyre char increased with the increase of activation time and activation temperature. Longer activation time provides more time for the carbon to react with activating agent. Activation is usually carried out at temperatures higher than 900 °C to maintain high reaction rates [39]. The adsorptive capacity of activated carbon is generally related to the BET surface area and porous texture [40]. Guo and Luo [40] studied the influence of activation temperatures on the BET surface area and porosity development of activated carbons prepared from oil palm stones and reported an increase in the BET surface areas with increasing activation temperatures from 750 to 900 °C. High activation temperatures were essential to enlarge the pores created during pyrolysis and to create new pores. A study of preparation of activated carbon from waste tyre was carried out by Ariyadejwanich et al. [34]. Physical activation of the tyre chars was carried out with steam at 850 °C and with a heating rate of 20 °C min<sup>-1</sup>. The BET surface area of the obtained activated carbon was found to be four times higher than the surface area of the chars.

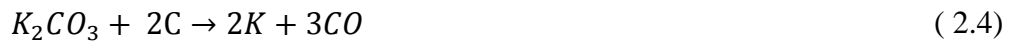
In addition, Buah and Williams [25] also investigated the influence of activation hold time on the porosity development of the activated carbons produced from RDF. At the same activation temperature, carbon yields linearly decreased with increasing holding time, as the degree of carbon burn-off via carbon gasification was observed to be proportional to the duration of activation. The BET surface area of the obtained activated carbons was found to increase with increasing the activation time, reaching the maximum value of 494 m<sup>2</sup> g<sup>-1</sup> after 3 hours of activation. Ash minerals could also have a significant influence on the pore formation during the activation process [35]. Thus, Ariyadejwanich et al. [34] carried out a study where tyre chars were demineralized with HCl before steam activation. The acid treatment was found to be highly effective for the removal of ash minerals that blocked the pore structure of the carbonised char, leading to the production of a highly mesoporous activated carbon with mesoporous volume and BET surface area up to 1.62 cm<sup>3</sup> g<sup>-1</sup> and 1119 m<sup>2</sup> g<sup>-1</sup>, respectively.

### 2.1.2.2 Chemical activation

Chemical activation has been shown to form carbons with high BET surface area and narrow micropores [41-42]. Preparation of activated carbon by chemical activation involves the impregnation of a raw or previously carbonised material with chemical activating agents at temperatures lower than 800 °C, under an inert atmosphere. The most widely used chemical activating agents are KOH, H<sub>3</sub>PO<sub>4</sub>, ZnCl<sub>2</sub>. However, the use of ZnCl<sub>2</sub> and H<sub>3</sub>PO<sub>4</sub> is less environmentally friendly due to environmental contamination and eutrophication issues associated with their use. In addition, alkali-metals-based compounds such as K<sub>2</sub>CO<sub>3</sub>, NaOH and Na<sub>2</sub>CO<sub>3</sub> have been effectively used as chemical agents for the production of chemically activated carbons. Among the alkali metal salts, KOH is the most effective activating agent in producing activated carbon with a well-developed porous texture and with an improvement in surface area [43]. Fierro et al. [44] concluded that chemical activation of lignin with KOH produced a microporous activated carbon with a BET surface area and micropore volume 1.5 and 1.2 times higher than the ones activated with NaOH. The same conclusion was reported by Hayashi et al. [45]. Generally, the mechanism of chemical activation depends on the type of precursor. For example, anthracites activated with NaOH had higher surface areas than those prepared with KOH [46]. This can be explained by the porous texture of the starting material; anthracite for example is already ultramicroporous, and with Na<sup>+</sup> being smaller than K<sup>+</sup>, it can penetrate more deeply into the carbon structure and generate smaller pores than K<sup>+</sup> [44]. The most widely used method of chemical activation consists of a preliminary carbonisation of the precursor, impregnation of the resultant char with an aqueous solution of the activating agent followed by drying and finally heat treatment of the resultant mixture at an inert atmosphere [47-49]. The second method involves the direct impregnation of the precursor in aqueous solution, followed by drying and heat treatment [45, 50]. A two-step chemical activation of rice straw, in which the raw material is first carbonised and subsequently activated with KOH, has been reported to lead to porous activated carbons with high BET surface area and high adsorption capacity [51]. Lin et al. [52] prepared activated carbon from waste tyres through a two-step chemical activation method. Waste tyres were carbonised first at 800 °C for 1 hour under nitrogen. Then, char was mixed with KOH at a KOH/carbon mass ratio of

4:1 and activated at 800 °C at different activation times ranging between 1 to 3 hours. The highest BET surface area of 758 m<sup>2</sup> g<sup>-1</sup> was obtained at an activation time of 2 hours.

Regarding the mechanism of the KOH activation of carbon, it is generally accepted by different researchers that the mechanism involves a series of chemical reactions and potassium intercalation into the lamella of the crystallites that form the carbon, thus widening the space between the carbon layers, which results in increasing the total surface area [52-53]. During the heat treatment under nitrogen, KOH reacts with disordered or amorphous carbon, which is oxidized to form potassium carbonate. Additionally, other decomposition product such as potassium is formed as follows [53-55]:



A number of researchers have investigated the influence of activation temperature and KOH-to sample ratio on the porous texture of the carbonaceous materials. For example, Evans et al. [56] showed that an activation temperature of 400 °C was ineffective to develop the porous texture and increase the surface area of a sucrose-derived char treated with KOH. According to the results of Yang et al. [57], 850 °C is an optimum activation temperature to obtain a mesoporous carbon from the mesophase pitch with high BET surface area using KOH as an activating agent. In another study, Guo and Luo [14] have activated palm shell with KOH at temperatures between 500 and 900 °C and observed an increase of BET surface area up to 800 °C. The decrease of BET surface area between 800 and 900 °C was attributed to the over burn-off of micropore walls which results in the formation of mesopores and macropores. In terms of correlation between porosity evolution and activation temperature, experimental tests conducted by Carvalho et al. [58] revealed that, during the preparation of activated carbons using chemically activated cork waste, mostly narrow micropores were created between 500 and 700 °C and at higher temperatures these were widened to from supermicropores.

Similar to the influence of activation temperature, increasing the amount of activating agent has also been found to have a strong influence on developing the BET surface area of activated carbon [41, 44]. In a study which set out to determine the optimum KOH/carbon weight ratio, Fierro et al. [44] reported a sharp increase in the BET surface area of KOH activated kraft lignin up to a KOH/carbon weight ratio of 2:1, and above this ratio the increase was not significant. In another study, commercial carbons were chemically activated with KOH at KOH-carbon ratios varied from 0.5 to 4 at 800 °C by Meng and Park [41]. The increase of chemical agent resulted in an increase in both BET surface area and total pore volumes. With a low KOH ratio of 1, micropores were favoured, while at a high ratio of 4, mesopores were found to form.

## **2.2 Waste derived materials applications**

### **2.2.1 Tar reduction**

Synthesis gas produced from waste or biomass gasification is considered as an alternative fuel to replace fossil fuels, however it also contains tar which can cause pipeline, injector and fuel line blockages, thereby restricting its end-use. Tar concentration in the syngas should be reduced to a level that complies with the specifications of end-use equipment such as engines or turbines. Depending on the operating parameters and the gasifier design, tar yields from biomass gasification are estimated to be between 0.5-100 g m<sup>-3</sup> [59]. The acceptable tar concentration in the syngas depends on the end application. For example, for fuel cells or methanol synthesis, less than 1 and 0.1 mg Nm<sup>-3</sup>, respectively is required, while for gas engines, the limit is less than 0.5 mg Nm<sup>-3</sup> [60-61].

#### **2.2.1.1 Tar definition and classification**

Tar is considered as one of the strongest barriers for the commercialization of gasification [61]. According to Milne [62], tar is defined as the organics produced under thermal treatment of any organic material and consists of a complex mixture of various compounds with a wide range of molecular weights [63], and some of the compounds, such as benzene and polyaromatic hydrocarbons (PAHs), are toxic and

could cause serious environmental hazards [59]. The typical composition of biomass tars is shown in Figure 2.2-1.

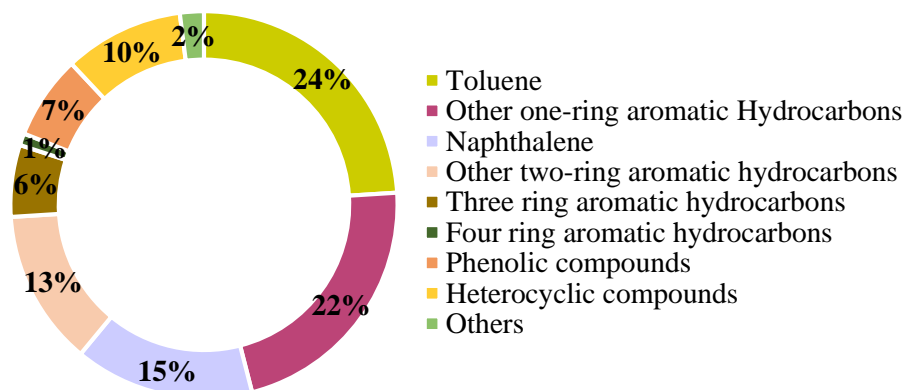


Figure 2.2-1. Biomass tar composition [64].

Different approaches are used to classify tar. According to Devi et al. [65] and Li and Suzuki [66], and based on the molecular weight, tar components are classified into five classes (Table 2.2-1). Class 2 includes tar compounds with heterocyclic compounds such as phenols. Class 3 refers to aromatics with 1-ring such as xylene; while light PAHs, with 2-3 rings, and heavy PAHs are grouped in class 4 and 5 respectively. This classification is based on the chemical, solubility, and condensability of tar compounds.

Table 2.2-1. Tar classification based on molecular weight of tar compounds [67].

| Tar class | Property   |
|-----------|--|
| Class 1   | GC undetectable heaviest tars which condense at high temperature   |
| Class 2   | Heterocyclic aromatic compounds such as phenol, pyridine and cresols   |
| Class 3   | Light hydrocarbon aromatic compounds (1 ring) such as toluene and xylenes  |
| Class 4   | Polyaromatic hydrocarbon compounds (2-3 rings) such as indene, naphthalenes, biphenyl, fluorene and phenanthrene |
| Class 5   | Heavy polyaromatic hydrocarbon compounds (4-7 rings) such as fluoranthene, pyrene and chrysene                   |

On the other hand, Milne et al. [62], classified tar species into four different groups depending on the reaction regimes as presented in Figure 2.2-2.

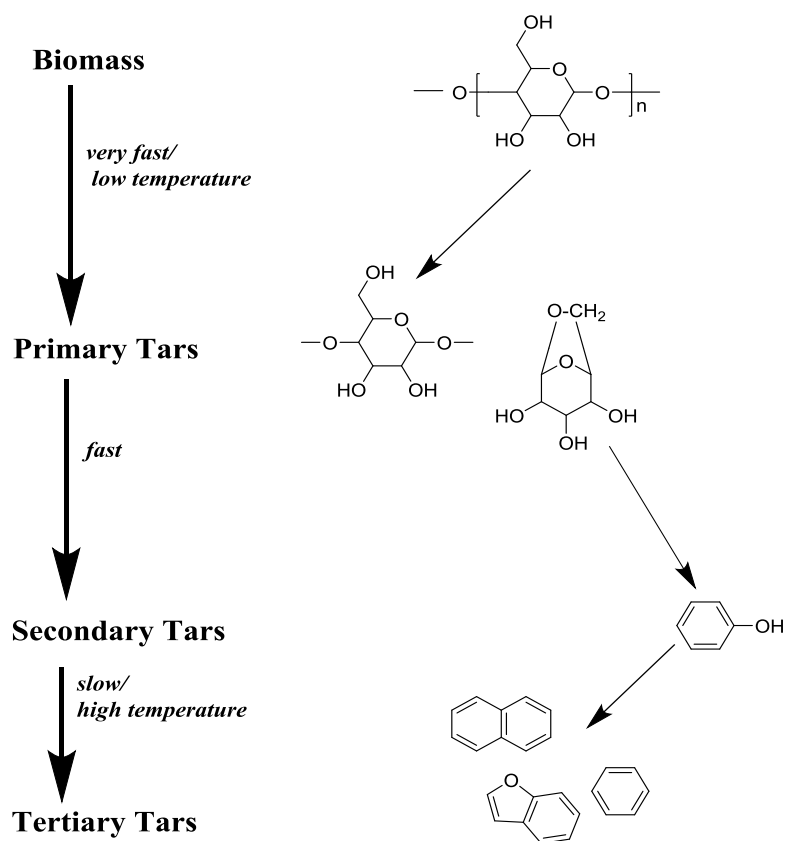


Figure 2.2-2. Tar classes as reported by Milne et al. [62].

### 2.2.1.2 Tar formation

The formation of tar chemical components depends highly on reaction temperature as shown in Figure 2.2-3, as temperature increases tar changes from mixed oxygenates at 400 °C to large PAH at 900 °C [68].

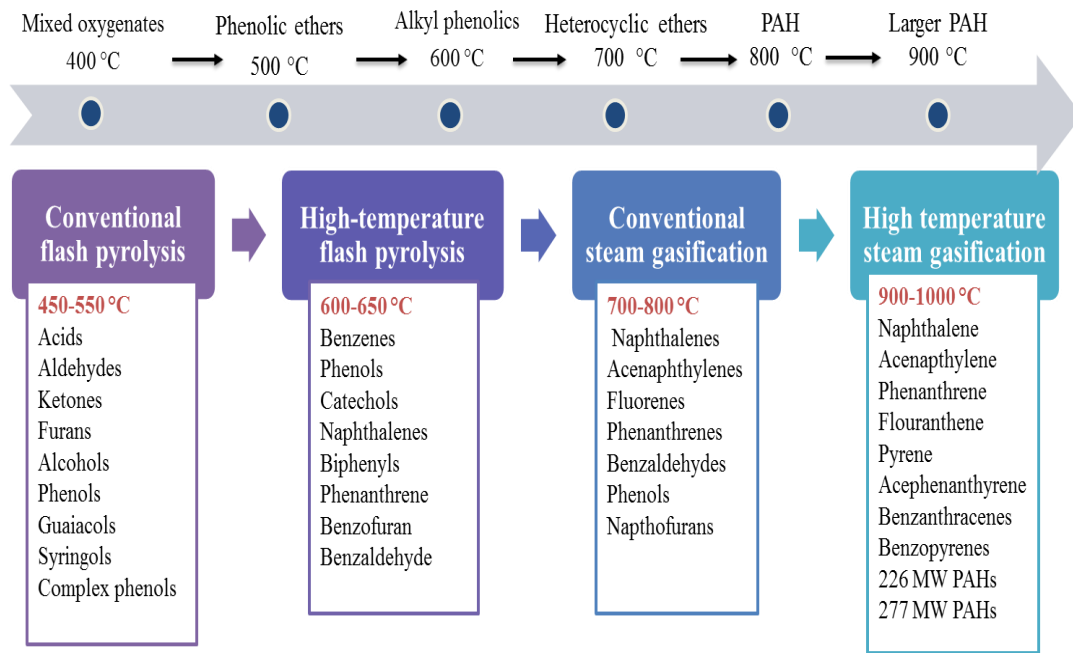


Figure 2.2-3. Chemical tar components formation with temperature [68].

Formation of PAH from biomass thermal decomposition can be explained by several pathways. Some researchers suggested that PAHs are formed through secondary reactions via a Diels-Alder mechanism [69-72]. Pyrolysis of alkanes at high temperatures is assumed to form alkenes via dehydrogenation, dienes via cyclization and then, through aromatization, aromatic compounds are produced [72]. Another route, for PAH formation, through deoxygenation of oxygenated aromatic compounds, at moderate to high temperatures, was also reported by other researchers [72-73].

The main components of biomass as shown in Figure 2.2-4 are cellulose, hemicellulose and lignin. During pyrolysis, biomass has been found to undergo the following four stages: at temperatures < 493 K moisture was evaporated; at temperatures of 493-588 K and 588-673 K decomposition of hemicellulose and cellulose respectively were observed; and lignin decomposition occurred mainly at temperatures > 673K [74]. Primary tar components formed from cellulose and hemicellulose are anhydrosugars, low molecular weight carbonyls, carboxylic acids and furans [75], while lignin forms mono aromatic such as phenols, guaiacols and its derivatives [74]. Secondary reactions of these primary tars produce catechols, cresols, xylenols, phenol, PAHs, coke and gases [74, 76].

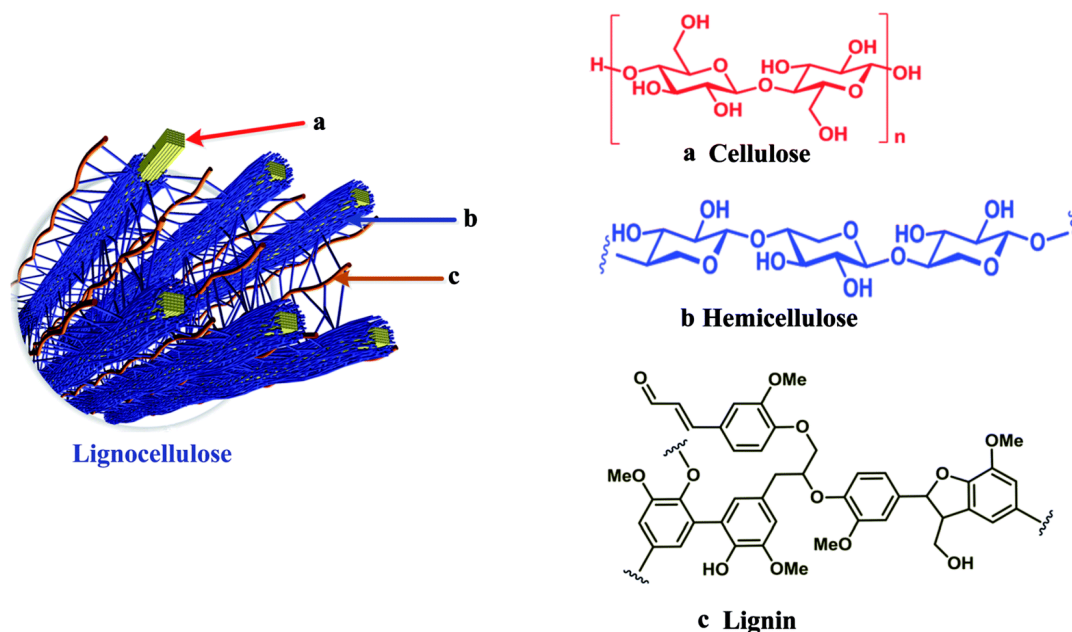


Figure 2.2-4. Biomass components (a) cellulose, (b) hemicellulose and (c) lignin [77].

Lignin, generally consists of 20 - 40 wt.% dry of biomass [74] and is the only part of biomass which is aromatic in nature; therefore it represents a potential precursor for tar generation. The pyrolysis of lignin units, vanillin ( $C_8H_8O_3$ ), guaiacol ( $C_7H_8O_2$ ), and catechol ( $C_6H_6O_2$ ) results in the formation of primary tars, and then by reaction with hydrogen it forms secondary tars [78]. Thermal decomposition of lignin is started by cleaving the weak  $\alpha$ -ether and  $\beta$ -ether bonds, forming guaiacyl and syringyl-type aromatics, which further react to form catechols and pyrogallols. Decomposition of these aromatics results in the formation of PAH [79-80] as presented in the reaction scheme shown in Figure 2.2-5 [80].

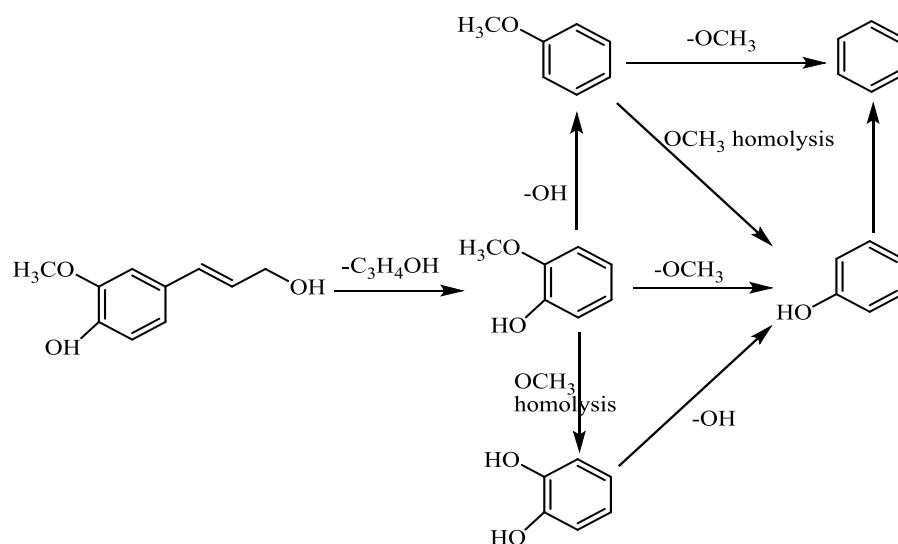


Figure 2.2-5. Lignin decomposition mechanism [80].

Tars can undergo a series of dehydrogenation, cyclization, and condensation reactions, forming larger polyaromatic hydrocarbons and soot. These large tar species can be generated from the aromatic structure either by a resonantly stabilized radical (RSR) mechanism or by hydrogen abstraction acetylene addition (HACA). However, the HACA mechanism is the most reported mechanism for PAH formation [81]. Single ring compounds such as benzene can be considered as PAH precursors, naphthalene can be formed from benzene via phenylacetylene [80].

### 2.2.1.3 Decomposition mechanism

Tar decomposition occurs mainly due to cracking, steam and dry reforming reactions [83]. The main reaction steps occur during tar cracking in both gasification atmosphere and in an inert atmosphere are: (1) radical-forming reactions, (2) propagation reactions, (3) hydrogen transfer, (4) isomerization reactions, and (5) termination reactions [84]. According to Van der Hoeven [85], at high reaction temperatures and long residence times, thermal conversion of tar includes both cracking and polymerization reactions as shown in Figure 2.2-6. Therefore, both cracking and polymerizations products are expected to be formed during the tar conversion process. The addition of hydrogen to the aromatics and subsequent breaking of the ring structures generally form cracking products. Methane, ethane, ethene and benzene were reported to be the most important cracking products formed during thermal tar treatment [85].

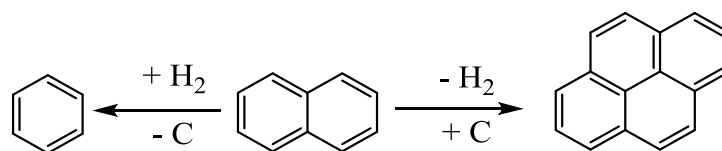


Figure 2.2-6. Cracking and polymerization products formed during tar conversion process [85].

Due to the complexity of the composition of real tar, tar model compounds have been used to study the decomposition mechanism. Benzene and naphthalene are considered as the two main tar components formed during biomass pyrolysis or gasification. Jess [86] studied the mechanism of thermal conversion of aromatic hydrocarbons in the presence of  $H_2$  and steam, using benzene, naphthalene and toluene as tar model compounds; the reaction scheme is shown in Figure 2.2-7, from which it can be seen that benzene is the key component in tar decomposition.

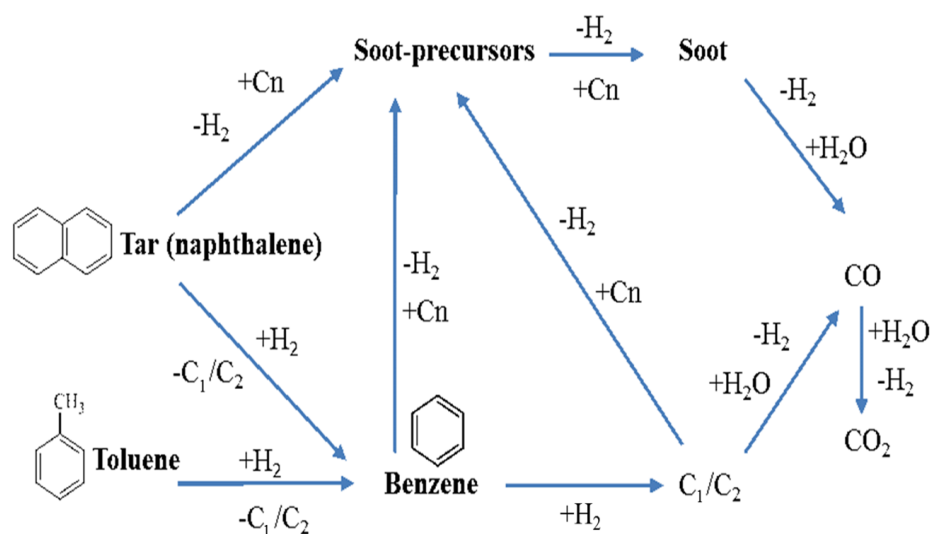


Figure 2.2-7. Simplified reaction scheme of tar conversion in the presence of hydrogen and steam [81].

In addition, hydration plays a significant role in the decomposition of both benzene and naphthalene tar species. For example, the ring breaks in benzene and through hydration reactions; methane, ethane and ethene are formed. While in the case of naphthalene, the reaction is started with a hydration, where naphthalene is converted to dihydronaphthalene, and with the further addition of hydrogen, benzene is produced

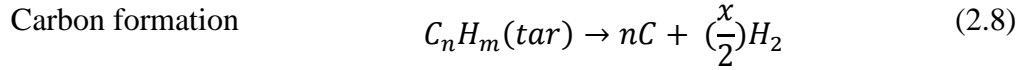
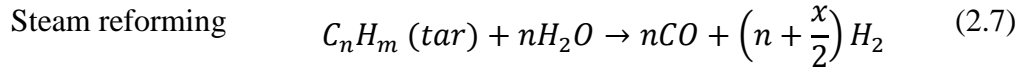
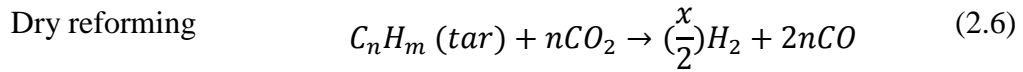
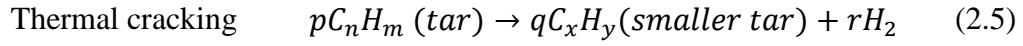


#### **2.2.1.4 Tar removal cracking methods**

Waste and biomass are recognized as a renewable source of energy [88]. Gasification, as a thermochemical process, enables the conversion of these materials into chemicals, syngas fuel, power and heat [89]. However, one of the issues associated with gasification is tar. Much research has been done in order to find a suitable and effective method for tar removal. Generally, tar removal technologies can be divided into two categories: treatments inside the gasifier (primary methods) and downstream from the gasifier where a separate reactor is used to reduce the tar content (secondary methods). Tar removal inside the gasifier is carried out by controlling the gasification operating conditions such as operating temperature, type of gasifying agent, equivalent ratio and type of in-bed catalysts [90]. In both primary and secondary methods, tar removal is achieved either by physical removal using a scrubber or ceramic filters, or chemical treatment which is mainly carried out by thermal and catalytic cracking. While physical methods are effective and easy to use, the tar content is often not fully destroyed. Thermal processes operate at a very high temperatures ( $>1000\text{ }^{\circ}\text{C}$ ), to crack the heavy tar compounds to less problematic species such as hydrogen, carbon monoxide and methane [91-92]. On the other hand, the catalytic tar removal process is an effective approach for gas cleaning, because lower reaction temperatures is required ( $600\text{-}800\text{ }^{\circ}\text{C}$ ) and tar removal efficiency can reach about 90-95% [60]. In addition, no tarry wastes are generated that require further treatment [92].

#### **2.2.1.5 Catalytic tar cracking**

According to Sutton et al. [93], the catalyst may be selected based on the following criteria: (1) effectiveness for tar removal, (2) ability to provide a suitable syngas ratio for the required purpose, (3) activity for reforming of heavy hydrocarbons, (4) resistance to deactivation, (5) should be stable and cheap, (6) easily regenerated. Tar decomposition occurs mainly due to a series of chemical reactions. The final product composition is a result of the following reactions [67]:



Various catalysts have been extensively investigated for tar reduction during the biomass gasification process, including non-metallic catalysts, such as minerals [65, 94-95], nickel based catalysts [96-98], zeolites [99], alkali metals [100] and others. Dolomite  $\text{CaO} \cdot \text{MgO} (\text{CO}_3)_2$  and olivine  $\text{FeMg} (\text{SiO}_4)_2$  are natural minerals that consist of magnesium and iron oxides which are responsible for the catalytic activity of these catalysts [64]. Dolomites are the most widely used non-metallic catalysts for tar removal [101] and they have been studied as a primary [102] and a secondary measure [103] for tar reduction in biomass gasification. Wei et al. [94] investigated biomass gasification for hydrogen production and concluded that dolomite exhibits a higher catalytic activity in terms of tar reduction and a significant increase in hydrogen production compared to that of limestone and olivine. In another study reported by Devi et al. [65], 63% and 43% tar conversions were observed over calcined dolomites and olivine respectively. Similarly, Gusta et al. [95] studied the catalytic decomposition of biomass tars over dolomites using a double bed micro-reactor in a two stage process and reported a good performance on tar conversion to gaseous species by an average of 21% over non-catalytic tests at a temperature of 750 °C. However, dolomites are physically softer and can be easily eroded [65]. On the other hand, olivine has been found to have a higher resistance to attrition and according to the results obtained by Devi et al. [65] and Rapagna et al. [104], olivine has been found to have a similar catalytic activity to dolomite. Although dolomites and olivine can decrease the tar content to a certain extent but the activity is still lower than that of the metallic catalysts, such as nickel oxides [105].

Significant work has been reported on the use of nickel catalysts for syngas cleaning during biomass gasification. The main advantages of Ni-based catalysts are their high

activity and selectivity to hydrogen [106]. To determine the influence of bed material on tar decomposition, Simell and Bredenberg [107] examined tar decomposition using various materials, such as Ni/Al<sub>2</sub>O<sub>3</sub>, dolomite, activated alumina, silica-alumina catalyst and silicon carbide and reported a complete tar decomposition was achieved with the nickel catalyst at a temperature and gas residence time of 900 °C and 0.3 s, respectively. Similarly, Zhang et al. [92] reported almost complete tar decomposition, using commercial nickel catalysts, accompanied with an increase in hydrogen concentration by 6-11 vol. %.

To improve the activity and stability of nickel catalysts, researchers have developed various catalyst supports, metal additives and preparation methods. The most widely used support materials are alumina [108-110], dolomite [108], silica [109], and magnesium oxide [111]. Srinakruang et al. [108], investigated the effectiveness of three catalyst supports, dolomite, Al<sub>2</sub>O<sub>3</sub> and silica-alumina mixed oxide (SiO<sub>2</sub>-Al<sub>2</sub>O<sub>3</sub>) on suppressing carbon deposition during tar reforming. Ni/ dolomite was prepared by a precipitation method while Ni/Al<sub>2</sub>O<sub>3</sub> and Ni/SiO-Al<sub>2</sub>O<sub>3</sub> were prepared by an impregnation method. The catalytic activity of the prepared catalysts in the steam reforming of toluene at a temperature of 700 °C and Ni loading of 15 wt.% was found to increase in the following order Ni/Al<sub>2</sub>O<sub>3</sub>> Ni/dolomite> Ni/SiO<sub>2</sub>-Al<sub>2</sub>O<sub>3</sub>. However, Ni on dolomite catalysts showed a high stability for toluene steam reforming, over 7 hours. Additionally, Ni-dolomites inhibited coke formation, while a significant amount of carbon of about 7.2 and 1.7 wt.% was detected on Ni/SiO-Al<sub>2</sub>O<sub>3</sub> and Ni-Al<sub>2</sub>O<sub>3</sub> respectively. Catalyst promoter metals such as cobalt [112], iron [112], copper [106], cerium [98, 113], platinum [114], and magnesium [115] have been also studied by researchers to improve the catalyst activity. Garcia et al. [116] have synthesised different Ni-based catalysts, supported on  $\alpha$ -Al<sub>2</sub>O<sub>3</sub>, for hydrogen production from the catalytic steam reforming of biomass. To improve the catalyst activity, magnesium and lanthanum were added as support modifiers to enhance the coke gasification rate, and cobalt and chromium were used as promoters to reduce the carbon deposition. In comparison to the other catalysts, the researchers concluded that chromium and cobalt promoted nickel supported on MgO-La<sub>2</sub>O- $\alpha$ -Al<sub>2</sub>O<sub>3</sub> performed the best in terms of stability and high hydrogen production

The main problems associated with the use of such catalysts are the high cost, difficulty of regeneration and the deactivation from sulphur coke deposition on the catalyst. Additionally, most of these catalysts are not environmentally sustainable. These disadvantages would inhibit the wide applications of such potentially commercial catalysts [78, 105]. As an alternative, waste materials have great potential as a raw carbon material for production of chars and activated carbons with catalytic properties [117]. Several studies have examined the use of carbonaceous char at high temperatures (500-800 °C) to act as a catalyst for tar decomposition [101, 118-121]. The use of char for tar decomposition is more advantageous than commercial catalysts due to many factors such as, char is a by-product of feedstock pyrolysis and gasification which is more economical. In addition, char does not need regeneration, because it can be either gasified or combusted if deactivated due to coking and moreover, char may be free from poisoning by sulfur or chlorine species [122].

#### **2.2.1.5.1 Char for catalytic tar conversion**

Pyrolysis and gasification processes have the potential to yield useful products such as char. Char is produced alongside tar during the pyrolysis process, therefore it is very attractive to use char as a cheap catalyst for tar cracking. Additionally, the spent char can be used as a solid fuel, therefore char deactivation is not a serious issue compared to other commercial catalysts [123]. Depending on the feedstock material, char contains minerals and abundant surface functional groups that make char a promising alternative to metal catalysts. Carbonaceous materials, including char and activated carbon, have been found to have some catalytic properties for removal of environmental pollutants [124-127] and for tar reforming [101, 118, 120-121]. Char can be used in various ways such as; an adsorbent, a catalyst support loaded with metals and it could also be gasified into gas species. The high efficiency of char and char supported catalysts is suggested to be due to its surface functional groups, porous texture and surface area [67]. Moliner et al. [128] investigated the influence of carbon textural properties and surface chemistry on methane decomposition. It was suggested that the surface oxygenated groups control the initial conversion rate and the long-term catalytic activity depends mainly on the char surface area and the pore size distribution. Mesoporous carbon with high BET surface area was found to be more

active in providing a stable and sustainable hydrogen production. In another study conducted by Jin [129], the difference in the BET surface area of the studied carbon samples was one of the reasons for the different performance of carbon catalysts during the catalytic upgrading of coal oil. Activated carbon with a BET surface area of  $803 \text{ m}^2 \text{ g}^{-1}$  had a higher efficiency than char with a BET surface area of  $2 \text{ m}^2 \text{ g}^{-1}$ . Additionally, Kreckkaiwan et al. [130], observed a higher catalytic activity of the blended coal and wood biomass char in the tar decomposition compared with either coal or biomass chars, in terms of higher  $\text{H}_2$  and higher carbon conversion into gas which was also attributed to its high BET surface area.

The most commonly used process conditions for catalytic tar reduction involve temperatures between 800 and 900 °C in an atmosphere of steam and  $\text{CO}_2$  [101]. In a study carried out by Zhao et al. [131], a two-stage pyrolysis-gasification reactor was used to investigate a range of process conditions for tar removal from the pyrolysis of rice straw using biomass char produced from the same raw material. They investigated the influence of different reforming agents,  $\text{CO}_2$ ,  $\text{H}_2\text{O}$  or  $\text{O}_2$  introduced into the second stage reactor and different char temperatures of 700-1000 °C. In comparison to the other reforming agents, the presence of steam was found to be the most effective for tar removal. They concluded that a higher temperature of char bed eliminated most of the tar. Zhao et al. [131], reported that in the absence of reforming agent, where catalytic cracking of tar over the char bed occurred, significant removal of tar was observed; for example 85% tar conversion at 700 °C and increased to 95% at 900 °C.

To further understand the role that char plays in tar reduction, it is of interest to investigate the reactions of biomass pyrolysis gases over a bed of pyrolysis char at high temperatures. A high temperature of biomass char bed for the cracking of biomass pyrolysis gases in a separate hot char reactor, at temperatures between 500 and 700 °C, was examined by Sun et al. [118]. Similarly Gilbert et al. [120] used a two-stage reactor system to investigate the cracking of biomass produced pyrolysis gas over a hot bed of wood char, with particles size of 10-15 mm, at temperatures between 500 and 800 °C. They reported a tar removal of 67%. In another study conducted by Dabai et al. [132], a tar removal of 97% was reported using spruce char at 800 °C. However, the amount of char in these studies were different, a char ratio of 5.4-7.4 was used in

Dabai et al. [132] study, whereas a ratio of only 0.6-1.8 was used by Gilbert et al. [120].

During the pyrolysis of biomass, steam is expected to be formed, through autogeneration, from the release of moisture and as a reaction product from pyrolysis of the biomass. Pyrolysis will also produce significant concentrations of CO<sub>2</sub>. Therefore, although pyrolysis and char cracking may take place in an inert atmosphere of nitrogen or argon [118, 120], the pyrolysis of biomass will produce a partial oxidation atmosphere through the formation of steam and CO<sub>2</sub> as reaction products which can further react with the char to produce CO, CO<sub>2</sub>, H<sub>2</sub>.

Guoxin and Hao [133] showed that biomass moisture content can autogenerate a steam atmosphere which can react with biomass pyrolysis gases to enhance reaction between the evolved intermediate products of pyrolysis due to the reforming of tar, methane and higher hydrocarbons, via reforming reactions and the water gas shift reaction. They found that the fastest reaction was observed with fast heating rates where the evolved autogenerated steam could react with the pyrolysis gases due to the fast drying and pyrolysis gases occurring over shorter residence times compared to slow heating rates. A direct correlation was observed with the high moisture content of the biomass and the higher hydrogen production. The presence of a downstream hot char bed at temperatures between 700 and 900 °C would provide a further zone for thermal and catalytic degradation of tar and higher hydrocarbons, together with autogenerated steam char gasification reactions and also steam reforming reactions of the pyrolysis tar and hydrocarbons.

However, in none of the reported studies was the decomposition of real biomass tar investigated in any detail and tar decomposition was not correlated to different char samples with different structures. Hosokai et al. [122] concluded that further research needs to be carried out to better understand the reaction mechanism taking place on the char surface during tar decomposition. It is hence worthwhile to investigate tar decomposition using different char structures.

### 2.2.1.5.2 Syngas production from biomass steam reforming

Pyrolysis vapor products can also undergo steam reforming for syngas and H<sub>2</sub> production [134]. Hydrogen is considered as an important fuel of the future, which can reduce the reliance on oil. Hydrogen can be generated via various chemical processes including ion exchange membranes, biomass gasification, ethanol and methanol steam reforming. However, fossil fuel reforming, mainly natural gas, is known to contribute to about 90% of the current total hydrogen production [135-136]. Therefore, there has been a growing effort to find alternative processes for hydrogen production. Gasification is one of the effective thermochemical conversion processes of biomass energy that lead to the formation of a hydrogen rich gas which can be used for fuel cell systems and synthesis reactions including Fischer-Tropsch and methanol reactions [67]. For these applications, there are certain requirements for the syngas composition, mostly in terms of H<sub>2</sub>/CO ratio [137]. Generally, a syngas with H<sub>2</sub>/CO ratio of 1-2 is needed to be fed to the downstream catalytic processes [138]. Therefore, it is extremely important to predict the overall gasification efficiency, in terms of chemical composition of the syngas, using char materials. There is a need to understand the catalytic activity of char for tar cracking and its consumption during the reforming process [139].

Various gasifying agents are used during the gasification process depending on the desired gas composition [140]. Steam is well-known to increase the heating value of syngas and produce a gas with a higher content of hydrogen [141]. With the use of steam as a gasifying agent during the biomass gasification process, hydrogen-rich syngas is expected to be formed. It has been reported that up to 60-70 vol.% of H<sub>2</sub> was generated using a fixed bed [142] and a pilot-scale fluidized bed [143]. Biomass is decomposed in the first stage to form gases, char and volatiles followed by a reforming stage where volatiles are reformed with the presence of steam and catalyst to syngas. The presence of steam during the char-volatiles reaction enhances the reforming of large and small ring aromatics. The C-C and C-O bonds on the char surface are expected to break during the reaction of steam with char, which may lead to the formation of radicals that would act as a catalyst for tar reforming. This reaction is also expected to form additional oxygen containing groups that increase the char

catalytic activity for tar cracking [144]. In addition, steam-char reactions enhanced the formation of additional oxygen containing groups. Which may also act as active sites to catalyse the tar cracking reactions during volatiles-char interactions as has been reported by Song et al. [144].

Choi et al. [145] investigated the gasification of a sewage sludge with the use of activated carbon as a catalyst and reported that the introduction of steam at 800 °C enhanced the steam reforming reactions and produced a free tar syngas with a high content of hydrogen (35-45 vol.%). The authors concluded that with this process the total condensed liquid decreased from 20 to 14.4 wt.% and the product syngas increased from 52.5 to 64.9 wt.%. In contrast, Striugos et al. [146] claimed that the conversion of tar during the steam reforming of biomass was only 1% higher than that with no steam. Biomass has a high percent of moisture, therefore the auto-generated steam during the catalytic cracking could also act as a gasifying agent and enhance the cracking of tar compounds. Regarding char gasification during the process of simultaneous reforming/gasification of pyrolysis oil and char, the volatiles formed during the pyrolysis process could be a strong inhibitor for char gasification [147-148]. The carbon deposits or coke could be formed during the interaction of volatiles with the char surface. However, the presence of minerals could facilitate or enhance the char gasification as was observed by Bayarsaikhan et al. [147]. They reported that the carbon conversion of the acid-treated char was found to be negative which suggests that the coke deposits on the char surface without being gasified or the tar deposition rate is faster than the steam gasification rate.

### **2.2.1.5.3 Tar model compounds**

Because of the complexity of real tar streams, most studies use tar model compounds, to study the reaction mechanism. Coll et al. [149] investigated the steam reforming of five tar model compounds with commercial nickel catalysts and found the following order of reactivity: benzene > toluene > anthracene > pyrene > naphthalene. In another study conducted by Burhenne and Aicher [150], the decomposition of benzene as a tar model compound on different wood char samples and commercial activated carbon using a fixed bed reactor was investigated at high temperatures (850-1050 °C). The

non-activated chars were found to exhibit a low activity, as the benzene conversion was almost similar to the experiments performed in an empty reactor. In contrast, char activated with CO<sub>2</sub> exhibited a high benzene removal of about 100% at the start of the experiment, however after 10-minute reaction time it dropped to 25% due to the deactivation of the char caused by coking. In contrast, the commercial activated carbon was found to have a higher benzene removal and the conversion of 50% was stable during 2-hour experimental time, which was attributed to the higher amount of mesopores. Similar results were observed by Moliner et al. [128], who concluded that mesoporous carbon provided a more stable decomposition of methane compared to the microporous carbon which was found to deactivate rapidly. In contrast, Park et al [151] reported a similar tar cracking behaviour for the investigated char samples despite the difference in the porous texture and mineral contents. The nature of the tar model compound has also been found to influence the char activity for tar decomposition [152]. Naphthalene is one of the most refractory compounds among the aromatic compounds [122] and represents the major fraction of two-ring aromatic compounds found in gasification tars [149], therefore, it is commonly used as a model tar compound [86]. In an investigation into the thermal decomposition of different tar model compounds, Jess [86] studied the thermal conversion of toluene, naphthalene and benzene in the presence of hydrogen and steam in a tubular flow reactor at temperatures of 700-1400 °C and residence times of 0.3-2 s. The reaction activity was found to follow the order of toluene > naphthalene > benzene. Jess [86] pointed out that steam had little effect on the decomposition of aromatics. He reported also that soot and methane could not be completely converted to hydrogen and CO, even at a high reaction temperature. In another study conducted by Fuentes-Cano et al. [152], catalytic conversion of both toluene and naphthalene over chars made of coal, coconut and sewage sludge, was examined in a fixed bed reactor with the presence of 15 vol.% steam. In spite of the difference in porous texture of the studied char materials, the tar conversion was found to be similar for the three types of chars. The initial conversion of naphthalene and toluene has been reported to be around 60 and 80% respectively, however, as the reaction proceeds a constant deactivation of char was observed and after a 60-minute reaction time the conversion for both tar model compounds decreased to about 40%.

### 2.2.1.6 Mechanism of tar cracking over char surface

Tar model compounds have been used to understand the tar cracking mechanism using carbonaceous materials [78]. The tar conversion mechanism over carbon is similar to that occurring with porous materials and involves various steps such as deposition, dehydrogenation and gasification of the carbon deposits if H<sub>2</sub>O or CO<sub>2</sub> are present [122, 153]. Hosokai et al. [122] investigated the decomposition of benzene, phenol, naphthalene, phenanthrene and pyrene over charcoal at temperatures in the range of 700-900 °C in the presence and absence of steam and concluded that the main mechanism of decomposition was coking rather than direct steam reforming and the micropores were the active sites for coking. It was also reported that the presence of steam enhanced the activity of charcoal by gasifying the coke and creating more micropores. The cracking activity of char may be associated with its porous texture which provides the active surfaces required for tar cracking, resulting in a longer residence time [105, 122, 154]. The presence of macropores and mesopores plays a crucial role in transporting the reactant compounds into the internal surface of the carbon as presented in Figure 2.2-10 [155]. Zeng et al. [154] concluded that char with higher BET surface area performed the best in terms of production of lower tar content in the product syngas.

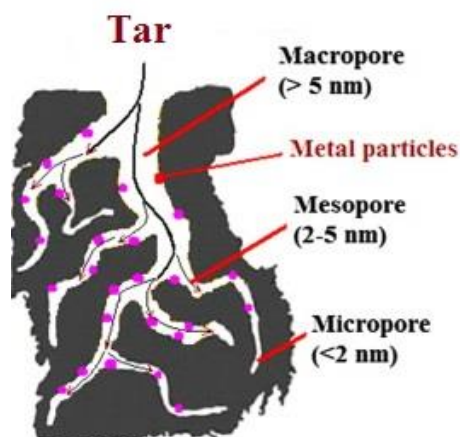


Figure 2.2-10. The role of carbon porous texture in tar cracking [64].

Tar removal mechanism was proposed to be based on coke formation [145, 152, 156], where tar adsorbed on the carbon surface and becomes dehydrogenated into coke. The

formed coke could then be gasified through reactions with gases and steam. As presented in Figure 2.2-11, tar is adsorbed on the char surface and undergoes polymerization reactions which results in the formation of  $H_2$  and soot, the formed soot could then block active sites present on the char surface and limit the interaction of gaseous tar compounds with the char surface [59, 152]. Therefore, the carbon gasification rate should be higher than the deposition rate, to avoid the soot accumulation over the char surface. The deactivation of carbon materials after tar decomposition due to coking has been reported by various researchers [145]. The deactivation is mainly due to the pore blockage by tar and coke. However, with the presence of steam, the deactivation has no major influence on the quality of syngas and, moreover at a longer reaction time the carbon deactivation was not significant as the deposited tar and coke, on the char surface, reacted continuously with steam [157]. Hosokai et al. [122] investigated decomposition of naphthalene and benzene over charcoal at a temperature of 900 °C and with a bed height of 30 mm in the absence of steam. They concluded that the aromatic compounds were decomposed over charcoal mainly by coking, as most of the carbon-containing gases were found to form due to the thermal cracking of charcoal itself instead of by direct cracking of aromatics. However, with the presence of steam, the activity of charcoal was maintained and the conversion of naphthalene and benzene increased to 84 and 99% respectively.

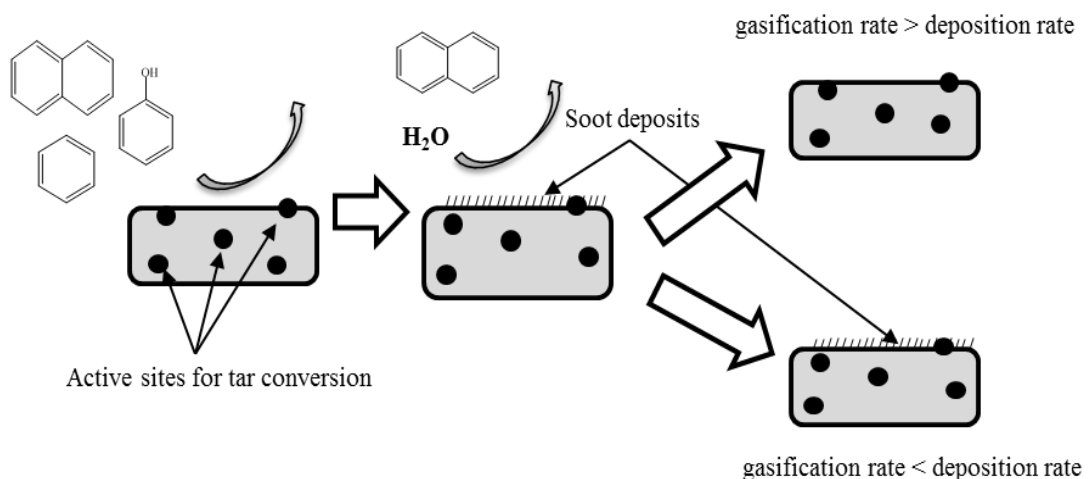


Figure 2.2-11. Mechanism of tar conversion over char [152].

Choi et al. [145], reported that the decrease in tar content in syngas during the gasification of sewage sludge, was accompanied with a significant increase in H<sub>2</sub> production. In comparison to the experiments without activated carbon, hydrogen production was found to increase from 28.1 to 45.4 vol.% with the use of activated carbon. The authors attributed the formation of hydrogen, with the use of activated carbon, to the process of thermal and catalytic cracking of adsorbed tar and coke over the carbon surface as presented in Figure 2.2-12.

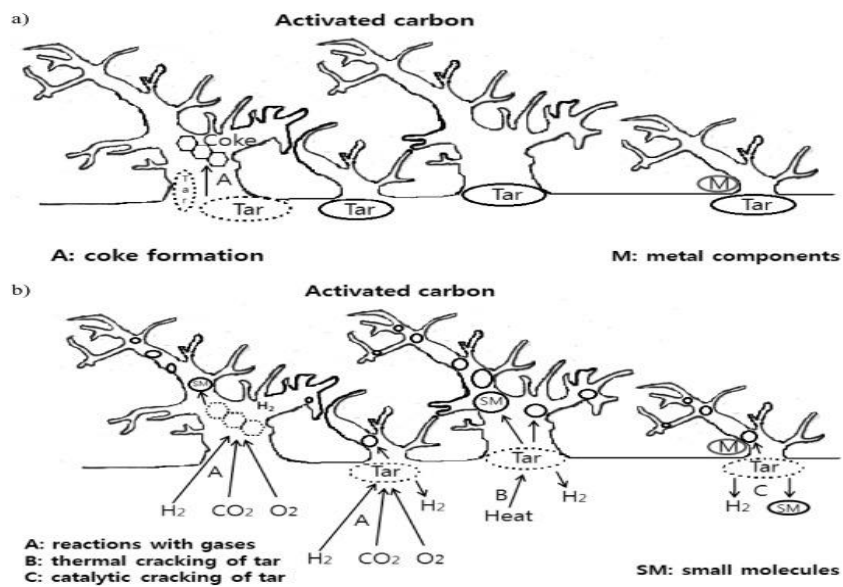


Figure 2.2-12. Tar cracking mechanism over activated carbon via reactions with gas components [145].

Another tar removal mechanism with carbon materials is based on tar cracking reactions, where the adsorbed tar components on the carbon surface undergoes various reactions resulting in cracking the tar and producing H<sub>2</sub> and small molecules according to steam reforming, dry reforming and thermal cracking [156].

The process of tar cracking is accompanied with an increase in total gas yield. Generally, more H<sub>2</sub> is produced due to the polymerization, cyclization and aromatization of tar components [158] and the oxygen in the tar is transferred into pyrolysis gas in the form of CO and CO<sub>2</sub> [158]. For example, Han et al. [158] observed a 30 % increase in total gas yield when char was used for the catalytic cracking of coal pyrolysis tar. The increase was observed mainly in H<sub>2</sub>, CH<sub>4</sub> and CO gaseous species,

while little change was observed with the production yields of CO<sub>2</sub> and C<sub>2</sub>-C<sub>3</sub> hydrocarbons.

## **2.2.2 NO<sub>x</sub> adsorption**

### **2.2.2.1 The NO<sub>x</sub> problem**

Atmospheric pollution is one of the greatest environmental problems that the world is facing today. The combustion of solid fuels is well-known to discharge various types of pollutants that cause several environmental impacts. One of these toxic pollutants is nitrogen oxides (NO<sub>x</sub>) which cause environmental problems such as acid rain and global warming [159]. Several types of nitrogen oxides with various chemical and physical properties are known to exist. However, NO<sub>x</sub> emissions in flue gas consist of a mixture which contains about 95% NO and 5% NO<sub>2</sub> [160]. Three different reaction paths are responsible for NO<sub>x</sub> formation: Fuel NO<sub>x</sub> is formed mainly from the oxidation of elemental nitrogen contained in waste fuels, thermal NO<sub>x</sub> is formed due to the reaction between nitrogen and oxygen present in the combustion air which is initiated at a high flame temperature of around 1100 °C and prompt NO<sub>x</sub> that forms as a result of reaction of hydrocarbon radicals and molecular nitrogen and oxygen [161].

### **2.2.2.2 Environmental Impacts**

NO<sub>x</sub> gases are known to cause various environmental issues such as acid rain, photochemical smog and ozone depletion [162]. NO can be easily oxidized to NO<sub>2</sub> which is considered as a highly toxic gas due to its ability to cause pulmonary edema and other severe effects [161]. In addition, NO is responsible for ozone formation in the troposphere layer of the atmosphere. In the presence of sunlight, NO reacts with oxygen to form NO<sub>2</sub> and ozone [161]. Also, NO<sub>x</sub> has been found to cause a wide variety of human health impacts such as respiratory diseases, damage to lung tissue, pneumonia, and premature death [163].

### **2.2.2.3 Abatement of NO<sub>x</sub>**

Various factors could influence the concentration of formed NO<sub>x</sub> such as flow velocity in the combustion space, temperature of combustion, burner design and fuel composition [164]. Due to the diversity of NO<sub>x</sub> containing exhaust gases, formed from various NO<sub>x</sub> sources, different control technologies have been established. However, NO<sub>x</sub> removal technologies can be classified into primary methods, which prevent the production of NO<sub>x</sub> by employing various techniques for combustion modification; and secondary methods that reduce the concentration of formed NO<sub>x</sub> in the resultant flue gas, such as selective catalytic or non-catalytic reduction and adsorption methods.

Several technologies have been developed to control NO<sub>x</sub> emissions [159, 165]. Ammonia (or urea) addition to the flue gases (selective non-catalytic reduction, SNCR) can reduce NO<sub>x</sub> by reaction to produce nitrogen and water, but is effective only over a narrow temperature range (~850 to 950 °C). Selective catalytic reduction (SCR) uses a catalyst in the presence of added ammonia which reproduces the ammonia reduction reaction but at a lower temperature (~250 to 400 °C). The effectiveness of SCR for NO<sub>x</sub> reduction can reach 85% and is a widely used technology [166]. However, the use of SCR has some drawbacks such as the difficulty of chemicals handling and storage, and ‘slippage’ of ammonia, because of less than 100% reaction [159, 165]. Additionally, SCR is a costly method and the catalyst is prone to deactivation when SO<sub>2</sub> is present in the flue gases. Therefore, there is interest in the development of low cost and efficient techniques to control NO<sub>x</sub> to meet the stringent emission limits in current environmental regulations.

#### **2.2.2.3.1 NO removal by activated carbon**

Activated carbons have been widely investigated as adsorbents for control of gases and vapours [167-168]. Removal of pollutants by adsorption is an effective method for the control of a range of pollutants. Although different adsorbents have been investigated including metal oxides, alumina, FeOOH and silica [169-172], activated carbon remains one of the main materials that can be used in numerous applications. Activated carbons have been used as adsorbents for many pollutants such as heavy

metals, SO<sub>2</sub> and NO<sub>x</sub>. The efficiency of activated carbon for pollutants adsorption is controlled by the degree of pore structure development and the chemical arrangement and the type and number of heteroatoms on the carbons' surfaces [105, 173].

Activated carbon is used as an adsorbent for many pollutants such as heavy metals (particularly mercury), SO<sub>2</sub> and NO<sub>x</sub>. The following properties make activated carbon suitable for adsorption applications: surface structure can be easily modified; they can be used in both acidic and basic conditions; their pore structure can be changed to be used for different purposes [12-13]. A fixed bed is the most effective arrangement for conducting experimental adsorption operations [174].

There have been several reports on the use of activated carbons to control NO<sub>x</sub>. The kinetics of NO<sub>x</sub> removal by carbon of commercial origin has been studied by many researchers [175-180] and it has been concluded that the origin of the precursor, the natural impurities in the feedstock, surface chemistry and the conditions used to prepare the activated carbon are the main factors which can control its efficiency for NO<sub>x</sub> reduction [181]. Although there has been much research into NO<sub>x</sub> control using activated carbons, the factors controlling the NO<sub>x</sub> adsorption process are still not clear.

Of particular interest for NO<sub>x</sub> control are low temperature processes where the NO<sub>x</sub> can be adsorbed after the gas scrubbing unit where very low levels of sulphur dioxide are found. Current NO<sub>x</sub> removal systems using selective catalytic reduction require temperatures typically between 200 and 400 °C, which may require some re-heating of the flue gases, resulting in an energy penalty for the process. Carbon-based adsorbents have been investigated to remove NO<sub>x</sub> at lower temperatures, for example between 25 °C and 200 °C [182]. Such temperatures occur after an acid gas scrubber unit to remove SO<sub>2</sub> and HCl which are known to interfere with the selective catalytic reduction NO<sub>x</sub> removal process [177]. Adsorption efficiency of activated carbon depends on various variables, including porous texture, temperature, NO concentration and surface chemistry of adsorbents.

### 2.2.2.3.2 The role of porous texture on NO removal

The narrow micropores found in activated carbons are very important for gas adsorption [183]. Zhang et al. [175] investigated the NO adsorption at a temperature of 25 °C using commercially activated carbons and concluded that NO conversion reached a maximum on an activated carbon with a micropore size of 7 Å [175]. Similarly, Gomez et al. [184] studied the influence of porous texture on NO conversion using several activated carbons made from coal, olive stones, almond shells and phenol-formaldehyde polymer resin and reported that no correlation was found between the NO reduction activity and carbon structure. In addition, all the available surface areas were effective for NO reduction and the accessibility problems due to the diffusion limitations were not important under the studied conditions. The results shown by Gomez et al. [184] were largely consistent with a number of other contributions found in the literature [185-187].

In another study carried out by Neathery et al. [182], NO<sub>x</sub> removal by activated carbon from gas containing CO<sub>2</sub>, H<sub>2</sub>O, N<sub>2</sub>, O<sub>2</sub>, SO<sub>2</sub> and NO<sub>x</sub> was investigated at adsorption temperatures between 20-140 °C. The authors reported that activated carbon can successfully adsorb NO<sub>x</sub> within a temperature of 35-120 °C. Their work, in which commercial activated carbon prepared from various precursors were used, showed that the NO adsorption efficiency of the examined activated carbon did not depend on their BET surface area and micropore volume. This was suggested from the results which showed that the activated carbon with an intermediate surface area and lowest total pore volume exhibited the highest NO adsorption capacity. In contrast, Rubio et al. [188] reported that the surface area and the carbon content were the main factors which influenced the removal efficiency of the activated carbon obtained from carbon enriched coal fly ashes. Kaneko et al. [189] also claimed that the adsorbability of activated carbon fibres in relation to NO, NH<sub>3</sub> and SO<sub>2</sub> at low temperature increased with specific surface area. Mochida et al. [179] reported that the main factor determining NO reduction activity of pitch-based active fibres, at room temperature, was the nitrogen content of the studied carbons. However, Gomez et al. [190] found no correlation between these two factors.

### 2.2.2.3.3 Effects of oxygen on adsorption

It has been reported by many studies that oxygen is important for NO adsorption [175, 181, 189, 191]. The presence of oxygen is believed to increase the adsorption of nitric oxide through the catalytic oxidation of NO to NO<sub>2</sub>, which results in an increase of the NO adsorption because of the higher adsorption potential of NO<sub>2</sub> [177, 192]. Some researchers reported that in the absence of oxygen, the removal capacity of NO by activated carbon was low [193-194].

According to Kong and Cha [191], the oxygen is first adsorbed on the char (Eq 2.9) and then reacts with NO to produce NO<sub>2</sub> (Eq 2.10).



Suzuki et al. [195] and Mochida et al. [196] noticed that during the adsorption, the created NO<sub>2</sub> is firstly adsorbed on the activated carbon and then during the desorption step it reacts to form NO according to the following equations;



Richter et al. [197] proposed that the presence of oxygen was effective in forming a carbon with an oxidized surface that acts as active sites for NO capture. On the contrary, the results obtained by Zhu et al. [198] disagreed with this observation. The pre-adsorption of O<sub>2</sub> on the activated carbon surface had a finite enhancing effect on the NO adsorption. A study carried out on pitch based active fibres by Mochida et al. [179] showed that oxygen at a level of 4% does not form any oxygen functional groups at ambient temperature.

According to Suzuki et al. [195], the enhancement rate of NO removal in the presence of O<sub>2</sub> is due to an increase in the amounts of carbon–oxygen complexes (Eq. 2.13)

which with decomposition produce free active carbon sites (Eq 2.14). Nitrogen containing species may form as in Eq. 2.15 and 2.1.6. N<sub>2</sub> gas is formed with the decomposition of these compounds according to Eq. 2.17 or 2.18. More carbon-oxygen complexes may form with an increase in the modification time [192].



Zhang et al. [175] investigated the influence of oxygen on NO adsorption using commercial activated carbon at a temperature of 25 °C and NO concentration of 500 ppm. It was found that NO removal efficiency was highly dependent on the presence of O<sub>2</sub> and increased with increasing O<sub>2</sub> concentration. The NO conversion increased from 3 % at an oxygen concentration of 0 % oxygen to about 50% with 10% oxygen. Chen et al. [199] reported that the adsorption capacity of NO reached a maximum (about 6.2 mg g<sup>-1</sup>) when the O<sub>2</sub> concentration was about 4% and declined when the O<sub>2</sub> content was higher than 8%. However, Guo et al. [185] claimed no relation between NO adsorption and oxygen and reported a 83 % NO conversion of active coconut carbon in the absence of oxygen. Kong and Cha [191] also concluded that NO<sub>x</sub> removal was independent of the presence of oxygen when the concentration was greater than 5%.

#### **2.2.2.4 Activated carbon modification methods of enhancement of gas adsorption**

Depending on the gas pollutant, the adsorption efficiency of activated carbon depends on various factors including pore size, surface functional groups, pore volume and BET surface area. The physical structure of activated carbon is determined mainly by the type of raw material, degree of activation and composition of activated carbon

[200]. Surface modified activated carbons were developed by researchers with the aim of enhancing NO adsorption. Impregnating chemicals, with high selective adsorptivities into carbonaceous materials, has been found to enhance NO<sub>x</sub> adsorption. Impregnation of the carbon materials with alkali metals has been found to enhance the NO removal, in particular, impregnating the activated carbon with KOH has been shown to enhance the carbon NO<sub>x</sub> adsorption capacity [201-203]. Lee et al. [201] examined the influence of impregnating coconut shell activated carbon with a KOH solution on NO<sub>2</sub> removal at a temperature of 130 °C [201]. The impregnation of coconut activated carbon with a KOH solution enhanced the NO<sub>x</sub> adsorption to be 4 times higher than that of the original activated carbon. Surface analysis of both carbons, using time of flight secondary ion mass spectrometry (ToF-SIMS), for the adsorbed species after adsorption showed the presence of NO<sub>3</sub><sup>-</sup> and NO<sub>2</sub><sup>-</sup> bonded on the surface of impregnated activated carbon with K<sup>+</sup> and produced crystals of KNO<sub>3</sub> and KNO<sub>2</sub>. The authors concluded that KOH contributes to the formation of adsorption sites for NO<sub>x</sub> adsorption, resulting in the production of oxide crystals of KNO<sub>x</sub> (x=2 or 3) due to the reaction with NO.

#### **2.2.2.5 NO reaction mechanism with activated carbon**

As proposed by Zhu et al. [198], NO adsorption on activated carbon, prepared from a commercial coal-derived semi coke, in the presence of oxygen is assumed to follow the pathway shown in Figure 2.2-13. According to this, there are two adsorption sites on activated carbon surface, adsorption site A is to adsorb both NO and NO<sub>2</sub> and adsorption site B is available only for NO<sub>2</sub>. Two pathways are responsible for NO<sub>2</sub> formation: (1) direct adsorption at the oxidized sites on activated carbon surface, and (2) through oxidation of the adsorbed NO species. The oxidized NO species, formed at site A, then move to site B and are stored there, probably as nitrate and nitrite species, resulting in the vacancy of site A for the continued adsorption process.

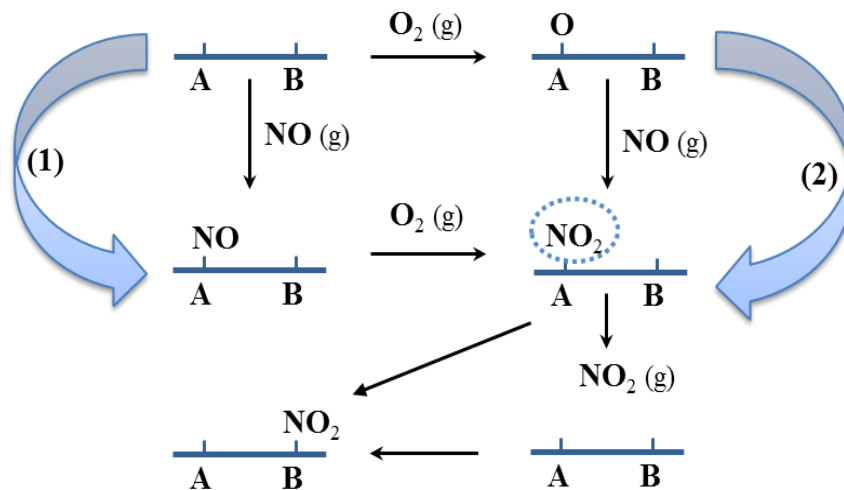


Figure 2.2-13. Reaction scheme of NO adsorption on activated carbon in the presence of oxygen [198].

The proposed NO adsorption mechanism was supported by the several adsorption sites formed on the carbon surface during the desorption experiments as presented in Figure 2.2-14. Four desorption peaks were identified at 70 °C (Low Temperature-LT), 110 °C (Mid Temperature 1-MT1), 160 °C (Mid Temperature 2-MT2) and 200 °C (High Temperature-HT), which strongly support the above mechanism that there are various NO adsorbed species on the activated coke surface formed during the NO adsorption experiments at 30 °C.

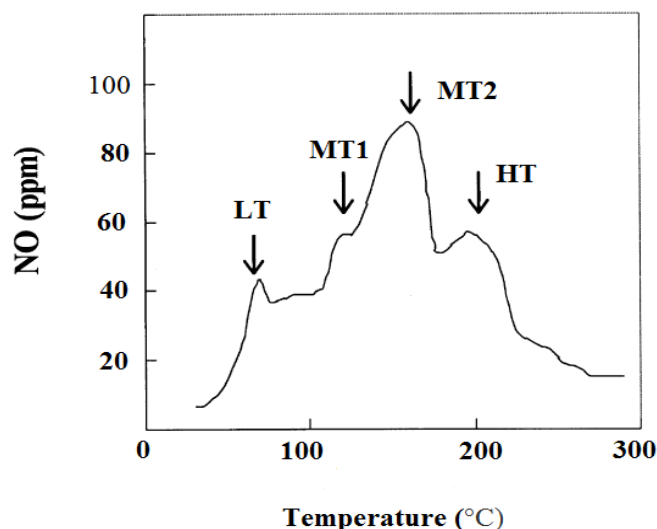


Figure 2.2-14. Temperature-programmed desorption pattern of NO after adsorption on activated carbon- NO desorption peaks showing the multiple adsorption sites on the activated carbon surface.

Another study carried out by Kong and Cha [191], where the NO adsorption mechanism on coal char, at 24 °C, was investigated in the presence of oxygen and H<sub>2</sub>O. The authors suggested that oxygen first adsorbed on the char surface, forming surface complexes (Eq. 2.19), which can then react with NO (Eq.2.20).



Zawadzki et al. [204] studied the adsorbed species formed during the reaction of carbon with NO in the presence of oxygen between 25 and 350 °C and found that carbon catalyzed the conversion of NO through oxidation to NO<sub>2</sub>, and other surface species such as C-ONO and C-NCO and anhydride structures were also formed. In the same way, Mochida et al. [205], reported that the main adsorbed species formed on activated carbon fiber during the NO+O<sub>2</sub> reaction at 30 °C is NO<sub>2</sub>. Rathore et al. [206] more recently proposed that both NO and O<sub>2</sub> adsorb on the active sites of carbon fibre, followed by oxidation to NO<sub>2</sub>. The adsorbed NO<sub>2</sub> further reacts and forms other adsorbed intermediates such as NO<sub>3</sub> and NO-NO<sub>3</sub>, which could then desorb as NO<sub>2</sub>. There is current research interest into the study of the mechanism of carbon-catalysed NO oxidation, however, due to the complexity of activated carbon, in terms of the variable chemical and physical properties, and NO auto-oxidation, characterizing NO oxidation mechanism is a challenge [207].

### 2.3 Summary

Literature on the production of carbonaceous materials has been reviewed in the current chapter. The catalytic activity of various carbonaceous materials used in tar cracking and NO removal have also been highlighted. However, most of the investigated carbons are commercial-based. The literature survey has not revealed any previous study concerning the use of carbonaceous materials derived from waste tyres, RDF and date stones for NO control at low temperature or tar control in the syngas produced from biomass gasification. To the author's best knowledge, the catalytic activity of these carbonaceous materials for NO removal and tar decomposition has

not been investigated yet. Therefore, the application of these waste-derived carbonaceous materials for NO control and tar removal would provide a more sustainable process and would also contribute to the waste management and conservation of resources.

It is necessary to determine the role of physical/chemical characteristics of the carbon, such as the porous texture and surface chemistry, on the adsorption of nitric oxide (NO) and degradation of tar species. There are some studies in the literature which have discussed the influence of these characteristics on the overall performance of the carbonaceous materials. However, there is a clear uncertainty about the effect of carbon characteristics on either NO removal or tar decomposition. Therefore, the aim of this research is to establish a comprehensive study to understand the factors affecting the catalytic activity of waste-derived carbonaceous materials.

## References

1. XIE, X. and B. GOODELL. Thermal Degradation and Conversion of Plant Biomass into High Value Carbon Products. *In: Deterioration and Protection of Sustainable Biomaterials*. American Chemical Society, 2014, pp.147-158.
2. BANDOSZ, T.J. *Activated Carbon Surfaces in Environmental Remediation*. First ed. New York, USA: Academic Press, 2006.
3. POLLARD, S.J.T., G.D. FOWLER, C.J. SOLLARS and R. PERRY. Low-cost adsorbents for waste and wastewater treatment: a review. *Science of The Total Environment*, 1992, **116**(1), pp.31-52.
4. MASCHIO, G., C. KOUFOPANOS and A. LUCCHESI. Pyrolysis, a promising route for biomass utilization. *Bioresource Technology*, 1992, **42**(3), pp.219-231.
5. DAI, X., X. YIN, C. WU, W. ZHANG and Y. CHEN. Pyrolysis of waste tires in a circulating fluidized-bed reactor. *Energy*, 2001, **26**(4), pp.385-399.
6. KAR, Y. Catalytic pyrolysis of car tire waste using expanded perlite. *Waste Management*, 2011, **31**(8), pp.1772-1782.
7. BUAH, W.K., A.M. CUNLIFFE and P.T. WILLIAMS. Characterization of Products from the Pyrolysis of Municipal Solid Waste. *Process Safety and Environmental Protection*, 2007, **85**(5), pp.450-457.
8. TIPPAYAWONG, N., J. KINORN and S. THAVORNUN. Yields and Gaseous Composition from Slow Pyrolysis of Refuse-derived Fuels. *Energy Sources, Part A: Recovery, Utilization, and Environmental Effects*, 2008, **30**(17), pp.1572-1580.
9. GUO, J. and A. CHONG LUA. Characterization of chars pyrolyzed from oil palm stones for the preparation of activated carbons. *Journal of Analytical and Applied Pyrolysis*, 1998, **46**(2), pp.113-125.
10. AMALRAJ, A. and A. PIUS. Removal of Selected Basic Dyes using Activated Carbon from Tannery Wastes. *Separation Science and Technology*, 2013, **49**(1), pp.90-100.
11. G.G. STAVROPOULOS , P.S., G.P. SAKELLAROPOULOS. Effect of activated carbons modification on porosity, surface structure and phenol adsorption. *Journal of Hazardous Materials*, 2008, **151**(2008), pp.414-421.
12. PIETRZAK, R., K. JUREWICZ, P. NOWICKI, K. BABEL and H. WACHOWSKA. Nitrogen-enriched bituminous coal-based active carbons as materials for supercapacitors. *Fuel*, 2010, **89**(11), pp.3457-3467.

13. ZENG, Z., P. LU, C. LI, L. MAI, Z. LI and Y. ZHANG. Removal of NO by carbonaceous materials at room temperature: A review. *Catalysis Science & Technology*, 2012, **2**(11), pp.2188-2199.
14. GUO, J., LUA, A.C.,. Effect of surface chemistry on gas-phase adsorption by activated carbon prepared from oil-palm stone with pre-impregnation. *Separation and Purification Technology*, 1999, **18**(2000), pp.47–55.
15. BHATNAGAR, A., W. HOGLAND, M. MARQUES and M. SILLANPÄÄ. An overview of the modification methods of activated carbon for its water treatment applications. *Chemical Engineering Journal*, 2013, **219**(0), pp.499-511.
16. MARSH, H. and F. RODRÍGUEZ-REINOSO. Chapter 8 - Applicability of Activated Carbon. *In: Activated Carbon*. Oxford: Elsevier Science Ltd, 2006, pp.383-453.
17. NAHIL, M.A. and P.T. WILLIAMS. Activated carbons from acrylic textile waste. *Journal of Analytical and Applied Pyrolysis*, 2010, **89**(1), pp.51-59.
18. WILLIAMS, P.T. and A.R. REED. High grade activated carbon matting derived from the chemical activation and pyrolysis of natural fibre textile waste. *Journal of Analytical and Applied Pyrolysis*, 2004, **71**(2), pp.971-986.
19. HAJIZADEH, Y., J.A. ONWUDILI and P.T. WILLIAMS. Removal potential of toxic 2378-substituted PCDD/F from incinerator flue gases by waste-derived activated carbons. *Waste Management*, 2011, **31**(6), pp.1194-1201.
20. GIL, R.R., B. RUIZ, M.S. LOZANO, M.J. MARTÍN and E. FUENTE. VOCs removal by adsorption onto activated carbons from biocollagenic wastes of vegetable tanning. *Chemical Engineering Journal*, 2014, **245**(0), pp.80-88.
21. GUPTA, V.K., A. NAYAK, S. AGARWAL and I. TYAGI. Potential of activated carbon from waste rubber tire for the adsorption of phenolics: Effect of pre-treatment conditions. *Journal of Colloid and Interface Science*, 2014, **417**(0), pp.420-430.
22. LIU, X., W. ZHANG and Z. ZHANG. Preparation and characteristics of activated carbon from waste fiberboard and its use for adsorption of Cu(II). *Materials Letters*, 2014, **116**(0), pp.304-306.
23. EL-KADY, A.A., H.H. ABDEL GHAFAR, M.B.M. IBRAHIM and M.A. ABDEL-WAHHAB. Utilization of activated carbon prepared from agricultural waste for the removal of organophosphorous pesticide from aqueous media. *Desalination and Water Treatment*, 2013, **51**(37-39), pp.7276-7285.
24. GUNDOGDU, A., C. DURAN, H.B. SENTURK, M. SOYLAK, M. IMAMOGLU and Y. ONAL. Physicochemical characteristics of a novel

- activated carbon produced from tea industry waste. *Journal of Analytical and Applied Pyrolysis*, 2013, **104**(0), pp.249-259.
25. BUAH, W.K. and P.T. WILLIAMS. Activated carbons prepared from refuse derived fuel and their gold adsorption characteristics. *Environmental Technology*, 2010, **31**(2), pp.125-137.
  26. WIGMANS, T. Proceedings of the Conference on Porosity and Carbon materials: Measurements and applications Industrial aspects of production and use of activated carbons. *Carbon*, 1989, **27**(1), pp.13-22.
  27. HADI, P., M. XU, C. NING, C. SZE KI LIN and G. MCKAY. A critical review on preparation, characterization and utilization of sludge-derived activated carbons for wastewater treatment. *Chemical Engineering Journal*, 2015, **260**, pp.895-906.
  28. RODRÍGUEZ-REINOSO, F., M. MOLINA-SABIO and M.T. GONZÁLEZ. The use of steam and CO<sub>2</sub> as activating agents in the preparation of activated carbons. *Carbon*, 1995, **33**(1), pp.15-23.
  29. MOLINA-SABIO, M., M.T. GONZALEZ, F. RODRIGUEZ-REINOSO and A. SEPÚLVEDA-ESCRIBANO. Effect of steam and carbon dioxide activation in the micropore size distribution of activated carbon. *Carbon*, 1996, **34**(4), pp.505-509.
  30. TENG, H., M.A. SERIO, M.A. WÓJTOWICZ, R. BASSILAKIS and P.R. SOLOMON. Reprocessing of used tires into activated carbon and other products. *Industrial and Engineering Chemistry Research*, 1995, **34**(9), pp.3102-3111.
  31. SAN MIGUEL, G., G.D. FOWLER and C.J. SOLLARS. A study of the characteristics of activated carbons produced by steam and carbon dioxide activation of waste tyre rubber. *Carbon*, 2003, **41**(5), pp.1009-1016.
  32. HAMADI, N.K., X.D. CHEN, M.M. FARID and M.G.Q. LU. Adsorption kinetics for the removal of chromium(VI) from aqueous solution by adsorbents derived from used tyres and sawdust. *Chemical Engineering Journal*, 2001, **84**(2), pp.95-105.
  33. SUN, J., T.A. BRADY, M.J. ROOD, C.M. LEHMANN, M. ROSTAM-ABADI and A.A. LIZZIO. Adsorbed natural gas storage with activated carbons made from Illinois coals and scrap tires. *Energy and Fuels*, 1997, **11**(2), pp.316-322.
  34. ARIYADEJWANICH, P., W. TANTHAPANICHAKOON, K. NAKAGAWA, S.R. MUKAI and H. TAMON. Preparation and characterization of mesoporous activated carbon from waste tires. *Carbon*, 2003, **41**(1), pp.157-164.

35. LEHMANN, C.M.B., M. ROSTAM-ABADI, M.J. ROOD and J. SUN. Reprocessing and Reuse of Waste Tire Rubber to Solve Air-Quality Related Problems. *Energy & Fuels*, 1998, **12**(6), pp.1095-1099.
36. GUO, J. and A.C. LUA. Characterization of adsorbent prepared from oil-palm shell by CO<sub>2</sub> activation for removal of gaseous pollutants. *Materials Letters*, 2002, **55**(5), pp.334-339.
37. YANG, T. and A.C. LUA. Characteristics of activated carbons prepared from pistachio-nut shells by physical activation. *Journal of Colloid and Interface Science*, 2003, **267**(2), pp.408-417.
38. FUNG, P.P.M., W.H. CHEUNG and G. MCKAY. Systematic Analysis of Carbon Dioxide Activation of Waste Tire by Factorial Design. *Chinese Journal of Chemical Engineering*, 2012, **20**(3), pp.497-504.
39. MUI, E.L.K., D.C.K. KO and G. MCKAY. Production of active carbons from waste tyres—a review. *Carbon*, 2004, **42**(14), pp.2789-2805.
40. GUO, J. and A.C. LUA. Effect of Heating Temperature on the Properties of Chars and Activated Carbons Prepared From Oil Palm Stones. *Journal of Thermal Analysis and Calorimetry*, 2000, **60**(2), pp.417-425.
41. MENG, L.-Y. and S.-J. PARK. MgO-templated porous carbons-based CO<sub>2</sub> adsorbents produced by KOH activation. *Materials Chemistry and Physics*, 2012, **137**(1), pp.91-96.
42. KIM, B.J., Y.S. LEE and S.J. PARK. Preparation of platinum-decorated porous graphite nanofibers, and their hydrogen storage behaviors. *Journal of Colloid and Interface Science*, 2008, **318**(2), pp.530-533.
43. HSU, L.-Y. and H. TENG. Influence of different chemical reagents on the preparation of activated carbons from bituminous coal. *Fuel Processing Technology*, 2000, **64**(1–3), pp.155-166.
44. FIERRO, V., V. TORNÉ-FERNÁNDEZ and A. CELZARD. Methodical study of the chemical activation of Kraft lignin with KOH and NaOH. *Microporous and Mesoporous Materials*, 2007, **101**(3), pp.419-431.
45. HAYASHI, J., A. KAZEHAYA, K. MUROYAMA and A.P. WATKINSON. Preparation of activated carbon from lignin by chemical activation. *Carbon*, 2000, **38**(13), pp.1873-1878.
46. LILLO-RÓDENAS, M.A., D. LOZANO-CASTELLÓ, D. CAZORLA-AMORÓS and A. LINARES-SOLANO. Preparation of activated carbons from Spanish anthracite - II. Activation by NaOH. *Carbon*, 2001, **39**(5), pp.751-759.

47. OLIVARES-MARÍN, M., C. FERNÁNDEZ-GONZÁLEZ, A. MACÍAS-GARCÍA and V. GÓMEZ-SERRANO. Preparation of activated carbons from cherry stones by activation with potassium hydroxide. *Applied Surface Science*, 2006, **252**(17), pp.5980-5983.
48. UBAGO-PÉREZ, R., F. CARRASCO-MARÍN, D. FAIRÉN-JIMÉNEZ and C. MORENO-CASTILLA. Granular and monolithic activated carbons from KOH-activation of olive stones. *Microporous and Mesoporous Materials*, 2006, **92**(1-3), pp.64-70.
49. WU, F.C. and R.L. TSENG. Preparation of highly porous carbon from fir wood by KOH etching and CO<sub>2</sub> gasification for adsorption of dyes and phenols from water. *Journal of Colloid and Interface Science*, 2006, **294**(1), pp.21-30.
50. GUO, Y., H. YUI, A. FUKAGAWA, S. KAMIYA, M. MASUDA, K. ITO and T. SHIMIZU. Alignment of glycolipid nanotubes on a planar glass substrate using a two-step microextrusion technique. *Journal of Nanoscience and Nanotechnology*, 2006, **6**(5), pp.1464-1466.
51. BASTA, A.H., V. FIERRO, H. EL-SAIED and A. CELZARD. 2-Steps KOH activation of rice straw: An efficient method for preparing high-performance activated carbons. *Bioresource Technology*, 2009, **100**(17), pp.3941-3947.
52. LIN, Y.-R. and H. TENG. Mesoporous carbons from waste tire char and their application in wastewater discoloration. *Microporous and Mesoporous Materials*, 2002, **54**(1-2), pp.167-174.
53. JI, Y., T. LI, L. ZHU, X. WANG and Q. LIN. Preparation of activated carbons by microwave heating KOH activation. *Applied Surface Science*, 2007, **254**(2), pp.506-512.
54. LILLO-RÓDENAS, M.A., D. CAZORLA-AMORÓS and A. LINARES-SOLANO. Understanding chemical reactions between carbons and NaOH and KOH: An insight into the chemical activation mechanism. *Carbon*, 2003, **41**(2), pp.267-275.
55. CHUNLAN, L., X. SHAOPING, G. YIXIONG, L. SHUQIN and L. CHANGHOU. Effect of pre-carbonization of petroleum cokes on chemical activation process with KOH. *Carbon*, 2005, **43**(11), pp.2295-2301.
56. EVANS, M.J.B., E. HALLIOP and J.A.F. MACDONALD. The production of chemically-activated carbon. *Carbon*, 1999, **37**(2), pp.269-274.
57. YANG, J., Z. SHEN and Z. HAO. Preparation of highly microporous and mesoporous carbon from the mesophase pitch and its carbon foams with KOH. *Carbon*, 2004, **42**(8-9), pp.1872-1875.

58. CARVALHO, A.P., B. CARDOSO, J. PIRES and M. BROTAS DE CARVALHO. Preparation of activated carbons from cork waste by chemical activation with KOH. *Carbon*, 2003, **41**(14), pp.2873-2876.
59. SHEN, Y. Chars as carbonaceous adsorbents/catalysts for tar elimination during biomass pyrolysis or gasification. *Renewable and Sustainable Energy Reviews*, 2015, **43**, pp.281-295.
60. BELGIORNO, V., G. DE FEO, C. DELLA ROCCA and R.M.A. NAPOLI. Energy from gasification of solid wastes. *Waste Management*, 2003, **23**(1), pp.1-15.
61. GARCÍA-LABIANO, F., P. GAYÁN, L.F. DE DIEGO, A. ABAD, T. MENDIARA, J. ADÁNEZ, M. NACKEN and S. HEIDENREICH. Tar abatement in a fixed bed catalytic filter candle during biomass gasification in a dual fluidized bed. *Applied Catalysis B: Environmental*, 2016, **188**, pp.198-206.
62. MILNE, T.A. and R.J. EVANS. Biomass gasifier “tars”: their nature, formation, and conversion. *Report no. NREL/TP-570-25357*, NREL, Golden, Colorado, USA, 1998.
63. NEVES, D., H. THUNMAN, A. MATOS, L. TARELHO and A. GÓMEZ-BAREA. Characterization and prediction of biomass pyrolysis products. *Progress in Energy and Combustion Science*, 2011, **37**(5), pp.611-630.
64. SHEN, Y. and K. YOSHIKAWA. Recent progresses in catalytic tar elimination during biomass gasification or pyrolysis—A review. *Renewable and Sustainable Energy Reviews*, 2013, **21**, pp.371-392.
65. DEVI, L., K.J. PTASINSKI, F.J.J.G. JANSSEN, S.V.B. VAN PAASEN, P.C.A. BERGMAN and J.H.A. KIEL. Catalytic decomposition of biomass tars: Use of dolomite and untreated olivine. *Renewable Energy*, 2005, **30**(4), pp.565-587.
66. LI, C. and K. SUZUKI. Tar property, analysis, reforming mechanism and model for biomass gasification—An overview. *Renewable and Sustainable Energy Reviews*, 2009, **13**(3), pp.594-604.
67. GUAN, G., M. KAEWPANHA, X. HAO and A. ABUDULA. Catalytic steam reforming of biomass tar: Prospects and challenges. *Renewable and Sustainable Energy Reviews*, 2016, **58**, pp.450-461.
68. HUBER, G.W., S. IBORRA and A. CORMA. Synthesis of Transportation Fuels from Biomass: Chemistry, Catalysts, and Engineering. *Chemical Reviews*, 2006, **106**(9), pp.4044-4098.

69. WILLIAMS, P.T. and S. BESLER. Polycyclic aromatic hydrocarbons in waste derived pyrolytic oils. *Journal of Analytical and Applied Pyrolysis*, 1994, **30**, pp.17-33.
70. CUNLIFFE, A.M. and P.T. WILLIAMS. Composition of oils derived from the batch pyrolysis of tyres. *Journal of Analytical and Applied Pyrolysis*, 1998, **44**(2), pp.131-152.
71. FAIRBURN, J.A., L.A. BEHIE and W.Y. SVRCEK. Ultrapyrolysis of n-hexadecane in a novel micro-reactor. *Fuel*, 1990, **69**(12), pp.1537-1545.
72. CYPRES, R. Aromatic hydrocarbons formation during coal pyrolysis. *Fuel Processing Technology*, 1987, **15**(C), pp.1-15.
73. SÁNCHEZ, M.E., J.A. MENÉNDEZ, A. DOMÍNGUEZ, J.J. PIS, O. MARTÍNEZ, L.F. CALVO and P.L. BERNAD. Effect of pyrolysis temperature on the composition of the oils obtained from sewage sludge. *Biomass and Bioenergy*, 2009, **33**(6-7), pp.933-940.
74. FONT PALMA, C. Modelling of tar formation and evolution for biomass gasification: A review. *Applied Energy*, 2013, **111**, pp.129-141.
75. HOSOYA, T., H. KAWAMOTO and S. SAKA. Pyrolysis gasification reactivities of primary tar and char fractions from cellulose and lignin as studied with a closed ampoule reactor. *Journal of Analytical and Applied Pyrolysis*, 2008, **83**(1), pp.71-77.
76. ASMADI, M., H. KAWAMOTO and S. SAKA. Gas- and solid/liquid-phase reactions during pyrolysis of softwood and hardwood lignins. *Journal of Analytical and Applied Pyrolysis*, 2011, **92**(2), pp.417-425.
77. SEBAYANG, A.H., H.H. MASJUKI, H.C. ONG, S. DHARMA, A.S. SILITONGA, T.M.I. MAHLIA and H.B. ADITIYA. A perspective on bioethanol production from biomass as alternative fuel for spark ignition engine. *RSC Advances*, 2016, **6**(18), pp.14964-14992.
78. SHEN, Y., J. WANG, X. GE and M. CHEN. By-products recycling for syngas cleanup in biomass pyrolysis – An overview. *Renewable and Sustainable Energy Reviews*, 2016, **59**, pp.1246-1268.
79. ASMADI, M., H. KAWAMOTO and S. SAKA. Thermal reactions of guaiacol and syringol as lignin model aromatic nuclei. *Journal of Analytical and Applied Pyrolysis*, 2011, **92**(1), pp.88-98.
80. ZHOU, H., C. WU, J.A. ONWUDILI, A. MENG, Y. ZHANG and P.T. WILLIAMS. Polycyclic aromatic hydrocarbons (PAH) formation from the pyrolysis of different municipal solid waste fractions. *Waste Management*, 2015, **36**, pp.136-146.

81. SHUKLA, B. and M. KOSHI. A novel route for PAH growth in HACA based mechanisms. *Combustion and Flame*, 2012, **159**(12), pp.3589-3596.
82. VIOLI, A., A. D'ANNA and A. D'ALESSIO. Modeling of particulate formation in combustion and pyrolysis. *Chemical Engineering Science*, 1999, **54**(15), pp.3433-3442.
83. DEVI, L., K.J. PTASINSKI and F.J.J.G. JANSSEN. Decomposition of Naphthalene as a Biomass Tar over Pretreated Olivine: Effect of Gas Composition, Kinetic Approach, and Reaction Scheme. *Industrial & Engineering Chemistry Research*, 2005, **44**(24), pp.9096-9104.
84. VREUGDENHIL, B.J. and R.W.R. ZWART. *Tar Formation in Pyrolysis and Gasification*. ECN-E--08-087. Energy and Research Center of Netherlands, 2004.
85. VANDER HOEVEN, T.A. Partial product gas combustion for tar reduction. Ph.D. Dissertation. *Eindhoven University*, 2007.
86. JESS, A. Mechanisms and kinetics of thermal reactions of aromatic hydrocarbons from pyrolysis of solid fuels. *Fuel*, 1996, **75**(12), pp.1441-1448.
87. NAIR, S.A., K. YAN, A.J.M. PEMEN, E.J.M. VAN HEESCH, K.J. PTASINSKI and A.A.H. DRINKENBURG. Tar Removal from Biomass-Derived Fuel Gas by Pulsed Corona Discharges. A Chemical Kinetic Study. *Industrial & Engineering Chemistry Research*, 2004, **43**(7), pp.1649-1658.
88. HAMAD, T.A., A.A. AGLL, Y.M. HAMAD and J.W. SHEFFIELD. Solid waste as renewable source of energy: current and future possibility in Libya. *Case Studies in Thermal Engineering*, 2014, **4**, pp.144-152.
89. BLASI, C.D. Dynamic behaviour of stratified downdraft gasifiers. *Chemical Engineering Science*, 2000, **55**, pp.2931-2944.
90. LIU, M. and P.V. ARAVIND. The fate of tars under solid oxide fuel cell conditions: A review. *Applied Thermal Engineering*, 2014, **70**(1), pp.687-693.
91. MILNE, T.A., N. ABATZOGLOU and R.J. EVANS. N.T. NATIONAL RENEWABLE ENERGY LABORATORY. TECHNICAL REPORT. *Biomass gasifier 'tars': their nature, formation, and conversion*. NREL/TP\_570\_25357. Golden, Colorado, USA, 1998.
92. ZHANG, R., R.C. BROWN, A. SUBY and K. CUMMER. Catalytic destruction of tar in biomass derived producer gas. *Energy Conversion and Management*, 2004, **45**(7-8), pp.995-1014.
93. SUTTON, D., B. KELLEHER and J.R.H. ROSS. Review of literature on catalysts for biomass gasification. *Fuel Processing Technology*, 2001, **73**(3), pp.155-173.

94. WEI, L., S. XU, L. ZHANG, C. LIU, H. ZHU and S. LIU. Steam gasification of biomass for hydrogen-rich gas in a free-fall reactor. *International Journal of Hydrogen Energy*, 2007, **32**(1), pp.24-31.
95. GUSTA, E., A.K. DALAI, M.A. UDDIN and E. SASAOKA. Catalytic Decomposition of Biomass Tars with Dolomites. *Energy & Fuels*, 2009, **23**(4), pp.2264-2272.
96. LI, C., D. HIRABAYASHI and K. SUZUKI. Development of new nickel based catalyst for biomass tar steam reforming producing H<sub>2</sub>-rich syngas. *Fuel Processing Technology*, 2009, **90**(6), pp.790-796.
97. CHEAH, S., K.R. GASTON, Y.O. PARENT, M.W. JARVIS, T.B. VINZANT, K.M. SMITH, N.E. THORNBURG, M.R. NIMLOS and K.A. MAGRINI-BAIR. Nickel cerium olivine catalyst for catalytic gasification of biomass. *Applied Catalysis B: Environmental*, 2013, **134–135**, pp.34-45.
98. KIMURA, T., T. MIYAZAWA, J. NISHIKAWA, S. KADO, K. OKUMURA, T. MIYAO, S. NAITO, K. KUNIMORI and K. TOMISHIGE. Development of Ni catalysts for tar removal by steam gasification of biomass. *Applied Catalysis B: Environmental*, 2006, **68**(3–4), pp.160-170.
99. DOU, B., J. GAO, X. SHA and S.W. BAEK. Catalytic cracking of tar component from high-temperature fuel gas. *Applied Thermal Engineering*, 2003, **23**(17), pp.2229-2239.
100. SUZUKI, T., H. OHME and Y. WATANABE. Alkali metal catalyzed CO<sub>2</sub> gasification of carbon. *Energy and Fuels*, 1992, **6**(4), pp.343-351.
101. ABU EL-RUB, Z., E.A. BRAMER and G. BREM. Experimental comparison of biomass chars with other catalysts for tar reduction. *Fuel*, 2008, **87**(10–11), pp.2243-2252.
102. DEVI, L., K.J. PTASINSKI and F.J.J.G. JANSSEN. A review of the primary measures for tar elimination in biomass gasification processes. *Biomass and Bioenergy*, 2003, **24**(2), pp.125-140.
103. DELGADO, J., M.P. AZNAR and J. CORELLA. Biomass Gasification with Steam in Fluidized Bed: Effectiveness of CaO, MgO, and CaO–MgO for Hot Raw Gas Cleaning. *Industrial & Engineering Chemistry Research*, 1997, **36**(5), pp.1535-1543.
104. RAPAGNÀ, S., N. JAND, A. KIENNEMANN and P.U. FOSCOLO. Steam-gasification of biomass in a fluidised-bed of olivine particles. *Biomass and Bioenergy*, 2000, **19**(3), pp.187-197.
105. ANIS, S. and Z.A. ZAINAL. Tar reduction in biomass producer gas via mechanical, catalytic and thermal methods: A review. *Renewable and Sustainable Energy Reviews*, 2011, **15**(5), pp.2355-2377.

106. BIMBELA, F., D. CHEN, J. RUIZ, L. GARCÍA and J. ARAUZO. Ni/Al coprecipitated catalysts modified with magnesium and copper for the catalytic steam reforming of model compounds from biomass pyrolysis liquids. *Applied Catalysis B: Environmental*, 2012, **119–120**, pp.1-12.
107. SIMELL, P.A. and J.B.S. BREDENBERG. Catalytic purification of tarry fuel gas. *Fuel*, 1990, **69**(10), pp.1219-1225.
108. SRINAKRUANG, J., K. SATO, T. VITIDSANT and K. FUJIMOTO. A highly efficient catalyst for tar gasification with steam. *Catalysis Communications*, 2005, **6**(6), pp.437-440.
109. EFIKA, C.E., C. WU and P.T. WILLIAMS. Syngas production from pyrolysis-catalytic steam reforming of waste biomass in a continuous screw kiln reactor. *Journal of Analytical and Applied Pyrolysis*, 2012, **95**, pp.87-94.
110. SUTTON, D., B. KELLEHER, A. DOYLE and J.R.H. ROSS. Investigation of nickel supported catalysts for the upgrading of brown peat derived gasification products. *Bioresource Technology*, 2001, **80**(2), pp.111-116.
111. KONG, M., J. FEI, S. WANG, W. LU and X. ZHENG. Influence of supports on catalytic behavior of nickel catalysts in carbon dioxide reforming of toluene as a model compound of tar from biomass gasification. *Bioresource Technology*, 2011, **102**(2), pp.2004-2008.
112. CHAIPRASERT, P. and T. VITIDSANT. Effects of promoters on biomass gasification using nickel/dolomite catalyst. *Korean Journal of Chemical Engineering*, 2009, **26**(6), pp.1545-1549.
113. ZHANG, R., Y. WANG and R.C. BROWN. Steam reforming of tar compounds over Ni/olivine catalysts doped with CeO<sub>2</sub>. *Energy Conversion and Management*, 2007, **48**(1), pp.68-77.
114. NISHIKAWA, J., K. NAKAMURA, M. ASADULLAH, T. MIYAZAWA, K. KUNIMORI and K. TOMISHIGE. Catalytic performance of Ni/CeO<sub>2</sub>/Al<sub>2</sub>O<sub>3</sub> modified with noble metals in steam gasification of biomass. *Catalysis Today*, 2008, **131**(1–4), pp.146-155.
115. MA, L., H. VERELST and G.V. BARON. Integrated high temperature gas cleaning: Tar removal in biomass gasification with a catalytic filter. *Catalysis Today*, 2005, **105**(3–4), pp.729-734.
116. GARCIA, L.A., R. FRENCH, S. CZERNIK and E. CHORNET. Catalytic steam reforming of bio-oils for the production of hydrogen: effects of catalyst composition. *Applied Catalysis A: General*, 2000, **201**(2), pp.225-239.
117. LIU, W.-J., H. JIANG and H.-Q. YU. Development of Biochar-Based Functional Materials: Toward a Sustainable Platform Carbon Material. *Chemical Reviews*, 2015, **115**(22), pp.12251-12285.

118. SUN, Q., S. YU, F. WANG and J. WANG. Decomposition and gasification of pyrolysis volatiles from pine wood through a bed of hot char. *Fuel*, 2011, **90**(3), pp.1041-1048.
119. PHUPHUAKRAT, T., T. NAMIOKA and K. YOSHIKAWA. Tar removal from biomass pyrolysis gas in two-step function of decomposition and adsorption. *Applied Energy*, 2010, **87**(7), pp.2203-2211.
120. GILBERT, P., C. RYU, V. SHARIFI and J. SWITHEBANK. Tar reduction in pyrolysis vapours from biomass over a hot char bed. *Bioresource Technology*, 2009, **100**(23), pp.6045-6051.
121. WANG, F.-J., S. ZHANG, Z.-D. CHEN, C. LIU and Y.-G. WANG. Tar reforming using char as catalyst during pyrolysis and gasification of Shengli brown coal. *Journal of Analytical and Applied Pyrolysis*, 2014, **105**, pp.269-275.
122. HOSOKAI, S., K. KUMABE, M. OHSHITA, K. NORINAGA, C.-Z. LI and J.-I. HAYASHI. Mechanism of decomposition of aromatics over charcoal and necessary condition for maintaining its activity. *Fuel*, 2008, **87**(13-14), pp.2914-2922.
123. SUEYASU, T., T. OIKE, A. MORI, S. KUDO, K. NORINAGA and J.-I. HAYASHI. Simultaneous Steam Reforming of Tar and Steam Gasification of Char from the Pyrolysis of Potassium-Loaded Woody Biomass. *Energy & Fuels*, 2012, **26**(1), pp.199-208.
124. ZHU, D., S. KWON and J.J. PIGNATELLO. Adsorption of Single-Ring Organic Compounds to Wood Charcoals Prepared under Different Thermochemical Conditions. *Environmental Science & Technology*, 2005, **39**(11), pp.3990-3998.
125. CHUN, Y., G. SHENG, C.T. CHIOU and B. XING. Compositions and Sorptive Properties of Crop Residue-Derived Chars. *Environmental Science & Technology*, 2004, **38**(17), pp.4649-4655.
126. QIU, Y., H. CHENG, C. XU and G.D. SHENG. Surface characteristics of crop-residue-derived black carbon and lead(II) adsorption. *Water Research*, 2008, **42**(3), pp.567-574.
127. MOHAN, D., C.U. PITTMAN JR, M. BRICKA, F. SMITH, B. YANCEY, J. MOHAMMAD, P.H. STEELE, M.F. ALEXANDRE-FRANCO, V. GÓMEZ-SERRANO and H. GONG. Sorption of arsenic, cadmium, and lead by chars produced from fast pyrolysis of wood and bark during bio-oil production. *Journal of Colloid and Interface Science*, 2007, **310**(1), pp.57-73.
128. MOLINER, R., I. SUELVE, M.J. LÁZARO and O. MORENO. Thermocatalytic decomposition of methane over activated carbons: influence

- of textural properties and surface chemistry. *International Journal of Hydrogen Energy*, 2005, **30**(3), pp.293-300.
129. JIN, L., X. BAI, Y. LI, C. DONG, H. HU and X. LI. In-situ catalytic upgrading of coal pyrolysis tar on carbon-based catalyst in a fixed-bed reactor. *Fuel Processing Technology*, 2016, **147**, pp.41-46.
  130. KRERKKAIWAN, S., S. MUEANGTA, P. THAMMARAT, L. JAISAT and P. KUCHONTHARA. Catalytic Biomass-Derived Tar Decomposition Using Char from the Co-pyrolysis of Coal and Giant Leucaena Wood Biomass. *Energy & Fuels*, 2015, **29**(5), pp.3119-3126.
  131. ZHAO, S., Y. LUO, Y. ZHANG and Y. LONG. Experimental investigation of the synergy effect of partial oxidation and bio-char on biomass tar reduction. *Journal of Analytical and Applied Pyrolysis*, 2015, **112**(0), pp.262-269.
  132. DABAI, F., N. PATERSON, M. MILLAN, P. FENNELL and R. KANDIYOTI. Tar formation and destruction in a fixed-bed reactor simulating downdraft gasification: Equipment development and characterization of tar-cracking products. *Energy and Fuels*, 2010, **24**(8), pp.4560-4570.
  133. GUOXIN, H. and H. HAO. Hydrogen rich fuel gas production by gasification of wet biomass using a CO<sub>2</sub> sorbent. *Biomass and Bioenergy*, 2009, **33**(5), pp.899-906.
  134. LIU, C., H. WANG, A.M. KARIM, J. SUN and Y. WANG. Catalytic fast pyrolysis of lignocellulosic biomass. *Chemical Society Reviews*, 2014, **43**(22), pp.7594-7623.
  135. GONZÁLEZ, J.F., S. ROMÁN, D. BRAGADO and M. CALDERÓN. Investigation on the reactions influencing biomass air and air/steam gasification for hydrogen production. *Fuel Processing Technology*, 2008, **89**(8), pp.764-772.
  136. HARYANTO, A., S. FERNANDO, N. MURALI and S. ADHIKARI. Current Status of Hydrogen Production Techniques by Steam Reforming of Ethanol: A Review. *Energy & Fuels*, 2005, **19**(5), pp.2098-2106.
  137. CHEN, C.-J., C.-I. HUNG and W.-H. CHEN. Numerical investigation on performance of coal gasification under various injection patterns in an entrained flow gasifier. *Applied Energy*, 2012, **100**, pp.218-228.
  138. MANENTI, F., S. CIERI and M. RESTELLI. Considerations on the steady-state modeling of methanol synthesis fixed-bed reactor. *Chemical Engineering Science*, 2011, **66**(2), pp.152-162.
  139. YAO, D., Q. HU, D. WANG, H. YANG, C. WU, X. WANG and H. CHEN. Hydrogen production from biomass gasification using biochar as a catalyst/support. *Bioresource Technology*, 2016, **216**, pp.159-164.

140. SHEN, Y., P. ZHAO, Q. SHAO, D. MA, F. TAKAHASHI and K. YOSHIKAWA. In-situ catalytic conversion of tar using rice husk char-supported nickel-iron catalysts for biomass pyrolysis/gasification. *Applied Catalysis B: Environmental*, 2014, **152-153**(1), pp.140-151.
141. LUO, S., B. XIAO, Z. HU, S. LIU, X. GUO and M. HE. Hydrogen-rich gas from catalytic steam gasification of biomass in a fixed bed reactor: Influence of temperature and steam on gasification performance. *International Journal of Hydrogen Energy*, 2009, **34**(5), pp.2191-2194.
142. TANG, Q., H. BIAN, J. RAN, Y. ZHU, J. YU and W. ZHU. Hydrogen-rich gas production from steam gasification of biomass using CaO and a Fe-Cr water-gas shift catalyst. *BioResources*, 2015, **10**(2), pp.2560-2569.
143. FREMAUX, S., S.-M. BEHESHTI, H. GHASSEMI and R. SHAHSAVAN-MARKADEH. An experimental study on hydrogen-rich gas production via steam gasification of biomass in a research-scale fluidized bed. *Energy Conversion and Management*, 2015, **91**, pp.427-432.
144. SONG, Y., Y. WANG, X. HU, S. HU, J. XIANG, L. ZHANG, S. ZHANG, Z. MIN and C.-Z. LI. Effects of volatile-char interactions on in situ destruction of nascent tar during the pyrolysis and gasification of biomass. Part I. Roles of nascent char. *Fuel*, 2014, **122**, pp.60-66.
145. CHOI, Y.-K., M.-H. CHO and J.-S. KIM. Steam/oxygen gasification of dried sewage sludge in a two-stage gasifier: Effects of the steam to fuel ratio and ash of the activated carbon on the production of hydrogen and tar removal. *Energy*, 2015, **91**, pp.160-167.
146. STRIŪGAS, N., K. ZAKARAUSKAS, G. STRAVINSKAS and V. GRIGAITIENĖ. Comparison of steam reforming and partial oxidation of biomass pyrolysis tars over activated carbon derived from waste tire. *Catalysis Today*, 2012, **196**(1), pp.67-74.
147. BAYARSAIKHAN, B., N. SONOYAMA, S. HOSOKAI, T. SHIMADA, J.-I. HAYASHI, C.-Z. LI and T. CHIBA. Inhibition of steam gasification of char by volatiles in a fluidized bed under continuous feeding of a brown coal. *Fuel*, 2006, **85**(3), pp.340-349.
148. LI, C.-Z. Some recent advances in the understanding of the pyrolysis and gasification behaviour of Victorian brown coal. *Fuel*, 2007, **86**(12-13), pp.1664-1683.
149. COLL, R., J. SALVADÓ, X. FARRIOL and D. MONTANÉ. Steam reforming model compounds of biomass gasification tars: conversion at different operating conditions and tendency towards coke formation. *Fuel Processing Technology*, 2001, **74**(1), pp.19-31.

150. BURHENNE, L. and T. AICHER. Benzene removal over a fixed bed of wood char: The effect of pyrolysis temperature and activation with CO<sub>2</sub> on the char reactivity. *Fuel Processing Technology*, 2014, **127**, pp.140-148.
151. PARK, J., Y. LEE and C. RYU. Reduction of primary tar vapor from biomass by hot char particles in fixed bed gasification. *Biomass and Bioenergy*, 2016, **90**, pp.114-121.
152. FUENTES-CANO, D., A. GÓMEZ-BAREA, S. NILSSON and P. OLLERO. Decomposition kinetics of model tar compounds over chars with different internal structure to model hot tar removal in biomass gasification. *Chemical Engineering Journal*, 2013, **228**, pp.1223-1233.
153. HOSOKAI, S., K. NORINAGA, T. KIMURA, M. NAKANO, C.-Z. LI and J.-I. HAYASHI. Reforming of Volatiles from the Biomass Pyrolysis over Charcoal in a Sequence of Coke Deposition and Steam Gasification of Coke. *Energy & Fuels*, 2011, **25**(11), pp.5387-5393.
154. ZENG, X., Y. WANG, J. YU, S. WU, J. HAN, S. XU and G. XU. Gas Upgrading in a Downdraft Fixed-Bed Reactor Downstream of a Fluidized-Bed Coal Pyrolyzer. *Energy & Fuels*, 2011, **25**(11), pp.5242-5249.
155. DABROWSKI, A. Adsorption from theory to practice. *Advances in Colloid and Interface Science*, 2001, **93**, pp.135-224.
156. CHO, M.-H., T.-Y. MUN and J.-S. KIM. Production of low-tar producer gas from air gasification of mixed plastic waste in a two-stage gasifier using olivine combined with activated carbon. *Energy*, 2013, **58**, pp.688-694.
157. CHO, M.-H., T.-Y. MUN, Y.-K. CHOI and J.-S. KIM. Two-stage air gasification of mixed plastic waste: Olivine as the bed material and effects of various additives and a nickel-plated distributor on the tar removal. *Energy*, 2014, **70**, pp.128-134.
158. HAN, J., X. WANG, J. YUE, S. GAO and G. XU. Catalytic upgrading of coal pyrolysis tar over char-based catalysts. *Fuel Processing Technology*, 2014, **122**, pp.98-106.
159. GÓMEZ-GARCÍA, M.A., V. PITCHON and A. KIENNEMANN. Pollution by nitrogen oxides: an approach to NO<sub>x</sub> abatement by using sorbing catalytic materials. *Environment International*, 2005, **31**(3), pp.445-467.
160. MATSUDA, S., M. TAKEUCHI, T. HISHINUMA, F. NAKAJIMA, T. NARITA, Y. WATANABE and M. IMANARI. Selective Reduction of Nitrogen Oxides In Combustion Flue Gases. *Journal of the Air Pollution Control Association*, 1978, **28**(4), pp.350-353.
161. BAUKAL, C. Everything you need to know about NO<sub>x</sub>. *Metal Finishing*, 2005, **103**(11), pp.18-24.

162. SHEN, Y., X. GE and M. CHEN. Catalytic oxidation of nitric oxide (NO) with carbonaceous materials. *RSC Advances*, 2016, **6**(10), pp.8469-8482.
163. MAUZERALL, D.L., B. SULTAN, N. KIM and D.F. BRADFORD. NO<sub>x</sub> emissions from large point sources: variability in ozone production, resulting health damages and economic costs. *Atmospheric Environment*, 2005, **39**(16), pp.2851-2866.
164. BAUKAL, C.E. *Industrial Combustion Pollution and Control*. New York: Marcel Dekker Inc, 2004.
165. SOUSA, J.P.S., M.F.R. PEREIRA and J.L. FIGUEIREDO. Modified activated carbon as catalyst for NO oxidation. *Fuel Processing Technology*, 2013, **106**(0), pp.727-733.
166. BELHACHEMI, M., M. JEGUIRIM, L. LIMOUSY and F. ADDOUN. Comparison of NO<sub>2</sub> removal using date pits activated carbon and modified commercialized activated carbon via different preparation methods: Effect of porosity and surface chemistry. *Chemical Engineering Journal*, 2014, **253**(0), pp.121-129.
167. YAN, R., T. CHIN, Y.L. NG, H. DUAN, D.T. LIANG and J.H. TAY. Influence of Surface Properties on the Mechanism of H<sub>2</sub>S Removal by Alkaline Activated Carbons. *Environmental Science & Technology*, 2004, **38**(1), pp.316-323.
168. BANDOSZ, T.J. On the Adsorption/Oxidation of Hydrogen Sulfide on Activated Carbons at Ambient Temperatures. *Journal of Colloid and Interface Science*, 2002, **246**(1), pp.1-20.
169. DIANA LOPEZ, R.B., ANTONIO SEPULVEDA-ESCRIBANO, FRANCISCO RODRÍGUEZ-REINOSO, AND FANOR MONDRAGON. Low-Temperature Catalytic Adsorption of NO on Activated Carbon Materials. *Langmuir*, 2007, **23**, pp.12131-12137.
170. AZAMBRE, B., L. ZENBOURY, A. KOCH and J.V. WEBER. Adsorption and Desorption of NO<sub>x</sub> on Commercial Ceria-Zirconia (Ce<sub>x</sub>Zr<sub>1-x</sub>O<sub>2</sub>) Mixed Oxides: A Combined TGA, TPD-MS, and DRIFTS study. *The Journal of Physical Chemistry C*, 2009, **113**(30), pp.13287-13299.
171. LEVASSEUR, B., A.M. EBRAHIM and T.J. BANDOSZ. Mesoporous silica SBA-15 modified with copper as an efficient NO<sub>2</sub> adsorbent at ambient conditions. *Journal of Colloid and Interface Science*, 2012, **377**(1), pp.347-354.
172. FLORENT, M., M. TOCCI and T.J. BANDOSZ. NO<sub>2</sub> adsorption at ambient temperature on urea-modified ordered mesoporous carbon. *Carbon*, 2013, **63**(0), pp.283-293.

173. KANTE, K., E. DELIYANNI and T.J. BANDOSZ. Interactions of NO<sub>2</sub> with activated carbons modified with cerium, lanthanum and sodium chlorides. *Journal of Hazardous Materials*, 2009, **165**(1–3), pp.704-713.
174. XU, L., J. GUO, F. JIN and H. ZENG. Removal of SO<sub>2</sub> from O<sub>2</sub>-containing flue gas by activated carbon fiber (ACF) impregnated with NH<sub>3</sub>. *Chemosphere*, 2006, **62**(5), pp.823-826.
175. ZHANG, W.J., S. RABIEI, A. BAGREEV, M.S. ZHUANG and F. RASOULI. Study of NO adsorption on activated carbons. *Applied Catalysis B: Environmental*, 2008, **83**(1–2), pp.63-71.
176. SHIRAHAMA, N., S.H. MOON, K.H. CHOI, T. ENJOJI, S. KAWANO, Y. KORAI, M. TANOURA and I. MOCHIDA. Mechanistic study on adsorption and reduction of NO<sub>2</sub> over activated carbon fibers. *Carbon*, 2002, **40**(14), pp.2605-2611.
177. KLOSE, W. and S. RINCÓN. Adsorption and reaction of NO on activated carbon in the presence of oxygen and water vapour. *Fuel*, 2007, **86**(1–2), pp.203-209.
178. CLAUDINO, A., J.L. SOARES, R.F.P.M. MOREIRA and H.J. JOSÉ. Adsorption equilibrium and breakthrough analysis for NO adsorption on activated carbons at low temperatures. *Carbon*, 2004, **42**(8–9), pp.1483-1490.
179. MOCHIDA, I., S. KISAMORI, M. HIRONAKA, S. KAWANO, Y. MATSUMURA and M. YOSHIKAWA. Oxidation of NO into NO<sub>2</sub> over active carbon fibers. *Energy and Fuels*, 1994, **8**(6), pp.1341-1344.
180. TENG, H. and E.M. SUUBERG. Chemisorption of nitric oxide on char. 1. Reversible nitric oxide sorption. *The Journal of Physical Chemistry*, 1993, **97**(2), pp.478-483.
181. X. H. XU, Y.S., S. H. LIU, H. P. WANG, AND S. G. CHANG. Method for the Control of NO<sub>x</sub> Emissions in Long-Range Space Travel. *Energy and Fuels*, 2003, **17**(5), pp.1303-1310.
182. NEATHERY, J.K., A.M. RUBEL and J.M. STENCEL. Uptake of NO<sub>x</sub> by activated carbons: bench-scale and pilot-plant testing. *Carbon*, 1997, **35**(9), pp.1321-1327.
183. LOZANO-CASTELLÓ, D., D. CAZORLA-AMORÓS, A. LINARES-SOLANO and D.F. QUINN. Influence of pore size distribution on methane storage at relatively low pressure: preparation of activated carbon with optimum pore size. *Carbon*, 2002, **40**(7), pp.989-1002.
184. ILLÁN-GÓMEZ, M.J., A. LINARES-SOLANO, C. SALINAS-MARTÍNEZ DE LECEA and J.M. CALO. NO reduction by activated carbons. 1. The role of carbon porosity and surface area. *Energy & Fuels*, 1993, **7**(1), pp.146-154.

185. GUO, Z., Y. XIE, I. HONG and J. KIM. Catalytic oxidation of NO to NO<sub>2</sub> on activated carbon. *Energy Conversion and Management*, 2001, **42**(15–17), pp.2005-2018.
186. RUIZ MACHADO W, A. and J. HALL P. Effects of porosity on carbon reactivity in NO and O<sub>2</sub>? *Energy & Fuels*, 1998, **12**(5), pp.958-962.
187. MOCHIDA, I., M. OGAKI, H. FUJITSU, Y. KOMATSUBARA and S. IDA. Reduction of nitric oxide with activated PAN fibres. *Fuel*, 1985, **64**(8), pp.1054-1057.
188. BEGOÑA RUBIO, M.T.I. Nitric Oxide Removal from Flue Gases by Carbon-enriched Coal Fly Ash. *Environmental Research, Engineering and Management*, 2013, **1**(63), pp.5-16.
189. KANEKO, K. Anomalous micropore filling of nitric oxide on .alpha.-iron hydroxide oxide-dispersed activated carbon fibers. *Langmuir*, 1987, **3**(3), pp.357-363.
190. ILLAN-GOMEZ, M.J., A. LINARES-SOLANO, C. SALINAS-MARTINEZ DE LECEA and J.M. CALO. Nitrogen oxide (NO) reduction by activated carbons. 1. The role of carbon porosity and surface area. *Energy & Fuels*, 1993, **7**(1), pp.146-154.
191. KONG, Y. and C.Y. CHA. NO<sub>x</sub> adsorption on char in presence of oxygen and moisture. *Carbon*, 1996, **34**(8), pp.1027-1033.
192. YANG, J., G. MESTL, D. HEREIN, R. SCHLÖGL and J. FIND. Reaction of NO with carbonaceous materials: 2. Effect of oxygen on the reaction of NO with ashless carbon black. *Carbon*, 2000, **38**(5), pp.729-740.
193. TENG, H. and E.M. SUUBERG. Chemisorption of nitric oxide on char. 1. Reversible nitric oxide sorption. *Journal of Physical Chemistry*, 1993, **97**(2), pp.478-483.
194. DEGROOT, W.F., T.H. OSTERHELD and G.N. RICHARDS. Chemisorption of oxygen and of nitric oxide on cellulosic chars. *Carbon*, 1991, **29**(2), pp.185-195.
195. SUZUKI, T., T. KYOTANI and A. TOMITA. Study on the carbon-nitric oxide reaction in the presence of oxygen. *Industrial and Engineering Chemistry Research*, 1994, **33**(11), pp.2840-2845.
196. MOCHIDA, I., Y. KORAI, M. SHIRAHAMA, S. KAWANO, T. HADA, Y. SEO, M. YOSHIKAWA and A. YASUTAKE. Removal of SO<sub>x</sub> and NO<sub>x</sub> over activated carbon fibers. *Carbon*, 2000, **38**(2), pp.227-239.

197. RICHTER, E., H.-J. SCHMIDT and H.-G. SCHECKER. Adsorption and catalytic reactions of NO and NH<sub>3</sub> on activated carbon. *Chemical Engineering and Technology*, 1990, **13**(5), pp.332-340.
198. ZHU, Z., Z. LIU, S. LIU and H. NIU. Adsorption and reduction of NO over activated coke at low temperature. *Fuel*, 2000, **79**(6), pp.651-658.
199. SHUANG-CHEN, M., J.J. YAO and L. GAO. Experimental study on removal of NO using adsorption of activated carbon/reduction decomposition of microwave heating. *Environ Technol*, 2012, **33**(13-15), pp.1811-7.
200. YIN, C.Y., M.K. AROUA and W.M.A.W. DAUD. Review of modifications of activated carbon for enhancing contaminant uptakes from aqueous solutions. *Separation and Purification Technology*, 2007, **52**(3), pp.403-415.
201. LEE, Y.-W., D.-K. CHOI and J.-W. PARK. Surface Chemical Characterization Using AES/SAM and ToF-SIMS on KOH-Impregnated Activated Carbon by Selective Adsorption of NO<sub>x</sub>. *Industrial & Engineering Chemistry Research*, 2001, **40**(15), pp.3337-3345.
202. ILLAN-GOMEZ, M.J., A. LINARES-SOLANO, L.R. RADOVIC and C. SALINAS-MARTINEZ DE LECEA. NO Reduction by Activated Carbons. 2. Catalytic Effect of Potassium. *Energy & Fuels*, 1995, **9**(1), pp.97-103.
203. LEE, Y.W., D.K. CHOI and J.W. PARK. Characteristics of NO<sub>x</sub> adsorption and surface chemistry on impregnated activated carbon. *Separation Science and Technology*, 2002, **37**(4), pp.937-956.
204. ZAWADZKI, J., M. WIŚNIEWSKI and K. SKOWROŃSKA. Heterogeneous reactions of NO<sub>2</sub> and NO–O<sub>2</sub> on the surface of carbons. *Carbon*, 2003, **41**(2), pp.235-246.
205. MOCHIDA, I., N. SHIRAHAMA, S. KAWANO, Y. KORAI, A. YASUTAKE, M. TANOURA, S. FUJII and M. YOSHIKAWA. NO oxidation over activated carbon fiber (ACF). Part 1. Extended kinetics over a pitch based ACF of very large surface area. *Fuel*, 2000, **79**(14), pp.1713-1723.
206. RATHORE, R.S., D.K. SRIVASTAVA, A.K. AGARWAL and N. VERMA. Development of surface functionalized activated carbon fiber for control of NO and particulate matter. *Journal of Hazardous Materials*, 2010, **173**(1–3), pp.211-222.
207. ZHANG, Z., J.D. ATKINSON, B. JIANG, M.J. ROOD and Z. YAN. Nitric oxide oxidation catalyzed by microporous activated carbon fiber cloth: An updated reaction mechanism. *Applied Catalysis B: Environmental*, 2014, **148–149**, pp.573-581.

## CHAPTER 3. METHODOLOGY

---

This chapter presents a description of the investigated waste materials and the experimental procedure used to prepare the chars and the activated carbons. The techniques used to characterize the materials and to analyse the products derived from the experiments are presented. Additionally, the procedure used to investigate the catalytic performance of the prepared materials for NO adsorption and tar cracking is also discussed. A two stage fixed bed reactor was used to carry out biomass gasification experiments. A fixed bed reactor connected to a Horiba on-line gas analyser was used to perform NO adsorption experiments.

The Methodology is divided into two parts;

Section 3.1; Part of this work was devoted to the preparation of chars and activated carbons from waste materials to be investigated for the tar cracking and NO adsorption experiments respectively. Activated carbons were tested for NO adsorption at low temperature. From the results obtained from these experiments, comparisons were made between the activated carbons in terms of their physical, chemical structure and NO removal efficiency.

Section 3.2; Gasification experiments of biomass using a two stage fixed bed reactor were performed with the use of chars as a catalyst for tar cracking. Comparisons were made between the three types of chars, syngas composition and tar reduction efficiency. A synopsis of the sequence of the experimental programme is schematically displayed in Figure 3.1.

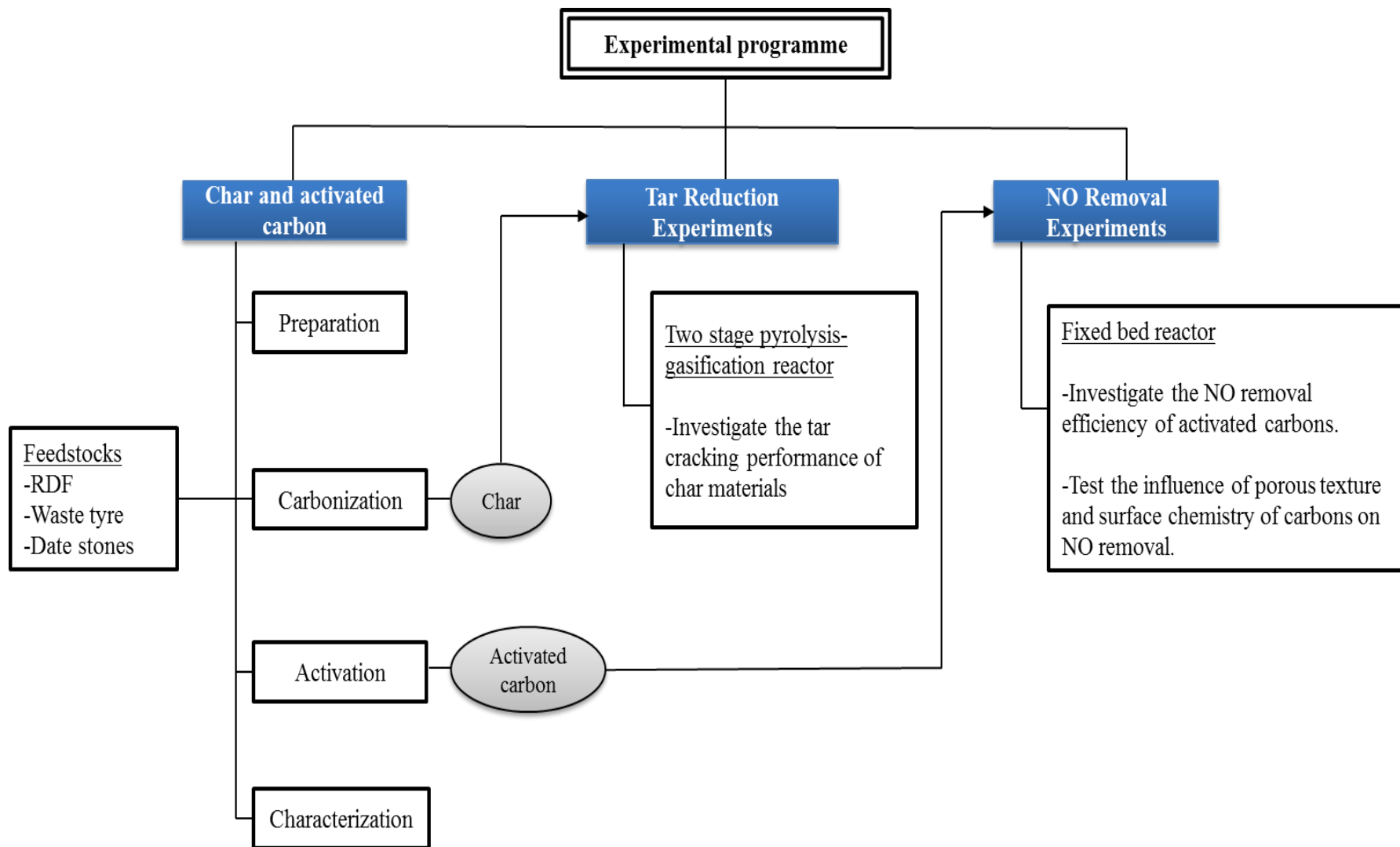


Figure 3.1. A synopsis of the sequence of the experimental programme

### **3.1 NO Adsorption Performance on the Activated carbons**

The main aim of this experimental investigation was to study the effectiveness of activated carbon produced from waste materials for NO removal. This section presents a description of the experimental procedure using a fixed bed reactor under which the reactions between activated carbons and NO took place, followed by a description of the gas analyser.

#### **3.1.1 Materials**

##### **3.1.1.1 Refuse derived fuel (RDF)**

About 85% of the un-segregated MSW is mainly organic which can be further processed by removing of non-combustible and low calorific materials to produce a refuse derived fuel (RDF) of higher calorific value, consisting of paper, plastics, textiles and other combustible materials. The processed RDF pellets had a calorific value of 18.0 MJ kg<sup>-1</sup>, while the raw MSW waste has a typical calorific value of 9.1 MJ kg<sup>-1</sup> [1]. Therefore, RDF was selected in this work to represent municipal solid waste with the elimination of recyclable materials such as metals and glass.

The RDF sample was carefully prepared from 2 kg of RDF and was mixed, coned and quartered and further shredded to enhance homogeneity. The RDF used in this study was in the form of pellets with 40 mm length and 20 mm diameter (Figure 3.1-1), obtained from a United Kingdom municipal waste treatment plant. The sample was shredded to get samples with a particle size of 8 mm to be used for the pyrolysis experiments. The proximate analysis of the RDF gave 72.0 wt.% volatiles, 5.0 wt.% moisture, 13.0 wt.% fixed carbon and 11.0 wt.% ash. Elemental analysis of the RDF sample gave 47.5 wt.% carbon, 5.8 wt.% hydrogen and 0.8 wt.% nitrogen. The solid composition of RDF is diverse; therefore slight variations in some parameters might be observed when comparing RDF samples from different sources.

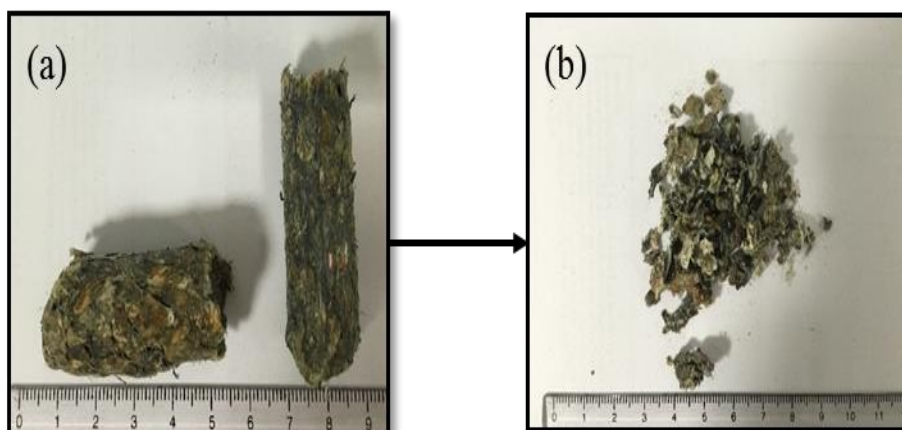


Figure 3.1-1. RDF sample (a) original pellets (b) shredded samples

### 3.1.1.2 Waste tyre

Shredded car passenger tyres of particle size of 1.7 mm were used in this work. The sample was prepared by removing the steel followed by shredding and sieving. The proximate analysis of waste tyre gave 62.2 wt.% volatiles, 1.3 wt.% moisture, 29.4 wt.% fixed carbon and 7.1 wt.% ash. Elemental analysis of the waste tyre gave 81.2 wt.% carbon, 7.2 wt.% hydrogen, 2.6 wt.% sulphur and 0.5 wt.% nitrogen.

### 3.1.1.3 Date stones

Date stones are one of the most available agricultural by-products in date palm growing countries including Oman which is considered as one of the top ten date-producing countries with an average annual production of 260,000 million tonnes [2]. Date stones were composed of 5-10 wt.% moisture, 55-56 wt.% carbohydrates, 5-7 wt.% protein, 7-10 wt.% oil, 10-20 wt.% crude fibre and 1-2 wt.% ash [3].

Thus, to utilize this abundant and cheap waste, date stones were used as the raw material to produce low-cost adsorbent. The date stones used in this study were obtained from Oman and were thoroughly cleaned with water and were sun-dried for 24 hours. The date stones as received of particle size of 30 mm were shredded and ground and sieved to obtain samples with a particle size of 8 mm (Figure 3.1-2).

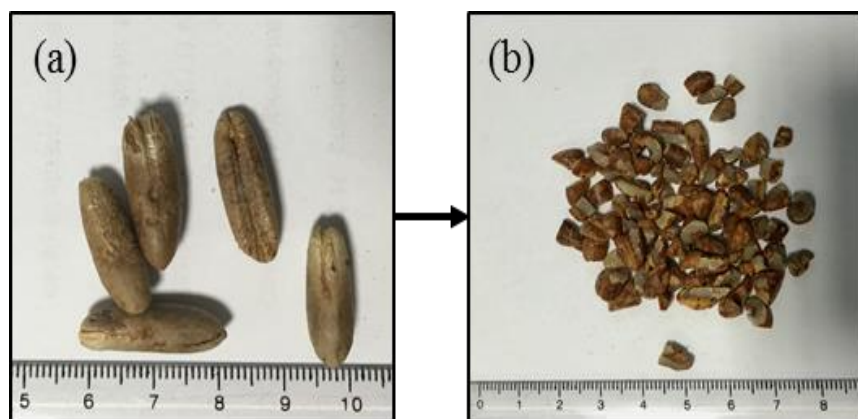


Figure 3.1-2. Date stones sample (a) original pellets (b) shredded samples

#### **3.1.1.4 Commercial activated carbons**

Four different commercial carbons (labelled C-AC1, C-AC2, C-AC3 and C-AC4) with different characteristics and porosity were used in this work and were obtained from Norit Ltd., Netherlands. The carbons were of particle size 0.15-3 mm. The NO removal efficiency of these carbons was compared to the waste derived activated carbons in chapter 4.

#### **3.1.2 Acid Demineralization**

The metallic mineral contents of tyre char might affect NO sorption. Therefore, to investigate the influence of the carbons mineral contents on NO capture, activated carbon produced from waste tyre was demineralized using 5% HCl to reduce its ash content. For this purpose, 20 ml of (5M) HCl was added to 1 g of tyre char followed by boiling the mixture for 20 minutes. Then, the char was washed several times with deionized water until the pH was 7, finally the demineralized tyre char was dried at 105 °C for 24 hours to ensure that almost all of the acid had been removed either from the washing step or evaporated in the furnace. Relevant results are reported in Chapter 4, Section 4.1.4

### 3.1.3 Production of chars

Three different waste materials, waste tyre, RDF and date stones were used to produce pyrolysis chars. Pyrolysis of the waste materials was carried out in a fixed bed reactor, 250 mm in length by 30 mm internal diameter. A schematic diagram of the reactor is shown in Figure 3.1-3. The reactor was fully instrumented in terms of gas flow control, furnace temperature control and temperature monitoring throughout. The waste (10 g) was held in a stainless steel sample crucible in the reactor and heated to final temperatures of 600 °C at a heating rate of 10 °C min<sup>-1</sup> and held at the final temperature for one hour. A slow heating rate of 10 °C min<sup>-1</sup> was chosen for char production, as lower heating rates have been reported to produce high yield of chars [1, 4-5]. Nitrogen with a flow rate of 200 ml min<sup>-1</sup> was used as the carrier gas to provide an inert atmosphere and to purge the evolved pyrolysis gases from the hot reactor and also to minimize any secondary reactions of the gases such as thermal cracking, recondensation and repolymerisation [6-7]. According to Katyal et al. [6], the presence of an inert purge gas during the slow pyrolysis of municipal solid waste minimized the secondary reactions of the evolved volatiles from the slow pyrolysis of municipal solid waste. A condenser system consisting of a water-cooled condenser and two dry ice-cooled condensers was used to trap the condensable liquids. The third condenser was packed with a glass wool to further trap any oil mist. A Dreschel bottle filled with de-ionised water, located after the final condenser, was used to dissolve any water soluble gases evolve from the experiment. At the end of the pyrolysis experiment, the furnace was allowed to cool down under nitrogen to room temperature. The char was then collected, weighed, ground and sieved to 1.5-2 mm particle size and dried at a temperature of 105 °C overnight. Repeat experiments were carried out to ensure the stability of the reactor and reproducibility of results and to obtain sufficient char amount for the subsequent experimental work.

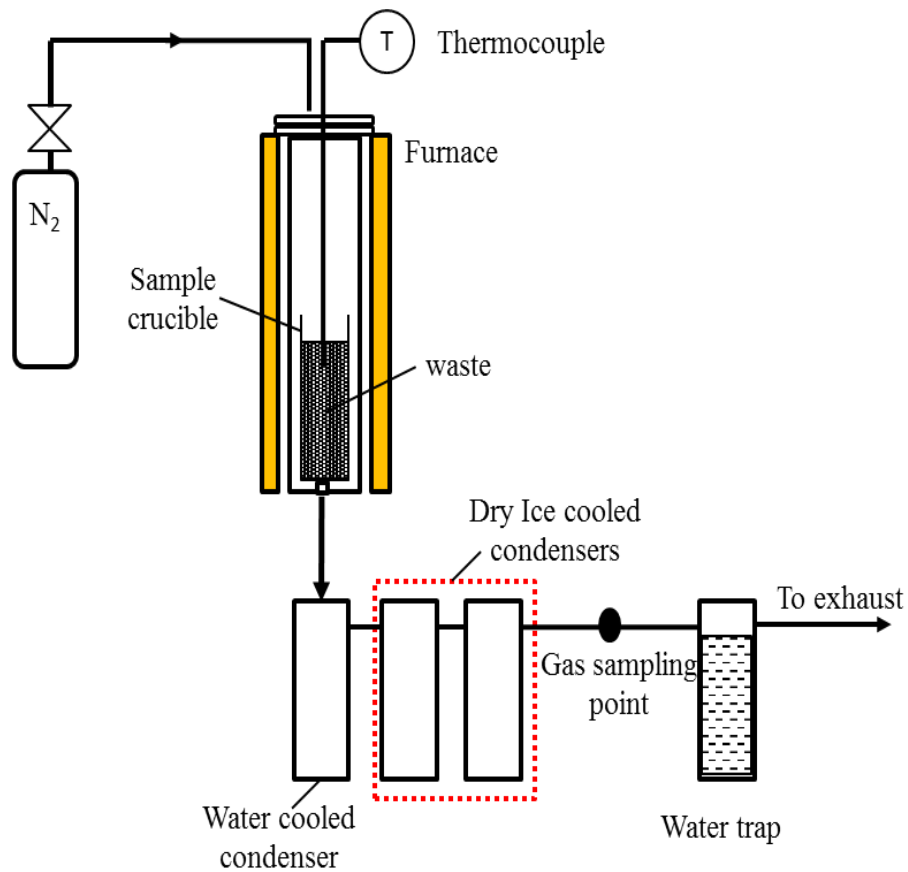


Figure 3.1-3. Schematic diagram of the waste pyrolysis reactor.

### 3.1.3.1 Repeatability of the pyrolysis procedure

The pyrolysis process was repeated five times to ensure the stability of the reactor and the consistency of the results. The yield of products from the pyrolysis of RDF and tyre at a pyrolysis temperature of 600 °C and holding time of 1 hour are presented in Table 3.1-1. The pyrolysis was repeated five times for each raw material, and repeatability was assessed according to the pyrolysis yield products. The descriptive statistics of the results showed good repeatability of the products.

Table 3.1-1. Repeatability of pyrolysis products

| Repeatable Parameters | RDF char              |       |       |       |       |       |                    |                       |  |
|-----------------------|-----------------------|-------|-------|-------|-------|-------|--------------------|-----------------------|--|
|                       | Pyrolysis Experiments |       |       |       |       | Mean  | SD                 | RSD (%)               |  |
|                       | 1                     | 2     | 3     | 4     | 5     |       |                    |                       |  |
| Char (wt.%)           | 30.70                 | 31.18 | 31.49 | 30.80 | 29.20 | 30.67 | 0.88               | 2.87                  |  |
| Liquid (wt.%)         | 54.30                 | 54.41 | 53.90 | 53.90 | 52.70 | 53.84 | 0.67               | 1.26                  |  |
| Gas (wt.%)            | 14.90                 | 14.41 | 14.60 | 15.30 | 15.01 | 15.46 | 0.34               | 2.35                  |  |
| Mass Balance          | 99.9                  | 100.0 | 99.9  | 100.0 | 96.9  | 99.35 | 1.37               | 1.38                  |  |
| Repeatable Parameters | Tyre char             |       |       |       |       |       |                    |                       |  |
|                       | Pyrolysis Experiments |       |       |       |       | Mean  | Standard Deviation | Relative Std. Dev (%) |  |
|                       | 1                     | 2     | 3     | 4     | 5     |       |                    |                       |  |
| Char (wt.%)           | 37.00                 | 36.80 | 38.00 | 36.90 | 35.40 | 36.82 | 0.93               | 2.50                  |  |
| Liquid (wt.%)         | 55.30                 | 54.40 | 54.20 | 56.70 | 56.10 | 55.34 | 1.07               | 1.94                  |  |
| Gas*(wt.%)            | 7.70                  | 7.80  | 7.80  | 7.50  | 7.40  | 7.64  | 0.18               | 2.38                  |  |
| Mass Balance          | 100.0                 | 99.0  | 100.0 | 101.0 | 98.9  | 99.8  | 0.86               | 0.86                  |  |

\* Calculated according to equations 3.17 and 3.18 (see page 104).

### **3.1.4 Production of activated carbons**

The influence of the activated carbon preparation process on the properties the derived carbons and the consequent influence on NO removal was investigated. Therefore, waste derived chars were activated via two different methods, physical activation with steam and chemical activation with alkali chemical agents. Chemical activation was performed for tyre char only, which was carried out to assess the influence of porous texture on NO removal.

#### **3.1.4.1 Physical activation**

The chars recovered from the pyrolysis reactor were ground and sieved to 1.5-2 mm and dried at a temperature of 105 °C overnight and then activated in steam in the pyrolysis reactor which was adapted to incorporate steam injection by the addition of preheater at the inlet to provide steam required to activate chars as presented in Figure 3.1-4. During the activation process the char samples (7g), obtained from the pyrolysis temperature of 600 °C, were placed in the reactor and were heated at a heating rate of 20 °C min<sup>-1</sup> to the activation temperature of 900 °C. Once the activation temperature was reached, the deionised was introduced into the nitrogen and then into a preheater maintained at 300 °C to generate steam as the activating agent.

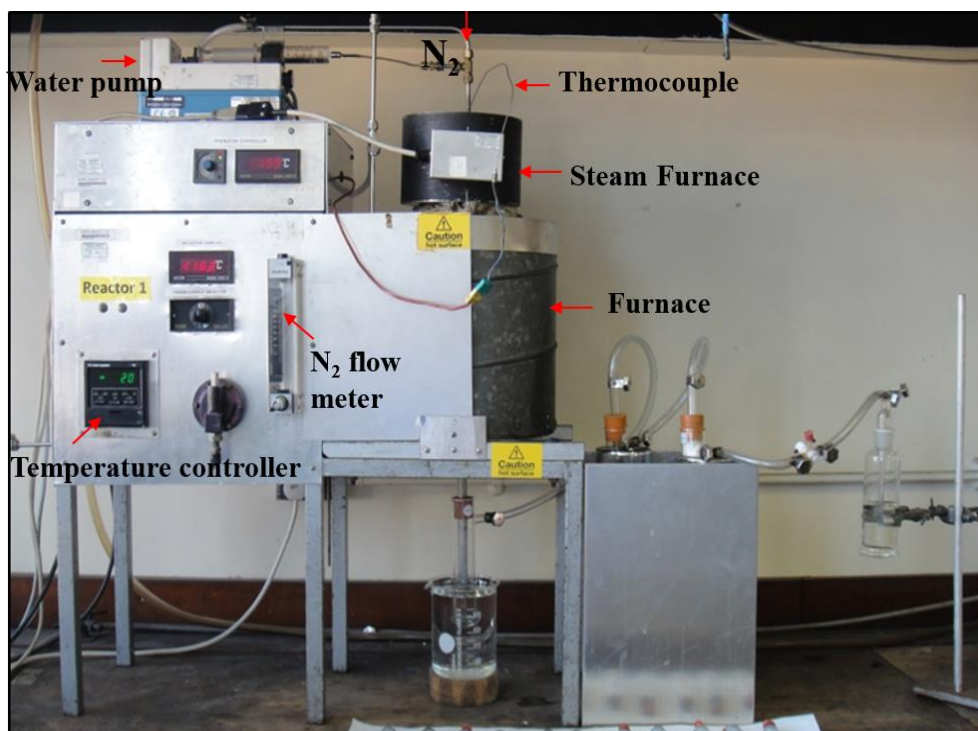


Figure 3.1-4. Photograph of the activation reactor.

A syringe pump was used to introduce the deionised water for a period of 3 hours. Nitrogen with a flow rate of  $200 \text{ ml min}^{-1}$  was used to purge the air from the system. A schematic diagram of the activation reactor is shown in Figure 3.1-5.

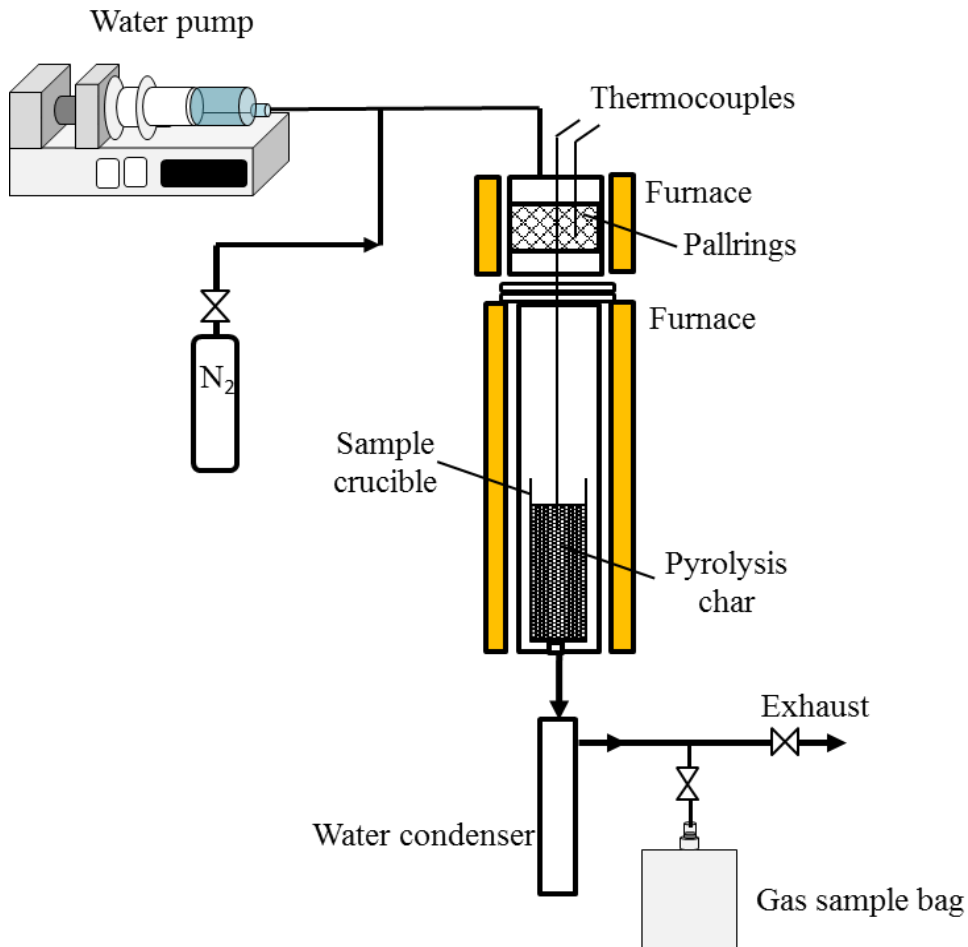


Figure 3.1-5. Schematic diagram of the char activation reactor

The repeatability of the activation procedure was assessed in terms of activated carbon yield, burn-off and surface area. Therefore, the activation of RDF chars, obtained at a pyrolysis temperature of 600 °C, in steam at 900 °C was repeated three times. The results presented in Table 3.1-2 showed good repeatability. From the results presented in Table 3.1-2, excellent repeatability was obtained with a very low relative standard deviation. The burn-off of the resultant activated carbon and the yield of carbon were obtained according to the following equations:

$$\text{Burn - off (w)} = \frac{w_1 - w_2}{w_1} \times 100\% \quad (3.1)$$

Where, W1 is the mass of char on a dry ash free basis, and W2 is the mass of carbon after activation on a dry basis.

$$\text{Yield (Y)} = \frac{W_2}{W_1} \times 100\% \quad (3.2)$$

Where, W1 is the initial dry mass of char (g), and W2 is the mass of carbon (g) after activation (g).

Table 3.1-2. Repeatability of the physical activation procedure.

| Activation experiments | RDF Activated carbon |                    |   |
|------------------------|----------------------|--------------------|---|
|                        | Yield<br>(wt.%)      | Burn-off<br>(wt.%) | Surface area<br>(m <sup>2</sup> g <sup>-1</sup> ) |
| 1                      | 61.25                | 57.23              | 337.91  |
| 2                      | 60.00                | 58.28              | 340.32  |
| 3                      | 62.25                | 56.53              | 341.51  |
| Mean                   | 61.17                | 57.35              | 339.91  |
| SD                     | 1.13                 | 0.88               | 1.83  |
| RSD (%)                | 1.84                 | 1.54               | 0.54  |

### 3.1.4.2 Chemical activation

Chemical activation was performed for tyre char only according to the procedure reported by Fierro et al. [8], where the char is physically mixed with the chemical agent. This chemical activation procedure has been found to lead to a higher BET surface area of the resulting activated carbons [9-10]. Also, this procedure was preferred to the wet impregnation procedure to avoid the preliminary carbonation of KOH with CO<sub>2</sub> from the atmosphere as reported by Illingworth [11].

Therefore, the activated carbons were prepared by pyrolysis followed by chemical activation with alkali metals. The char was subjected to chemical activation with the use of KOH, K<sub>2</sub>CO<sub>3</sub>, NaOH and Na<sub>2</sub>CO<sub>3</sub> as the activating agents. The char was physically mixed with the alkali chemical agent with a weight ratio of 1:3. The influence of the chemical impregnation ratio was also investigated using KOH, where char was physically mixed with KOH with various weight ratios (0.5, 1, 3 and 4:1). All the activations took place at an activation temperature of 900 °C. Additionally, the influence of varying the activation temperature on the porous texture of the final

product was tested. Char was mixed with a 1:3 weight ratio of KOH and activated at 700, 800 and 900 °C for 3 hours under nitrogen.

The activation process for the chemically impregnated char samples involved heating the char under nitrogen at a heating rate of 20 °C min<sup>-1</sup> to the final activation temperature. After the activation, the carbons were cooled under N<sub>2</sub>, and then washed first with 1 M HCl and later with distilled water until the pH of the washed solution was about 7. Finally, the washed samples were dried at 105 °C overnight.

### **3.1.5 Analysis of the raw materials, chars and activated carbons**

#### **3.1.5.1 Ultimate analysis**

The elemental analysis of the raw materials and their representative chars and activated carbons was carried out using an elemental analyser (Flash EA2000). A schematic diagram of the instrument is presented in Figure 3.1-6. About 2.5-3 mg of sample is weighed and sealed in a tin capsule. Each sample was prepared in duplicate. The tin capsules were then placed into an auto-sampler and introduced into a combustion chamber maintained at 900-1000 °C. Then a fixed amount of oxygen was injected into the combustion chamber via a helium carrier gas. Once the capsules react with the oxygen, an exothermic reaction is generated which results in increasing the temperature to 1800 °C causing the oxidation of the sample. The combustion gaseous products were then swept through the reduction chamber, where H<sub>2</sub>O, NO<sub>2</sub>, CO<sub>2</sub> and SO<sub>2</sub> are formed. The gases were then separated in a chromatography column and detected by thermal conductivity detector (TCD), which is calibrated via standards with known elemental composition. Gases were then converted into weight percentages of hydrogen (H), nitrogen (N), carbon (C), and sulphur (S) via computer software.

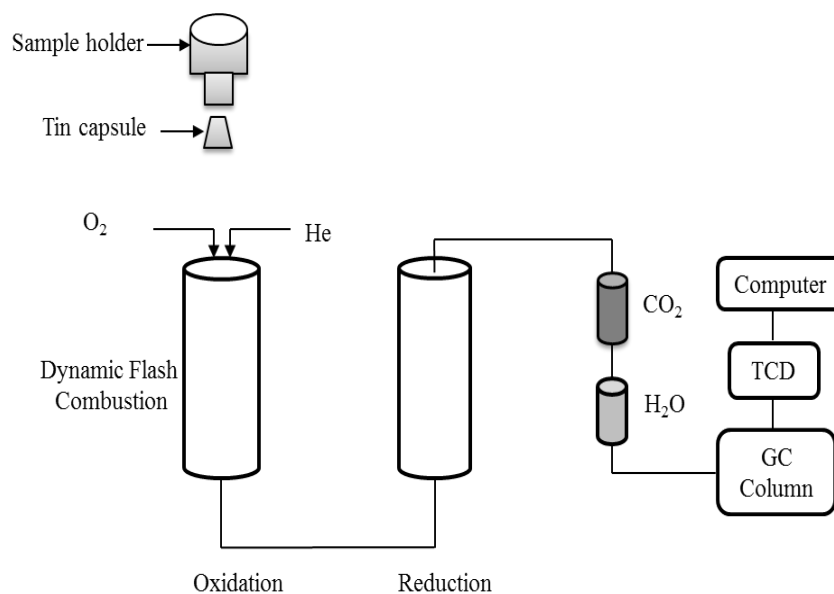


Figure 3.1-6. Schematic diagram of the Flash EA2000 Elemental analyser.

### 3.1.5.2 Proximate analysis

The proximate analysis of the samples was carried out using a Shimadzu TGA-50H thermogravimetric analyser to obtain a measure of the moisture, fixed carbon, volatile matter and ash content of the raw samples, chars and activated carbons. The analysis was carried out in three stages. In the first stage, the sample was heated under nitrogen to a temperature of 110 °C and held at this temperature for 10 minutes. The weight loss that occurred during this stage corresponds to the moisture content of the sample. Then in the second stage, the sample was heated to 900 °C and held for 15 minutes. The weight loss occurring during this stage represents the weight of the volatile content. Finally, and after the sample had been heated to 900 °C, air was used instead of nitrogen to burn-off the fixed carbon leaving the ash in the aluminium pan. An example of thermogram for the proximate analysis of RDF is shown in Figure 3.1-7.

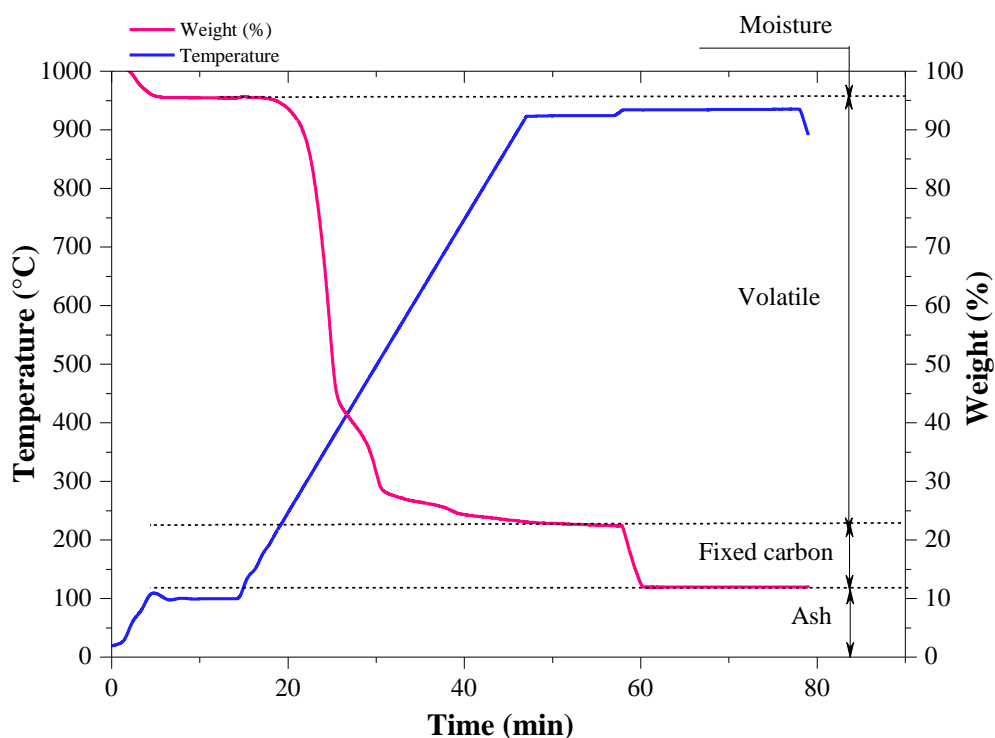


Figure 3.1-7. A TGA Thermogram for the proximate analysis of RDF.

### 3.1.5.3 Scanning Electron Microscope (SEM) and Energy-Dispersive X-ray spectroscopy (EDXS)

A SEM LEO 1530 high-resolution scanning electron microscope (SEM) coupled to an energy-dispersive X-ray spectroscope (EDXS) was used to characterize and examine the surface morphology of the prepared carbons with EDXS providing an indication of the metal content of the carbons. The main components of the SEM are an electron gun, lenses, sample chamber and detector. The microscope was operated at a working distance of 8 to 9 mm and an accelerating voltage of 25 kV. The samples were coated with a 30.0 nm layer of gold using an Emscope SC500 specimen vacuum gold coater at 20 mA to improve the charge dissipation. The samples were then placed on the specimen stand and analysed. An example of a SEM-EDXS for tyre activated carbon is presented in Figure 3.1-8.

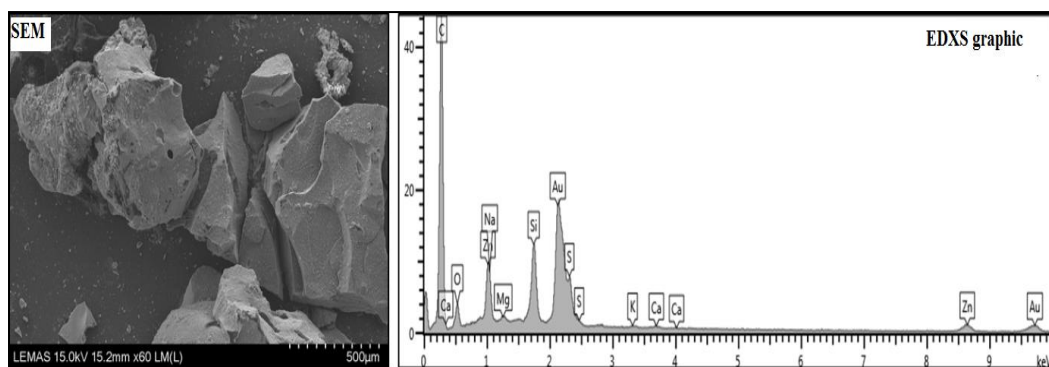


Figure 3.1-8. SEM-EDXS results for tyre char activated carbon.

A semi-quantitative analysis of the inorganic components of selected chars and activated carbons samples was conducted using EDXS. The EDXS technique depends on the detection of X-ray energy emitted when the inner shell electrons are displaced by an incident beam of electrons interacting with the sample. Each element emits a specific X-ray energy. A semi-conductor detector is used to detect the X-ray according to its energy. The energy from the X-rays is converted into pulses of current proportional to the photon energy by a lithium drifted silicon crystal disc. Aztec software was used to obtain EDXS spectra and to determine the elemental composition. The energy peaks appearing in the EDX spectra correspond to various elements in the sample.

#### 3.1.5.4 Boehm titration

The Boehm titration method was used to determine the acidic and basic oxygen groups of the commercial and waste derived activated carbons. The basic sites were determined by mixing 1g of activated carbon with 50 ml of 0.05 M HCl in a closed flask and shaken for 24 hours. The solution was then filtered, and an aliquot of 5 ml was taken and titrated with 0.05 M NaOH. The acidic groups were determined by a similar procedure, where activated carbon was mixed with 0.05 M NaOH and the titrant solution was 0.05 HCl. The amounts of acidic and basic groups were calculated as shown in equations (3.3) and (3.4) respectively.

$$\text{Acidic groups (mmol/g)} = \frac{[\text{NaOH}] \cdot V_{\text{NaOH,mix}} - ([\text{HCl}] \cdot V_{\text{HCl,cons}})}{m_{\text{carbon}}} \quad (3.3)$$

$$\text{Basic groups (mmol/g)} = \frac{[\text{HCl}] \cdot V_{\text{HCl,mix}} - ([\text{NaOH}] \cdot V_{\text{NaOH,cons}})}{m_{\text{carbon}}} \quad (3.4)$$

### 3.1.5.5 Fourier Transform Infrared spectrometry (FTIR)

Fourier Transform Infrared spectrometry (FTIR) is a technique used to determine the different functional groups present in solid or an organic liquid by absorbing infrared spectra light across a wide range of wavelengths. The technique was used to identify the NO adsorbed species formed on the carbon surface after the NO adsorption tests. FTIR spectra of the activated carbons were determined using a Thermo Nicolet Corporation iS10 (Thermo Scientific), over a wave number range of 4000-600  $\text{cm}^{-1}$ . IR spectrum consists of the wave number ( $\text{cm}^{-1}$ ) against intensity (% transmittance or absorbance). A detailed description of this technique can be found elsewhere [12].

### 3.1.5.6 Metal analysis

The presence of metals are known to influence the catalytic properties of carbons; therefore the metal content of the waste samples was determined since these will end up in the product carbon. A semi-quantitative analysis of the raw material samples (RDF, tyre and date stones) was carried out using a Thermo Advant XP X-ray fluorescence (XRF) spectrometer. The device was equipped with a Rh source. The samples were prepared as fused beads to provide a homogenous sample. The three waste materials were ashed in a furnace at 550  $^{\circ}\text{C}$  for several hours. A lithium borate flux was added to the ash and heated to 900  $^{\circ}\text{C}$  in a platinum crucible and then cast into a mould with a flat bottom. The resultant fused bead was presented to the XRF spectrometer for analysis. The fused bead was analysed using OXSAS programme. As both waste tyre and RDF had high ash content, therefore it was worth carrying out a quantitative analysis of these two samples. Therefore, mineral matter characterization was performed using a Varian Fast Sequential Atomic Absorption Spectrophotometer (Varian AA240FS). The waste sample was converted to ash, and the ash was subsequently dissolved in a concentrated solution of nitric acid; 0.1 g of ash was

digested with 10 ml HNO<sub>3</sub> at 240 °C. The samples were prepared in duplicate. Table 3.1-3 shows the metal contents of Tyre and RDF waste raw materials.

Table 3.1-3. Metals composition of tyre and RDF waste raw materials.

| Element<br>(wt.%) | Tyre  |       |         | RDF   |       |         |
|-------------------|-------|-------|---------|-------|-------|---------|
|                   | 1     | 2     | Average | 1     | 2     | Average |
| Ca                | 0.200 | 0.203 | 0.202   | 1.258 | 1.414 | 1.336   |
| Zn                | 2.560 | 2.575 | 2.568   | 0.033 | 0.033 | 0.033   |
| K                 | 0.037 | 0.033 | 0.035   | 0.152 | 0.176 | 0.164   |
| Fe                | 0.081 | 0.095 | 0.088   | 0.214 | 0.164 | 0.189   |
| Cu                | 0.010 | 0.010 | 0.010   | 0.000 | 0.000 | 0.000   |
| Al                | 0.032 | 0.033 | 0.032   | 1.447 | 1.213 | 1.330   |
| Na                | 0.025 | 0.024 | 0.025   | 0.165 | 0.154 | 0.159   |

### 3.1.5.7 Pore structure characterization

The BET surface area and porosity parameters of the chars and activated carbons were determined from the measurements of nitrogen adsorption-desorption at 77 K with the use of a Nova gas analyser (Figure 3.1-9).

The physical gas adsorption is usually the technique used to analyse the pore characteristics of materials which is based on the determination of the amount of gas adsorbed into a solid sample. The adsorption isotherm results from the physical adsorption of gas and provides the required information for determining the BET surface area, pore volumes and pore size distribution [13].



Figure 3.1-9. QuantaChrome NOVA 2200e.

The measurements are based on the static volumetric principle, which consists of admitting known amounts of nitrogen, as adsorptive gas, to the sample, which is kept at liquid nitrogen temperature (77 K). The solid then adsorbs some of the admitted gas, thus implying a variation in gas pressure inside the sample cell, which will change until equilibrium occurs. However, if equilibrium is not reached, another dose of gas is applied. Once equilibrium is reached, the quantity of gas adsorbed is then calculated as the difference between the amount of gas admitted and the amount of gas filling the dead space (i.e. space not occupied by the solid material) at the equilibrium pressure [13]. The plot of the amount of gas adsorbed/desorbed onto/from a sample against the relative pressure is called the adsorption isotherm at a constant temperature (77 K). The determination of the adsorption/desorption isotherm is useful to identify the structure of the analysed solid material. The samples were prepared for analysis, i.e.,

about 0.1 g of the char or activated carbon samples were degassed under vacuum for 3 hours at a temperature of 300 °C for the purpose of removing the moisture and the adsorbed molecules from the surface of the adsorbent. To do this, the sample cell was placed inside a heating mantle, which was connected to a temperature controller. The degassing conditions depended upon the type of sample analysed.

### 3.1.5.7.1 Determination of BET surface area by Brunauer-Emmer-Teller (BET) method

The surface area of chars and activated carbons were determined using the BET method. The method of Brunauer, Emmett and Teller (BET) is the most accepted method for the calculation of surface area of solid materials. Two stages are involved in the determination of surface area according to the BET method. Firstly, the BET monolayer capacity ( $W_m$ ) from the BET plot is determined. In the second stage, the BET area is calculated from  $W_m$  and the cross-sectional area occupied by the adsorbate molecule in the complete monolayer [14-15]. The BET equation used for the calculation of surface area can be expressed as (3.5):

$$\frac{1}{W \cdot \left(\frac{P_0}{P} - 1\right)} = \frac{1}{W_m \cdot C} + \frac{C - 1}{W_m \cdot C} \left(\frac{P}{P_0}\right) \quad (3.5)$$

Where,  $W$  is the amount of gas adsorbed at a relative pressure ( $P/P_0$ ),  $P_0$  is the saturated vapour pressure of nitrogen,  $P$  is the absolute pressure of adsorbate (i.e. nitrogen),  $W_m$  is the weight of adsorbate of monolayer formed over the surface of the adsorbent, and  $C$  is the BET constant which is related to the strength of interaction between gas and solid.

The plot of  $P/P_0$  vs  $1/[W (P_0/P)-1]$  should yield a straight line normally in the  $P/P_0$  range of 0.05 to 0.35. A sample BET plot for tyre char is shown in Figure 3.1-10.

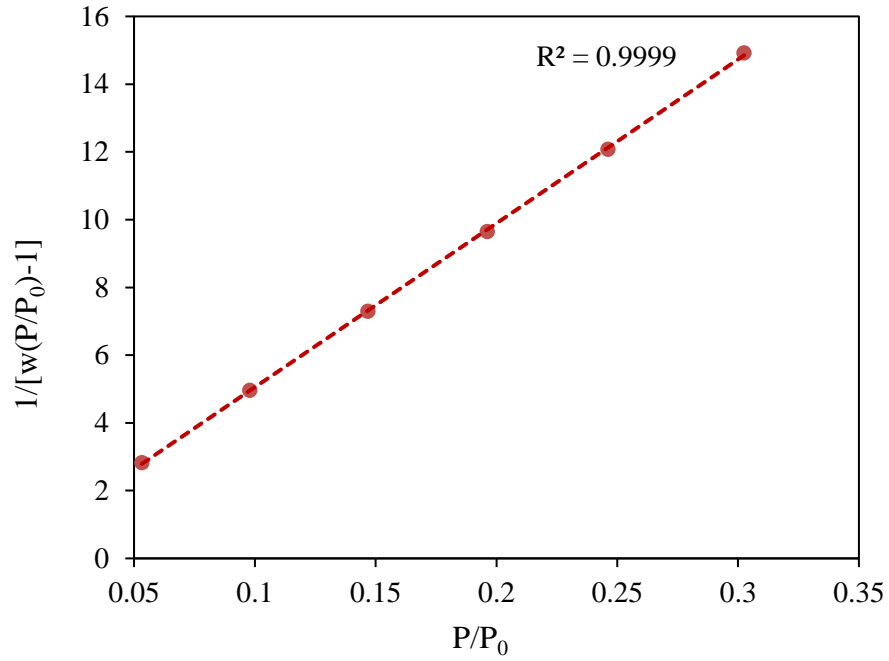


Figure 3.1-10. Sample BET Plots for tyre char

The weight of adsorbate monolayer ( $W_m$ ) can be then calculated from the slope ( $S$ ) and intercept ( $I$ ) of the BET plot by solving the following equations (3.6) and (3.7).

$$S = \frac{C - 1}{W_m \cdot C} \quad (3.6)$$

$$I = \frac{1}{W_m \cdot C} \quad (3.7)$$

Then  $W_m$  can be expressed as:

$$W_m = \frac{1}{S + I} \quad (3.8)$$

Thus, the total surface area ( $S_t$ ) can be calculated based on the following equation

$$S_t = \frac{W_m \cdot N \cdot A_{CS}}{M} \quad (3.9)$$

Where N is the Avogadro's number,  $A_{CS}$  is the cross-sectional area of the adsorbate, which is 16.2 m<sup>2</sup> for nitrogen, and M is the molecular weight of the adsorbate (28 g.mol<sup>-1</sup> for Nitrogen). The specific surface area (S) in m<sup>2</sup> g<sup>-1</sup> can then be obtained from the total surface area ( $S_t$ ) and the sample weight ( $W_s$ ) as follows [16]:

$$S = \frac{S_t}{W_s} \quad (3.10)$$

### **3.1.5.7.2 Determination of mesopore volume (BJH) method**

The method of Barrett, Joyner, and Halenda (BJH) is used to calculate the mesopore size based on the assumption that the pores have a cylindrical shape and the pore radius is given by the kelvin radius plus the thickness of the adsorbate layer which is adsorbed onto the pore walls prior to condensation during adsorption or which remains on pore walls after evaporation during desorption. The BJH model was applied to the desorption leg of the N<sub>2</sub> isotherm, in particular for relative pressure (P/P<sub>0</sub>) in the range of 0.4 to 0.96 [17].

### **3.1.5.7.3 Determination of micropore volume – Dubinin-Radushkevich (DR) method**

The micropore volume of chars and activated carbons was determined using the Dubinin Radushkevich method which is based on the Polanyi potential theory of adsorption. Dubinin proposed that in very fine pores the adsorption occurs through pore filling from the smallest to the largest pores rather than the adsorption via layers and there is an adsorption potential into which adsorbate molecules falls. Dubinin and Radushkevich assumed that the volume filled by liquid adsorbate at various adsorption potentials can be expressed as [16]:

$$V = V_0 \exp \left[ - \left( \frac{A}{\beta E_0} \right)^2 \right] \quad (3.11)$$

Where A is the adsorption potential and is given by the equation (3.12)

$$A = RT \ln \left( \frac{P_0}{P} \right) \quad (3.12)$$

V is the adsorption volume of the liquid adsorbate,  $V_0$  is the micropore volume,  $E_0$  represents the characteristic energy of adsorption, and  $\beta$  is the affinity coefficient which can be determined by the liquid molar volume of a given adsorbate and benzene (used as the reference liquid) as in equation (3.13) [16]

$$\beta = \frac{V}{V_{C_6H_6}} \quad (3.13)$$

After substituting for E in Eq 3.11 from Eq 3.12, the Dubinin Radushkevich equation can then be written in logarithmic form as:

$$\log V = \log V_0 - 2.302 \left( \frac{RT}{\beta E_0} \right)^2 \log(P_0/P)^2 \quad (3.14)$$

A plot of the logarithm of the amount adsorbed ( $\log V_{ads}$ ) versus the square of adsorption potential  $\log [(P_0/P)^2]$  should give a straight line. The micropore volume ( $V_0$ ) and energy of adsorption ( $E_0$ ) can be then calculated from the intercept ( $\log V_0$ ) and the slope  $(-RT/E)^2$  respectively.

#### 3.1.5.7.4 Pore size distribution by Density Functional Theory (DFT)

Density functional method was applied for the determination of the pore size distribution from the adsorption isotherms. This method provides a microscopic

description of fluids (i.e. the liquid adsorbate) in confined pores which allows obtaining a more accurate analysis of narrow micro and mesopores. Additionally, compared to the methods based on the thermodynamic and macroscopic approaches, such as the DR and BJH methods which are applicable for a certain pore size analysis and do not provide a description of the filling of micropores and narrow mesopores, this method determines the distribution of pore sizes over both micropore and mesopore size ranges [15].

### 3.1.6 Analysis of Gaseous Products

All the gases collected from the experiments carried out in this research work were analysed as described below in sections 3.1.6.2 and 3.1.6.3. The gaseous products collected in the gas bag were analysed off-line by packed column chromatography. The gas chromatograph consists of several components including, injection port, carrier gas, column, oven and detector. A microsyringe is used to introduce the sample through a rubber septum and into the vaporization chamber. A carrier gas is used to transport the analytes through the column. The sample is separated into its components in the column based on the strength of interaction of the compounds with the stationary phase. The main components of a gas chromatography are shown in Figure 3.1-11.

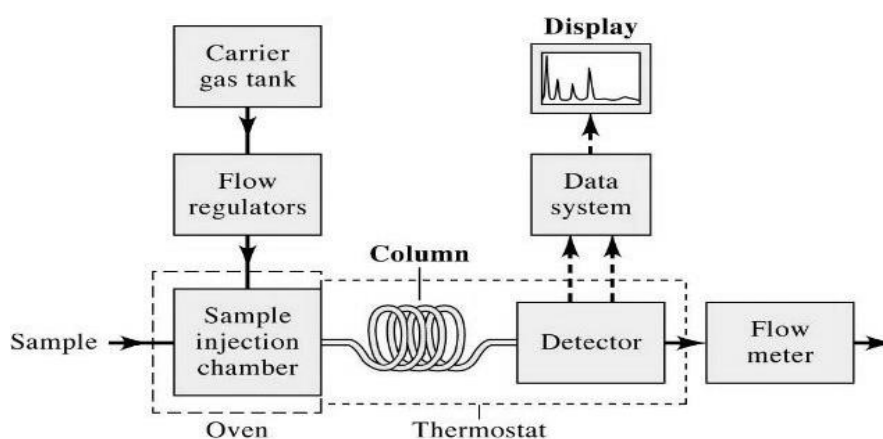


Figure 3.1-11. GC Chromatography equipment and general layout of a typical GC.

### 3.1.6.1 Calibration of the Gas Chromatograph Instruments

The gas chromatographs were regularly calibrated with standard gas mixtures to ensure accurate quantitation. The standard gases were used to create calibration curves and used as a reference for compositional calculation of each gas. For permanent gases, the calibration was carried out using a standard gas mixture obtained from Supelco, UK. The mixture typically contained 0.994 vol.% H<sub>2</sub>, 0.999 vol.% CO, 0.992 vol.% CO<sub>2</sub>, 1 vol.% O<sub>2</sub> and 96 vol.% of N<sub>2</sub>.

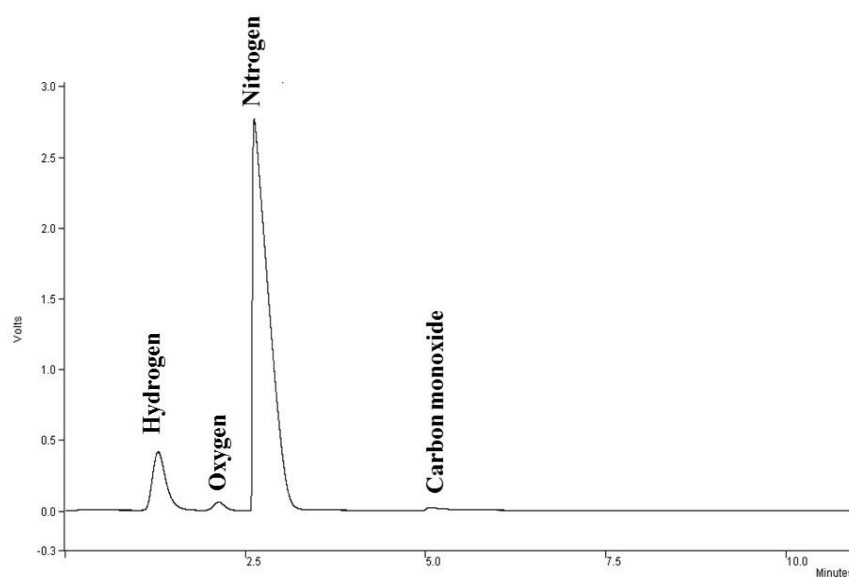


Figure 3.1-12. GC response peaks for a standard gas mixture of permanent gases (H<sub>2</sub>, O<sub>2</sub>, N<sub>2</sub>, CO).

However, for hydrocarbons, the calibration was performed using two different gas standards of alkanes and alkenes. The standard alkane mixture contained 1 vol.% each of CH<sub>4</sub>, C<sub>2</sub>H<sub>6</sub>, C<sub>3</sub>H<sub>8</sub> and C<sub>4</sub>H<sub>10</sub>; and the standard alkene mixture contained 1 vol.% each of C<sub>2</sub>H<sub>4</sub>, C<sub>3</sub>H<sub>6</sub> and 2 vol.% of C<sub>4</sub>H<sub>8</sub>. In all cases, 1.0 cm<sup>3</sup> of each standard was injected into the GC. Examples of the resulting chromatograms for the permanent gases and hydrocarbon standard gas mixtures and the corresponding areas are shown in Figures 3.1-12 and 3.1-13 respectively.

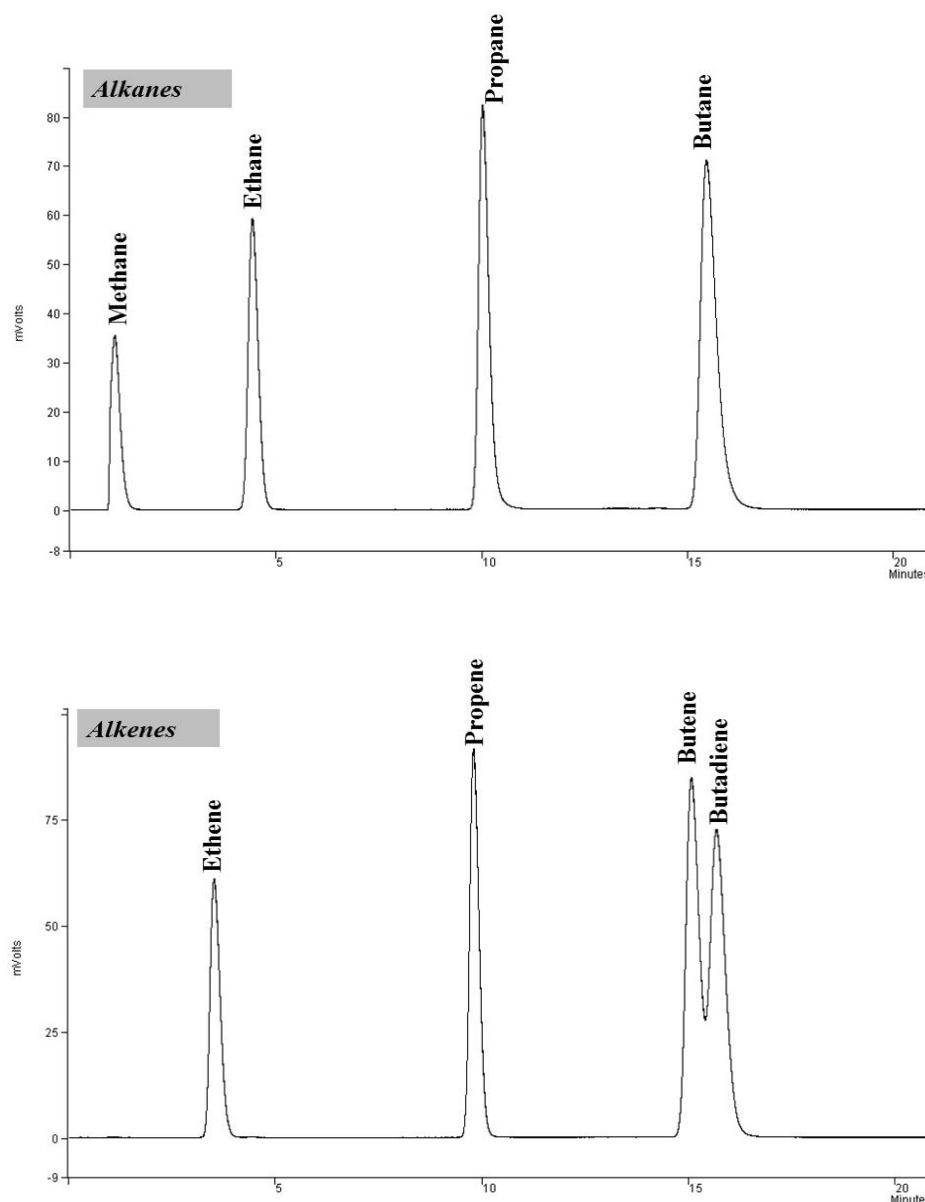


Figure 3.1-13. GC response peaks for standard gas mixture of hydrocarbons (C<sub>1</sub>-C<sub>4</sub>).

### 3.1.6.2 Permanent gases analyses

The permanent gases (N<sub>2</sub>, H<sub>2</sub>, CO, CO<sub>2</sub>) were analysed using a Varian CP-3380 gas chromatograph with a thermal conductivity detector (GC/TCD) equipped with a 2 meters-long column with a 2 mm diameter packed with 60-80 mesh molecular sieve. Argon was used as the carrier gas. Nitrogen, the purge gas used during the char preparation experiments was also determined, and the volumetric flow rates of the evolved gases were calculated by comparison with the N<sub>2</sub> flow rate. The gas chromatograph oven was isothermally held at a temperature of 30 °C during the

analysis; the injector and detector temperatures were set at 120 °C and the filament temperature at 160 °C. Carbon dioxide was analysed by another Varian CP-3380 (GC/TCD) on a 2 m length by 2 mm diameter column and packed with a HayeSep 80-100 molecular mesh, and argon was also used as the carrier gas.

### 3.1.6.3 Hydrocarbon gases analyses

Hydrocarbon gases from C<sub>1</sub> to C<sub>4</sub> were analysed using a separate Varian CP-3380 GC with a flame ionisation detector (FID). The column used was 2 m long with 2 mm diameter packed with 80-100 mesh HayeSep. Nitrogen was used as the carrier gas. The injector was held at 150 °C, while the detector temperature was 200 °C. The oven temperature was set at 60 °C for 3 min, then ramped at 10 °C min<sup>-1</sup> to 100 °C, held for 3 min and finally ramped to 120 °C at 20 °C min<sup>-1</sup> heating rate.

### 3.1.6.4 Calculation of gas concentration

The calculation of the volume percentage of the gas products was determined in relation to the results produced by the analysis of standard gases. The area values recognized by the digital integrator by converting the voltage signal from the detector were used to obtain response factors for each gas species in the standard gases. The response factor (RF) was calculated according to the following equation:

$$RF = \frac{\textit{peak area of standard gas}}{\textit{vol \% of standard gas}} \quad (3.15)$$

After obtaining the response factor values, then the volume percent of each gas can be calculated by using the following equation:

$$\textit{vol. \%} = \frac{\textit{peak area of each analytical gas sample}}{\textit{RF of the standard gas}} \quad (3.16)$$

At standard conditions of temperature and pressure, one mole of gas has a volume of 22.4 litres. The mass of each gas species 'x' can then be calculated based on the concentration of nitrogen present as follows:

$$Mass_x = R_m \cdot \left( \frac{C_x}{100} \cdot V_{total} \right) / 22.4 \quad (3.17)$$

Where  $Mass_x$  is the mass of the compound 'x' produced,  $R_m$  is the molecular weight of the compound 'x',  $C_x$  is the concentration of gas 'x' in percent obtained from GC analysis and  $V_{total}$  is the total volume of the gas sample collected which was calculated as follows:

$$V_{total} = Q_n \cdot t_c \cdot \frac{100}{C_n} \quad (3.18)$$

Where  $V_{total}$  is the total volume of the gas sample collected,  $Q_n$  is the flow rate of nitrogen used in the experiment,  $t_c$  is the gas collection time and  $C_n$  is the concentration of nitrogen in the gas in percent.

The total mass of the gases produced can then be calculated by summing the masses for each gas compound.

#### **3.1.6.5 Repeatability of the gas analysis**

To evaluate the repeatability of the gas analysis procedure, repeat injections were carried out using the gas sample collected in the same gas bag. Figure 3.1-14 shows an example of the obtained chromatograms which clearly indicates that the gas analysis procedure is accurate. The repeatability of the analyses of gaseous species found in the sample is shown in Table 3.1-4. The repeatability was estimated from the relative standard deviation. Relative standard deviation of less than 10% indicates an

excellent repeatability with minimal errors. The relative standard deviation was in the range of 0.06-6.67% showing the excellent repeatability of the gas analysis procedure.

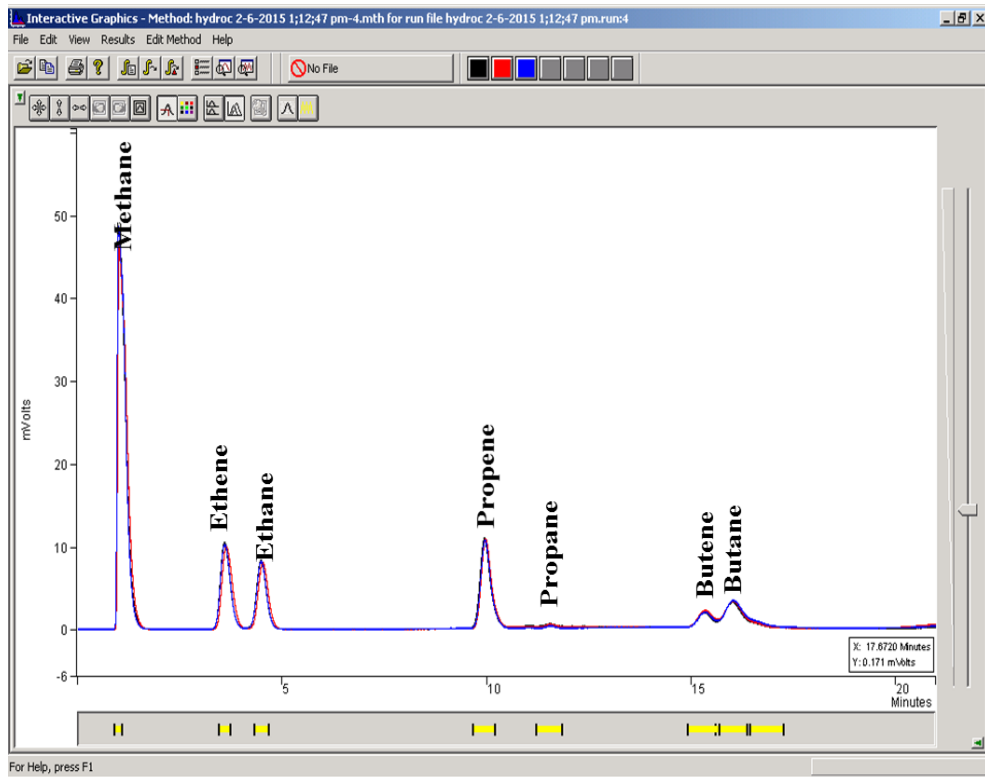


Figure 3.1-14. Overlying Chromatograms indicating repeatability of GC analysis results

Table 3.1-4. Repeatability of GC analysis

| Gas                            | Rf      | Peak Area<br>sample 1 | Conc (Vol.%) | Peak area<br>sample 2 | Conc (Vol.%) | Peak area<br>sample 3 | Conc (Vol.%) | Peak area<br>sample 4 | Conc (Vol.%) | Average<br>(conc.%) | SD    | RSD   |
|--------------------------------|---------|-----------------------|--------------|-----------------------|--------------|-----------------------|--------------|-----------------------|--------------|---------------------|-------|-------|
| CO                             | 48427   | 157689                | 3.26         | 154163                | 3.18         | 154163                | 3.18         | 155830                | 3.22         | 3.21                | 0.035 | 1.081 |
| H <sub>2</sub>                 | 593758  | 1326581               | 2.23         | 1320714               | 2.22         | 1346077               | 2.27         | 1322020               | 2.23         | 2.24                | 0.020 | 0.893 |
| N <sub>2</sub>                 | 48100   | 4514386               | 93.85        | 4503660               | 93.63        | 4571144               | 95.03        | 4541752               | 94.42        | 94.24               | 0.063 | 0.067 |
| CO <sub>2</sub>                | 12115   | 33891                 | 2.80         | 32550                 | 2.69         | 32795                 | 2.71         | 33891                 | 2.80         | 2.75                | 0.059 | 2.145 |
| CH <sub>4</sub>                | 587018  | 682456                | 1.16         | 695617                | 1.19         | 695699                | 1.19         | 682456                | 1.16         | 1.17                | 0.013 | 1.111 |
| C <sub>2</sub> H <sub>4</sub>  | 982709  | 174236                | 0.18         | 177677                | 0.18         | 177349                | 0.18         | 174236                | 0.18         | 0.18                | 0.002 | 1.111 |
| C <sub>2</sub> H <sub>6</sub>  | 1072273 | 137614                | 0.13         | 140257                | 0.13         | 140181                | 0.13         | 137614                | 0.13         | 0.13                | 0.001 | 0.769 |
| C <sub>3</sub> H <sub>6</sub>  | 1385398 | 189177                | 0.14         | 192679                | 0.14         | 192976                | 0.14         | 189177                | 0.14         | 0.14                | 0.002 | 1.451 |
| C <sub>3</sub> H <sub>8</sub>  | 1585587 | 3760                  | 0.00         | 3760                  | 0.00         | 3652                  | 0.00         | 3712                  | 0.00         | 0.00                | 0.000 | 0.000 |
| C <sub>4</sub> H <sub>8</sub>  | 1781254 | 44235                 | 0.02         | 50829                 | 0.03         | 43710                 | 0.02         | 44235                 | 0.02         | 0.03                | 0.002 | 6.670 |
| C <sub>4</sub> H <sub>10</sub> | 2191162 | 118301                | 0.05         | 110096                | 0.05         | 102813                | 0.05         | 118301                | 0.05         | 0.05                | 0.003 | 5.849 |

Peak areas in microvolts per unit time; Response factor is microvolts per unit time per vol.%

### 3.1.7 NO adsorption experiments

The nitrogen oxide adsorption tests on the commercial and waste derived activated carbons, described in sections 3.1.1.4 and 3.1.4 respectively, were conducted using a stainless steel fixed bed reactor externally heated by an electrical furnace (Figure 3.1-15). The reactor system consisted of a gas mixing unit, the activated carbon-NO adsorption reactor and on-line gas analysis system. The air and NO/N<sub>2</sub> with an NO concentration of 1000 ppm were supplied by B.O.C Special Gases Ltd., UK. Nitrogen was used as a carrier gas. The gases were mixed together before entering the reactor in a gas mixing unit. The NO adsorption reactor was of 20 cm height and 2.2 cm internal diameter, with a 10 cm (long) sample holder used to hold the activated carbon bed inside the reactor. The temperature of the carbon was controlled and monitored with a thermocouple. The adsorption tests were conducted with a fixed activated carbon mass of 2.8 g which was previously treated under nitrogen at 500 °C for 30 min in order to clean the surface oxides and desorb the adsorbed gases on the carbon surface [18-19].

The bed depth was about 3 cm which gave ~1.7 s gas residence time through the carbon bed. A gas mixture with a flow rate of 500 ml min<sup>-1</sup> passed through the reactor, and the outlet gas was directed to the gas analyser system. The adsorption was carried out for two hours at a temperature of 50 °C and in the presence of 5% O<sub>2</sub> and 800 ppm NO. The presence of oxygen in the gas mixture is essential since it increases the adsorption of nitric oxide through the catalytic oxidation of NO to NO<sub>2</sub>, which results in an increase of the NO adsorption because of the higher adsorption potential of NO<sub>2</sub> [20-21]. In the absence of oxygen, the NO removal efficiency was only about 5%, similar findings have been reported in the literature [22-23]. The gas composition was recorded every minute using a gas analyser unit supplied by Horiba Instruments UK Ltd. and consisted of a Horiba VA-3000 chemiluminescence analyser for NO/NO<sub>x</sub> and a separate Horiba VA-3000 paramagnetic analyser for oxygen. Similar experimental conditions have been used by other researchers for the NO<sub>x</sub> removal by activated carbon [24-26].

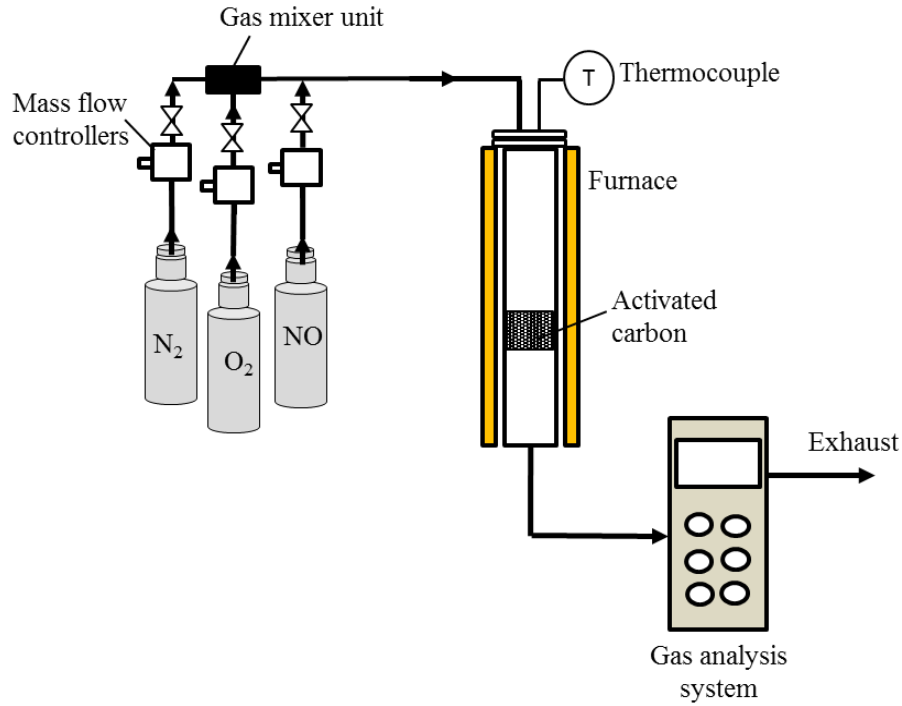


Figure 3.1-15. A Schematic diagram of the gas adsorption reactor

The NO removal efficiency of the used adsorbents was calculated according to the relation (Eq. 3.19):

$$\text{NO removal efficiency (\%)} = \frac{(C_0\text{NO} - \text{CNO})}{C_0\text{NO}} \times 100 \% \quad (3.19)$$

Where  $C_0\text{NO}$  and  $\text{CNO}$  are the NO concentration before and after adsorption respectively.

The carbon's NO adsorption capacity was calculated as follows [27]:

$$C_b = C_a + \left[ \frac{\left( \text{NO}_{inlet} - \left( \frac{c_a + b_b}{2} \right) \right) (t_b - t_a) FM_{\text{NO}273}}{10^6 m_{\text{carbon}} 22.4 (273 + T)} \right] \quad (3.20)$$

Where  $C_b$  is the capacity in ( $\text{mg g}^{-1}$ ) after time  $t_b$ ,  $C_a$  is the capacity ( $\text{mg g}^{-1}$ ) after time  $t_a$ ,  $c_b$  is the detected NO concentration (ppm) after time  $t_b$ ,  $c_a$  is the detected NO

concentration (ppm) after time  $t_a$ ,  $F$  is the total gas flow rate ( $\text{ml min}^{-1}$ ),  $M_{\text{NO}}$  is the molecular mass of NO,  $m_{\text{carbon}}$  is the mass of activated carbon used (g), and  $T$  is the temperature of measurement ( $^{\circ}\text{C}$ ).

### 3.1.7.1 Chemiluminescent $\text{NO}_x$ Analyser

The analyser (Figure 3.1-16) used to measure NO concentration is based on the chemiluminescent reaction of NO with ozone according to the following equations:



Where  $h$  is the Planck's constant ( $6.6 \times 10^{-34}$  Js) and  $\nu$  is the frequency of radiation (Hz).

The nitric oxide (NO) reacts with ozone ( $\text{O}_3$ ) in the reaction chamber and results in the generation of excited  $\text{NO}_2^*$  molecules (equation 3.21). When these molecules decay to their ground state, they emit light with an intensity proportional to NO concentration (equation 3.22) [28].



Figure 3.1-16. Horiba VS3000/VA3000 multi gas analyser; (a) Analyser pump,(b) Sample pump, (c) Mist catcher, (d) Selector valve, (e) Filter, (f) Sample flowmeter, (g) Calibration gas flow meter, (h) VS-3000 Gas sampling unit, (i) VA-3000 Multi – gas analyser unit.

Figure 3.1-17 shows a diagram of the main components of the chemiluminescent analyser. Two gas flow meters are used to regulate a constant flow rate of the sample and ozone to the reaction chamber. The sample inlet has two flow modes; one mode is for NO and it provides a direct path of the sample to the reaction chamber. The second mode is to measure NO<sub>x</sub>. However, only NO in the sample reacts with ozone. Thus, to measure NO<sub>x</sub> the sample must first pass to the converter in order to convert NO<sub>2</sub> to NO. NO<sub>2</sub> concentration can be measured from the difference of the total NO<sub>x</sub> and NO [28]. However, the gas analyser used in this work required a gas inlet with a

minimum flow rate of  $1500 \text{ ml min}^{-1}$  which cannot be used with a small-scale reactor. The gas residence time with this high flow rate is only 0.01 second. Therefore, to solve this the connections inside the gas analyser were modified, and the sample gas had to pass directly to the converter instead of passing first to the mist catcher and drain separator. The drain separator is used to dry the gas sample by removing the moisture from the sample and because of this step the flow rate decreased before it reached the analyser unit. Therefore, it was decided to pass the sample directly to the converter. This modification had improved the required gas sample flow rate. With this modification, a sample inlet of  $500 \text{ ml min}^{-1}$  gave the same NO concentration in supply (1010 ppm). However, when the gas sample ( $\text{NO} + \text{O}_2$ ) was passed to the converter to measure total  $\text{NO}_x$  ( $\text{NO} + \text{NO}_2$ ), total  $\text{NO}_x$  gave the same concentration as NO. Therefore, the experiments were carried out with NO measurement only. To measure the NO concentration, the sample inlet after passing through various components for treatment was mixed with ozone, which was generated within the instrument from the air. The resulting chemiluminescence from the reaction of NO and  $\text{O}_3$  is monitored through a filter by a photomultiplier detector placed at the end of the reaction chamber. The output from the photomultiplier is proportional to NO concentration [29]. A mixture of NO in  $\text{N}_2$  with a certified concentration of 1010 ppm was used to calibrate the analyser.

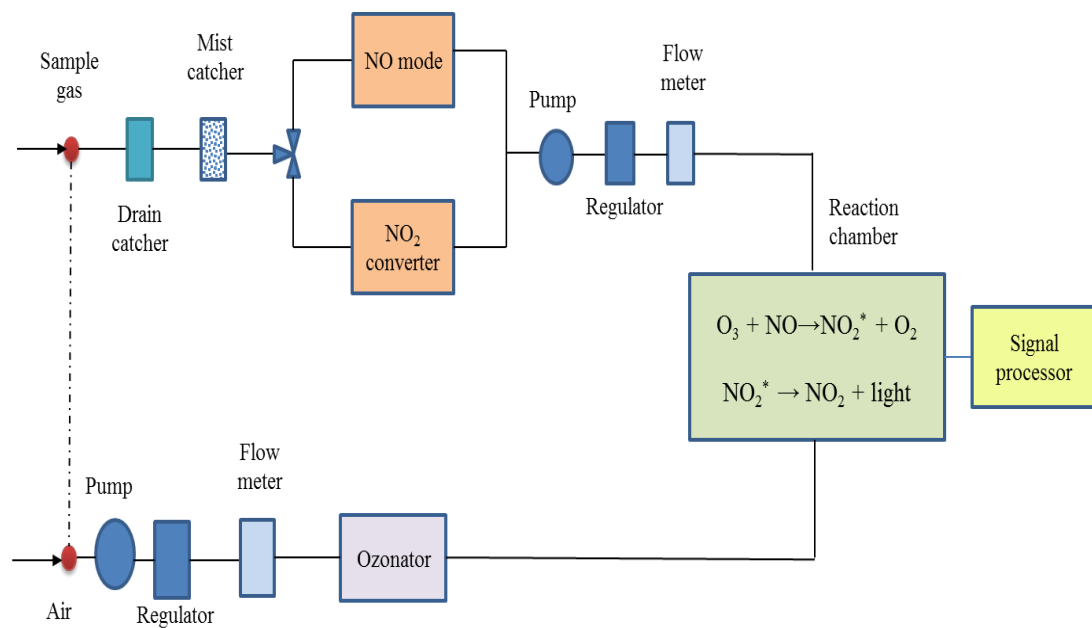


Figure 3.1-17. The principle of operation of the gas analyser.

### 3.1.7.2 The precision assessment of the used gas analyser

Multipoint calibrations with different NO concentrations were carried out to assess the linearity of the gas analyser. The NO calibration gas was diluted with zero air in order to prepare calibration mixture of NO with different concentrations. The required flow rate for each concentration was calculated according to the following equations [30]:

$$\text{Multiplication Factor (MF)} = \text{Total flow} \times \text{Required NO concentration} \quad (3.23)$$

$$\text{The required flow rate} = \text{MF} \times (\text{Total flow } 100/\text{NO in supply } \%) \quad (3.24)$$

For a total flow rate higher than  $100 \text{ ml min}^{-1}$ , the result must be multiplied by the total flow rate /100, as the above calculation is applied only for a total flow rate of  $100 \text{ ml min}^{-1}$  [30]. Thus, for a concentration of 800 ppm NO, the result is:

|  |   |
|--|---|
| The concentration of the supplied NO   | = 1000 ppm  |
| The required NO concentration          | = 800 ppm   |
| MF                                     | = 0.08  |
| The required flow rate                 | = $0.08 \times (100 / 0.1)$                               |
|  | = 80 (This for $100 \text{ ml min}^{-1}$ total flow rate) |
| For 500 total flow rate, the result is | = $80 \times 500/100$                                     |
|  | = $400 \text{ ml min}^{-1}$                               |

So a flow rate of  $400 \text{ ml min}^{-1}$  in a total flow rate of  $500 \text{ ml min}^{-1}$  for a supply of 1000 ppm NO gave a concentration of 800 ppm NO [30]. Table 3.1-5 shows the multipoint calibration with the required flow rate used to test the reliability of the instrument.

Table 3.1-5. Test the reliability of the instrument with multipoint calibration

| Total flow rate (ml min <sup>-1</sup> ) | Required flow rate (ml min <sup>-1</sup> ) | NO delivered to the instrument (ppm) | NO displayed by the instrument (ppm) |
|---|--|--------------------------------------|--------------------------------------|
| 500                                     | 500  | 1010                                 | 1013                                 |
| 500                                     | 400  | 800                                  | 802                                  |
| 500                                     | 350  | 707                                  | 691                                  |
| 500                                     | 300  | 606                                  | 595                                  |
| 500                                     | 250  | 505                                  | 486                                  |
| 500                                     | 200  | 404                                  | 380                                  |
| 500                                     | 150  | 303                                  | 290                                  |
| 500                                     | 100  | 202                                  | 195                                  |

Based on the data shown in Figure 3.1-18, the  $r$  (correlation coefficient) value of 0.999 indicates a strong linear correlation. The uncertainty of the gas analyser was within the manufacturer's range of 1% uncertainty. The gas analyser was routinely calibrated by using a reference NO gas mixture with known concentration.

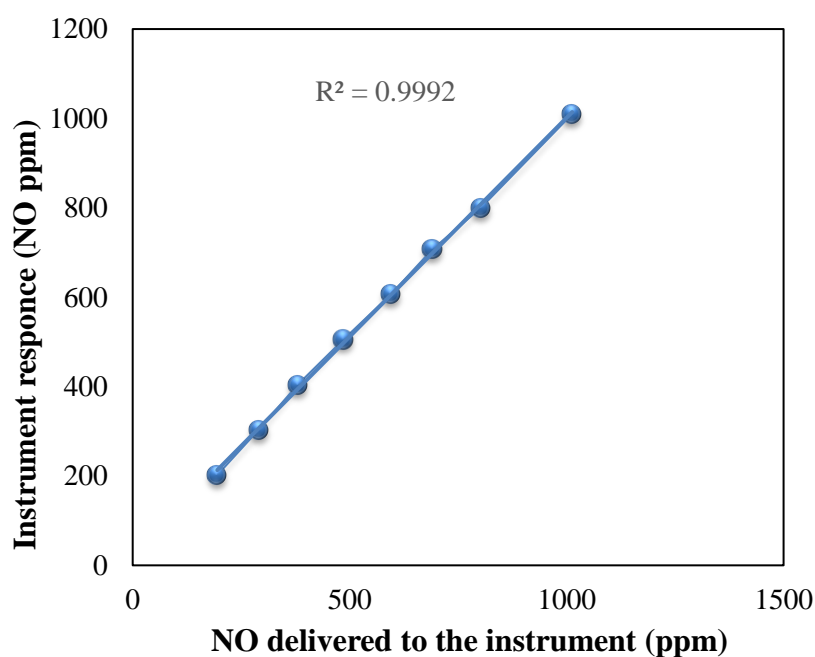


Figure 3.1-18. Calibration mixtures to test the uncertainty of the gas analyser

### 3.1.7.3 Estimation of Errors in NO measurements

Problems may exist in NO sampling and analysis. The presence of metal traces may catalyse the NO/carbon reaction. Some sampling probes have been found to reduce

NO when used to sample hot combustion gases. Stainless steel tubes were found to have a high catalytic activity which results in low measured NO concentration [31]. To assess the possibility of interaction of NO with the solid surfaces and the chance of NO oxidation to NO<sub>2</sub> in the presence of air, an NO adsorption test was undertaken in the presence of 800 ppm and 5% O<sub>2</sub> at 50 °C in an empty reactor. It was found that the NO outlet concentration was almost equal to the inlet which indicates that NO oxidation in the gas phase does not contribute to the NO removal efficiency.

#### 3.1.7.4 Repeatability of the NO adsorption performance of the activated carbons

To ensure the repeatability of the results, experiments with the same conditions were repeated three times. Figure 3.1-19 presents the repeatability of the results. The adsorption tests were conducted with the use of a commercial activated carbon (Norit RST 3) at a temperature of 50 °C and in the presence of 5% O<sub>2</sub> and NO concentration of 800 ppm.

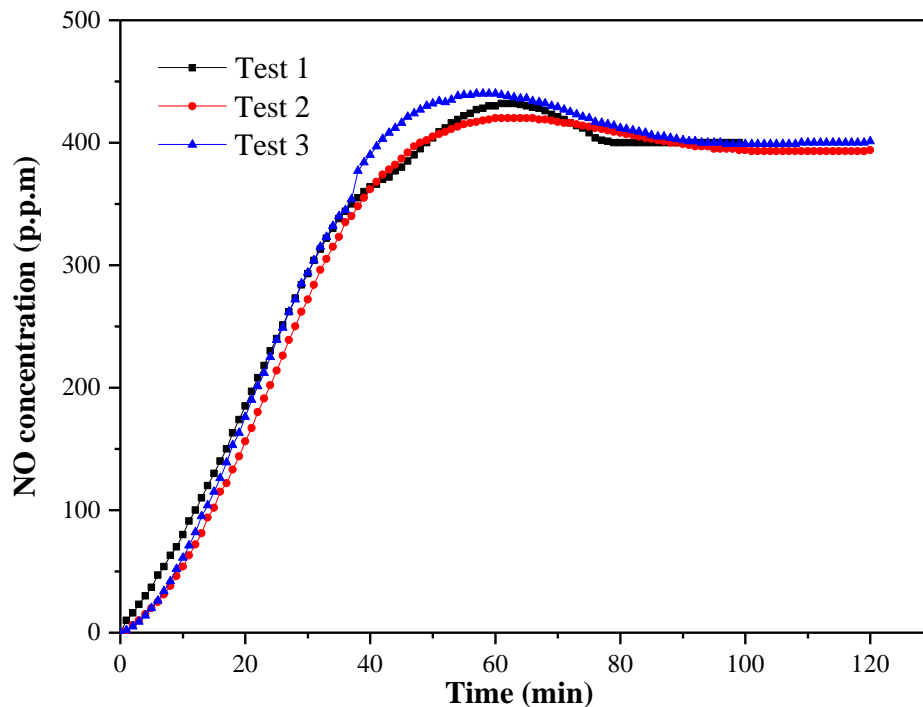


Figure 3.1-19. Repeatability of NO adsorption experiments

## 3.2 Tar conversion over a hot bed of char

This section presents the experimental setup used for the assessment of char effectiveness for the conversion of biomass pyrolysis gases including the heavier molecular weight hydrocarbons (tar) from the pyrolysis of biomass, waste wood pellets. Biomass is composed of cellulose, hemicellulose and lignin, whose structures are different from each other. Lignin is aromatic in nature, while cellulose and hemicellulose are polysaccharides [32]. During the biomass pyrolysis, lignin breaks down to form mono aromatics, while hemicellulose and cellulose forms the primary tar compounds such as furans [33]. In the vapour phase, these primary tar compounds undergo series reactions of cracking, oxidation, reforming and polymerization, resulting in the formation of secondary and tertiary tars at temperatures higher than 500 °C [34]. Thus, in this work cracking of biomass tar vapour was investigated using waste derived char materials. The catalytic removal of tar is generally known as hot gas cleaning [35].

### 3.2.1 Materials

#### 3.2.1.1 Biomass feedstock

The wood pellets were used as the biomass feedstock for the pyrolysis which generated the pyrolysis gases for subsequent cracking in the hot bed of char, relevant results are reported in Chapter 5, sections 5.1 and 5.3. The wood pellets were produced as compressed saw dust pellets from waste wood processing by Liverpool Wood Pellets Ltd, Liverpool, UK. The wood pellets were then ground and sieved to obtain a sample with 1 mm particle size (Figure 3.2-1).

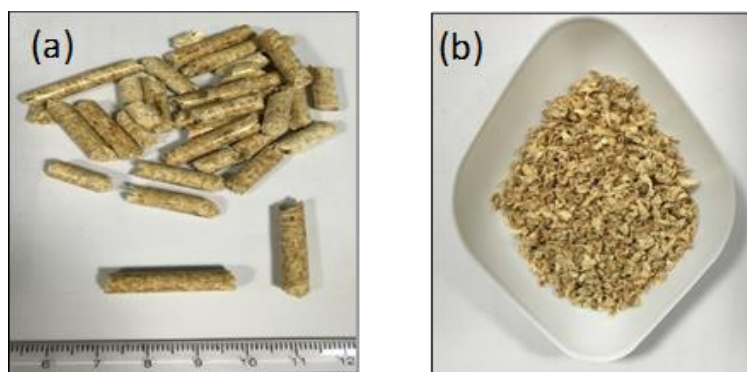


Figure 3.2-1. Wood pellets.

The proximate analysis of the wood pellets gave 75.0 wt.% volatiles, 7.0 wt.% moisture, 2.0 wt.% ash and 15.0 wt.% fixed carbon. Elemental analysis of the pellets gave 46.0 wt.% carbon, 5.6 wt.% hydrogen, 0.7 wt.% nitrogen and 45.7 wt.% oxygen.

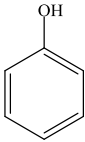
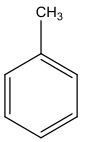
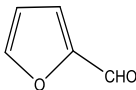
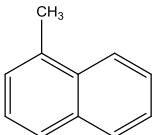
### **3.2.1.2 Chars**

The waste pyrolysis derived char materials were prepared from tyres, RDF and date stones as described in section 3.1-3.

### **3.2.1.3 Tar model compounds**

To get a better understanding of the influence of textural properties and surface chemistry of carbons on the tar decomposition, four model compounds were used including phenol, furfural, toluene and methylnaphthalene to simulate typical biomass tar compounds produced during biomass gasification. Benzene, phenol, toluene and naphthalene are commonly used as tar model compounds which represent the main types of biomass gasification tar [36-37]. The chemical properties and structures are presented in Table 3.2-1. These tar model compounds were chosen for the purpose of investigating how the structure of the aromatic molecule affects tar conversion and the char catalytic activity individually for each aromatic compound [38]. Relevant results are reported in Chapter 5, section 5.2.

Table 3.2-1. Aromatic model compounds studied in this study.

| Name              | Tar class | Structure  | Chemical formula                             | Molar mass (g mol <sup>-1</sup> ) | Boiling point (°C) |
|-------------------|-----------|--|--|-----------------------------------|--------------------|
| Phenol            | 2         |   | C <sub>6</sub> H <sub>6</sub> O              | 94                                | 182                |
| Toluene           | 3         |   | C <sub>7</sub> H <sub>8</sub>                | 92                                | 111                |
| Furfural          | 2         |   | C <sub>5</sub> H <sub>4</sub> O <sub>2</sub> | 96                                | 161.7              |
| Methylnaphthalene | 4         |  | C <sub>11</sub> H <sub>10</sub>              | 142                               | 246                |

### 3.2.2 Acid treatment

To assess the influence of oxygen functional groups on tar conversion, a commercial carbon, designed as AC1 and provided by Norit, was treated with HNO<sub>3</sub> with molar concentrations of 1-4 M. The treatment was carried out in a 25 ml Teflon bottle containing 7 g AC and 50 ml 1-4 M HNO<sub>3</sub>. The treatment was carried at 70 °C for 8h and 150 rpm. Later, the treated carbons were washed several times with distilled water and dried at 105 °C for 48h [39]. Relevant results are reported in Chapter 5 section 5.2.

In addition, to investigate the role of ash minerals on the catalytic performance of char for tar decomposition, the metals were removed from tyre char following the procedure described earlier in section 3.1.2, and the performance of the de-ashed char was compared to that of the raw char. This was performed only for tyre char; relevant results are reported in Chapter 5, section 5.3.

### **3.2.3 Two stage-Fixed bed pyrolysis/cracking reactor**

A two stage fixed bed reactor was used to test the tar conversion efficiency of chars prepared from waste tyres, RDF and date stones.

#### **3.2.3.1 Reactor set-up**

The use of waste derived pyrolysis chars for bio-oil/tar catalytic cracking was investigated in a two-stage fixed bed reactor made of stainless steel with an inner diameter of 22 mm and a length of 160 mm and was fully instrumented with monitoring and control of gas flow and temperature. Both stages were thermally heated independently, and two thermocouples were located in each reactor to control the temperature. The pyrolysis process of the wood pellets took place within the first stage; while the catalytic cracking was carried out in the second stage. Both furnaces were mounted in a vertical arrangement with pyrolysis in the upper stage and catalytic cracking in the lower stage. The assembled and main parts of the reaction system are shown in Figure 3.2-2.



Figure 3.2-2. Assembled and main parts of the pyrolysis-gasification reactor; (a) Syringe pump, (b) Thermocouple, (c) 1<sup>st</sup> stage pyrolysis reactor, (d) 2<sup>nd</sup> stage catalytic reactor, (e) Furnace controller, and (f) Mass flow controller.

### 3.2.3.2 Experimental procedure

To investigate the influence of the presence of char on the production of tar and hydrogen in the effluent gas, a series of experiments were carried out. The investigation can be divided into the following groups of experiments:

- i. Biomass pyrolysis oil-char reactions
  - a. Tar cracking-RDF, date stones and tyre chars without steam
- ii. Tar model compounds cracking-char reactions
  - a. Tar model compounds cracking-Tyre char
- iii. Biomass tar reforming
  - a. Tar reforming-Tyre char with steam

### 3.2.3.2.1 Tar cracking using waste derived chars

Experiments were performed with 2 grams of biomass loaded into a sample boat and placed within the first pyrolysis stage, and 2 grams of waste derived pyrolysis chars kept within the second stage and maintained at the required temperature. A schematic diagram of the reactor is shown in Figure 3.2-3. The experiments consisted of the initial heating of the second stage hot char reactor to the desired temperature (600, 700 and 800 °C) at a heating rate of 40 °C min<sup>-1</sup>. Once the temperature of the char reactor was stable, the first stage pyrolysis reactor was heated at a heating rate of 40 °C min<sup>-1</sup> to a final temperature of 500 °C. This temperature is suitable for complete decomposition of cellulose and hemicellulose, and partial decomposition of lignin [40]. In addition, tar is favoured to form from the release of heavy molecular weight compounds during the pyrolysis at a temperature within the range of 300-500 °C.

The two-stage reactor system was continually purged with nitrogen (90 ml min<sup>-1</sup>). Further experiments were undertaken using a biomass: tyre char ratio of 1:1-1:3 to determine the influence of the ratio of biomass to char on the conversion of tar from the pyrolysis gases produced from the pyrolysis of the biomass waste wood pellets. The evolved pyrolysis gases, including tar, higher hydrocarbons, product autogenerated steam and non-condensable gases such as methane, ethane, hydrocarbons, carbon dioxide and carbon monoxide were passed directly to the hot char reactor where the range of gasification, reforming, thermal and catalytic cracking reactions occurred. Experiments were also undertaken in the absence of char for comparison using sand. The product gases were passed to a series of dry ice condensers where condensable tar/bio-oil and water were condensed. The uncondensed gases were collected in a Tedlar™ gas sample bag. After the experiment, the gases were analysed using gas chromatography and with the known flow rates and molecular mass of each gas, the total mass of gases could be determined. The pyrolysis char from pyrolysis of the biomass wood pellets was collected from the first stage pyrolysis reactor and weighed.

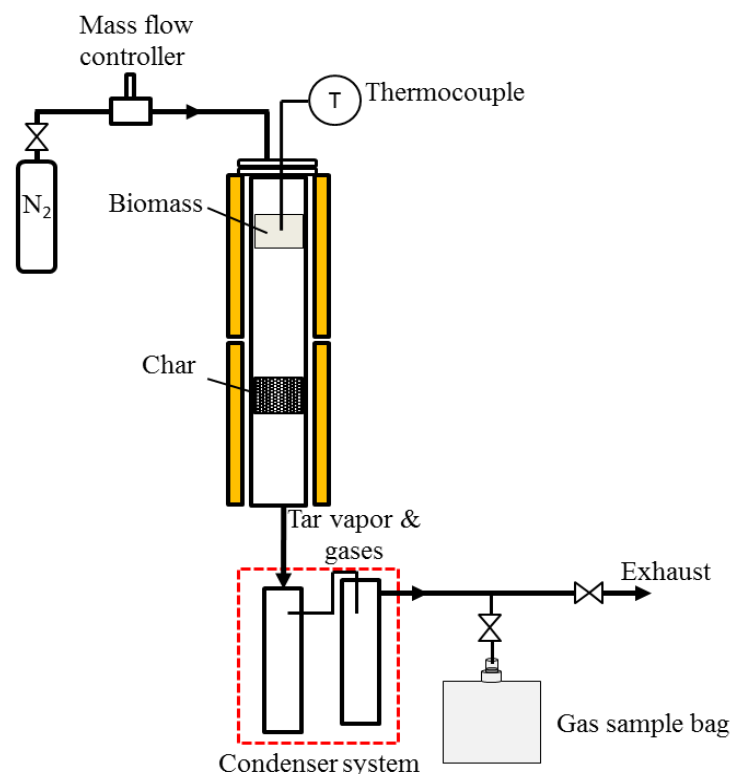


Figure 3.2-3. Schematic two-stage pyrolysis-gasification reaction system

### 3.2.3.2.2 Char catalytic performance for tar model compounds cracking

The catalytic activity of carbonaceous materials for tar cracking depends on many factors such as the porous texture and the surface chemistry of the used carbon and also on the nature of tar compound [41]. Therefore, to get a better understanding of the influence of textural properties and surface chemistry of carbons on the tar decomposition and to study more deeply the char catalytic performance for tar cracking and understand the overall process, tar model compounds were used, and the investigation was carried out with the use of tyre char only. The effectiveness of tyre char for decomposing of model tar compounds was studied using a two stage fixed bed reactor (described in section 3.2.3.2.1) and at a bed temperature of 700 °C. The compounds were fed continuously for 60 min using methanol as a solvent, with a methanol and model compound carbon molar ratio 1. Before reaction, the second stage reactor, where tyre char is located (2 g), was heated to the required temperature at a heating rate of 40 °C min<sup>-1</sup> and the first furnace was kept at 250 °C in order to vaporize the tar model compounds before entering the second reactor where the reaction occurred with the tyre char. When the furnace of both reactors reached the desired

temperature, the tar compounds were fed continuously into the reactor with a flow rate of 3.8 ml h<sup>-1</sup> using a syringe pump. Nitrogen was used as the carrier gas with a flow rate of 90 ml min<sup>-1</sup>. The volatile stream produced was passed to a series of dry ice condensers where condensable liquid and the unconverted model compounds were collected. The amount of unconverted reactant was calculated by weighing both condensers and syringe before and after the experiments. The non-condensable gases were collected in a Tedlar™ gas sample bag and analysed as described in section 3.1.6.

In order to quantify the products of the cracking process, carbon conversion and product yields were calculated. The carbon conversion was defined as the moles of carbon in the gaseous products divided by the moles of carbon fed. The total amount of carbon moles in the gas were calculated from the moles of CO, CO<sub>2</sub> and C<sub>1</sub>-C<sub>4</sub> hydrocarbons formed during the reaction which were determined from the GC analyses. The moles of carbon in the feed were calculated from the total amount of model compound fed into the reactor.

$$\text{Carbon conversion}(\%) = \frac{\text{moles of carbon in the product gas}}{\text{moles of carbon in the feed}} \times 100 \quad (3.25)$$

The yield of gaseous species was calculated as follows:

$$\text{Yield}(\%) = \frac{\text{g of the compound in the product gas}}{\text{g of the model compound fed}} \times 100 \quad (3.26)$$

### 3.2.3.2.3 Steam reforming reaction system

Additional experimental tests were carried out using tyre char for tar reforming and hydrogen production through a gas-solid simultaneous reforming/gasification process. The experimental system consisted of a two-stage pyrolysis-reforming reactor, as described in section 3.2.3.2.1. Biomass was used as the feedstock to generate tar/syngas and waste tyre derived pyrolysis char was used as a sacrificial catalyst in a steam reforming process to produce a hydrogen-rich syngas. The experimental procedure was described previously in section 3.2.3.2.1. However, a syringe pump was used to inject water at the feeding rate of 6.64 g h<sup>-1</sup> (steam/biomass (S/B) ratio of

3.32) into the second stage of the reactor, and mixed with the evolved pyrolysis gas and passed over the tyre char. The influence of the experimental conditions on the gas composition and reforming/gasification process was investigated. The experimental parameters used were, bed temperature (700-900 °C), S/B mass ratio (1.82-6.00) and reaction time (1-4 h).

### **3.2.3.3 Experiment repeatability and validation of the reactor**

The repeatability of the experimental system was ensured via repeat experiments. The general process conditions were: 2 g of biomass, pyrolysis temperature 500 °C, N<sub>2</sub> flow rate 90 ml min<sup>-1</sup>. The experimental data in relation to the validation of the two stage pyrolysis-gasification reactor is displayed in Tables 3.2-2 & 3.2-3 and the experiments are repeatable. For example, several repeated experiments with biomass in the absence of char (where sand was used) gave a standard deviation on char recovered mass of 0.4 wt.%, for liquid 0.7 wt.% and gas yield of 1.9 wt.%. Gas compositional analysis for the same repeated experiment gave a standard deviation for CO of 3.4 vol.%, H<sub>2</sub> of 1.1 vol.%, CO<sub>2</sub> of 2.4 vol.%, CH<sub>4</sub> of 2 vol.% and C<sub>2</sub>-C<sub>4</sub> of 4.9 vol.%.

Table 3.2-2. Validation of the two stage fixed bed reactor.

|  | Without char |      |       |      | RDF char |      |         | Tyre char |      |         | Date stones char |      |         |
|--|--------------|------|-------|------|----------|------|---------|-----------|------|---------|------------------|------|---------|
|  | 1            | 2    | 3     | SD   | 1        | 2    | Average | 1         | 2    | Average | 1                | 2    | Average |
| <b>General conditions</b>                        |              |      |       |      |          |      |         |           |      |         |                  |      |         |
| Biomass sample weight (g)                        | 2            |      |       |      | 2        |      |         | 2         |      |         | 2                |      |         |
| Pyrolysis temperature (°C)                       | 500          |      |       |      | 500      |      |         | 500       |      |         | 500              |      |         |
| Cracking temperature (°C)                        | 600          |      |       |      | 700      |      |         | 700       |      |         | 700              |      |         |
| H <sub>2</sub> O flow rate (ml h <sup>-1</sup> ) | -            |      |       |      | -        |      |         | -         |      |         | -                |      |         |
| <b>Mass Balance</b>                              |              |      |       |      |          |      |         |           |      |         |                  |      |         |
| Residual Biomass char (wt.%)                     | 24.0         | 23.5 | 23.0  | 0.41 | 24.0     | 24.0 | 24.0    | 23.5      | 24   | 23.8    | 24.0             | 24.0 | 24.0    |
| Liquid (wt.%)                                    | 49.0         | 50.5 | 50.5  | 2.45 | 25.5     | 24.5 | 25.0    | 9.5       | 8.5  | 9.0     | 24.5             | 26.0 | 25.25   |
| Gas (wt.%)                                       | 22.4         | 23.4 | 27.3  | 1.9  | 44.3     | 41.9 | 43.1    | 57.5      | 55.9 | 56.7    | 50.6             | 49.5 | 50.03   |
| <b>Gas composition (vol.%)</b>                   |              |      |       |      |          |      |         |           |      |         |                  |      |         |
| CO   | 48.2         | 38.8 | 41.9  | 3.4  | 32.2     | 35.0 | 33.6    | 34.0      | 33.2 | 33.6    | 39.2             | 38.8 | 39.0    |
| H <sub>2</sub>                                   | 9.6          | 7.6  | 6.5   | 1.1  | 27.2     | 26.7 | 26.9    | 29.0      | 28.7 | 28.9    | 24.4             | 26.3 | 25.4    |
| CO <sub>2</sub>                                  | 21.9         | 25.9 | 23.0  | 2.4  | 23.7     | 19.8 | 21.7    | 20.3      | 20.7 | 20.5    | 15.9             | 17.3 | 16.6    |
| CH <sub>4</sub>                                  | 13.4         | 8.0  | 11.6  | 2.0  | 11.4     | 12.5 | 11.9    | 12.1      | 12.3 | 12.2    | 12.5             | 9.6  | 11.1    |
| C <sub>2</sub> -C <sub>4</sub>                   | 7.0          | 19.8 | 17.0  | 4.9  | 5.5      | 6.0  | 5.75    | 4.7       | 5.0  | 4.9     | 5.8              | 4.5  | 5.2     |
| Mass Balance (%)                                 | 95.4         | 97.4 | 100.8 | 3.3  | 93.8     | 90.4 | 92.1    | 90.5      | 88.4 | 89.4    | 99.1             | 99.5 | 99.3    |

Table 3.2-3. Validation of the two stage fixed bed reactor.

|  | Tyre char |       |         |       |        |         |
|--|-----------|-------|---------|-------|--------|---------|
|  | 1         | 2     | Average | 1     | 2      | Average |
| Biomass sample weight (g)                                      | 2         |       |         | 2     |        |         |
| Pyrolysis temperature (°C)                                     | 500       |       |         | 500   |        |         |
| Reforming temperature (°C)                                     | 700       |       |         | 800   |        |         |
| H <sub>2</sub> O flow rate (ml h <sup>-1</sup> )               | 6.64      |       |         | 6.64  |        |         |
| <i>Mass balance based on the biomass sample + water (wt.%)</i> |           |       |         |       |        |         |
| Liquid   | 82.76     | 82.75 | 82.75   | 75.06 | 78.68  | 76.87   |
| Gas  | 12.9      | 11.39 | 12.15   | 16.55 | 16.59  | 16.57   |
| Biomass char   | 5.50      | 5.67  | 5.59    | 5.62  | 5.86   | 5.74    |
| Mass Balance (%)   | 101.1     | 99.8  | 100.5   | 97.20 | 101.10 | 99.18   |
| Tyre char recovered (%)  | 100       | 100   | 100.0   | 90.50 | 91.5   | 91.0    |
| <i>Mass balance based on the biomass sample (wt.%)</i>         |           |       |         |       |        |         |
| Gas  | 52.8      | 47.22 | 50.0    | 67.7  | 66.5   | 67.1    |
| Biomass char   | 22.5      | 23.5  | 23.0    | 23.0  | 23.5   | 23.25   |

### 3.2.4 Products analyses

#### 3.2.4.1 Liquid Effluent analyses

The condensed liquid products (tar/oil/water) obtained from the pyrolysis-catalysis of biomass using waste derived char materials were collected in the condenser system and weighed and then separated into a hydrocarbon oil/tar fraction and water fraction using Karl Fischer titration with a Metrohm 890 Titrando analytical system. The liquid fraction was then further prepared (Figure 3.2-4) to identify the aromatic and oxygenated compounds using GC-MS.

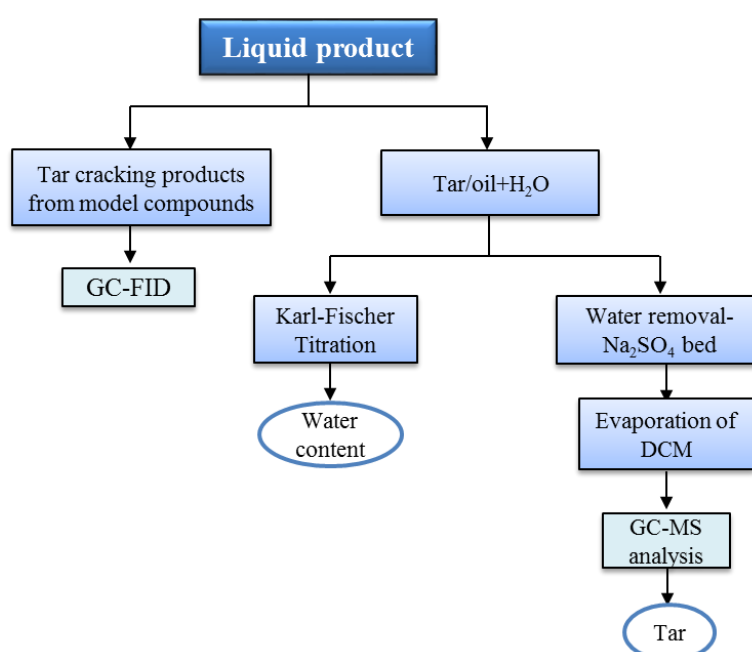


Figure 3.2-4. Flowchart of liquid analysis route.

##### 3.2.4.1.1 Karl-Fischer Titration (KFT)

The condensed fraction trapped in the condensers during the pyrolysis-cracking of biomass experiments was a mixture of water and tar/oil products. The water content was determined using a Karl-Fischer titration. This technique is recommended by several authors for water determination of pyrolysis oils [42-43]. The water is derived from the release of moisture in the biomass and could lower the heating value [43]. The water amount was determined to obtain the tar yield. In addition, the behaviour of water; the amount of water reacted and condensed during the biomass pyrolysis-

cracking process using char is useful to determine the occurrence of char-steam reactions

Therefore, the water content of tar/bio-oil samples was determined using volumetric Karl fisher method, and the titrations were carried out using a KF Titrand 890 Metrohm (Switzerland). The amount of water present in the sample is determined from the consumed amount of iodine as a result of a redox reaction of water with Iodine and sulphur dioxide in the presence of base and alcohol such as methanol as follows:



In this reaction, water and Iodine are consumed in an equimolar ratio; therefore the amount of water can be determined from the consumed amount of Iodine. The analysis was carried out using Hydranol 5K as a titrant which contains iodine, imidazole and sulphur dioxide, whereas the working medium was a Hydranal-Ketosolver. To perform the analysis, a beaker containing a magnetic stirrer was filled with a fresh solvent and the Karl Fischer apparatus was calibrated using a standard mixture solution of methanol and water with a 3:1 mass ratio. For the water determination, an empty syringe was weighed, and then about 0.1 ml of the sample was taken, and the syringe was weighed. Then the sample was injected into the titration beaker of the KF device and the syringe was back-weighed. The weight difference (sample weight) was entered manually and recorded by the apparatus software. The end point (+100) is detected with a double platinum electrode (type Pt1400) [44]. Each sample was measured in duplicate.

The method involves two steps; firstly the standardization of reagent in which the amount of titre is determined as in equation (3.30):

$$\text{The water equivalence factor of reagent (F)} = W/V \quad (3.30)$$

Where, W is the weight of water contained in the standard (mg) and V is the volume of reagent (KF solution) used in the titration (ml). Then the amount of water is

calculated from this titre according to the following equation:

$$\text{Water (\%)} = S \times F / \text{weight of sample (mg)} \cdot 100 \quad (3.31)$$

Where, S is the volume in ml of the consumed reagent in the second titration.

#### 3.2.4.1.2 Gas Chromatography/Mass Spectrometry

The composition of the condensed product bio-oil/tar obtained from the biomass pyrolysis-gasification experiments was analysed for the main hydrocarbon, and oxygenated hydrocarbon compounds present using coupled gas chromatography-mass spectrometry (GC-MS). The condensed liquid at the bottom of the condensers was collected using dichloromethane. Before GC-MS analysis the water contained in the oil mixed with dichloromethane (DCM, Fischer Scientific) samples was extracted by passing the liquid fraction through a bed of sodium sulphate ( $\text{Na}_2\text{SO}_4$ ). The DCM was then evaporated at around 39 °C using an evaporation system. The GC-MS used was a Varian CP-3800 GC connected to a Varian Saturn 2200 MS fitted with a 30 m  $\times$  0.25  $\mu\text{m}$  DB-5 equivalent column with helium as a carrier gas. Gas chromatography-mass spectrometry is an instrument used to separate, identify and quantify complex mixtures of chemicals. The chemical sample is injected into the hot GC inlet where it is vaporised and swept onto a chromatographic column by the carrier gas (helium). The molecules in the mixture are separated based on their relative affinity for the stationary phase (coating of the column) and the molecules with lower boiling points elute faster than those with higher boiling points. The molecules elute from the column at different times called the retention times. As the compounds elute from the column and pass through the transfer line, they are then introduced to a mass detector. In the mass detector, the stream of gas phase molecules passes into the ionization chamber where the beam of molecular ions and fragment ions are generated. The most widely used ionization method is electron impact ionization, where the compounds are bombarded with a beam of electrons produced by a heated filament and resulting in the loss of an electron and produce a radical cation  $\text{M}^+$  which has the same molecular weight of a compound being analysed. Due to the large energy imparted, the radical cation

fragments and produces smaller ions. The resultant positive ions are then repelled out of the ionization chamber by a repeller. The formed ions are then accelerated and passed through a series of slits to produce a focused beam. The formed ions are then moved to the mass analyser (Ion trap) where the ions are separated according to their mass/charge ratio ( $m/z$ ). The  $m/z$  ratio represent the molecular weight of the fragment. The ions are then deflected by a magnetic field. The degree of deflection depends on the mass and charge of ion, the lighter ions are deflected to a greater extent than the heavier ones. The separated ions then enter the detector, and a plot of intensity versus  $m/z$  ratio (mass spectrum) is produced. A schematic diagram of a typical GC-MS system is shown in Figure 3.2-5.

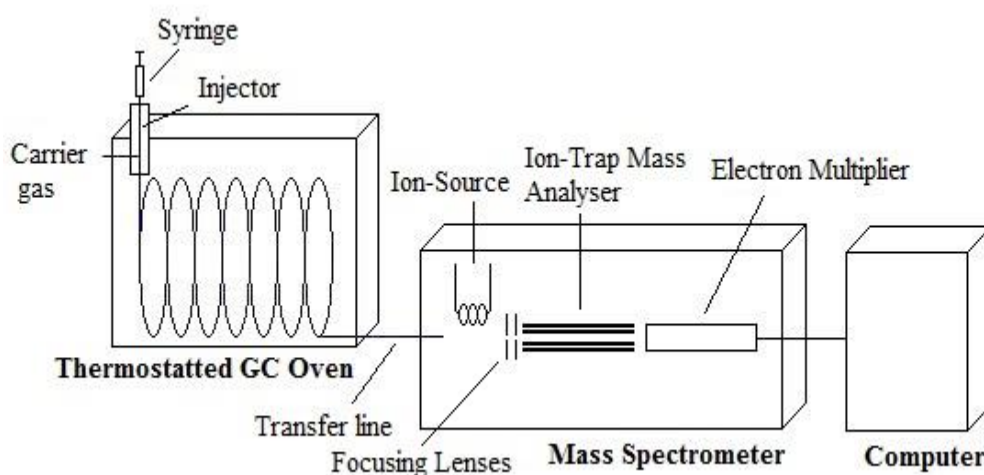


Figure 3.2-5. General diagram of GC-MS.

An aliquot (2  $\mu\text{l}$ ) of the bio-oil/tar dissolved in DCM was injected via auto sampler system into the GC injection port. The GC injector was held at 290  $^{\circ}\text{C}$  and the GC oven was programmed to start analysis at 40  $^{\circ}\text{C}$  and held for 2 min, then ramped to 280  $^{\circ}\text{C}$  at 5  $^{\circ}\text{C min}^{-1}$  heating rate, and finally held at 280  $^{\circ}\text{C}$  for 10 min. The transfer line between the GC and MS was kept at 280  $^{\circ}\text{C}$ , and the ion trap temperature was held at 200  $^{\circ}\text{C}$ . The Internal standard method was used to quantify the compounds present in the oil samples with the use of 2-hydroxyacetophenone as an internal standard. The ion-mass spectra derived were automatically compared to the NIST 2008 spectral library and similarity indexes of >70% were used to identify compounds.

The GC-MS was calibrated using a solution containing standards of different aromatic and oxygenated compounds. A mass of 0.1 g of each compound was dissolved in 10 ml of dichloromethane (DCM) to obtain a solution with a concentration of 10000 ppm for each compound. Then 1 ml of this solution was further diluted with 100 ml of DCM to get a final stock solution with a concentration of 100 ppm. From this concentrated solution, four different diluted standard solutions were prepared with concentrations of 20, 40, 80 and 100 ppm used to create a 4-point calibration curve. Examples of some calibration curves are shown in Figure 3.2-6 which gave  $R^2$  values close to 1.

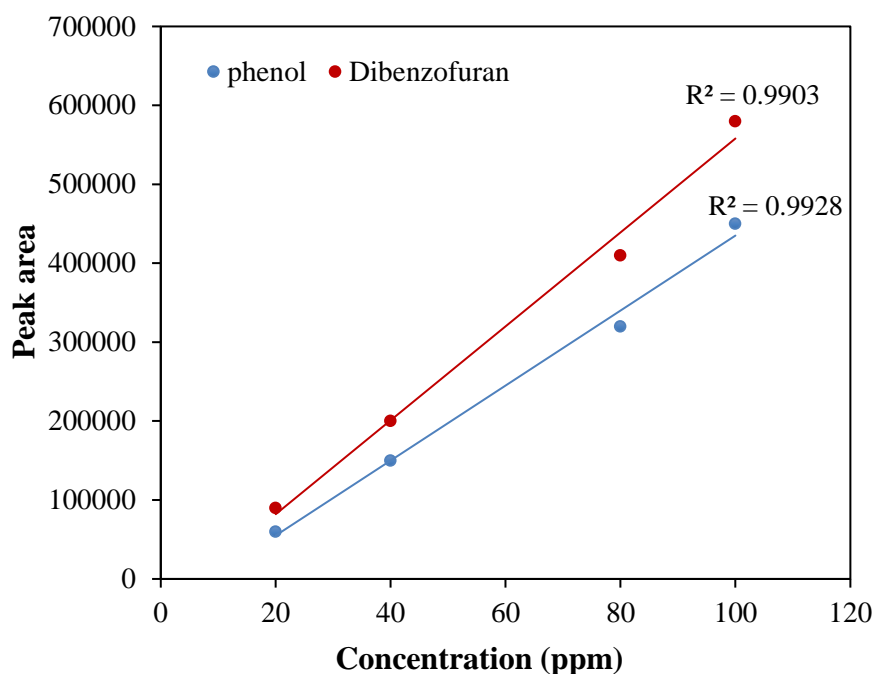


Figure 3.2-6. Calibration curves for dibenzofuran and phenol.

Results of oil analyses were quantified using the calibration line. In some cases, spectral searches on the installed NIST2008 were used for the qualitative identification of the unknown compounds.

The yield of each individual compound was then obtained as (3.32):

$$\text{Individual compound yield } (\mu\text{g/g}) \text{ of biomass} = \frac{\text{Tar concentration (ppm)} \cdot \text{Volume of solution ml}}{\text{weight of biomass (g)}} \quad (3.32)$$

Where tar concentration is the concentration of individual tar compound in the sample analysed and volume of solution is the total volume of the oil obtained during the experiment. However, where the characterization was more important than the tar quantification, some of the results were presented in peak area (%). Figure 3.2-7 shows an example of GC-MS chromatogram of tar/bio-oil sample obtained at a cracking temperature of 800 °C without char.

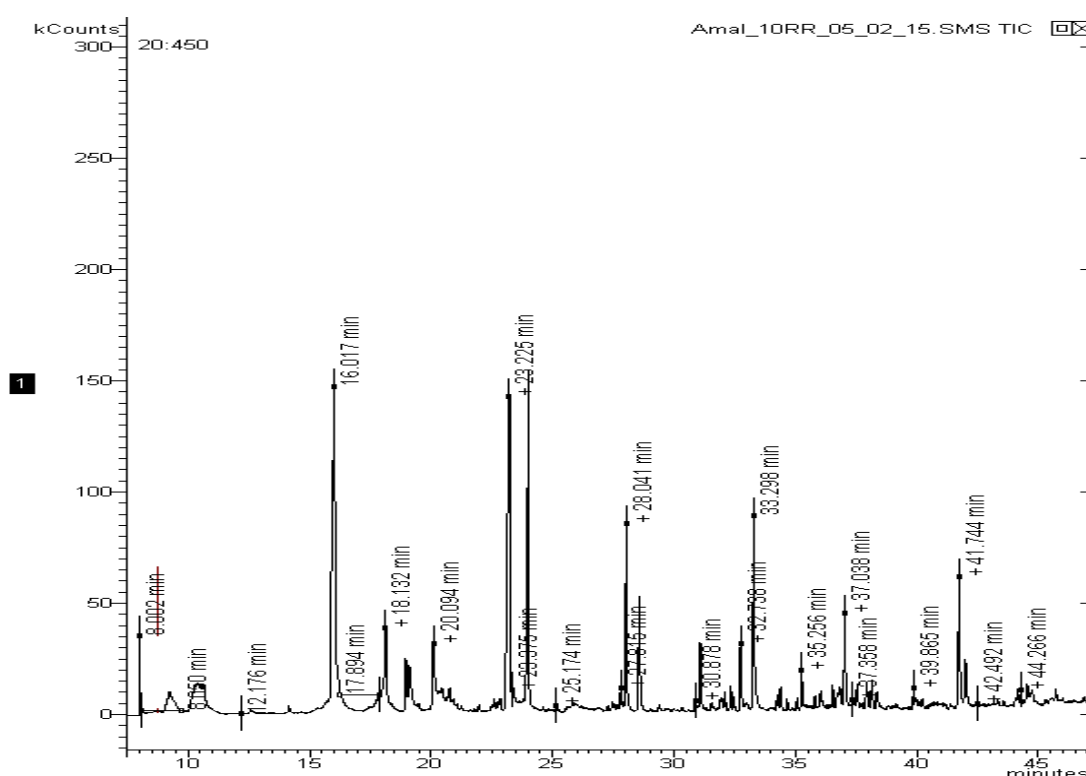


Figure 3.2-7. An example of a GC-MS chromatogram.

### 3.2.4.1.3 Size Exclusion Chromatography

Size exclusion chromatography was used to analyse tar samples to obtain information about the molecular mass distribution. The SEC instrument used was a Perkin-Elmer Series 200 HPLC instrument equipped with a Varian PGE column of 30 cm length and 7.5 mm diameter. Tetrahydrofuran was used as a mobile phase with a flow rate of 0.8 ml min<sup>-1</sup>, and the detector used was a Perkin-Elmer 200a refractive index detector. The samples were prepared by dissolving a small amount of pure oil sample collected during the experiment without any solvent in tetrahydrofuran (THF), with an

approximate concentration of 0.2 vol.%. The instrument calibration was performed using a polystyrene molecular weight standard with molecular weight range of 800-860000. Figure 3.2-8 shows an example of size exclusion chromatogram of tar/bio-oil from the pyrolysis-cracking of biomass.

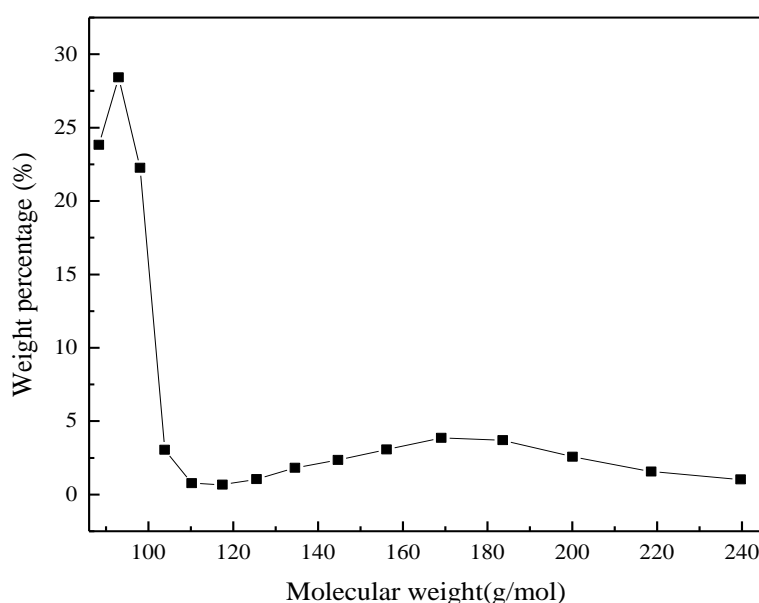


Figure 3.2-8. Size exclusion chromatogram of tar/oil sample.

#### 3.2.4.2 Effluent Gas Analyses

The collected gaseous products were analysed off-line as described earlier in section 3.1-6.

#### 3.2.4.3 Char characterization

Chars were analysed as described in section 3.1-5. In addition, thermogravimetric analysis (TGA) of char was performed using a Stanton-Redcroft thermogravimetric analyser interfaced to a Nicolet Magna IR-560 Fourier transform infra-red spectrometer (FTIR). About 28 mg sample was heated from 25 to 900 °C with a heating rate of 20 °C min<sup>-1</sup> using nitrogen as the carrier gas and holding time of 30 min at the final temperature. The sample weight loss, together with time and temperature and CO, CO<sub>2</sub> detected by FTIR were continuously monitored.

## References

1. BUAH, W.K. and P.T. WILLIAMS. Activated carbons prepared from refuse derived fuel and their gold adsorption characteristics. *Environmental Technology*, 2010, **31**(2), pp.125-137.
2. AL-YAHYAI, R. and M.M. KHAN. Date Palm Status and Perspective in Oman. In: M.J. AL-KHAYRI, M.S. JAIN and V.D. JOHNSON, eds. *Date Palm Genetic Resources and Utilization: Volume 2: Asia and Europe*. Dordrecht: Springer Netherlands, 2015, pp.207-240.
3. BOUCHELTA, C., M.S. MEDJRAM, O. BERTRAND and J.-P. BELLAT. Preparation and characterization of activated carbon from date stones by physical activation with steam. *Journal of Analytical and Applied Pyrolysis*, 2008, **82**(1), pp.70-77.
4. WILLIAMS, P.T. and S. BESLER. The pyrolysis of municipal solid waste. *Journal of the Institute of Energy*, 1992, **65**(465), pp.192-200.
5. ONAY, O. Influence of pyrolysis temperature and heating rate on the production of bio-oil and char from safflower seed by pyrolysis, using a well-swept fixed-bed reactor. *Fuel Processing Technology*, 2007, **88**(5), pp.523-531.
6. KATYAL, S., K. THAMBIMUTHU and M. VALIX. Carbonisation of bagasse in a fixed bed reactor: influence of process variables on char yield and characteristics. *Renewable Energy*, 2003, **28**(5), pp.713-725.
7. YORGUN, S., S. ŞENSÖZ and Ö.M. KOÇKAR. Characterization of the pyrolysis oil produced in the slow pyrolysis of sunflower-extracted bagasse. *Biomass and Bioenergy*, 2001, **20**(2), pp.141-148.
8. FIERRO, V., V. TORNÉ-FERNÁNDEZ and A. CELZARD. Studies in surface science and catalysis. Amsterdam: Elsevier, 2007.
9. BASTA, A.H., V. FIERRO, H. EL-SAIED and A. CELZARD. 2-Steps KOH activation of rice straw: An efficient method for preparing high-performance activated carbons. *Bioresource Technology*, 2009, **100**(17), pp.3941-3947.
10. OH, G.H. and C.R. PARK. Preparation and characteristics of rice-straw-based porous carbons with high adsorption capacity. *Fuel*, 2002, **81**(3), pp.327-336.
11. ILLINGWORTH, J. Chemical activation of biomass fibre with alkali metal salts. Ph.D thesis, University of Leeds, 2005.
12. SMITH, B.C. Infrared Spectral Interpretation: A Systematic Approach. Taylor & Francis, 1998.

13. SINGH, K.S.W., D.H. EVERETT, R.A.W. HAUL, L. MOSCOU, R.A. PIEROTTI, J. ROUQUEROL, AND T. SIEMIENIEWSKA, IUPAC, Reporting physisorption data for gas/solid systems with special reference to the determination of surface area and porosity (Recommendations 1984), in *Pure and Applied Chemistry*, 1985. **57** (4):p. 603-619
14. LEOFANTI, G., M. PADOVAN, G. TOZZOLA and B. VENTURELLI. Surface area and pore texture of catalysts. *Catalysis Today*, 1998, **41**(1-3), pp.207-219.
15. THOMMES, M., K. KANEKO, V. NEIMARK ALEXANDER, P. OLIVIER JAMES, F. RODRIGUEZ-REINSO, J. ROUQUEROL, AND S.W. SING KENNETH, Physisorption of gases, with special reference to the evaluation of surface area and pore size distribution (IUPAC Technical Report), in *Pure and Applied Chemistry* 2015. p. 1051.
16. QUANTACHROME INSTRUMENTS. Gas sorption system operating manual. Quntachrome, 2008.
17. MERINO, E.G., P.D. NEVES, I.M. FONSECA, F. DANÉDE, A. IDRISSE, C.J. DIAS, M. DIONÍSIO and N.T. CORREIA. Detection of Two Glass Transitions on Triton X-100 under Confinement. *The Journal of Physical Chemistry C*, 2013, **117**(41), pp.21516-21528.
18. LÓPEZ, D., R. BUITRAGO, A. SEPÚLVEDA-ESCRIBANO, F. RODRÍGUEZ-REINOSO and F. MONDRAGÓN. Low-Temperature Catalytic Adsorption of NO on Activated Carbon Materials. *Langmuir*, 2007, **23**(24), pp.12131-12137.
19. CLAUDINO, A., J.L. SOARES, R.F.P.M. MOREIRA and H.J. JOSÉ. Adsorption equilibrium and breakthrough analysis for NO adsorption on activated carbons at low temperatures. *Carbon*, 2004, **42**(8-9), pp.1483-1490.
20. KLOSE, W. and S. RINCÓN. Adsorption and reaction of NO on activated carbon in the presence of oxygen and water vapour. *Fuel*, 2007, **86**(1-2), pp.203-209.
21. YANG, J., G. MESTL, D. HEREIN, R. SCHLÖGL and J. FIND. Reaction of NO with carbonaceous materials: 2. Effect of oxygen on the reaction of NO with ashless carbon black. *Carbon*, 2000, **38**(5), pp.729-740.
22. TENG, H. and E.M. SUUBERG. Chemisorption of nitric oxide on char. 1. Reversible nitric oxide sorption. *The Journal of Physical Chemistry*, 1993, **97**(2), pp.478-483.
23. DEGROOT, W.F., T.H. OSTERHELD and G.N. RICHARDS. Chemisorption of oxygen and of nitric oxide on cellulosic chars. *Carbon*, 1991, **29**(2), pp.185-195.

24. GUO, Z., Y. XIE, I. HONG and J. KIM. Catalytic oxidation of NO to NO<sub>2</sub> on activated carbon. *Energy Conversion and Management*, 2001, **42**(15–17), pp.2005-2018.
25. KONG, Y. and C.Y. CHA. NO<sub>x</sub> adsorption on char in presence of oxygen and moisture. *Carbon*, 1996, **34**(8), pp.1027-1033.
26. SOUSA, J.P.S., M.F.R. PEREIRA and J.L. FIGUEIREDO. Catalytic oxidation of NO to NO<sub>2</sub> on N-doped activated carbons. *Catalysis Today*, 2011, **176**(1), pp.383-387.
27. NOWICKI, P., H. WACHOWSKA and R. PIETRZAK. Active carbons prepared by chemical activation of plum stones and their application in removal of NO<sub>2</sub>. *Journal of Hazardous Materials*, 2010, **181**(1–3), pp.1088-1094.
28. JERNIGAN, J.R. *Chemiluminescence NO<sub>x</sub> and GFC NDIR CO Analyzers For Low Level Source Monitoring*. Massachusetts.
29. INSTRUCTION MANUAL. *Multi-gas Analyzer unit VA-3000*, Horiba, 2010.
30. MADILL, D. *Low temperature selective catalytic reduction (SCR) of nitric oxide (NO) on active carbon fibre (ACF) supported transition metal catalysts*. PhD thesis, University of Leeds, 2002.
31. ENGLAND, C., J. HOUSEMAN and D.P. TEIXEIRA. Sampling nitric oxide from combustion gases. *Combustion and Flame*, 1973, **20**(3), pp.439-442.
32. DU, Z.-Y., X. WANG, Z.-H. ZHANG, J. FENG, Y.-H. QIN, B.-B. ZHANG and W.-Y. LI. Evolution properties of cellulose- and lignin-derived pyrolysis tars after interacting with coal chars. *Journal of Analytical and Applied Pyrolysis*.
33. HOSOYA, T., H. KAWAMOTO and S. SAKA. Pyrolysis gasification reactivities of primary tar and char fractions from cellulose and lignin as studied with a closed ampoule reactor. *Journal of Analytical and Applied Pyrolysis*, 2008, **83**(1), pp.71-77.
34. EVANS, R.J. and T.A. MILNE. Molecular characterization of the pyrolysis of biomass. *Energy & Fuels*, 1987, **1**(2), pp.123-137.
35. BRIDGWATER, A.V. Catalysis in thermal biomass conversion. *Applied Catalysis A: General*, 1994, **116**(1), pp.5-47.
36. LI, D., M. TAMURA, Y. NAKAGAWA and K. TOMISHIGE. Metal catalysts for steam reforming of tar derived from the gasification of lignocellulosic biomass. *Bioresource Technology*, 2015, **178**, pp.53-64.

37. FENG, D., Y. ZHAO, Y. ZHANG, S. SUN, S. MENG, Y. GUO and Y. HUANG. Effects of K and Ca on reforming of model tar compounds with pyrolysis biochars under H<sub>2</sub>O or CO<sub>2</sub>. *Chemical Engineering Journal*, 2016, **306**, pp.422-432.
38. COLL, R., J. SALVADÓ, X. FARRIOL and D. MONTANÉ. Steam reforming model compounds of biomass gasification tars: conversion at different operating conditions and tendency towards coke formation. *Fuel Processing Technology*, 2001, **74**(1), pp.19-31.
39. LI, B., Z. LEI and Z. HUANG. Surface-Treated Activated Carbon for Removal of Aromatic Compounds from Water. *Chemical Engineering & Technology*, 2009, **32**(5), pp.763-770.
40. PARK, J., Y. LEE and C. RYU. Reduction of primary tar vapor from biomass by hot char particles in fixed bed gasification. *Biomass and Bioenergy*, 2016, **90**, pp.114-121.
41. HOSOKAI, S., K. KUMABE, M. OHSHITA, K. NORINAGA, C.Z. LI and J.I. HAYASHI. Mechanism of decomposition of aromatics over charcoal and necessary condition for maintaining its activity. *Fuel*, 2008, **87**(13-14), pp.2914-2922.
42. OASMAA, A. and D. MEIER. Norms and standards for fast pyrolysis liquids: 1. Round robin test. *Journal of Analytical and Applied Pyrolysis*, 2005, **73**(2), pp.323-334.
43. MOHAN, D., C.U. PITTMAN and P.H. STEELE. Pyrolysis of Wood/Biomass for Bio-oil: A Critical Review. *Energy & Fuels*, 2006, **20**(3), pp.848-889.
44. SMETS, K., P. ADRIAENSENS, J. VANDEWIJNGAARDEN, M. STALS, T. CORNELISSEN, S. SCHREURS, R. CARLEER and J. YPERMAN. Water content of pyrolysis oil: Comparison between Karl Fischer titration, GC/MS-corrected azeotropic distillation and <sup>1</sup>H NMR spectroscopy. *Journal of Analytical and Applied Pyrolysis*, 2011, **90**(2), pp.100-105.

## **CHAPTER 4.NO REMOVAL USING WASTE DERIVED ACTIVATED CARBONS**

---

This chapter is divided into two sections, which focus on the assessment of the efficiency of waste derived activated carbons for control of nitrogen oxides (NO<sub>x</sub>) at low temperature. The NO<sub>x</sub> investigated was in the form of nitric oxide (NO), and adsorption tests were conducted using a fixed bed reactor system described in Chapter 3, Section 3.1.7. A brief description of each section is given below.

Section 4.1 contains results obtained from the carbonisation and physical activation of RDF, waste tyre and date stones. The produced activated carbons were investigated in relation to NO removal. The influence of temperature, oxygen concentration and NO concentration on NO removal was also investigated. In addition, the efficiency of these produced activated carbons for NO removal was compared with commercial carbons with varied porous texture and surface chemistry.

Section 4.2 reports results of the production of activated carbons from waste tyres using a chemical activation process with different alkali-activating agents, KOH, K<sub>2</sub>CO<sub>3</sub>, NaOH and Na<sub>2</sub>CO<sub>3</sub>, to determine their influence on the characteristics of the product activated carbons. The activated carbons were tested in terms of their ability to adsorb NO at low temperature (25 °C) from a simulated flue gas in relation to the various characteristics, particularly surface area and porosity of the carbons.

## **4.1 Nitrogen oxide removal using commercial and waste-derived physically activated carbons**

This section describes NO removal from a simulated flue gas stream using waste derived activated carbons produced from waste materials compared with commercially obtained carbons. The activated carbons were prepared using a fixed bed reactor following the procedure described in chapter 3, section 3.1.1. The activated carbon samples were designated as AC-D for the date stones biomass waste, AC-R for the activated carbon produced from refuse derived fuel (RDF) and AC-T for the carbons produced from waste tyres. In addition, the efficiency of these activated carbons in terms of NO removal from the gas stream was compared to different commercial carbons (labelled C-AC1, C-AC2, C-AC3 and C-AC4) with varied porous texture and surface chemistry to determine the main carbon properties that influence nitrogen oxide adsorption. The nitrogen oxide adsorption was investigated at a low temperature of 50 °C.

### **4.1.1 Properties of the raw precursors**

Table 4.1-1 shows the properties of the raw waste RDF, tyre and date stones. The RDF had a significant ash content at 11.0 wt.% consisting of mainly alumina-silicates and also a significant metal content, including heavy metals. The tyre also had a high ash content at 7.1 wt.%, with zinc as a prominent constituent which was derived from the tyre as an additive to the tyre manufacturing process and also with the presence of other metals and filler materials. The date stones had the lowest ash content at 4.0 wt.% consisting of mainly calcium, potassium, magnesium and phosphorus.

Table 4.1-1. Composition of the raw waste materials.

| <b>Proximate analysis (wt.%)</b> | <b>RDF</b> | <b>Tyre</b> | <b>Date Stones</b> |
|----------------------------------|------------|-------------|--------------------|
| Volatiles                        | 72.0       | 62.2        | 69.9               |
| Moisture                         | 4.0        | 1.4         | 7.5                |
| Ash                              | 11.0       | 7.1         | 4.0                |
| Fixed carbon                     | 13.0       | 29.4        | 18.2               |
| <b>Minerals analysis (wt.%)</b>  |            |             |                    |
| ZnO                              | 0.06       | 2.95        | 0.01               |
| SiO <sub>2</sub>                 | 4.64       | 1.74        | 0.14               |
| Fe <sub>2</sub> O <sub>3</sub>   | 0.36       | 0.40        | 0.03               |
| CaO                              | 1.86       | 0.24        | 0.21               |
| K <sub>2</sub> O                 | 0.28       | 0.07        | 1.98               |
| Al <sub>2</sub> O <sub>3</sub>   | 2.31       | 0.17        | 0.04               |
| P <sub>2</sub> O <sub>5</sub>    | 0.05       | 0.03        | 0.90               |
| CuO                              | 0.01       | 0.06        | <0.01              |
| MgO                              | 0.50       | 0.05        | 0.61               |

#### 4.1.2 Product Yield from the Fixed Bed Pyrolysis of the Waste Materials

Table 4.1-2 shows the product yield (solid, liquid and gas) from the pyrolysis of RDF, waste tyre and date stones. The yield was calculated according to the following expression:

$$\text{Mass Balance} = \frac{\text{Weight of gas, oil and char residue}}{\text{Weight of sample}} \times 100 \quad \text{Eq. 4.1-1}$$

The pyrolysis was carried out in a fixed bed reactor at a heating rate of 10 °C min<sup>-1</sup> to a final temperature of 600 °C and held at that temperature for 1 hour. Repeat pyrolysis experiments were carried out using the fixed bed reactor described in section 3.1.3 and an excellent repeatability was obtained.

Table 4.1-2. Product yield from the pyrolysis of waste materials

| Raw Material                   | RDF   | Tyre  | Date stones |
|--------------------------------|-------|-------|-------------|
| <b>Products Yield (wt.%)</b>   |       |       |             |
| Char                           | 30.67 | 36.82 | 23.66       |
| Liquid                         | 53.84 | 55.34 | 58.93       |
| Gas                            | 15.46 | 7.64  | 18.94       |
| <b>Gas composition (vol.%)</b> |       |       |             |
| CO                             | 60.31 | 18.60 | 39.00       |
| H <sub>2</sub>                 | 20.93 | 4.40  | 33.00       |
| CO <sub>2</sub>                | 13.21 | 25.20 | 12.70       |
| CH <sub>4</sub>                | 2.39  | 17.80 | 6.60        |
| C <sub>2</sub> —C <sub>4</sub> | 3.16  | 33.57 | 8.66        |
| Mass balance (%)               | 99.35 | 99.8  | 101.52      |

The mass balances obtained were all close to 100 %. As the main product being pyrolysis oil, the use of three cooled condensers systems had helped to get a good mass balance. The largest char yield of about 36 wt.% was obtained for waste tyre. Pyrolysis of waste tyre by other researchers reported similar amounts of char [1-3]. They showed that tyre rubber starts to decompose at a temperature of 450 °C and the process was complete at a temperature of 500-600 °C and gave char yields between 33-42 wt.%. Date stones yielded the highest gaseous and liquid product. The pyrolysis products for the studied precursors were in the range of values obtained by previous researchers [4-5].

The gaseous composition obtained from the pyrolysis of the three waste materials are shown in Table 4.1-2. The gases are generated due to the thermal breakdown of waste components and also through the secondary cracking reactions of the primary products [4]. RDF and date stones have a high oxygen content; therefore the main pyrolysis gases are carbon dioxide and carbon monoxide generated from the thermal degradation of cellulose, hemicellulose and lignin. On the other hand, the pyrolysis of waste tyre produced a higher concentration of hydrocarbons gases. Waste tyre is less oxygenated and is made of about (60-65%) rubber mainly butyl rubber and styrene-butadiene rubber which with the thermal degradation produces a high concentration of C<sub>4</sub> compounds [6].

### 4.1.3 Properties of the commercial and waste-derived activated carbons

The proximate and ultimate analyses of the commercial activated carbons and the activated carbons produced from the waste materials are shown in Table 4.1-3. The activated carbon samples were designated as AC-D for the date stones biomass waste, AC-R for the activated carbon produced from refuse derived fuel (RDF) and AC-T for the carbons produced from waste tyres. For comparison, commercial carbons described in Chapter 3, section 3.1.1.4 (labelled C-AC1, C-AC2, C-AC3 and C-AC4) were used.

Table 4.1-3. Proximate and ultimate analysis of the activated carbons.

| Sample             | Proximate analysis (wt.%) |      |              | Elemental analysis (wt.%) |     |     |                |
|--------------------|---------------------------|------|--------------|---------------------------|-----|-----|----------------|
|                    | Volatiles                 | Ash  | Fixed carbon | C                         | H   | N   | O <sup>a</sup> |
| C-AC1              | 2.5                       | 2.4  | 85.6         | 89.9                      | 0.3 | 0.8 | 6.0            |
| C-AC2              | 5.1                       | 5.0  | 90.9         | 90.8                      | 0.3 | 0.8 | 0.3            |
| C-AC3              | 5.5                       | 1.3  | 89.3         | 93.5                      | 0.6 | 0.4 | 4.1            |
| C-AC4              | 1.7                       | 8.2  | 85.6         | 88.0                      | 0.3 | 0.6 | 2.0            |
| AC-R (RDF)         | 6.1                       | 60.9 | 28.9         | 36.4                      | 0.4 | 1.5 | 0.4            |
| AC-T (Tyre)        | 2.8                       | 23.9 | 73.3         | 61.1                      | 0.2 | 1.4 | 9.3            |
| AC-D (Date stones) | 4.1                       | 10.0 | 83.9         | 74.5                      | 0.6 | 2.1 | 12.8           |

There are large differences in the ash content of the commercial carbons compared to the activated carbons produced from the waste materials, particularly the carbons produced from refuse derived fuel and tyres. The mineral matter found in the original feedstock becomes progressively concentrated through the process of pyrolysis, due to the reduction of the mass of solid product through loss of volatiles to produce the char. Additionally, during the subsequent activation process, the mineral matter is further concentrated as the carbon reacts with the steam to produce gases, such as carbon dioxide, carbon monoxide, hydrogen, methane etc., as the char is activated (gasified). As can be observed from Table 4.1-3, the commercial carbons have high carbon content (88-93 wt.%). Among the used waste materials, date stones showed the highest elemental carbon content (74 wt.%), fixed carbon (83.9 wt.%) and had a significant amount of nitrogen (2.10 wt.%). These properties have been reported to

accelerate NO adsorption by carbon [7]. The abundance of nitrogen content in AC-D could have a role in enhancing NO adsorption as reported by Rathore et al. [8] in which the highest NO adsorption at room temperature was found with the sample containing the highest amount of nitrogen containing groups. Bashkova and Bandosz [9] concluded that a high NO<sub>2</sub> adsorption was found with carbon containing quaternary nitrogen groups, which was ascribed to the presence of positive charge centres for the adsorption of NO<sub>2</sub> and NO which can be further reduced to N<sub>2</sub> or oxidized to nitrate.

Table 4.1-4 shows the analysis of the commercially obtained activated carbons for their metal contents using X-ray fluorescence (XRF). There were clear differences between the carbons in terms of their ash composition. These differences may be attributed to the composition of the original precursor raw material (which was not known due to being company proprietary information) or related to additives to the carbons during the commercial preparation process (again, information could not be obtained).

Table 4.1-4. Mineral composition of the commercial activated carbons

| Minerals analysis (wt.%)       | C-AC1 | C-AC2 | C-AC3 | C-AC4 |
|--------------------------------|-------|-------|-------|-------|
| SiO <sub>2</sub>               | 0.15  | 0.07  | 0.04  | 1.07  |
| Fe <sub>2</sub> O <sub>3</sub> | 0.39  | 0.22  | 0.06  | 3.44  |
| CaO                            | 0.74  | 1.78  | 0.14  | 1.97  |
| K <sub>2</sub> O               | 0.47  | 0.92  | 0.81  | 0.08  |
| Al <sub>2</sub> O <sub>3</sub> | 0.02  | 0.01  | <0.01 | 0.52  |
| P <sub>2</sub> O <sub>5</sub>  | 0.47  | 0.10  | 0.05  | 0.08  |
| MgO                            | 0.03  | 0.04  | 0.01  | 0.07  |
| MnO                            | 0.03  | 0.13  | 0.01  | 0.04  |

The metal contents and surface morphology of the activated carbons produced from the waste materials were estimated from the SEM-EDXS analysis and are presented in Figure 4.1-1. The SEM images show that the type of activated carbon precursor has a strong influence on the development of porous texture of the resulting activated carbon. As shown in Figure 4.1-1, both the activated carbons derived from waste tyres and date stones (AC-T and AC-D) present a smooth and a regular surface, while the RDF activated carbon (AC-R) shows a heterogeneous structure. The EDX spectra

indicate the existence of a high percentage of calcium, sodium and other minerals with AC-R, while AC-T showed the presence of a high amount of zinc. The presence of abundant amounts of alkaline minerals in a sample cannot be assumed to give high reactivity for NO<sub>x</sub>, for example, Ahmed et al. [10] reported a high nitrogen oxide adsorption activity with a sample contained the lowest mineral content of alkaline metal oxides (calcium oxide, magnesium oxide and sodium oxide).

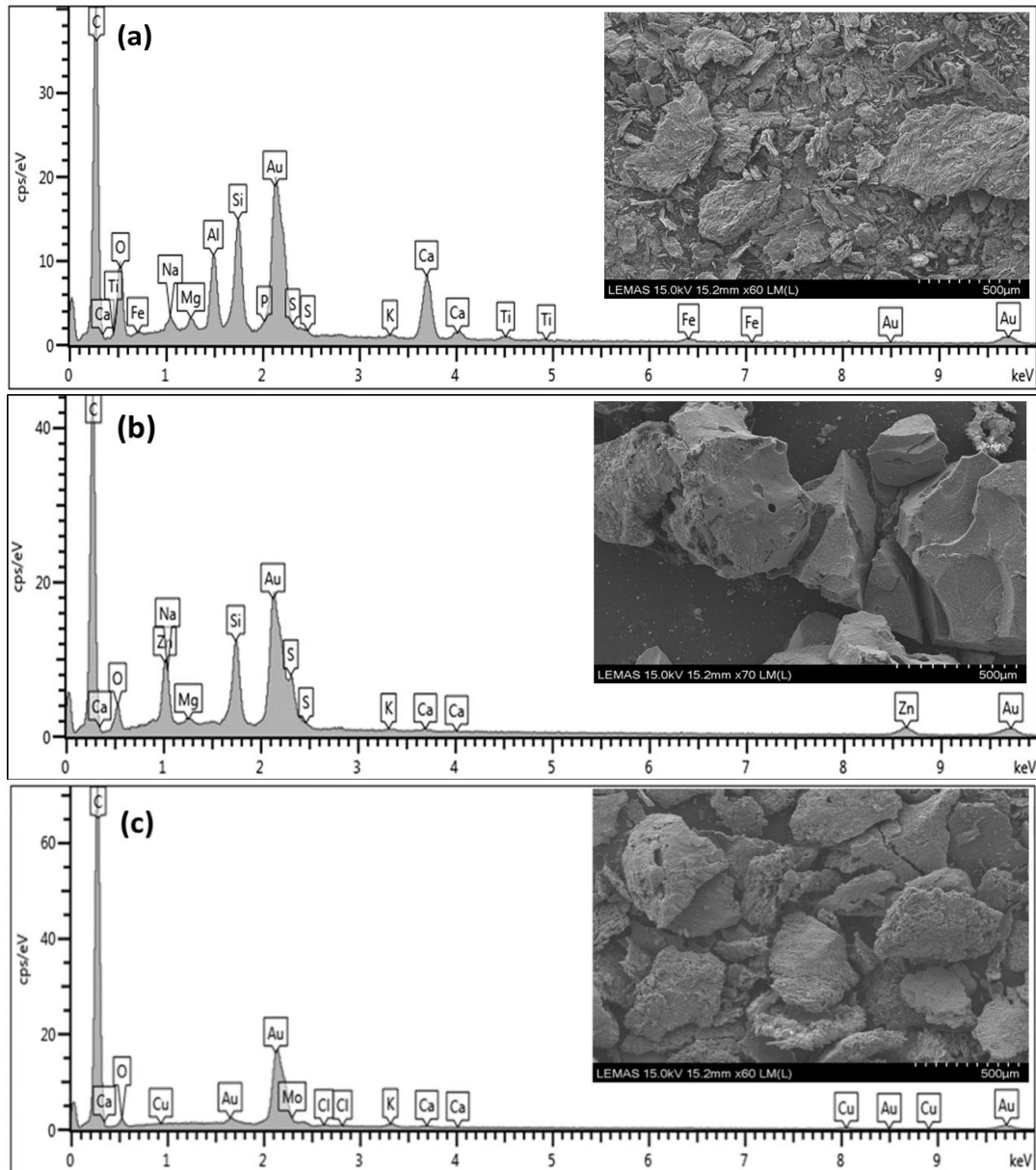


Figure 4.1-1. SEM-EDXS results of the waste-derived activated carbons: (a) activated carbon from RDF (AC-R); (b) activated carbon from waste tyre (AC-T); and (c) activated carbon from date stones (AC-D)

#### **4.1.4 NO removal using commercial and waste derived activated carbons**

Waste derived activated carbons and the commercially obtained activated carbons were investigated for their NO adsorption characteristics with the NO adsorption reactor using a gas mixture of NO (800 ppm) and air (5 vol.% oxygen) and at 50 °C adsorption temperature. The reactor system used was described in Chapter 3, Section 3.1.7. The NO removal efficiency curves for the commercial activated carbons and the waste derived activated carbon are shown in Figure 4.1-2 (a) and (b) respectively. There is an initial high adsorption of the NO by the activated carbons, but the level of adsorption decreases before reaching a steady level of adsorption. The highest removal efficiency was found for the commercial C-AC1 activated carbon at 60% removal efficiency achieved after the 120 minutes test time.

The other commercial activated carbons achieved about 40% NO removal after 120 minutes. For the waste derived activated carbons, the NO concentration after 2 hours adsorption was reduced to 630 ppm with the tyre derived activated carbon, to 585 ppm for the refuse derived fuel carbon and to 480 ppm for the biomass (date stones) activated carbon. The waste derived activated carbons showed a lower, but still an effective level of NO adsorption, with removal efficiencies of 40%, 26% and 21% for the AC-D, AC-R and AC-T respectively at 120 minutes.

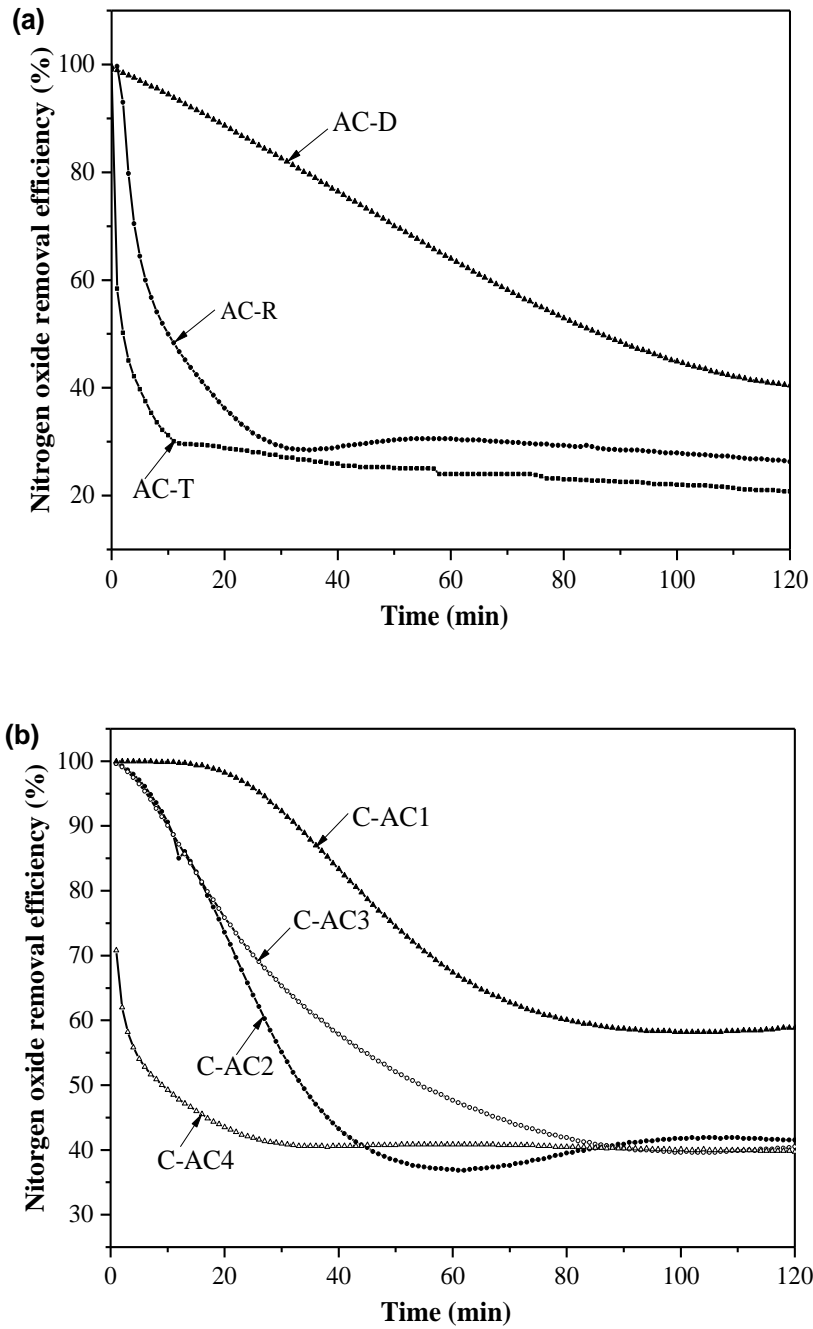


Figure 4.1-2. The NO removal efficiency curves for (a) the commercial activated carbons and (b) the waste derived activated carbons at 50 °C adsorption temperature

The NO adsorption capacity obtained by the waste derived activated carbons and the commercial carbons was calculated according to the formula (3.20) described in Chapter 3 (Section 3.1.7), with results listed in Table 4.1-5.

Table 4.1-5. Adsorption amount of NO ( $\text{mg g}^{-1}$ ) and as NO per mass of carbon

| <b>Activated carbon</b>             | <b>NO<sub>ads</sub> (<math>\text{mg g}^{-1}</math>)</b> | <b>NO<sub>ads</sub> (<math>\text{mg g}^{-1}</math>) per mass of carbon</b> |
|-------------------------------------|---|--|
| <i>Commercial activated carbons</i> |   |  |
| C-AC1                               | 28.03   | 28.72  |
| C-AC2                               | 19.02   | 19.48  |
| C-AC3                               | 20.78   | 21.05  |
| C-AC4                               | 15.92   | 17.34  |
| <i>Waste derived carbons</i>        |   |  |
| AC-T(Tyre)                          | 9.68  | 12.69  |
| AC-R (RDF)                          | 12.51   | 30.06  |
| AC-D (date stones)                  | 15.26   | 17.05  |

The greatest NO adsorption capacity of  $28.03 \text{ mg g}^{-1}$  was obtained for the commercial activated carbon C-AC1. Waste derived activated carbons; in particular, AC-R and AC-T, showed much lower NO sorption capacity. It should be noted that the lower performance of the tyre and refuse derived fuel activated carbons is linked to the high ash contents of these carbons. Consequently, from Table 4.1-3, the actual mass of carbon present in the NO adsorption reactor for the RDF activated carbon (60.9 wt.% ash) was only 40% of that used for the commercial activated carbon experiments. Similarly, for the waste tyre activated carbon (23.9 wt.% ash), there was only 76% of carbon present compared to the tests using the commercial activated carbons. The adsorption capacity of the original RDF activated carbon (with ash) was  $12.5 \text{ mg g}^{-1}$ , however, on the basis of the actual mass of carbon used, the adsorption was found to be  $30.06 \text{ mg NO per gram of carbon}$ . Therefore, to achieve comparable NO adsorption efficiencies to those obtained from commercially available activated carbons, a higher mass of waste derived activated carbon would be needed.

To verify that the low sorption capacity of AC-T and AC-R is probably related to the high content of mineral matter in their structure, waste tyre was demineralized with HCl to reduce the catalytic mineral content. The acid demineralization was effective in reducing the mineral content of AC-T to 5%. The demineralized AC-T was then examined for NO removal. As presented in Figure 4.1-3, the demineralized AC-T exhibited a higher NO adsorption capacity than the original AC-T. This could be due to the availability of more free active sites on the demineralized carbon because of the ash removal. Thus, the BET surface area of AC-T increased after demineralization. The same observation was reported by others [11-12]. Lenz et al. [11] also reported an increase in NO adsorption capacity of brown coal coke after being demineralized with hydrochloric acid. Rubio et al. [12] believed that the increase of BET surface area, after demineralization, is the main factor for the increase in NO removal for the demineralized sample.

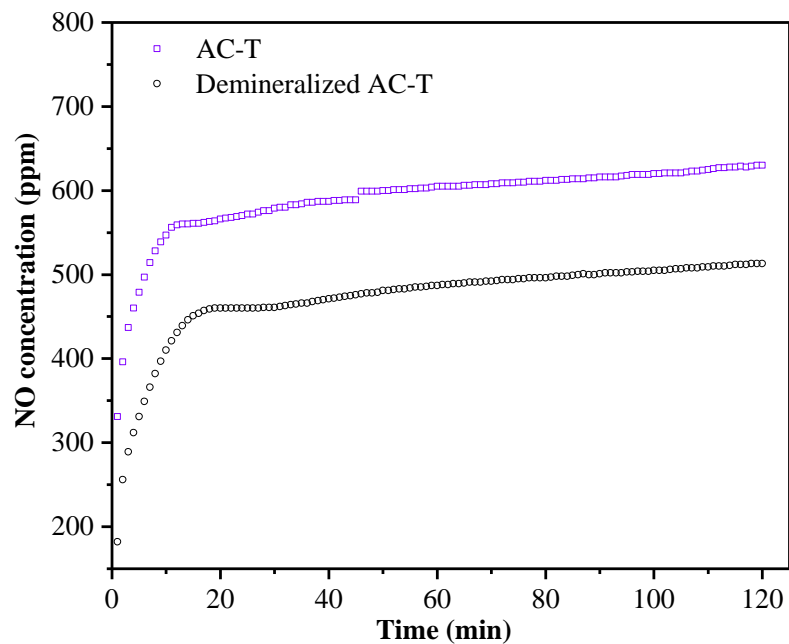


Figure 4.1-3. Comparison of NO breakthrough curve obtained for AC-T sample before and after demineralization

#### 4.1.5 Surface Area and Pore Characteristics of the Activated Carbons

To understand the differing level of NO removal efficiency found by the different adsorbents, the properties of surface area and porosity of the activated carbons were

investigated. The pore size distribution for activated carbons are classified into average pore size classes; micropores are of pore width  $< 2$  nm, mesopores of pore width 2-50 nm and macropores are of pore width  $> 50$  nm [13].

The pore width refers to the distance between the walls of slit-shaped pores or the radius of cylindrical shaped pores. The nitrogen adsorption-desorption isotherms of waste derived activated carbons and the commercial carbons are shown in Figure 4.1-4(a) and 4.1-4(b) respectively. The data suggest that the activated carbons for the C-AC1, C-AC2, C-AC3, C-AC4 produced adsorption-desorption isotherms characteristic of Type I and Type IV isotherms according to the IUPAC classification [14]. Therefore, these activated carbons contained both micropores and mesopores. The Type I isotherm is characterized by the initial steep portion of the adsorption isotherm at low relative pressures which represents the filling of the micropores by the adsorbate. The isotherm then reaches a plateau indicating the amount adsorbed by a unit mass of activated carbon reaches a limiting value. The Type IV isotherm exhibits a significant adsorption-desorption hysteresis loop indicating the filling and emptying of mesopores by capillary condensation. The isotherms obtained for AC-T and AC-R were more similar to Type 5 isotherms [14] which indicate a more mesoporous type of activated carbon. The amount of nitrogen adsorbed by activated carbons derived from waste is smaller than that of the commercial activated carbons and they exhibit a hysteresis loop, which indicates the presence of mesopores.

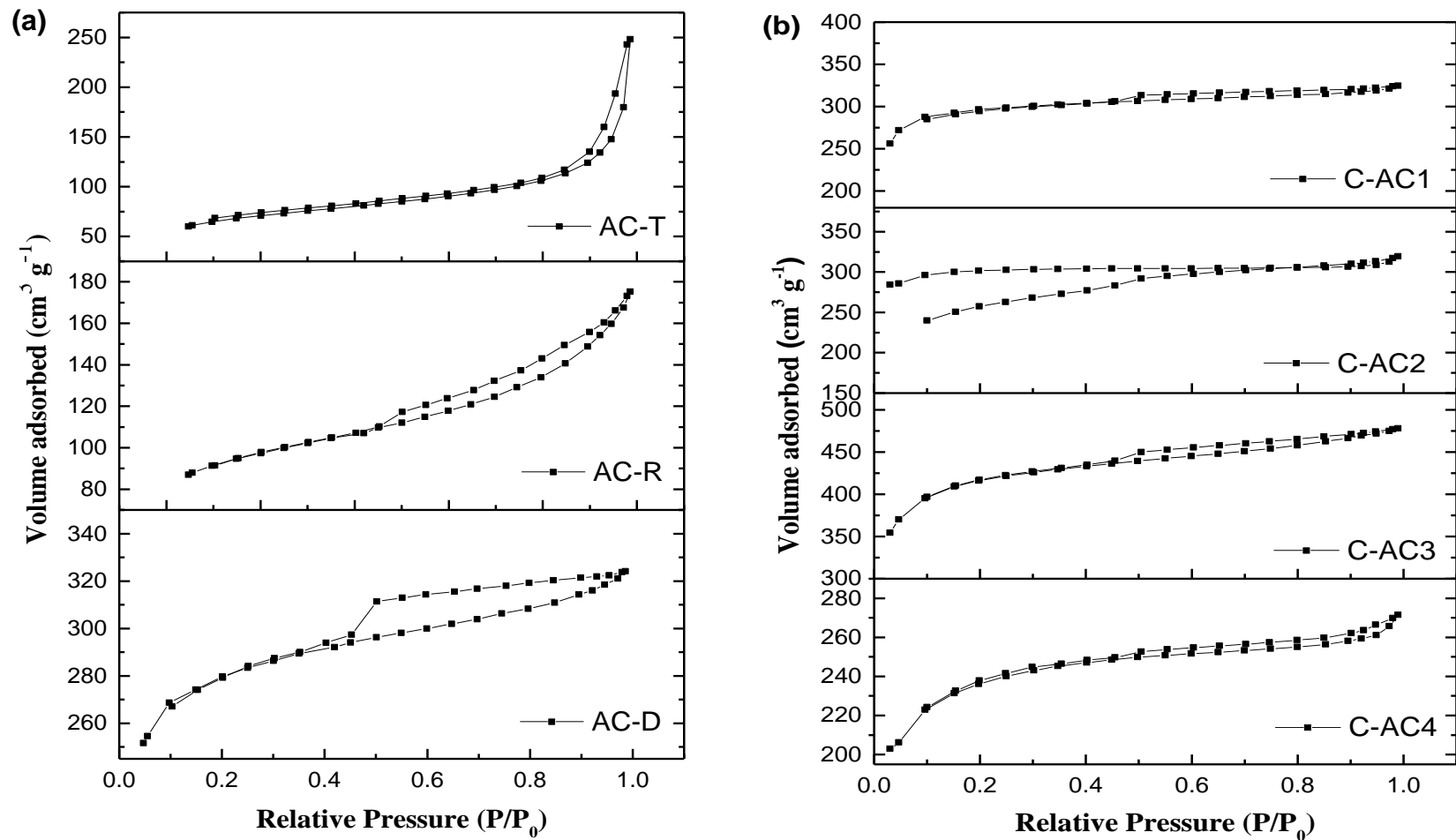


Figure 4.1-4. Nitrogen adsorption-desorption isotherms for the (a) waste derived activated carbons and (b) commercial activated carbons

Table 4.1-6 shows the surface area, mesopore and micropore volumes of the activated carbons as determined by a Nova gas analyser (Chapter 3, Section 3.1.5.7). The development of the surface area and porosity characteristics of an activated carbon produced by the pyrolysis of the waste raw material followed by char-steam activation is determined by the characteristics of the original raw materials and the process conditions of pyrolysis and activation. The commercial activated carbons had high surface areas, ranging from 558 m<sup>2</sup> g<sup>-1</sup> to 988 m<sup>2</sup> g<sup>-1</sup>. In the case of the activated carbons produced from waste, surface areas were somewhat lower than the commercial activated carbons at 270 m<sup>2</sup> g<sup>-1</sup> for the AC-T, 340 m<sup>2</sup> g<sup>-1</sup> for the AC-R, but the activated carbon produced from date stones had a high BET surface area of 867 m<sup>2</sup> g<sup>-1</sup>.

Table 4.1-6. Surface area and pore size characteristics of the commercial and waste derived activated carbons.

| <b>Sample</b>      | <b>Surface area<br/>(m<sup>2</sup> g<sup>-1</sup>)</b> | <b>Micropore volume<br/>(cm<sup>3</sup> g<sup>-1</sup>)</b> | <b>Mesopore volume<br/>(cm<sup>3</sup> g<sup>-1</sup>)</b> |
|--------------------|--|---|--|
| C-AC1              | 944  | 0.479   | 0.304  |
| C-AC2              | 912  | 0.466   | 0.109  |
| C-AC3              | 988  | 0.510   | 0.324  |
| C-AC4              | 750  | 0.350   | 0.145  |
| AC-T (Tyre)        | 270  | 0.214   | 0.784  |
| AC-R (RDF)         | 340  | 0.223   | 0.620  |
| AC-D (Date stones) | 867  | 0.478   | 0.203  |

In relation to the influence of the surface area and pore size characteristics of the activated carbons on NO adsorption, the BET surface area showed no clear correlation with NO removal efficiency. For example, the highest NO adsorption (60%) was achieved with the C-AC1 carbon which had the second highest surface area of 944 m<sup>2</sup> g<sup>-1</sup>, but C-AC2 and C-AC3 had high surface areas of 912 m<sup>2</sup> g<sup>-1</sup> and 988 m<sup>2</sup> g<sup>-1</sup> respectively but had very different NO adsorption efficiencies. Additionally, date stones with a surface area of 867 m<sup>2</sup> g<sup>-1</sup> showed similar NO removal efficiency to the C-AC2 commercial carbon with a surface area of up to 900 m<sup>2</sup> g<sup>-1</sup>.

There is also disagreement in the literature regarding the influence of surface area and porosity on the rate of NO reduction on a carbon surface. Several authors [15-16] have

considered that the rate of NO adsorption is proportional to the internal surface area of the char. However, Neathery et al. [17] observed that the NO adsorption capacity of the studied activated carbons was not directly related to their surface areas and micropore volumes. The same conclusion was derived by Ruiz Machado and Hall [16] and Guo et al. [15]. Other overriding factors which may influence NO adsorption over the carbon surface area, are the size of the molecule being adsorbed such that the pollutant cannot enter the micropores of the carbon and the surface chemistry of the carbon which may not be conducive to NO adsorption [18].

The pore size characteristics presented in Table 4.1-6 showed that C-AC1, C-AC2 and C-AC3 contained a mixture of micropores and mesopores, and the C-AC4 was microporous. However, the tyre (AC-T) and refuse fuel derived activated carbons (AC-R) were mainly mesoporous, while AC-D contained a mixture of micropores and mesopores.

Figures 4.1-5(a) and 4.1-5 (b) show the pore size distribution of the activated carbons produced from wastes and also the commercial adsorbents respectively as calculated by the DFT method (Chapter 3, Section 3.1.5.7.4). The lower removal efficiency of activated carbons produced from waste tyre and RDF compared to those of commercial carbons or date stones is suggested to be largely because of the differences in porous structure. The pores of the commercial activated carbons and biomass date stones are mostly located in the micropore range of 1-2 nm while the activated carbons produced from RDF and tyre have a much greater number of pores with diameters in the range of 2-10 nm particularly many pores greater than 4 nm. Pores of these sizes are probably unsuitable for effective NO adsorption, since the kinetic diameter of NO is 0.317 nm, suggesting microporous activated carbons would be more suitable for NO adsorption. The prevalence of mesopores in the tyre and the RDF derived carbons seems to reduce the efficiency of the product activated carbon to capture NO.

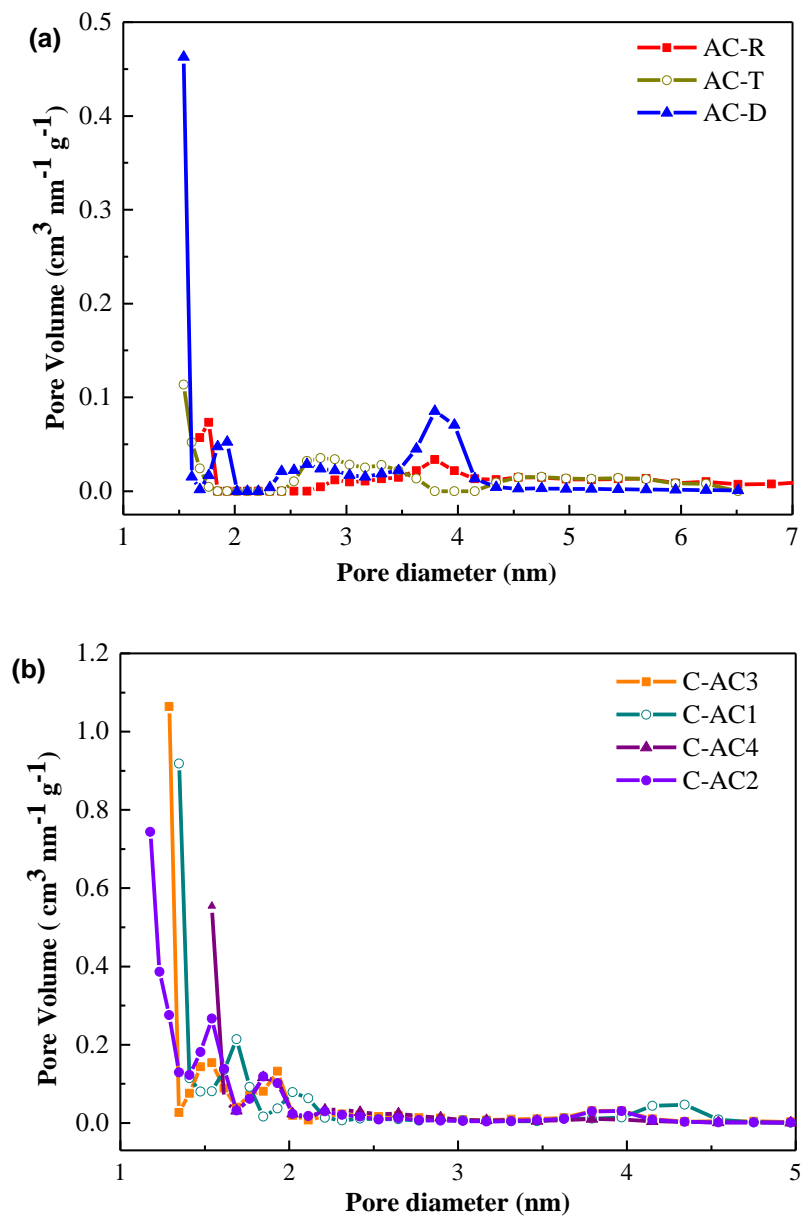


Figure 4.1-5. Pore size distribution for (a) the waste-derived activated carbons and (b) the commercial activated carbons

To further study the influence of surface area and porosity on NO adsorption, one of the waste materials (waste tyre) was activated to different degrees of carbon burn off, to prepare activated carbons with different surface area and pore size characteristics together with the NO adsorption efficiency after 120 minutes of operation (Table 4.1-6). The activation process is described in Chapter 3, Section 3.1.4.1. The data presented in Table 4.1-7, show that increasing the activation time led to an increase in the BET surface area and micropore volume, which was accompanied by a

proportional increase in NO removal. This suggests that the porous texture has an important role in determining the NO capture by the studied carbons. However, there appeared to be no correlation with the mesoporosity of the tyre derived activated carbons and NO removal efficiency.

Table 4.1-7. Influence of surface area, mesopore volume and micropore volume of the tyre derived activated carbons on NO removal efficiency at 120 minutes.

| Sample      | Activation time (min) | Surface area ( $\text{m}^2 \text{g}^{-1}$ ) | Mesopore volume ( $\text{cm}^3 \text{g}^{-1}$ ) | Micropore volume ( $\text{cm}^3 \text{g}^{-1}$ ) | NO (%) |
|-------------|-----------------------|---|---|--|--------|
| AC-T (Tyre) | 45 min                | 88  | 0.61  | 0.09   | 9      |
| AC-T (Tyre) | 90 min                | 70  | 0.54  | 0.08   | 7      |
| AC-T (Tyre) | 180 min               | 270   | 0.78  | 0.21   | 23     |

#### 4.1.5.1 Acid-base properties

The surface chemistry of the product activated carbons may also influence the uptake of NO. The chemical structure of activated carbons are associated with heteroatoms (hydrogen, oxygen, nitrogen, sulphur) which are bonded at the edges of aromatic carbon sheets or to carbon atoms within the carbon matrix forming various surface functional groups which can be acidic, basic or neutral [19]. These functional groups are responsible for the uptake of pollutants. The commercial and the waste derived activated carbons were therefore analysed by Boehm titration to determine the concentration of basic and acidic chemical groups on the carbon surface (as described in Chapter 3, Section 3.1.5.4). The results are shown in Table 4.1-8. For the commercial carbons, the content of the basic surface groups varied in the range of 0.66-1.22  $\text{mmol g}^{-1}$ , while for the RDF waste derived activated carbon, the content of basic surface groups was almost double (2.65  $\text{mmol g}^{-1}$ ). The very high content of basic groups with RDF could be due to the presence of the high mineral components and metal compounds found in the raw precursor material (Table 4.1-1) and also as shown by the SEM-EDXS analysis of the waste derived activated carbons (Figure 4.1-1).

Table 4.1-8. Acid and base properties of the activated carbons

| Sample         | pH    | Basic groups<br>(mmol g <sup>-1</sup> ) | Acidic groups<br>(mmol g <sup>-1</sup> ) | Total content of surface<br>oxides (mmol g <sup>-1</sup> ) |
|----------------|-------|---|--|--|
| C-AC1          | 9.52  | 1.22                                    | 0.05                                     | 1.27   |
| C-AC2          | 9.20  | 1.17                                    | 0.13                                     | 1.30   |
| C-AC3          | 9.24  | 0.66                                    | 0.02                                     | 0.68   |
| C-AC4          | 7.58  | 0.69                                    | 0.00                                     | 0.69   |
| AC-R(RDF)      | 10.67 | 2.65                                    | 0.00                                     | 2.65   |
| AC-T (Tyre)    | 8.11  | 0.51                                    | 0.30                                     | 0.81   |
| AC-D (Biomass) | 7.53  | 0.71                                    | 0.00                                     | 0.71   |

Hu et al. [20] and Nowicki and Pietrzak [21] found that activated carbons with the highest content of basic groups and the lowest content of acidic groups had the highest NO sorption capacity. Comparison of the acidic and basic groups on the activated carbons (Table 4.1-8) with the NO removal data shown in Figure 4.1-2, showed that the commercial activated carbon with the highest basic groups C-AC-1, had the highest NO removal efficiency. C-AC1 and C-AC2 have a similar amount of basic groups but C-AC2 has a higher amount of acidic groups which could be the reason for the lower NO removal efficiency of C-AC2. The inhibitory effect of acidic groups in relation to the NO adsorption capacity of carbons has been reported in the literature [21]. For the activated carbon produced from waste, the AC-R had the highest concentration of basic groups but showed no significant influence on NO removal compared to the other activated carbons, suggesting other inhibitory factors related to metal content or pore structure that influence NO adsorption for the RDF activated carbon.

#### 4.1.6 Influence of Temperature, NO Concentration and Oxygen on NO Adsorption

To determine the optimal conditions needed to obtain the maximum NO removal efficiency, the influence of the process parameters of adsorption temperature and NO gas concentration on the adsorption of NO were examined for tyre and biomass-derived activated carbons. The RDF activated carbon was not further investigated because of the high ash content of the product carbon. Figure 4.1-6 shows the influence

of activated carbon temperature using the NO adsorption reactor (Chapter 3, Section 3.1.7). Adsorption experiments were carried out at temperatures of 25, 50 and 100 °C and at a fixed NO concentration of 800 ppm and oxygen concentration of 5%.

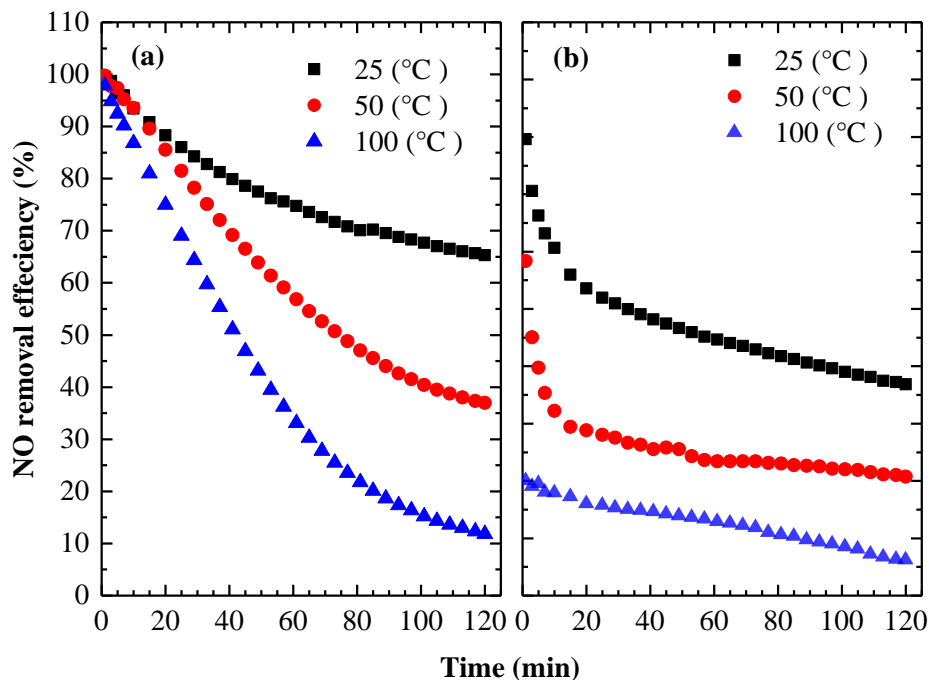


Figure 4.1-6. Influence of temperature on NO removal efficiency at 120 minutes for (a) date stones (AC-D) and (b) tyre (AC-T) derived activated carbons.

Both the tyre derived carbon and the biomass derived carbon showed a decrease in NO removal efficiency as the adsorption temperature was increased. At low temperature, physisorption of the NO takes place on the carbon surface which means that activated carbon acts as a medium for adsorbing the reactants and not as a catalyst (chemisorption), this will lead to a decrease in the NO conversion with increasing temperature. Guo et al. [15] also reported a decrease in the adsorption of NO onto activated carbon fibres with an increase in temperature from 30 °C to 100 °C. The decrease of NO adsorption with the increase in temperature suggests that NO adsorption is a physical process and the forces exist between the NO and the activated carbon are weak Vander Waals forces. A higher temperature decreases the physisorption but enhance the chemisorption rate. The same observation was reported by others [22-23]. Choo et al. [24] reported that an increase in the operating temperature caused a decrease in the adsorption capacity of the activated carbon

because at higher temperature the vapour pressure of adsorbate increase and therefore increasing the energy level of the adsorbate molecules to overcome the Vander Waals attraction and migrate back to the bulk gas phase.

The NO removal efficiency of carbon will also depend on the NO concentration in the flue gas. The effect of varying the inlet flue gas NO concentration on the adsorption capacity of activated carbons produced from waste tyre and biomass date stones was assessed. Figure 4.1-7 shows the influence of NO concentration on NO removal. Experiments were carried out with NO inlet concentration of 200, 400, 800 ppm in the flue gas and with a fixed O<sub>2</sub> concentration of 5% and at an adsorption temperature of 25 °C.

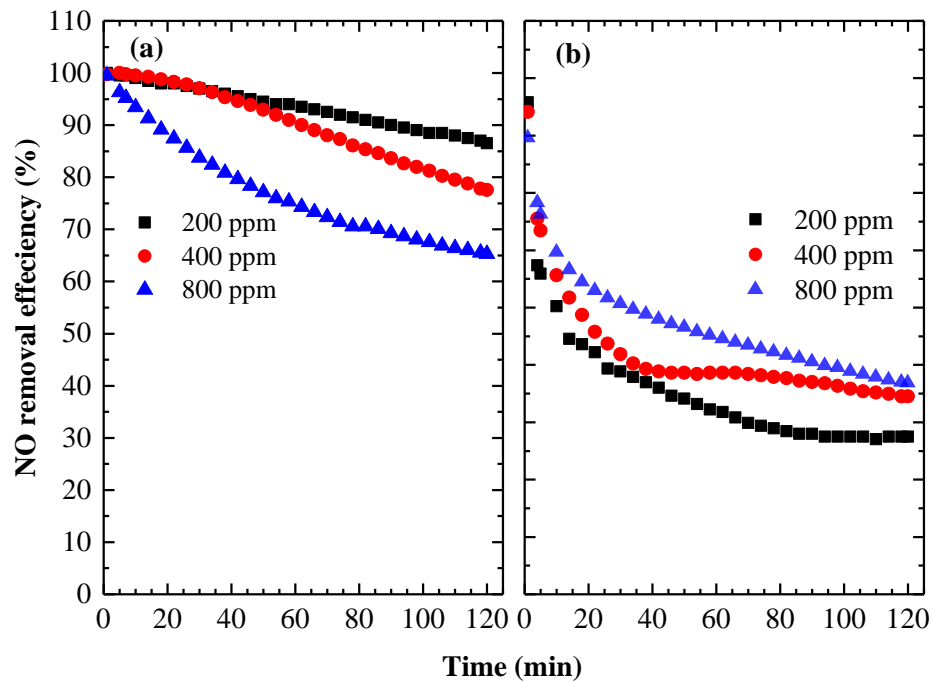


Figure 4.1-7. Influence of NO concentration (ppm) on NO removal efficiency at 120 minutes for (a) date stones (AC-D) and (b) tyre (AC-T) derived activated carbons.

The effect of increasing the NO concentration did not reveal the same trend for both carbons; this could be due to the difference in the surface chemistry of the adsorbents. For the date stones, there was a substantial decrease in adsorption as the NO was increased from 200 ppm to 800 ppm. In the case of waste tyre, NO removal efficiency increased with increasing NO concentration (Figure 4.1-7). A similar behaviour was

observed by others [15, 25]. For example, Guo et al. [15] investigated the influence of NO concentration on NO adsorption with activated carbon and reported a 69% NO adsorption capacity at 600 ppm NO concentration, reducing to 65% at 200 ppm but reducing markedly to 40% at 50 ppm. On the contrary, Klose and Rincon [26] observed a different trend on using activated carbon synthesized from oil palm shells at a temperature of 100 °C. They reported a decrease in the adsorption capacity as the influent NO concentrations were increased from 400 ppm to 1200 ppm.

In addition, another set of experiments were carried out to study the influence of oxygen concentration on NO removal. For this purpose, the oxygen concentration was varied between 5-13% (Figure 4.1-8). Experiments were carried out with a fixed NO inlet concentration of 400 ppm and at an adsorption temperature of 25 °C.

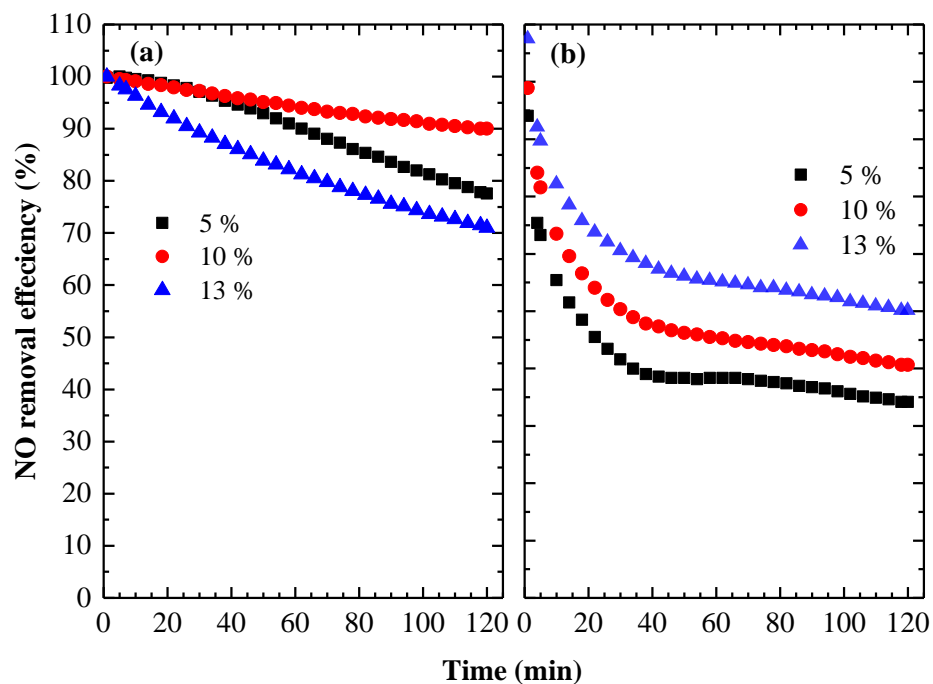
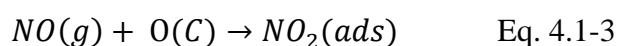


Figure 4.1-8. Influence of oxygen concentration on NO removal efficiency at 120 minutes for (a) date stones (AC-D) and (b) tyre (AC-T) derived activated carbons.

It is evident from the results shown in Figure 4.1-8 that the NO adsorption for both carbons (waste tyre and date stones) increased with the increase of oxygen concentration in the simulated flue gas from 5 to 10%. However, increasing the oxygen concentration to 13% led to a decrease in the NO removal of date stones to about 70%.

In a study by Xu [27], in which activated carbon produced from wheat straw was used for NO adsorption at a temperature of 20 °C. A 100 % NO removal efficiency was obtained with 10 % oxygen. However, the residence time used was about 10 s, which was quite high compared to the one used in this research (1.7 s). The presence of oxygen is crucial for the effective NO capture by carbon. It is well reported by various researchers that the presence of oxygen enhances the reaction rate between NO and carbon. This could be explained by the catalytic oxidation of NO by O<sub>2</sub> to NO<sub>2</sub> and then NO<sub>2</sub> is adsorbed on the carbon surface, which has been reported to have a higher adsorption potential by carbon than NO [26-28]. Yang et al. [28] also observed a higher reactivity of NO<sub>2</sub> with carbon than that with NO.

It has been suggested that oxygen first adsorbed on the carbon surface (Eq. 4.1-2) and then reacts with NO to form NO<sub>2</sub> (Eq. 4.1-3) [29].



Where (g) is the species in the gas phase and O (C) refers to the oxygen complexes from on the carbon surface.

Increasing the oxygen concentration led to a different trend depending on the type of the raw material used to prepare the activated carbon. According to the literature different material behaves differently. For example, Chen et al. [30], claimed that the highest NO adsorption capacity was found with oxygen concentration of 4% and efficiency declined when the oxygen content was higher than 8%. In contrast, Kong and Cha [29] reported no relation between the NO removal and oxygen concentration when the oxygen concentration was higher than 5%.

#### **4.1.7 Reaction mechanism of NO adsorption**

FTIR analysis was carried out to identify the nature of NO adsorbed species formed on the carbon surface during the NO adsorption experiment using waste derived activated carbons. The analytical procedure is described in Chapter 3, Section 3.1.5.5).

As shown in Figure 4.1-9, by comparing the IR vibrational bands before and after adsorption, a remarkable band at around  $1400\text{ cm}^{-1}$  was observed with AC-R after adsorption which is likely to be due to the presence of nitrates [31-33]. Additionally, the appearance of another band at around  $850\text{ cm}^{-1}$  is ascribed also to the presence of organic nitrates ( $\text{R-O-NO}_2$ ) [9].

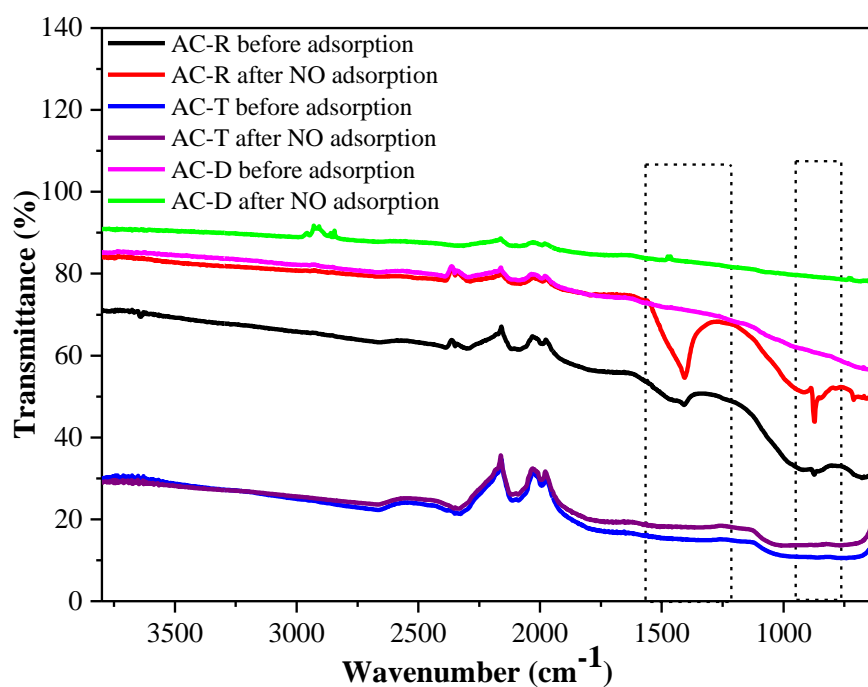


Figure 4.1-9. FTIR spectra for the waste derived activated carbons before and after NO removal at  $50\text{ }^{\circ}\text{C}$ .

However, these bands were observed only with AC-R as RDF contains more inorganic species compared to tyre and date stones. The type and concentration of mineral matter could influence the adsorption ability of carbon due to the formation of nitrate through the reaction of NO with ash. A weak absorption band was found with AC-D at  $1500\text{ cm}^{-1}$ , such a band can be assigned to the adsorbed  $\text{NO}_2$  species [32, 34]. Long and Yang [34] concluded that the main NO adsorbed species formed on carbon after NO adsorption at room temperature, were nitrate,  $\text{NO}_2$  dimers and  $\text{NO}_2$ .

The nitro compounds such as nitrate and nitrite are expected to form on carbon surface during NO adsorption; therefore the adsorbents after adsorption were soaked into

deionized water for one week. The filtered solution was then analysed by ionic chromatography. During the leaching step of activated carbon, following NO capture experiments, the nitrate ions were found in important quantities in AC-R, AC-D and AC-T. The concentration of the detected nitrates were largely higher than the detected nitrite ions, this may suggest the presence of adsorbed  $\text{NO}_2$  over activated carbons, which during the leaching process react with  $\text{H}_2\text{O}$  leading to the formation of nitric acid ( $\text{HNO}_3$ ) which dissociate to form  $\text{NO}_3^-$  or also it could be due to the oxidation of NO to  $\text{NO}_2$  which then adsorbed on the carbon surface as nitrates. Long and Yang [34] also studied the NO adsorption at room temperature using carbon nanotubes and reported the oxidation of NO to  $\text{NO}_2$  which then adsorbed on the carbon surface as nitrates. Therefore nitrates were identified as the dominant adsorbed species. Lopez et al. [35] observed by XPS the formation of nitro and nitrate complexes during the adsorption of NO on activated carbon produced from Sub-bituminous coal at  $30^\circ\text{C}$ . Therefore, it can be suggested that the main NO adsorbed species formed during the NO adsorption are  $\text{NO}_2$  and  $\text{NO}_3^-$  (Figure 4.1-10).

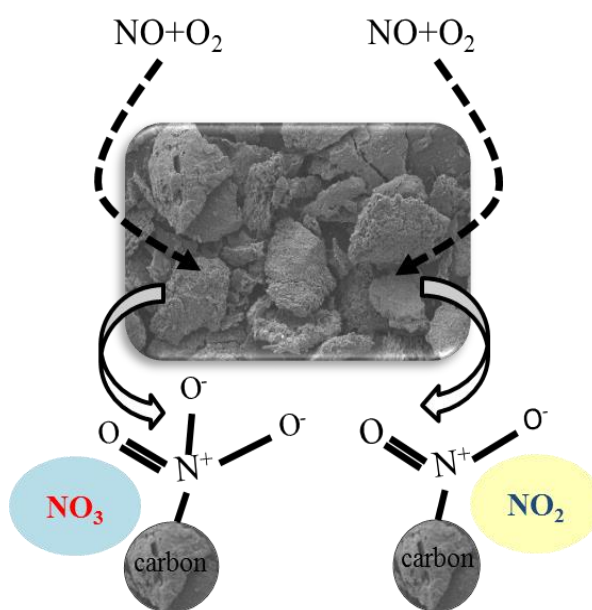


Figure 4.1-10. The nature of NO adsorbed species formed on carbon (adapted from [35]).

Different mechanisms have been proposed to describe the interaction of NO with carbon. Mochida et al. [25] identified through XPS and IR the presence of  $\text{NO}_2$  as the

main adsorbed species on carbon during NO adsorption over activated carbon fibre at 30 °C. With the presence of oxygen, activated carbon acts as a catalyst to oxidize NO into NO<sub>2</sub> which is then adsorbed on the carbon micropores. The adsorbed NO<sub>2</sub> may further react with carbon and form various nitro compounds such as NO<sub>3</sub> and NO-NO<sub>3</sub> [8, 36].

Adapa [37] more recently proposed Langmuir-Hinshelwood and Eley-Rideal mechanisms for the NO oxidation over carbon (Table 4.1-9). In Langmuir-Hinshelwood mechanism (mechanism 1), both NO and oxygen are assumed to adsorb on the free active sites on carbon (Eq.4.1-4 and 4.1-5), followed by the oxidation of the adsorbed NO species into NO<sub>2</sub>. Various intermediates such as NO<sub>3</sub> and NO-NO<sub>3</sub> are expected to form due to the reaction of adsorbed NO<sub>2</sub>. Finally, the NO-NO<sub>3</sub> is desorbed as NO<sub>2</sub> [8]. In the Eley-Rideal mechanism (mechanism 2), the adsorbed NO reacts directly with the gaseous O<sub>2</sub> instead of C-O (mechanism 2, Eq. 4.1-10) and form NO<sub>2</sub> adsorbed species [38]. However, Hui et al. [39], reported that the gaseous O<sub>2</sub> oxidizes the adsorbed NO rather than the adsorbed O<sub>2</sub>. NO<sub>2</sub> can be easily removed by water; therefore catalytic oxidation of NO to NO<sub>2</sub> is an effective process to control NO without the need for use of reducing agents such as ammonia [40].

Table 4.1-9. Proposed reaction mechanisms of NO oxidation to NO<sub>2</sub> on carbon [37].

| <b>Mechanism 1</b>                                    |            |
|---|------------|
| $NO + C_f \rightarrow C - NO$                         | Eq. 4.1-4  |
| $O_2 + 2C_f \rightarrow 2C - O$                       | Eq. 4.1-5  |
| $C - NO + C - O \rightarrow C - NO_2 + C_f$           | Eq. 4.1-6  |
| $C - NO_2 + C - NO_2 \rightarrow C - NO_3 + NO + C_f$ | Eq. 4.1-7  |
| $C - NO_3 + C - NO \rightarrow C - NO - NO_3 + C_f$   | Eq. 4.1-8  |
| <b>Mechanism 2</b>                                    |            |
| $NO + C_f \rightarrow C - NO$                         | Eq. 4.1-9  |
| $2C - NO + O_2 \rightarrow 2C - NO_2$                 | Eq. 4.1-10 |
| $C - NO_2 + C - NO_2 \rightarrow C - NO_3 + NO + C_f$ | Eq. 4.1-11 |
| $C - NO_3 + C - NO \rightarrow C - NO - NO_3 + C_f$   | Eq. 4.1-12 |
| $C - NO - NO_3 \rightarrow 2NO_2 + C_f$               | Eq. 4.1-13 |

#### **4.1.8 Summary of section 4.1**

Adsorption of NO at low temperature was studied using activated carbon produced from waste materials. Different commercial carbons with different porous texture and surface chemistry were used for the comparison. The porous structure and surface chemistry of the studied adsorbents were analysed and compared to the NO removal efficiency of carbons. From the presented results and analysis, it can be concluded that the micropore size and the pore width play an important role in determining the efficiency of activated carbons for NO capture, but less so for surface area. The differences in performance of the activated carbons could also be attributed to the influence of porous texture and surface chemistry. The waste-derived activated carbons had NO removal efficiencies of 40%, 26% and 21% for the carbons derived from date stones, refuse derived fuel and waste tyres respectively at 50 °C adsorption temperature. Commercially produced activated carbons had NO removal efficiencies of between 40% and 60%. Therefore, although the waste derived activated carbons were somewhat less effective than commercially produced carbons they still showed a high and effective level of NO removal. In addition, the use of waste materials for the minimisation of a problematic pollutant is a novel re-use of resources.

## 4.2 Activated Carbons from Chemical Activation of Waste Tyres for Low Temperature NO Control

Section 4.1 examined the adsorption of NO using waste derived activated carbons produced by physical activation of different waste materials. Section 4.2 examines the influence of surface area and porosity of the waste tyre activated carbons produced via chemical activation with different alkali chemical activating agents to investigate their effect on NO capture at low temperature (25 °C). Tyre chars were activated with alkali chemical agents, KOH, K<sub>2</sub>CO<sub>3</sub>, NaOH and Na<sub>2</sub>CO<sub>3</sub> to produce waste tyre derived activated carbons. The aim was to improve NO removal of waste tyre activated carbon by improving the porosity. Therefore, the influence of varying the chemical activation conditions on the porous texture and corresponding NO removal from the flue gas was investigated.

### 4.2.1 Activated carbon preparation and characterization

Details regarding the preparation method of the waste tyre chemically activated carbons used in this section can be found in Chapter 3, Section 3.1.4.2 The designation of the produced activated carbons are shown in Table 4.2-1.

Table 4.2-1. Preparation conditions of the activated carbons

| Sample Designation                 | Activating agent                | Wt. ratio (Char: Chemical agent) | Activation Temperature (°C) |
|------------------------------------|---------------------------------|----------------------------------|-----------------------------|
| TA-KOH0.5                          | KOH                             | 1:0.5                            | 900°C                       |
| TA-KOH1                            | KOH                             | 1:1                              | 900°C                       |
| TA-KOH3                            | KOH                             | 1:3                              | 900°C                       |
| TA-KOH4                            | KOH                             | 1:4                              | 900°C                       |
| TA-KOH3-700                        | KOH                             | 1:3                              | 700°C                       |
| TA-KOH3-800                        | KOH                             | 1:3                              | 800°C                       |
| TA-K <sub>2</sub> CO <sub>3</sub>  | K <sub>2</sub> CO <sub>3</sub>  | 1:3                              | 900°C                       |
| TA-NaOH                            | NaOH                            | 1:3                              | 900°C                       |
| TA-Na <sub>2</sub> CO <sub>3</sub> | Na <sub>2</sub> CO <sub>3</sub> | 1:3                              | 900°C                       |

The elemental analysis of the prepared adsorbents is shown in Table 4.2-2. The carbon content varied from 65 to 88 wt.%. Increasing the char: activating agent for KOH increased the carbon content of the activated carbon products. Samples activated with KOH showed a greater content of carbon and a lower content of hydrogen and sulfur than those prepared with  $K_2CO_3$ ,  $Na_2CO_3$  and NaOH. Additionally, increasing the activation temperature led to higher carbon content and lower hydrogen and the sulfur contents in the product activated carbons. Similar results have been reported by Hofman and Pietrzak [41]. No correlation was found between the elemental compositions of the prepared samples and their NO capture capacity.

Table 4.2-2. Elemental analysis of the waste derived activated carbons.

| <b>Activated Carbon Sample</b> | <b>C<br/>(wt.%)</b> | <b>H<br/>(wt.%)</b> | <b>N<br/>(wt.%)</b> | <b>S<br/>(wt.%)</b> |
|--------------------------------|---------------------|---------------------|---------------------|---------------------|
| TA-KOH0.5                      | 65.00               | 3.19                | 1.60                | 0                   |
| TA-KOH1                        | 64.51               | 2.35                | 1.40                | 0                   |
| TA-KOH3                        | 88.26               | 2.44                | 1.51                | 0                   |
| TA-KOH4                        | 88.02               | 2.78                | 0.62                | 0                   |
| TA-KOH3-700                    | 69.67               | 5.37                | 2.25                | 0.53                |
| TA-KOH3-800                    | 83.97               | 4.58                | 1.76                | 0.55                |
| TA- $K_2CO_3$                  | 87.02               | 3.61                | 1.52                | 0.39                |
| TA-NaOH                        | 80.01               | 3.04                | 1.52                | 0.38                |
| TA- $Na_2CO_3$                 | 76.20               | 3.37                | 1.25                | 0.27                |

The textural properties of the activated carbon samples are shown in Table 4.2-3. The BET surface area, micropore and mesopore volumes of the carbons were obtained from the adsorption/desorption isotherms of  $N_2$  at 77 K. The results indicate the positive influence of the type of activating agent and the activation temperature on the porosity development. The modification of active carbons by KOH results in the formation of active carbons with high BET surface area and microporous structure as also reported by Hayashi et al. [42].

The influence of the char: KOH impregnation ratio on the porosity of the product carbons was investigated at 900 °C activation temperature. As presented in Table 4.2-3, the BET surface area and the micropore volume increased in relation to increasing impregnation ratio (TA-KOH3), and then decreased (TA-KOH4). The BET surface

area and micropore volume of TA-KOH3 were 621 m<sup>2</sup> g<sup>-1</sup> and 0.437 cm<sup>3</sup> g<sup>-1</sup> respectively. However, with the char to KOH ratio of 4 both the BET surface and pore volumes decreased.

Table 4.2-3. Porous properties of the waste derived activated carbons

| Sample                             | Total surface area <sup>a</sup><br>[m <sup>2</sup> g <sup>-1</sup> ] | Micropore volume <sup>b</sup><br>[cm <sup>3</sup> g <sup>-1</sup> ] | Mesopore volume <sup>c</sup><br>[cm <sup>3</sup> g <sup>-1</sup> ] | Pore diameter <sup>d</sup><br>(nm) |
|------------------------------------|--|---|--|------------------------------------|
| TA-KOH0.5                          | 202  | 0.185   | 0.611  | 1.038                              |
| TA-KOH1                            | 287  | 0.240   | 0.728  | 1.098                              |
| TA-KOH3                            | 621  | 0.437   | 0.884  | 0.962                              |
| TA-KOH4                            | 315  | 0.269   | 0.775  | 0.905                              |
| TA-KOH3-700                        | 170  | 0.184   | 0.690  | 1.675                              |
| TA-KOH3-800                        | 243  | 0.192   | 0.427  | 1.443                              |
| TA-K <sub>2</sub> CO <sub>3</sub>  | 133  | 0.201   | 0.788  | 2.450                              |
| TA-NaOH                            | 128  | 0.173   | 0.543  | 2.426                              |
| TA-Na <sub>2</sub> CO <sub>3</sub> | 92   | 0.132   | 0.490  | 2.446                              |

<sup>a</sup> Multi-Point Brunauer, Emmett & Teller (BET) Method.

<sup>b</sup> Dubinin-Radushkevich (DR) Method.

<sup>c</sup> Barrett, Joyner & Halenda (BJH) Method.

<sup>d</sup> Density Functional Theory (DFT) Method.

The higher KOH content producing increased activation, due to the fact that the potassium salt complexes, potassium oxide and potassium carbonate, which are formed in the carbons before carbonisation act as active sites for gasification according to Eq 4.2-1 & Eq 4.2-2 [43]. The formation of CO is the result of a gasification reaction of the carbon by the alkaline oxide or carbonate. This reaction is expected to occur at a temperature of about 900 °C and is related to the hydroxide content of the impregnated carbon [43]. Therefore the higher the amount of KOH, the higher the activation process will be.



The decrease in surface area and micro and mesopore volume at the higher KOH ratio (TA-KOH4) has also been reported by Meng and Park [44]. They prepared various

nano porous carbons using KOH chemical activation with KOH:carbon ratios between 0.5 and 4. The authors reported a decrease in the micropore volume when the KOH: carbon ratio was increased to 4. It could be suggested that at the higher levels of KOH addition, blockage of pores by potassium leads to a decrease in surface area and microporosity and mesoporosity of the activated carbons.

In contrast to KOH, activation with other alkali metals led to the formation of samples with less developed porosity (Table 4.2-3). Using the  $K_2CO_3$ , NaOH and  $Na_2CO_3$  as activating agents resulted in the formation of active carbons with BET surface areas of  $133\text{ m}^2\text{ g}^{-1}$ ,  $128\text{ m}^2\text{ g}^{-1}$  and  $92\text{ m}^2\text{ g}^{-1}$  respectively. The increase in microporosity appears to depend more on the nature of the cation used ( $Na^+$  or  $K^+$ ). Lillo-Rodenas et al. [28], concluded that the chemical activation of anthracite with  $Na_2CO_3$  had no effect on porosity development. Mitani et al. [45], tried to prepare activated carbon from tar pitch derived needle coke by chemical activation with  $K_2CO_3$  at an activation temperature of  $900\text{ }^\circ\text{C}$  for 3 h and observed that  $K_2CO_3$  was not effective as an activating agent, as the surface area of the obtained activated carbon was only  $20\text{ m}^2\text{ g}^{-1}$ . However, the activation of the same sample with KOH led to an active carbon with a BET surface area of  $2300\text{ m}^2\text{ g}^{-1}$ . March et al. [46], used different chemical agents for the chemical activation of petroleum coke and concluded that the BET surface area decreased in the following order:  $KOH > NaOH > K_2CO_3 > Na_2CO_3$  [46]. However, the porosity and surface area developments depended on the activation parameters and most importantly on the carbon origin [47].

Besides the type of activating agent, the activation temperature also has an influence on the BET surface area and the porosity development. The influence of the activation temperature was investigated for the sample with a 3:1, KOH: char ratio and activated at various temperatures of 700, 800 and  $900\text{ }^\circ\text{C}$  under nitrogen. The sample obtained at the activation temperature of  $900\text{ }^\circ\text{C}$  had a more developed porous structure with BET surface area and micropore volume about five times greater than the sample activated at  $700\text{ }^\circ\text{C}$ . In the study carried out by Hsu et al. [48], the maximum porosity of the activated carbons produced from bituminous coal treated with KOH was produced at a temperature  $800\text{ }^\circ\text{C}$ , but at a higher temperature, the porosity was found to decrease due to the breakdown of cross-links in the carbon matrix.

From Table 4.2-3, the activated carbons exhibited a high mesoporous volume which confirms the mesoporous properties of the prepared carbons. For the series of samples prepared with different KOH ratios, the higher BET surface area of around  $600 \text{ m}^2\text{g}^{-1}$  was reported for the sample prepared with a KOH-char ratio of 3. This sample also shows a high micropore and mesopore volume.

The porosity development of the prepared samples was investigated by  $\text{N}_2$  adsorption at 77K. The mesoporous character of the prepared samples was confirmed by the typical adsorption-desorption isotherms of carbons shown in Figure 4.2-1 (a), (b) and (c). The IUPAC designation system for such isotherms classifies them as Type IV which shows a hysteresis loop at relative pressures ( $P/P_0$ ) above 0.4 suggesting a mesoporous carbon [49]. The isotherms show a widening of the microporosity and higher mesoporosity as the activation temperature was raised (Figure 4.2-1a).

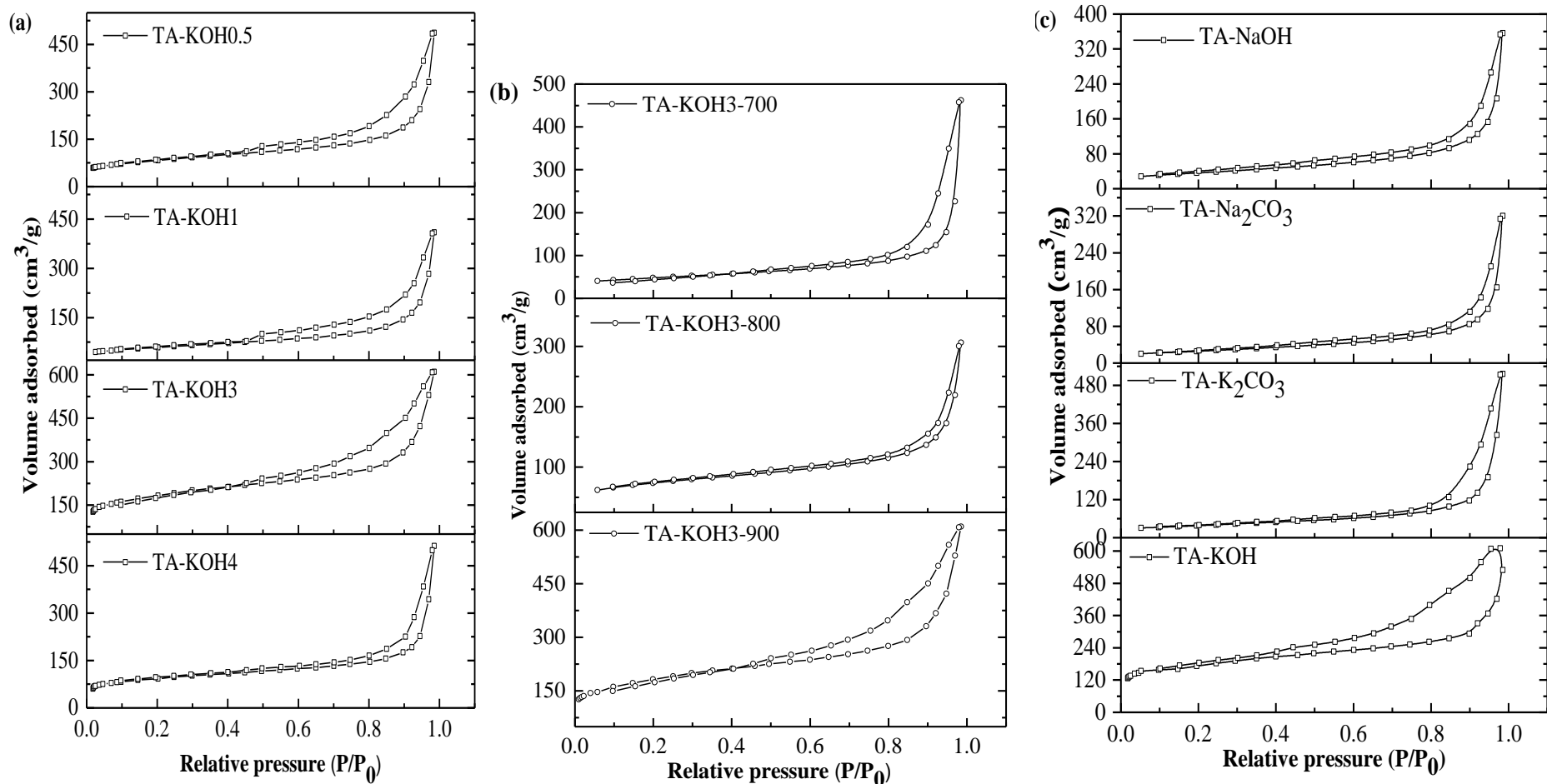


Figure 4.2-1. Adsorption and desorption isotherms of the waste tyre derived activated carbons in relation to (a) char:KOH impregnation ratio (b) activation temperature with KOH char impregnation (c) type of alkali activating agent

The pore size distribution is one of the main factors to consider while developing a carbon adsorbent with high NO capture efficiency. The DFT pore size distribution plots of the produced adsorbents are shown in Figure 4.2-2.

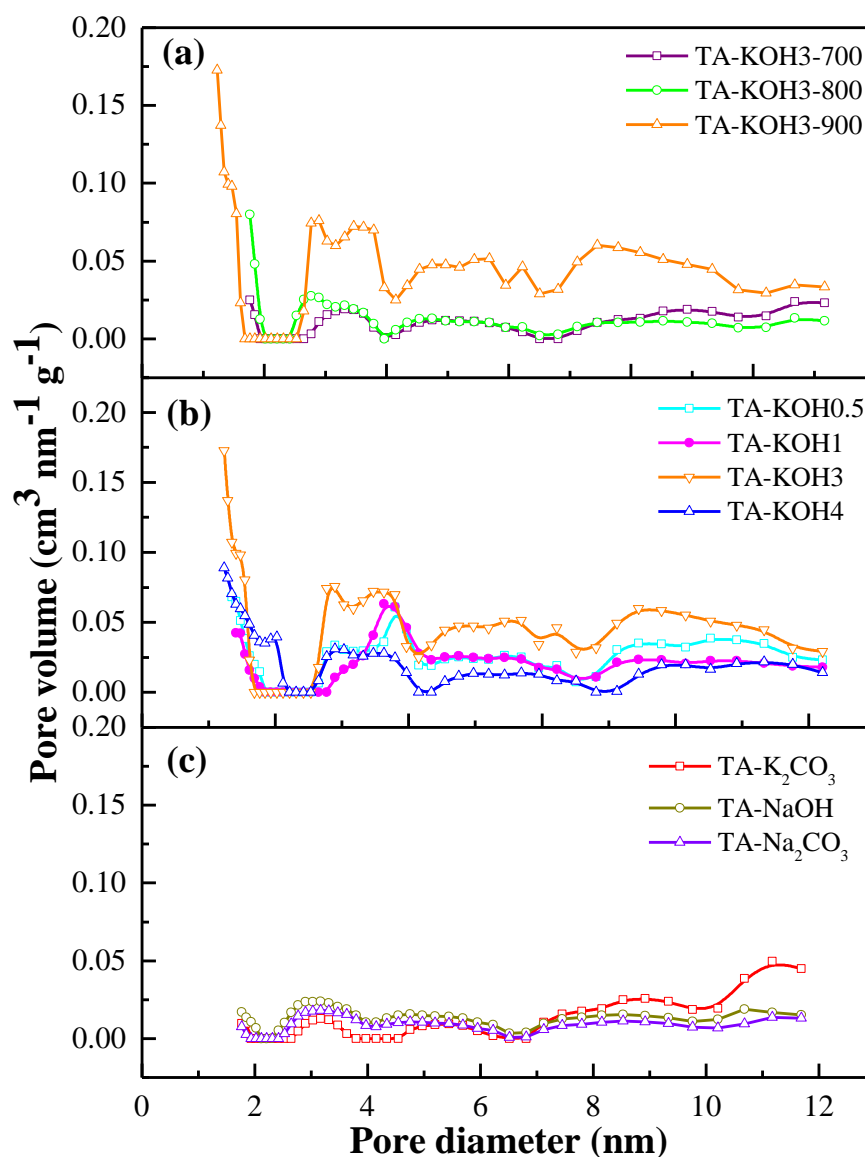


Figure 4.2-2. Pore size distribution (DFT) of the waste derived activated carbons in relation to (a) activation temperature with KOH char impregnation (b) char:KOH impregnation ratio (c) type of alkali activating agent

The micropore structure was predominantly enhanced with the use of KOH as an activating agent. Most of the micropores of the waste tyre derived activated carbon were enhanced by chemical activation with KOH at a temperature of 900 °C and with a KOH: char ratio of 3:1 (TA-KOH3). Additionally, mesopore development is suggested around the pore width of 4 nm. With increasing KOH: char ratio, the high intensity of gasification reactions results in the breakthrough of micropore walls leading to an increase in the mesopore volume. As reported in the literature, the porous structure of carbons activated with KOH is highly dependent on the KOH: char ratio [50]. As shown in Figure 4.2-2 (a), the change in activation temperature has influenced the pore size distribution with the proportion of micropore and mesopore volumes increasing with increasing temperature.

The SEM images for the activated carbons treated with different alkali metals are presented in Figure 4.2-3. Similar morphologies were observed for TANA<sub>2</sub>CO<sub>3</sub> (Figure 4.2-3 (c)), and TAK<sub>2</sub>CO<sub>3</sub> (Figure 4.2-3 (d)) which showed small grains. Whereas TAKOH had small aggregated particles.

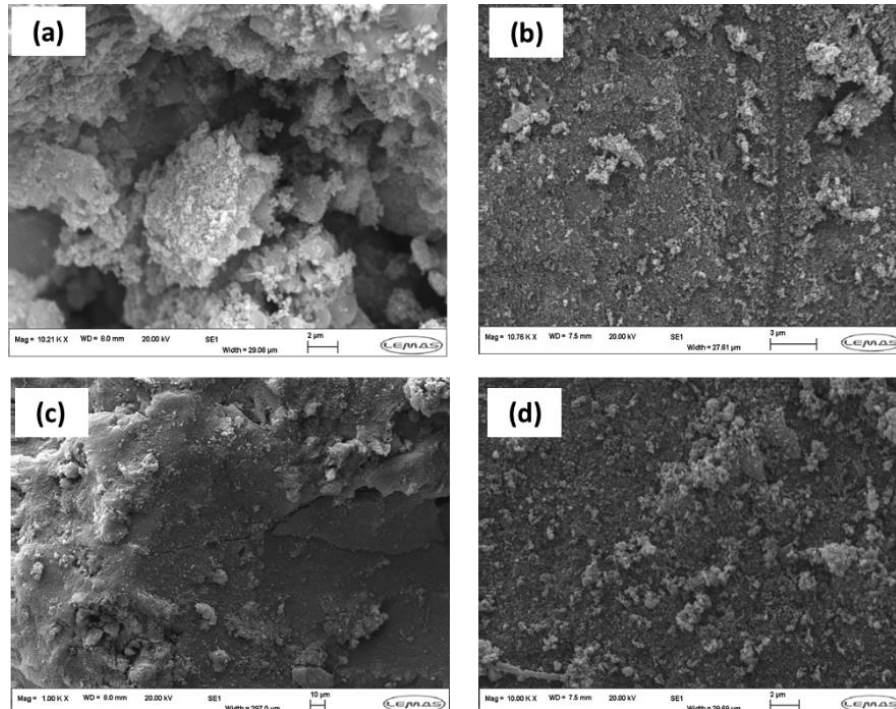


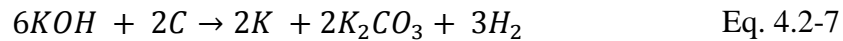
Figure 4.2-3. SEM images for (a) TAKOH, (b)TANA<sub>2</sub>CO<sub>3</sub>, (c)TANA<sub>2</sub>CO<sub>3</sub>, (d) TAK<sub>2</sub>CO<sub>3</sub>

It can be concluded that KOH is more effective in developing the porosity of the activated carbons than  $K_2CO_3$ , NaOH and  $Na_2CO_3$ . During carbonisation, these reagents play different roles which can significantly affect the porosity. Potassium hydroxide is a strong base and has the ability to interact with the carbon atoms, catalyzing the dehydrogenation reaction and leading to a carbon with developed porous structure [43].

According to Otowa et al. [51], at a temperature below 700 °C, the chemical activation with KOH followed the reactions described below, and the main products are  $H_2$ ,  $H_2O$ ,  $K_2O$ , CO,  $CO_2$ . The carbon is gasified through the reaction of carbon with  $H_2O$  (Eq.4.2-4).



However, the widening of pore distribution at higher activation temperature  $> 800$  °C is due to the following redox reactions;



According to recent studies,  $K_2CO_3$  is formed at a temperature of 400 °C and at temperatures higher than 700 °C; it decomposes to  $CO_2$  and  $K_2O$  (Eq. 4.2-8). At temperatures higher than 700 °C, the formed potassium compounds in (Eq. 4.2-7 & Eq. 4.2-8) are reduced to produce potassium as in Eq. 4.2-9, Eq. 4.2-10 & Eq. 4.2-11. The produced metallic potassium intercalates into the carbon matrix as shown in Figure 4.2-4(b), resulting in widening the carbon layers. The carbon lattice cannot return to the original state (a), even after the removal of the intercalated potassium by

washing, thus resulting in opening the carbon pores (Figure 4.2-4 (c)). These chemical reactions are responsible for producing an activated carbon with a well-developed porous texture [12, 47].

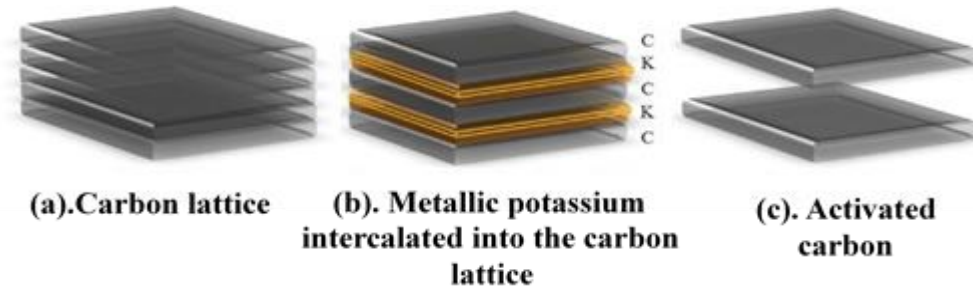


Figure 4.2-4. KOH activation mechanism at a temperature above 700 °C and the expansion of carbon lattice due to the intercalation of potassium [12]

According to the reaction shown in Eq. 4.2-7,  $K_2CO_3$  is one of the reaction products that is formed during the KOH activation, which plays an important role in the porosity development (Eq. 4.2-11). However, it is less effective when it was used as the activating agent. This is because  $K_2CO_3$  diffuses more slowly on carbon than KOH. In addition, when KOH is used as the activating agent;  $K_2CO_3$  is produced as an intermediate inside the pores of carbon at which it reacts with carbon [15, 52]. Lu et al. [15], reported that with the direct  $K_2CO_3$  activation, it was hardly for  $K_2CO_3$  to enter the pores of petroleum coke.

#### 4.2.2 Nitrogen Oxide adsorption

The NO adsorption efficiency of the prepared activated carbon adsorbents was investigated at a temperature of 25 °C and with an inlet NO concentration of 400 ppm and in the presence of 10% oxygen. The addition of  $O_2$  was essential, since it increases the adsorption of nitric oxide via the catalytic oxidation of NO to  $NO_2$ , producing an increase of the NO adsorption because of the higher adsorption potential of  $NO_2$  [26, 28]. In the absence of oxygen, the NO removal efficiency was only about 5%, similar findings have been reported in the literature [45, 53]. Prior to any test, the samples were dried under an inert  $N_2$  atmosphere. NO adsorption capacity of the tested carbons is presented in Table 4.2-4.

Table 4.2-4. NO adsorption capacity of the activated carbons obtained ( $\text{mg g}^{-1}$  ads)

| Sample                             | NO ads ( $\text{mg g}^{-1}$ ) |
|------------------------------------|-------------------------------|
| TA-KOH0.5                          | 8.67                          |
| TA-KOH1                            | 13.71                         |
| TA-KOH3                            | 17.23                         |
| TA-KOH4                            | 15.63                         |
| TA-KOH3-700                        | 10.18                         |
| TA-KOH3-800                        | 14.12                         |
| TA-K <sub>2</sub> CO <sub>3</sub>  | 10.91                         |
| TA-NaOH                            | 9.28                          |
| TA-Na <sub>2</sub> CO <sub>3</sub> | 5.69                          |

The maximum NO adsorption capacity of  $17.23 \text{ mg g}^{-1}$  was found for TA-KOH 1-3 sample obtained by activation of tyre char with KOH at an activation temperature of  $900 \text{ }^\circ\text{C}$  with char: KOH ratio of 1:3. The least effective adsorbent, of adsorption capacity much smaller than those of other samples, was TA-Na<sub>2</sub>CO<sub>3</sub>, whose adsorption capacity towards NO was only  $5.69 \text{ mg g}^{-1}$ . A maximum NO adsorption capacity of  $6.2 \text{ mg g}^{-1}$  was reported by Chen et al. [30]. In another study carried out by Zhang et al. [7], an uptake amount of  $4.5 \text{ mg g}^{-1}$  ( $0.15 \text{ mmol g}^{-1}$ ) was obtained after 2.5 h adsorption when a mixture 500 ppm NO + 5% O<sub>2</sub> was introduced to a commercial activated carbon at room temperature. Kaneko [54] reported about 15-17 mg of NO per gram was adsorbed on activated carbon at  $30 \text{ }^\circ\text{C}$ . This comparison shows that TAKOH3 is a good sorbent for NO removal.

The NO breakthrough curves and the NO removal efficiency curves of the prepared activated carbons in relation to char: KOH activating agent ratio are shown in Figure 4.2-5.

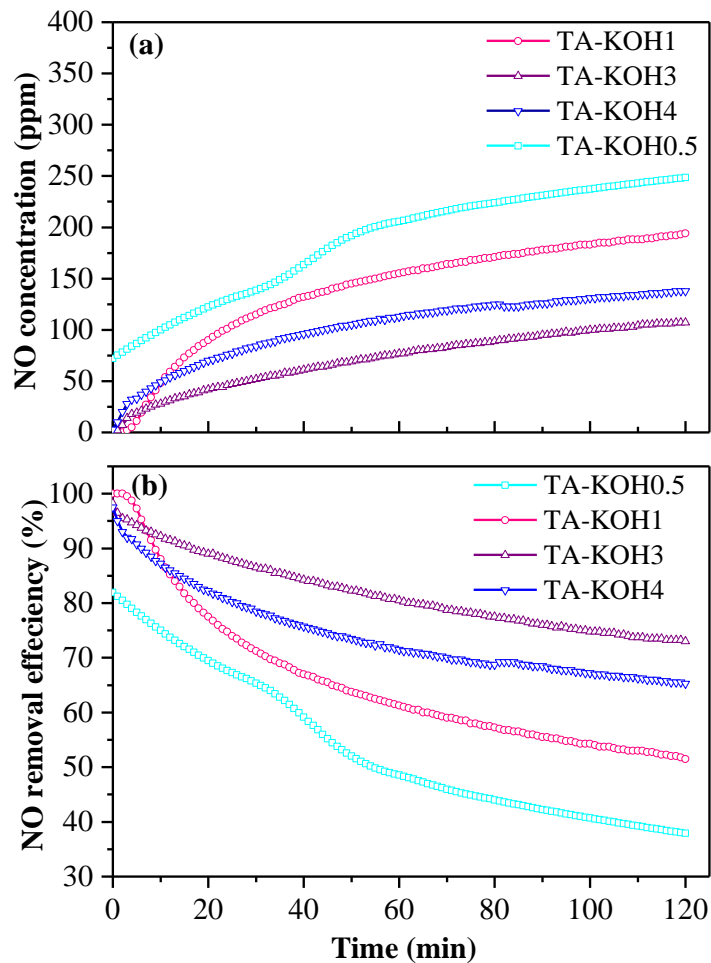


Figure 4.2-5. (a) NO breakthrough curves and (b) removal efficiency of the waste tyre derived activated carbons in relation to char: KOH ratio

The NO breakthrough curve for the lowest concentration of activating agent impregnation (char: KOH ratio of 1:0.5) showed an immediate breakthrough of NO through the activated carbon bed of 75 ppm in relation to the inlet NO concentration of 400 ppm and reached an NO outlet concentration of 250 ppm after 120 minutes. For the activated carbons produced at higher char: KOH impregnation ratios, the NO breakthrough occurred after about 1 minute and the carbons were much more effective in removing NO. The NO removal efficiencies after 120 minutes were highest for the char: KOH impregnation ratio of 1:3 at 75% (Figure 4.2-5). A comparison of the NO removal efficiency with the porous texture data for the activated carbon products (Table 4.2-3) and the pore size distribution (Figure 4.2-2) indicates that the TA-KOH3 carbon produced at the char: KOH ratio of 1:3 had the highest NO removal efficiency which correlated with the highest micropore volume of  $0.437 \text{ cm}^3 \text{ g}^{-1}$  and highest

surface area of  $621 \text{ m}^2 \text{ g}^{-1}$ . Both TA-KOH1 and TA-KOH4 showed almost the same micropore and mesopore volumes. However, the NO conversion with TA-KOH4 was higher than that with TA-KOH1.

The results obtained for the waste tyre activated carbon products may be compared with results from the literature, for example, Lee et al. [55] studied  $\text{NO}_2$  adsorption at a temperature of  $130 \text{ }^\circ\text{C}$  using KOH impregnated commercial activated carbon produced from coconut shells. The removal efficiency was found to decrease with increasing  $\text{NO}_2$  concentration, with  $\text{NO}_2$  concentration of 400 ppm, the removal efficiency was  $\sim 20 \%$ . The influence of varying the amount of added KOH, over the range 0-2.0 wt%, to chars produced from coal on NO removal efficiency has been studied by Zhong and Zhang [56]. Increasing the KOH content to 1.0 wt.% led to an increase on NO reduction. However, when the KOH content in char was increased to 2.0 wt.%, the NO reduction capacity remained almost the same. The authors concluded that with increasing KOH content to 1.0 wt.%, the activation energy decreased and the collision frequency factor for the carbon and nitrogen oxide increased. Consequently, the NO reduction capacity of the studied carbons increased. However, a further increase of KOH content to about 2.0 wt.% had no major influence on the collision frequency factor. Therefore, the NO reduction remained unaffected. Cha et al. [57] produced chemically activated carbons using rice straw char and sewage sludge char and investigated NO removal at a temperature of  $50 \text{ }^\circ\text{C}$  using a fixed bed reactor. The chemically activated carbons treated with KOH exhibited a higher NO removal efficiency compared to the physically activated carbons. This was attributed to the differences in the number of oxygen functional groups, pore volumes and BET surface areas which were dependent on the activation process. The maximum NO removal efficiency was observed with the rice straw activated carbon at 85%, while the sewage sludge-activated carbon showed a NO removal efficiency of 45%.

Materials with different pore width are expected to exhibit different behavior during the gas adsorption. The results presented in Table 4.2-3 suggested the high dependence of NO conversion with the pore diameter of the carbon. Considering the kinetic diameter of NO is 0.3 nm, so carbonaceous materials with pore diameter similar to this should have higher adsorption efficiency than others with higher pore diameter.

Carbons with pore diameters of 1.1 nm have been found to have a much higher capacity for NO adsorption than those with pore diameters larger than 1.1 nm [17]. In this work, a maximum conversion was observed on a carbon with an average pore diameter of 0.9 nm. In the Zhang et al. [7] study, carbon with an average micropore size of 0.7 nm was found to produce the highest NO adsorption at about 52%. These results suggest the dependence of NO adsorption on the average pore diameter along with the BET surface area of the activated carbon products.

In order to further ascertain if the porosity and BET surface area affect the NO capture, the sample treated with KOH at a char: KOH weight ratio of 1:3 was activated to 700 and 800 °C. The results shown in Figure 4.2-6 indicate that activation temperature had a significant role in influencing the surface area and porosity of the activated carbon products and in turn influencing the NO capture capacity.

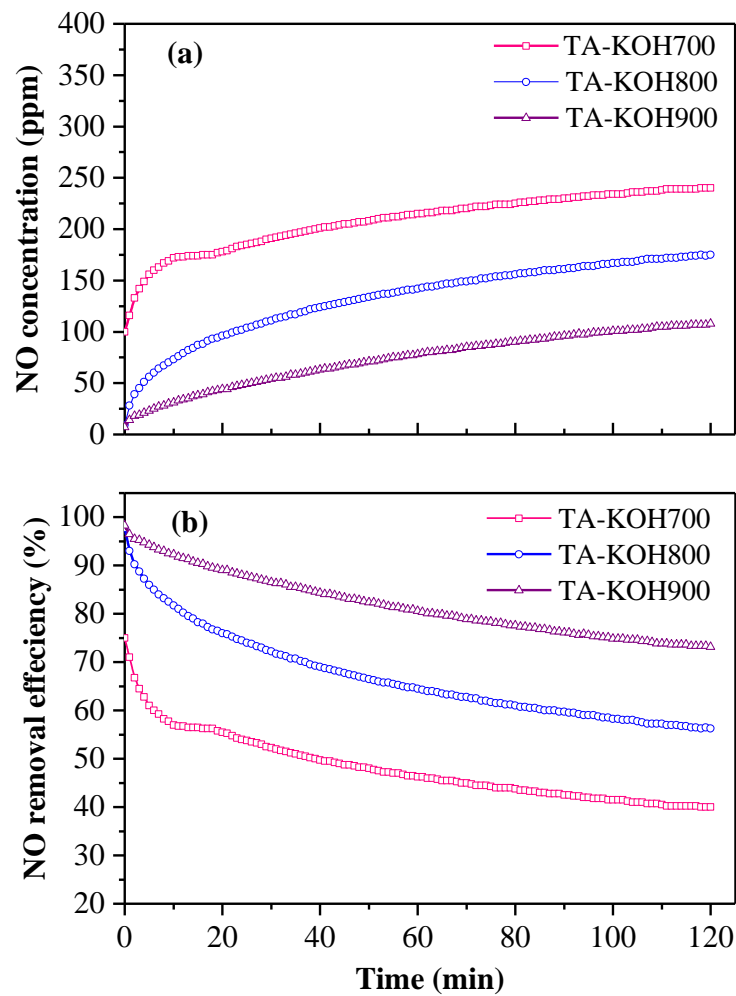


Figure 4.2-6. (a) NO breakthrough curves and (b) removal efficiency of the waste tyre derived activated carbons in relation to activation temperature

The surface area of the carbons increased from  $170 \text{ m}^2 \text{ g}^{-1}$  at  $700 \text{ }^\circ\text{C}$  activation temperature, to  $243 \text{ m}^2 \text{ g}^{-1}$  at  $800 \text{ }^\circ\text{C}$  and to  $621 \text{ m}^2 \text{ g}^{-1}$  at  $900 \text{ }^\circ\text{C}$  activation temperature (Table 4.2-3). There was a similar increase in microporosity from  $0.184 \text{ cm}^3 \text{ g}^{-1}$  at  $700 \text{ }^\circ\text{C}$  to  $0.437 \text{ cm}^3 \text{ g}^{-1}$  at  $900 \text{ }^\circ\text{C}$ . Both increasing surface area and increasing microporosity of the activated carbons correlating directly with increased NO breakthrough and NO removal efficiency. The results found in this study are in good agreement with the results reported by Illan-Gomez et al. [58] where they reported a direct correlation between NO adsorption capacity and BET surface area of the samples used.

To determine the influence of the type of alkali-activating agent on the characteristics and NO removal efficiency of the activated carbon products from different types of activating agents ( $\text{K}_2\text{CO}_3$ ,  $\text{NaOH}$  and  $\text{Na}_2\text{CO}_3$ ) were physically mixed with the tyre char and compared to the results obtained with the chemical activation with  $\text{KOH}$ . All the carbons were prepared at an activating agent impregnation ratio of 1:3, char: activating agent and a final activation temperature of  $900 \text{ }^\circ\text{C}$ . According to the results shown in Figure 4.2-7, the type of activating agent used during the chemical activation significantly influenced the NO adsorption ability,  $\text{KOH}$  was the most effective in providing the best NO removal efficiency with around 75% after 120 minutes, followed by  $\text{K}_2\text{CO}_3$ ,  $\text{NaOH}$  and  $\text{Na}_2\text{CO}_3$  with 37, 30 and 19% respectively.

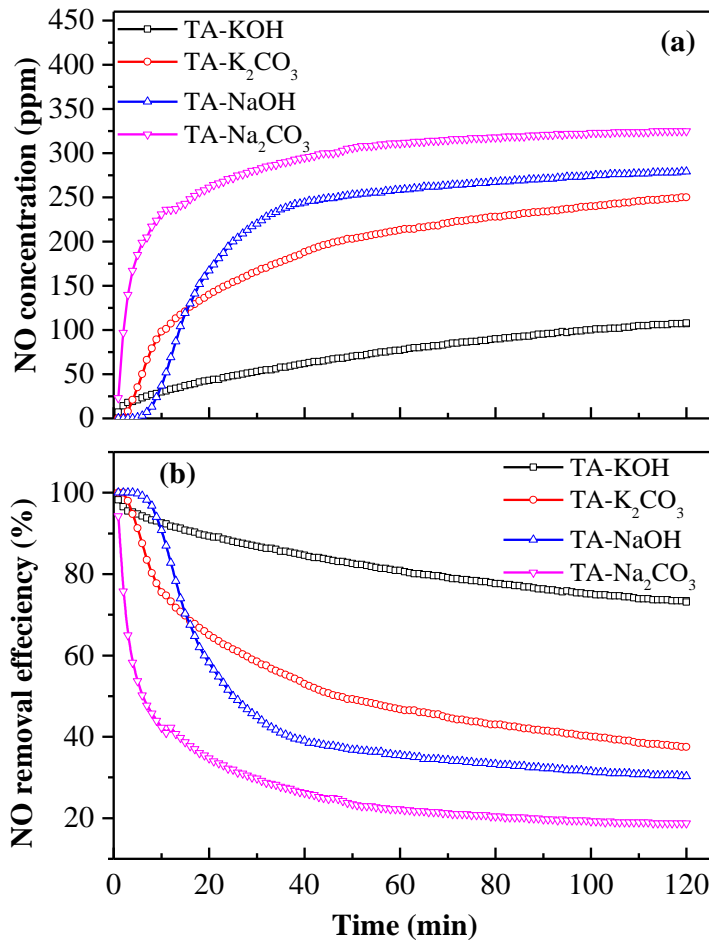


Figure 4.2-7. (a) NO breakthrough curves and (b) removal efficiency of the waste tyre derived activated carbons in relation to char: activating agent

Based on the textural properties shown in Table 4.2-3, the chemical activation of waste tyre with KOH produced a sample with a much more developed structure than those activated with other alkali metals, which was found to markedly enhance the NO sorption capacity. As mentioned before, the activation with KOH and at a higher temperature (900 °C) resulted in the formation of active carbon with a high BET surface area and well developed porous structure. As a consequence, the NO removal efficiency was higher with this sample than those activated with other alkali metals. Potassium has been shown to have high catalytic activity in the NO carbon reaction [59]. The NO reduction capacity by coal char samples has been found to increase from 3% to 63% when the char was loaded with 4 wt.% potassium.

According to studies by Lee et al. [60] and Nowicki et al. [61], the high NO capture by carbons treated with KOH is due to the basic nature of hydroxides provided on the carbon surface. Regarding the chemical state of crystals formed on the carbon, Lee et al [60] found that  $\text{KNO}_3$  was present in high amounts on the carbon surface after the NO adsorption on KOH-impregnated activated carbon.

Thus, the reaction was suggested to be:



However, with the experimental conditions carried out in this research, this reaction is not expected, as the carbon materials were activated at 900 °C whereas in the study by Lee et al [60], the KOH-impregnated activated carbons were activated at a temperature of only 140 °C. Therefore, at low temperature KOH is expected to be on the carbon surface. Lu et al [62] had tried to analyze the products formed on the carbon surface after KOH activation at a temperature of 700 °C using XRD and observed that KOH peaks were no longer observed.

The adsorption ability of the treated carbons in this study can be explained by the reaction mechanism shown in Figure 4.2-8 [46, 61].

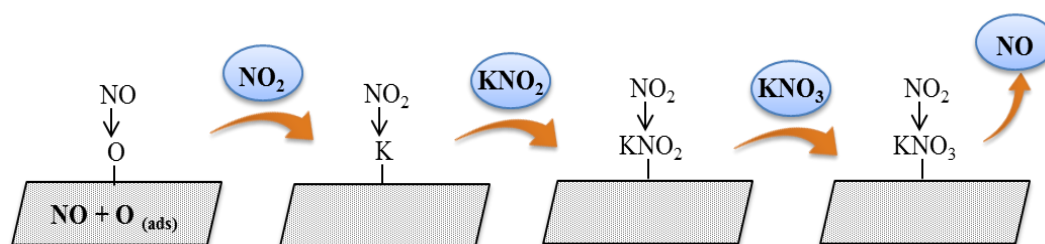


Figure 4.2-8.Expected reaction mechanism of NO with TA-KOH

The presence of potassium metal on the KOH treated waste tyre derived activated carbon was verified through EDX analysis (Figure 4.2-9) which showed that potassium was dispersed well on the carbon. The treated carbon had about 4 wt.% of potassium.

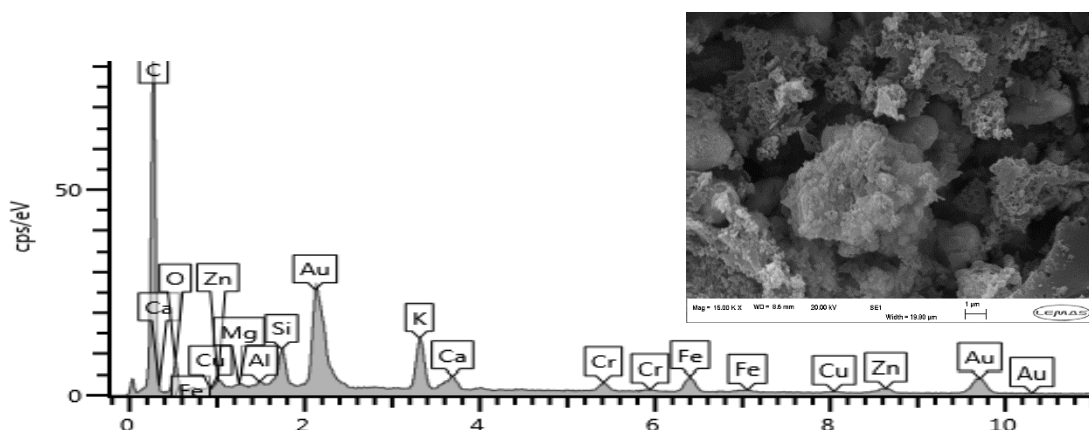


Figure 4.2-9.SEM-EDX of TA-KOH900

Therefore, the metallic potassium left after the chemical activation of waste tyre with KOH (Eq. 4.2-9, Eq. 4.2-10, Eq. 4.2-11), could react with  $\text{NO}_2$ , which is expected to be formed due to the oxidation of NO, to produce  $\text{KNO}_2$ . The formed  $\text{KNO}_2$  may react with another  $\text{NO}_2$  to form  $\text{KNO}_3$  (Eq. 4.2-13)[46, 61].



The NO removal efficiency of the waste tyre derived activated carbons produced in this work may be compared with NO removal efficiencies reported for other more conventionally produced activated carbons. For example, Guo et al [15] prepared pitch based activated carbons with a BET surface area of  $1000 \text{ m}^2 \text{ g}^{-1}$  and investigated NO adsorption at a temperature of  $30 \text{ }^\circ\text{C}$  in the presence of oxygen. The NO removal efficiency of the investigated activated carbons was found to be in the range of 44-75%. In another study carried out by Zhang et al [7] commercial activated carbons were used for NO conversion at a low temperature. In the presence of  $\sim 10\%$  oxygen, the NO conversion of the activated carbons was found to be 50%. The results suggest that waste tyres, which represent a waste disposal problem, have the potential to be processed through pyrolysis and chemical activation to produce activated carbons which are effective in NO removal and are comparable with conventionally produced carbons. However, a full techno-economic assessment would be required to determine

whether the proposed process would be comparable to currently produced activated carbons using conventional feedstocks.

#### **4.2.3 Summary of section 4.2**

In this section of work, the influence of treating the activated carbon with various alkali chemical agents (KOH,  $K_2CO_3$ , NaOH and  $Na_2CO_3$ ) on the porous texture was studied. The influence of surface area and porosity of the carbons produced with the different alkali chemical activating agents on NO capture from the simulated flue gas was investigated. In addition, the influence of varying the chemical activation conditions on the porous texture and corresponding NO removal from the flue gas was studied. The chemical activation of waste tyre with KOH has been shown to effectively enhance the NO reduction at room temperature to about 75% removal in direct relation to the increase in BET surface area and micropore volume. The textural properties seem to be the dominant factor affecting the NO adsorption. Treating the waste tyre with other alkali agents ( $K_2CO_3$ , NaOH,  $Na_2CO_3$ ) produced much lower NO removal efficiencies. The textural properties of the product activated carbon adsorbents were determined mainly by the type of chemical agent and the temperature of activation. Adsorbents prepared by KOH activation had a well-developed porous texture compared to those treated with  $K_2CO_3$ , NaOH and  $Na_2CO_3$  which enhanced the NO capture. The NO capture activity of the activated carbons produced from waste tyre decreased in the order of alkali impregnation as  $KOH > K_2CO_3 > NaOH > Na_2CO_3$ .

## References

1. MUI, E.L.K., D.C.K. KO and G. MCKAY. Production of active carbons from waste tyres—a review. *Carbon*, 2004, **42**(14), pp.2789-2805.
2. CUNLIFFE, A.M. and P.T. WILLIAMS. Influence of process conditions on the rate of activation of chars derived from pyrolysis of used tires. *Energy and Fuels*, 1999, **13**(1), pp.166-175.
3. MERCHANT, A.A. and M.A. PETRICH. Preparation and characterization of activated carbons from scrap tires, almond shells, and Illinois coal. *Chemical Engineering Communications*, 1992, **118**, pp.251-263.
4. BUAH, W.K., A.M. CUNLIFFE and P.T. WILLIAMS. Characterization of Products from the Pyrolysis of Municipal Solid Waste. *Process Safety and Environmental Protection*, 2007, **85**(5), pp.450-457.
5. WILLIAMS, P.T., S. BESLER and D.T. TAYLOR. The pyrolysis of scrap automotive tyres: The influence of temperature and heating rate on product composition. *Fuel*, 1990, **69**(12), pp.1474-1482.
6. MARTÍNEZ, J.D., N. PUY, R. MURILLO, T. GARCÍA, M.V. NAVARRO and A.M. MASTRAL. Waste tyre pyrolysis – A review. *Renewable and Sustainable Energy Reviews*, 2013, **23**, pp.179-213.
7. ZHANG, W.J., S. RABIEI, A. BAGREEV, M.S. ZHUANG and F. RASOULI. Study of NO adsorption on activated carbons. *Applied Catalysis B: Environmental*, 2008, **83**(1–2), pp.63-71.
8. RATHORE, R.S., D.K. SRIVASTAVA, A.K. AGARWAL and N. VERMA. Development of surface functionalized activated carbon fiber for control of NO and particulate matter. *Journal of Hazardous Materials*, 2010, **173**(1–3), pp.211-222.
9. BASHKOVA, S. and T.J. BANDOSZ. The effects of urea modification and heat treatment on the process of NO<sub>2</sub> removal by wood-based activated carbon. *Journal of Colloid and Interface Science*, 2009, **333**(1), pp.97-103.
10. AHMED, S.N., J.M. STENCEL, F.J. DERBYSHIRE and R.M. BALDWIN. Activated carbons for the removal of nitric oxide. *Fuel Processing Technology*, 1993, **34**(2), pp.123-136.
11. U.LENZ, H.P. PAEFFGEN and E.WOLFRUM. Development of a process for removal of SO<sub>2</sub> and NO<sub>x</sub> from flue gas using brown coal coke. In: P.F. SENS and J.K. WILKINSON, eds. *Flue gas and Fly ash*. Taylor & Francis, 1989, pp.24-35.

12. RUBIO, B., M.T. IZQUIERDO, M.C. MAYORAL, M.T. BONA and J.M. ANDRES. Unburnt carbon from coal fly ashes as a precursor of activated carbon for nitric oxide removal. *Journal of Hazardous Materials*, 2007, **143**(1–2), pp.561-566.
13. GROEN, J.C., L.A.A. PEFFER and J. PÉREZ-RAMÍREZ. Pore size determination in modified micro- and mesoporous materials. Pitfalls and limitations in gas adsorption data analysis. *Microporous and Mesoporous Materials*, 2003, **60**(1–3), pp.1-17.
14. SING, K.S.W., D.H. EVERETT, R.A.W. HAUL, L. MOSCOU, R.A. PIEROTTI, J. ROUQUEROL and T. SIEMIENIEWSKA. Reporting physisorption data for gas solid systems with special reference to the determination of surface area and porosity. *Pure & Applied Chemistry*, 1985, **57**(4), pp.603-619.
15. GUO, Z., Y. XIE, I. HONG and J. KIM. Catalytic oxidation of NO to NO<sub>2</sub> on activated carbon. *Energy Conversion and Management*, 2001, **42**(15–17), pp.2005-2018.
16. RUIZ MACHADO, W.A. and P.J. HALL. Effects of Porosity on Carbon Reactivity in NO and O<sub>2</sub>. *Energy & Fuels*, 1998, **12**(5), pp.958-962.
17. NEATHERY, J.K., A.M. RUBEL and J.M. STENCEL. Uptake of NO<sub>x</sub> by activated carbons: bench-scale and pilot-plant testing. *Carbon*, 1997, **35**(9), pp.1321-1327.
18. MOHAN, D. and C.U. PITTMAN JR. Activated carbons and low cost adsorbents for remediation of tri- and hexavalent chromium from water. *Journal of Hazardous Materials*, 2006, **137**(2), pp.762-811.
19. GUO, J. and A.C. LUA. Effect of surface chemistry on gas-phase adsorption by activated carbon prepared from oil-palm stone with pre-impregnation. *Separation and Purification Technology*, 1999, **18**(1), pp.47-55.
20. HU, H., X. LU, F. WANG, J. HE, J. LI and M. FAN. Activated carbon based selective purification of medical grade NO starting from arc discharge method. *Carbon*, 2011, **49**(7), pp.2197-2205.
21. NOWICKI, P. and R. PIETRZAK. Effect of ammoxidation of activated carbons obtained from sub-bituminous coal on their NO<sub>2</sub> sorption capacity under dry conditions. *Chemical Engineering Journal*, 2011, **166**(3), pp.1039-1043.
22. XIAO, Y., S. WANG, D. WU and Q. YUAN. Experimental and simulation study of hydrogen sulfide adsorption on impregnated activated carbon under anaerobic conditions. *Journal of Hazardous Materials*, 2008, **153**(3), pp.1193-1200.

23. SINGH, V.K. and E. ANIL KUMAR. Measurement and analysis of adsorption isotherms of CO<sub>2</sub> on activated carbon. *Applied Thermal Engineering*, 2016, **97**, pp.77-86.
24. CHOO, H.S., L.C. LAU, A.R. MOHAMED and K.T. LEE. Hydrogen sulfide adsorption by alkaline impregnated coconut shell activated carbon. *Journal of Engineering Science and Technology*, 2013, **8**(6), pp.741-753.
25. MOCHIDA, I., N. SHIRAHAMA, S. KAWANO, Y. KORAI, A. YASUTAKE, M. TANOURA, S. FUJII and M. YOSHIKAWA. NO oxidation over activated carbon fiber (ACF). Part 1. Extended kinetics over a pitch based ACF of very large surface area. *Fuel*, 2000, **79**(14), pp.1713-1723.
26. KLOSE, W. and S. RINCÓN. Adsorption and reaction of NO on activated carbon in the presence of oxygen and water vapour. *Fuel*, 2007, **86**(1-2), pp.203-209.
27. XU, X.H., Y. SHI, S.H. LIU, H.P. WANG, S.G. CHANG, J.W. FISHER, S. PISHARODY, M. MORAN and K. WIGNARAJAH. Method for the Control of NO<sub>x</sub> Emissions in Long-Range Space Travel. *Energy & Fuels*, 2003, **17**(5), pp.1303-1310.
28. YANG, J., G. MESTL, D. HEREIN, R. SCHLÖGL and J. FIND. Reaction of NO with carbonaceous materials: 2. Effect of oxygen on the reaction of NO with ashless carbon black. *Carbon*, 2000, **38**(5), pp.729-740.
29. KONG, Y. and C.Y. CHA. NO<sub>x</sub> adsorption on char in presence of oxygen and moisture. *Carbon*, 1996, **34**(8), pp.1027-1033.
30. SHUANG-CHEN, M., J.J. YAO and L. GAO. Experimental study on removal of NO using adsorption of activated carbon/reduction decomposition of microwave heating. *Environ Technol*, 2012, **33**(13-15), pp.1811-7.
31. SHIRAHAMA, N., S.H. MOON, K.H. CHOI, T. ENJOJI, S. KAWANO, Y. KORAI, M. TANOURA and I. MOCHIDA. Mechanistic study on adsorption and reduction of NO<sub>2</sub> over activated carbon fibers. *Carbon*, 2002, **40**(14), pp.2605-2611.
32. RAJ, A., T.H.N. LE, S. KALIAGUINE and A. AUROUX. Involvement of nitrate species in the SCR of NO by NH<sub>3</sub> at ambient conditions over TS-1 catalysts. *Applied Catalysis B: Environmental*, 1998, **15**(3), pp.259-267.
33. PIETRZAK, R. and T.J. BANDOSZ. Activated carbons modified with sewage sludge derived phase and their application in the process of NO<sub>2</sub> removal. *Carbon*, 2007, **45**(13), pp.2537-2546.
34. LONG, R.Q. and R.T. YANG. Carbon Nanotubes as a Superior Sorbent for Nitrogen Oxides. *Industrial & Engineering Chemistry Research*, 2001, **40**(20), pp.4288-4291.

35. LÓPEZ, D., R. BUITRAGO, A. SEPÚLVEDA-ESCRIBANO, F. RODRÍGUEZ-REINOSO and F. MONDRAGÓN. Low-Temperature Catalytic Adsorption of NO on Activated Carbon Materials. *Langmuir*, 2007, **23**(24), pp.12131-12137.
36. SOUSA, J.P.S., M.F.R. PEREIRA and J.L. FIGUEIREDO. Modified activated carbon as catalyst for NO oxidation. *Fuel Processing Technology*, 2013, **106**(0), pp.727-733.
37. ADAPA, S., V. GAUR and N. VERMA. Catalytic oxidation of NO by activated carbon fiber (ACF). *Chemical Engineering Journal*, 2006, **116**(1), pp.25-37.
38. SHEN, Y., X. GE and M. CHEN. Catalytic oxidation of nitric oxide (NO) with carbonaceous materials. *RSC Advances*, 2016, **6**(10), pp.8469-8482.
39. YANG, H., H. LIU, K. ZHOU, Z.-Q. YAN, R. ZHAO, Z.-H. LIU, Z.-H. LIU and J.-R. QIU. Oxidation path analysis of NO in the adsorption and removal process using activated carbon fibers. *Journal of Fuel Chemistry and Technology*, 2012, **40**(8), pp.1002-1008.
40. ZENG, Z., P. LU, C. LI, L. MAI, Z. LI and Y. ZHANG. Removal of NO by carbonaceous materials at room temperature: A review. *Catalysis Science & Technology*, 2012, **2**(11), pp.2188-2199.
41. HOFMAN, M. and R. PIETRZAK. Adsorbents obtained from waste tires for NO<sub>2</sub> removal under dry conditions at room temperature. *Chemical Engineering Journal*, 2011, **170**(1), pp.202-208.
42. HAYASHI, J.I., A. KAZEHAYA, K. MUROYAMA and A.P. WATKINSON. Preparation of activated carbon from lignin by chemical activation. *Carbon*, 2000, **38**(13), pp.1873-1878.
43. EHRBURGER, P., A. ADDOUN, F. ADDOUN and J.B. DONNET. Carbonization of coals in the presence of alkaline hydroxides and carbonates: Formation of activated carbons. *Fuel*, 1986, **65**(10), pp.1447-1449.
44. MENG, L.-Y. and S.-J. PARK. MgO-templated porous carbons-based CO<sub>2</sub> adsorbents produced by KOH activation. *Materials Chemistry and Physics*, 2012, **137**(1), pp.91-96.
45. TENG, H. and E.M. SUUBERG. Chemisorption of nitric oxide on char. 1. Reversible nitric oxide sorption. *The Journal of Physical Chemistry*, 1993, **97**(2), pp.478-483.
46. LEE, Y.-W., J.-W. PARK, J.-H. YUN, J.-H. LEE and D.-K. CHOI. Studies on the Surface Chemistry Based on Competitive Adsorption of NO<sub>x</sub>-SO<sub>2</sub> onto a KOH Impregnated Activated Carbon in Excess O<sub>2</sub>. *Environmental Science & Technology*, 2002, **36**(22), pp.4928-4935.

47. WU, C., Z. WANG, P.T. WILLIAMS and J. HUANG. Renewable hydrogen and carbon nanotubes from biodiesel waste glycerol. *Scientific Reports*, 2013, **3**, p.2742.
48. HSU, L.Y. and H. TENG. Influence of different chemical reagents on the preparation of activated carbons from bituminous coal. *Fuel processing technology*, 2000, **64**(1), pp.155-166.
49. PEVIDA, C., M.G. PLAZA, B. ARIAS, J. FERMOSO, F. RUBIERA and J.J. PIS. Surface modification of activated carbons for CO<sub>2</sub> capture. *Applied Surface Science*, 2008, **254**(22), pp.7165-7172.
50. DÍEZ, N., P. ÁLVAREZ, M. GRANDA, C. BLANCO, R. SANTAMARÍA and R. MENÉNDEZ. A novel approach for the production of chemically activated carbon fibers. *Chemical Engineering Journal*, 2015, **260**(0), pp.463-468.
51. OTOWA, T., R. TANIBATA and M. ITOH. Production and adsorption characteristics of MAXSORB: High-surface-area active carbon. *Gas Separation & Purification*, 1993, **7**(4), pp.241-245.
52. VIRLA, L.D., V. MONTES, J. WU, S.F. KETEP and J.M. HILL. Synthesis of porous carbon from petroleum coke using steam, potassium and sodium: Combining treatments to create mesoporosity. *Microporous and Mesoporous Materials*, 2016, **234**, pp.239-247.
53. DEGROOT, W.F., T.H. OSTERHELD and G.N. RICHARDS. Chemisorption of oxygen and of nitric oxide on cellulosic chars. *Carbon*, 1991, **29**(2), pp.185-195.
54. KANEKO, K. Control of supercritical gases with solid nanospace — environmental aspects. In: A. DĄBROWSKI, ed. *Studies in Surface Science and Catalysis*. Elsevier, 1999, pp.635-657.
55. LEE, Y.-W., D.-K. CHOI and J.-W. PARK. Surface Chemical Characterization Using AES/SAM and ToF-SIMS on KOH-Impregnated Activated Carbon by Selective Adsorption of NO<sub>x</sub>. *Industrial & Engineering Chemistry Research*, 2001, **40**(15), pp.3337-3345.
56. ZHONG, B.J. and H.S. ZHANG. Reduction of NO by low-volatile coal chars with or without catalyst addition. *Combustion Science and Technology*, 2003, **175**(12), pp.2181-2199.
57. CHA, J.S., J.-C. CHOI, J.H. KO, Y.-K. PARK, S.H. PARK, K.-E. JEONG, S.-S. KIM and J.-K. JEON. The low-temperature SCR of NO over rice straw and sewage sludge derived char. *Chemical Engineering Journal*, 2010, **156**(2), pp.321-327.

58. ILLAN-GOMEZ, M.J., A. LINARES-SOLANO, C. SALINAS-MARTINEZ DE LECEA and J.M. CALO. Nitrogen oxide (NO) reduction by activated carbons. 1. The role of carbon porosity and surface area. *Energy & Fuels*, 1993, **7**(1), pp.146-154.
59. BUENO-LÓPEZ, A., A. GARCÍA-GARCÍA, M.J. ILLÁN-GÓMEZ, A. LINARES-SOLANO and C. SALINAS-MARTÍNEZ DE LECEA. Advances in Potassium Catalyzed NO<sub>x</sub> Reduction by Carbon Materials: An Overview. *Industrial & Engineering Chemistry Research*, 2007, **46**(12), pp.3891-3903.
60. LEE, Y.-W., D.-K. CHOI and J.-W. PARK. Performance of fixed-bed KOH impregnated activated carbon adsorber for NO and NO<sub>2</sub> removal in the presence of oxygen. *Carbon*, 2002, **40**(9), pp.1409-1417.
61. NOWICKI, P., R. PIETRZAK and H. WACHOWSKA. Sorption properties of active carbons obtained from walnut shells by chemical and physical activation. *Catalysis Today*, 2010, **150**(1-2), pp.107-114.
62. LU, C., S. XU and C. LIU. The role of K<sub>2</sub>CO<sub>3</sub> during the chemical activation of petroleum coke with KOH. *Journal of Analytical and Applied Pyrolysis*, 2010, **87**(2), pp.282-287.

## **CHAPTER 5. TAR REDUCTION USING WASTE DERIVED PYROLYSIS CHAR**

---

This chapter consists of three sections, which focus on tar conversion over a hot bed of char materials. The tar conversion experiments were conducted using a two stage fixed bed reactor described in Chapter 3, section 3.2.3.1. A brief description of each section is given below.

Section 5.1 examines the effectiveness of using different pyrolysis char materials, produced from the pyrolysis of tyre, RDF and biomass, for tar decomposition during the pyrolysis-gasification of biomass. The selected char materials were chosen for the purpose of studying the influence of porous texture on tar decomposition and chars derived from different waste precursor materials. Biomass was used to generate a range of hydrocarbon gases typically found in biomass gasification tars through the pyrolysis of the biomass. The influence of operating conditions including char cracking temperature and biomass to char ratio on tar reduction and gas composition have been investigated.

Section 5.2 focuses on understanding the tar decomposition mechanism over carbonaceous materials. Therefore, tar model compounds were used. The influence of porous texture and surface chemistry of carbons on tar cracking was investigated.

Section 5.3 focuses on improving the quality of syngas and promoting H<sub>2</sub> production via using steam as a gasifying agent. The influence of steam to biomass mass ratio, reaction time and the presence of ash metals in the char on syngas composition and hydrogen production is reported.

## 5.1 Thermal decomposition and gasification of biomass pyrolysis gases using a hot bed of waste derived pyrolysis char

This section of work focuses on investigating the effectiveness of char materials derived from the pyrolysis of waste materials for tar cracking during the pyrolysis-gasification of biomass using a two-stage fixed bed reactor, described in chapter 3, section 3.2.3.1 at char temperatures of 600 to 800 °C. Chars were obtained from the pyrolysis of waste tyres, municipal solid waste in the form of refuse derived fuel (RDF) and biomass wastes in the form of date stones. In addition, the influence of char catalytic cracking temperature and char to biomass ratio on gas and tar compositions was investigated.

### 5.1.1 Biomass pyrolysis gas conversion using waste derived pyrolysis chars

The properties of the feed biomass used in the pyrolysis stage and the waste derived char materials used in the cracking/gasification stage are shown in Table 5.1-1.

Table 5.1-1. Composition of the biomass waste wood and the waste derived char samples.

| Sample                | Proximate analysis (wt.%) |       |              | Elemental analysis (wt.%) |      |      |                |
|-----------------------|---------------------------|-------|--------------|---------------------------|------|------|----------------|
|                       | Volatiles                 | Ash   | Fixed carbon | C                         | H    | N    | O <sup>a</sup> |
| Wood                  | 75.01                     | 2.00  | 15.01        | 46.01                     | 5.60 | 0.66 | 45.70          |
| <b>Char materials</b> |                           |       |              |                           |      |      |                |
| Tyre char             | 2.00                      | 18.90 | 78.80        | 70.10                     | 0.28 | 0.83 | 5.15           |
| RDF char              | 4.50                      | 44.01 | 48.30        | 44.80                     | 0.38 | 1.08 | 9.28           |
| Date stones char      | 3.90                      | 5.50  | 85.50        | 85.70                     | 0.57 | 2.25 | 5.90           |

The waste derived pyrolysis chars produced from waste tyres, RDF and date stones were investigated for their effectiveness in the conversion of biomass pyrolysis gases including the heavier molecular weight hydrocarbons (tar) from the pyrolysis of biomass, waste wood pellets. The biomass pyrolysis gases was passed through a hot bed of char maintained at 600, 700 and 800 °C. The catalytic effect of each char

material was investigated on the basis of the changes of tar yield and gaseous composition.

The results are presented in Table 5.1-2. For comparison, the results without char are also presented where sand was substituted for the waste char sample. In Table 5.1-1, the char yield represents the residual yield of char in the first stage pyrolysis reactor produced from the pyrolysis of the biomass wood pellets. The biomass pyrolysis char yield was always ~24wt%, since the pyrolysis of the biomass was always at ambient temperature raising to 500 °C and the same heating rate and the process would be unaffected by the reactions downstream of the evolved pyrolysis gases with the hot bed of char.

Table 5.1-2. Influence of waste derived pyrolysis char on the product yield from the pyrolysis-gasification of biomass.

|                                | Without char |      |      | Tyre char |      |      | RDF char |      |      | Date stones char |       |      |
|--------------------------------|--------------|------|------|-----------|------|------|----------|------|------|------------------|-------|------|
| Temperature (°C)               | 600          | 700  | 800  | 600       | 700  | 800  | 600      | 700  | 800  | 600              | 700   | 800  |
| Residual Biomass Char (wt.%)   | 24.0         | 23.5 | 23.0 | 24.5      | 24.5 | 23.5 | 24.0     | 24.0 | 23.5 | 24.0             | 23.0  | 24   |
| Liquid (wt.%)                  | 49.0         | 36.0 | 28.5 | 34.0      | 25.5 | 8.5  | 43.5     | 25.5 | 17.0 | 45.5             | 40.5  | 24.5 |
| Tar (wt.%)                     | 28.0         | 20.1 | 15.3 | 14.8      | 4.7  | 4.6  | 25.1     | 9.2  | 7.6  | 26.1             | 21.5  | 13.9 |
| Water (wt.%)                   | 21.0         | 15.9 | 13.3 | 19.15     | 20.8 | 3.9  | 18.4     | 16.3 | 9.4  | 19.15            | 19.0  | 10.6 |
| Gas yield (wt.%)               | 22.4         | 33.5 | 46.6 | 31.0      | 41.0 | 57.5 | 33.0     | 44.3 | 59.5 | 26.3             | 38.75 | 50.6 |
| Gas composition (vol.%)        |              |      |      |           |      |      |          |      |      |                  |       |      |
| CO                             | 48.2         | 47.1 | 42.3 | 35.2      | 35.1 | 34.0 | 31.7     | 32.2 | 29.9 | 41.7             | 44.2  | 40.1 |
| H <sub>2</sub>                 | 9.6          | 12.1 | 19.6 | 17.6      | 23.5 | 29.0 | 22.0     | 27.2 | 34.0 | 11.1             | 19.2  | 25   |
| CO <sub>2</sub>                | 21.9         | 18.4 | 16.2 | 29.6      | 22.8 | 20.3 | 27.0     | 23.7 | 21.7 | 27.1             | 17.0  | 16.2 |
| CH <sub>4</sub>                | 13.4         | 13.6 | 15.1 | 11.6      | 12.5 | 12.1 | 14.1     | 11.4 | 10.5 | 13.7             | 12.5  | 12.8 |
| C <sub>2</sub> —C <sub>4</sub> | 7.0          | 8.9  | 6.7  | 6.1       | 6.2  | 4.7  | 5.2      | 5.5  | 3.9  | 6.5              | 7.0   | 5.9  |
| Mass balance (%)               | 95.4         | 93.0 | 98.0 | 89.6      | 91.0 | 89.5 | 103      | 93.8 | 99.9 | 95.8             | 102   | 99.1 |

In the absence of char, the tar yield decreased with an increase in the second stage char cracking temperature from 28.0 wt.% at 600 °C to 15.3 wt.% at 800 °C. These results are comparable with the results reported in the literature [1]. This is due to the change in tar composition with temperature due to tar cracking to produce increase gas yields. With the use of char materials, it can be observed from Table 5.1-2 that the tar yields decreased significantly with all the waste char derived materials used in comparison to the experiments without char. The tyre derived pyrolysis char produced the largest conversion of the biomass tar to gas, reducing the condensed bio-oil/tar from 14.8 wt.% tar at 600 °C to 4.6 wt.% at 800 °C with a corresponding increase in gas yield from 31 wt.% at 600 °C to 57.5 wt.% at 800 °C. The RDF char and biomass date stones char producing lower conversion of bio-oil/tar, for example, 7.6 wt.% and 13.9 wt.% tar respectively at 800 °C. Under the same studied experimental conditions, at a char cracking temperature of 800 °C, the total bio-oil/tar yield decreased by 70, 50 and 9% with tyre, RDF and date stones char respectively compared to that without char. These results are in agreement with the results obtained by Park et al. [1], in which the tar yields at 800 °C was 7.7 wt.% with wood char. Sun et al. [2] used biomass char as a catalyst for tar cracking from pyrolysis of pine wood and reported a significant decrease of tar yield from 35% without char to 11% with char at a cracking temperature of 700 °C.

The product liquid collected in the condensers was a mixture of a pale yellow coloured oil and water (Figure 5.1-1). A noticeable difference was observed with the colour of the obtained fractions with the absence of char compared with the presence of char, particularly with tyre char. The dark brown colour of the condensed product collected with no char became a clear liquid with the introduction of tyre char in the second stage reactor during the pyrolysis-gasification of biomass.

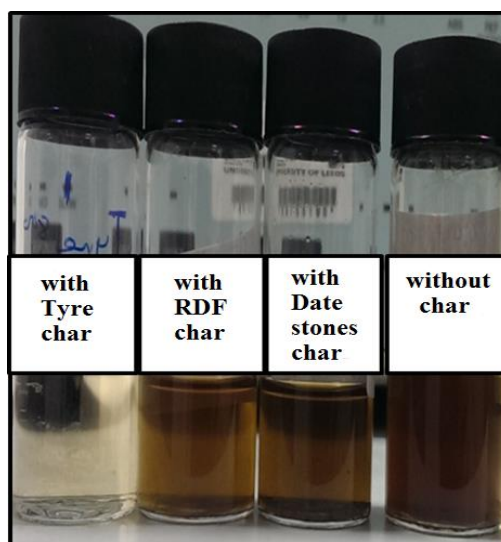


Figure 5.1-1. Photographs of bio-oil/tar samples during the pyrolysis-gasification of biomass with and without char.

The yield of condensed water produced from the pyrolysis of the biomass and from the moisture content of the biomass decreased with increasing second stage (sand) temperature as shown in Table 5.1-2. This was also the case when each of the waste-derived chars was introduced into the second stage-cracking reactor but to a greater extent. The decrease in the water content with the use of chars at high cracking temperature (800 °C) may be due to the results of tar reforming over the chars or could be also due to the reaction of the autogenerated steam, formed from the release of biomass moisture, with char. The data shown in Table 5.1-2 shows the total liquid yield and also the yield of water and tar in the liquid as determined by the Karl Fischer analysis. These results showed that char has a significant catalytic effect in reducing the total tar yield during the biomass-gasification of biomass. The catalytic activity of char produced from biomass for tar removal has been studied by Gilbert et al. [3]. The investigated char was effective in enhancing heavy tar cracking in a fixed bed reactor but not to such a high degree as found in this work. Abu El Rub et al. [4] reported about 85% removal of naphthalene by biomass char, however, the same char could remove only 58% of real biomass produced tar.

One of the products of char induced conversion of tar is gas. An increase in the total gas yield was observed with the introduction of char in the second stage reactor (Table 5.1-2). For example, at a char cracking temperature of 800 °C, the highest gas yield

(59.5 wt.%) which was obtained with the use of RDF char while date stones char produced the lowest yield (50.6 wt.%). The influence of waste derived pyrolysis chars on the gas product composition obtained for tar cracking is presented in Table 5.1-2. It is clear that the introduction of char resulted in a significant influence on gas compositions particularly with the H<sub>2</sub> and CO<sub>2</sub> production. For example, with the use of tyre char at a cracking temperature of 800 °C, the total H<sub>2</sub> and CO<sub>2</sub> yields were 32% and 20% higher respectively than those without char. This is most likely due to the water-gas shift reaction (Table 5.1-2). Sun et al. [2] investigated the effects of using charcoal as a catalyst for tar reduction and observed an increase of H<sub>2</sub> and CO<sub>2</sub> yields of 3.9 and 2.9% compared to that without charcoal. The author attributed the increase of H<sub>2</sub> and CO<sub>2</sub> to the auto-generated steam gasification of char.

However, the analysis of the produced gases obtained with the presence of tyre, RDF and date stones chars showed that the main gas concentration that increased was hydrogen. At a cracking temperature of 800 °C, the H<sub>2</sub> concentration increased to 34, 29 and 25 vol.% with the presence of RDF, tyre and date stones chars, respectively compared to that without char. Cracking of the bio-oil/tar hydrocarbons would produce a range of lower molecular weight hydrocarbons, including methane and C<sub>2</sub>–C<sub>4</sub> hydrocarbon gases and also hydrogen.

The production of hydrogen could also be from autogeneration of steam and subsequent reactions of the steam with the generated biomass pyrolysis hydrocarbons and the waste derived char through gasification, water gas shift, methanation and reforming reactions [5, 6] (Table 5.1-3);

Table 5.1-3. Tar decomposition reactions

| Reaction type            | Chemical reaction  | Reaction number |
|--------------------------|--|-----------------|
| Steam Reforming          | $C_nH_m + nH_2O \leftrightarrow nCO + \left(n + \frac{m}{2}\right)H_2$ | R. 5.1-1        |
| Dry Reforming            | $C_nH_m + nCO_2 \leftrightarrow 2nCO + \left(\frac{m}{2}\right)H_2$    | R. 5.1-2        |
| Thermal cracking         | $C_nH_m \leftrightarrow C^* + C_xH_y + gas$                            | R. 5.1-3        |
| Tars hydrocracking       | $C_nH_m + H_2 \leftrightarrow CO + H_2 + CH_4 + \dots + coke$          | R. 5.1-4        |
| Water-gas shift reaction | $CO + H_2O \leftrightarrow CO_2 + H_2$                                 | R. 5.1-5        |

( $C_nH_m$  hydrocarbons representing tars.  $C_xH_y$  hydrocarbons representing lighter tar)

The presence of char promotes the hydrocarbon cracking reactions; thus hydrocarbon gases were found to decrease compared to that without char. The decrease was higher with RDF char; therefore more gas production was obtained from the cracked hydrocarbons when RDF char was used.

### 5.1.2 Tar analysis

The analysis of tar samples collected from the pyrolysis/gasification of biomass was carried out using GC-MS and SEC analytical techniques, as described in chapter 3, section 3.2.4.1.

### 5.1.3 GC-MS analysis of the tar composition

The composition of the condensed bio-oil/tar products from the pyrolysis of biomass in the presence of the tyre char, RDF char and date stones char at the hot char reaction temperature of 800 °C were analysed using GC-MS. Figure 5.1-2 shows the total ion chromatograms for the bio-oil/tar collected after passing through the waste derived tyre, RDF and date stones chars and compared to the bio-oil/tar in the absence of char (with sand as a blank). Comparing the chromatograms obtained without char (Figure 5.1-2 (a)) and with chars (Figure 5.1-2 (b,c,d)), a large decrease in the concentration

of hydrocarbon compounds was observed with char materials, particularly with tyre char, compared to that without char which clearly demonstrate that chars promoted the tar cracking reactions.

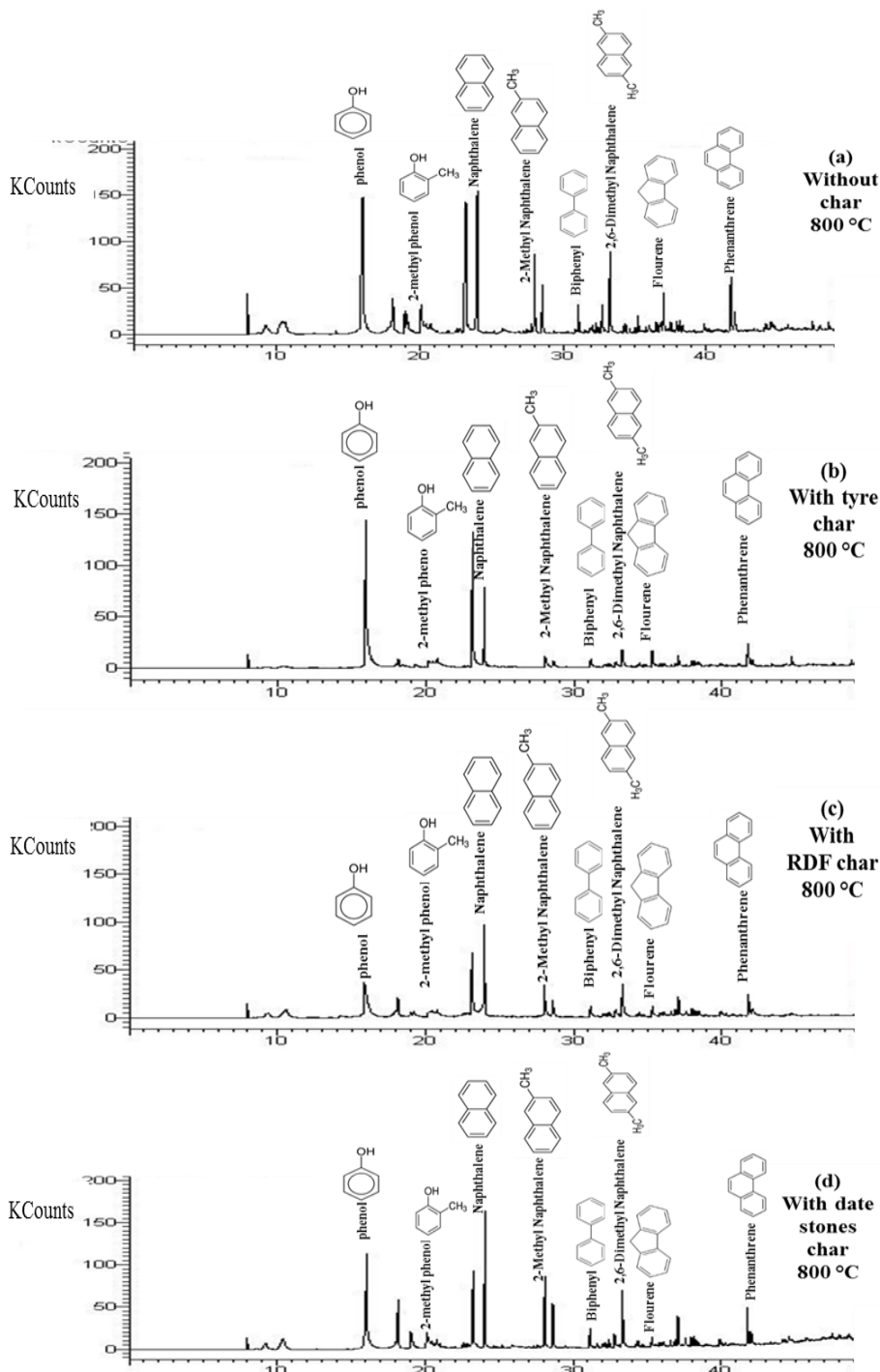


Figure 5.1-2. Effect of char type over tar composition at a cracking temperature of 800 °C.

The main compounds detected were phenolic compounds and polycyclic aromatic hydrocarbons (PAH). The relative peak area was calculated in proportion to the total peak area found with the oil produced with the experiment where no char was present in the second stage. The oil components were classified into phenols and polycyclic hydrocarbons (PAH). The class denoted as phenols included phenol and alkyl phenols; PAHs included naphthalene, alkyl naphthalenes, fluorene, phenanthrene, fluoranthene and pyrene. Figure 5.1-3 shows the total phenolic compounds and PAH for each of the bio-oil/tars in relation to each of the waste cracking chars at a char temperature of 800 °C. The results obtained from the non-catalytic experiments are presented for comparison of the efficiency of different types of char materials for the decomposition of hydrocarbon compounds.

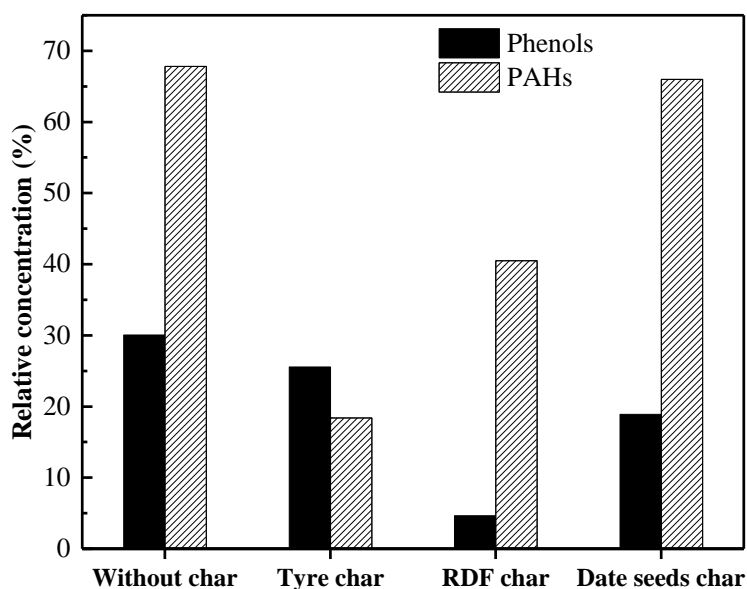


Figure 5.1-3. Tar composition with different carbon samples at a cracking temperature of 800 °C.

The oxygenated phenolic compounds decreased with all the waste derived char materials compared to the experiment in the absence of char. In particular, the presence of the RDF char produced the lowest concentration of phenolic compounds in the condensed bio-oil/tar. With regard to the fraction of polycyclic aromatic hydrocarbons in the bio-oil/tar at a cracking temperature of 800 °C (Figure 5.1-3), the fraction decreased significantly with the use of tyre char compared to the experiment without

char. Many factors could contribute to the high catalytic activity of char. Char contains metals and oxygen functional groups which can act as the active sites for tar cracking. The oxygen functional groups on the surface of char can combine with tar species and enhance the tar cracking reactions, as has been reported by Ren et al. [7]. However, others believed that this could only be the case for low temperature reactions [8, 9].

The porosity and the acidity of the produced char samples could play a role in affecting the product distribution of the produced oil. The acidic properties of the catalytic materials have a significant role during pyrolysis catalytic processes. The acidic sites have been found to induce isomerization, cracking and aromatization reactions. The activity of alumino silicate materials for oil cracking and conversion of large hydrocarbons have been found to depend greatly on the strength of their acidic groups. The materials with moderate acid strength present a higher activity than the classical silica-alumina catalysts [10]. Iliopoulou et al. [11] investigated the catalytic pyrolysis of biomass using mesoporous alumina silicate materials with various acidity, the material with the higher number of acidic groups reduced the organic phase of the liquids products by 55% compared to the material with less acidic groups. The authors concluded that the materials with a higher acidity induced higher concentrations of phenols compared to the non-acidic materials. Additionally, it has been found that increasing the number of acid sites of catalysts led to a decrease of the PAHs compared to the untreated sample. Thus the difference in the catalytic activity of the studied char materials for tar reduction could be due to the difference of their surface chemistry and their acidic and basic groups. The tyre char had a higher number of acidic groups than date stones and RDF char which were found to be basic in nature [12]. The influence of the acidity is discussed in detail in section 5.2.

The high ash content of tyre and RDF char compared to that of date stones char (Table 5.1-1) could be another reason for the low activity in conversion of bio-oil/tar hydrocarbons for the biomass date stones char. For comparison, in separate experiments, wood char with an ash content of 2% was investigated for bio-oil/tar removal at the studied conditions at a char cracking temperature of 700 °C. It was found that wood char had a lower bio-oil/tar cracking activity than the other types of char. The ash composition and the type of metal present in the ash could play a role in

enhancing tar reduction due to catalytic effects. Therefore, the significant reactivity of tar with tyre char could be due to the catalytic effects of the minerals such as Zn, which was present in high concentration [13]. For example, in the study by Oztas [14], coal samples were impregnated with several metals including Zn. The author observed some catalytic effect of Zn and Ni in decomposing many of the tar compounds. Direct correlation between the porosity, acidic properties and metal species and the oil product yields during pyrolysis-reforming of biomass would need further study [11]. The influence of these factors on tar conversion is discussed in more detail in Sections 5.2 and 5.3.

For the tyre char sample, the influence of char cracking temperature from 600 °C to 800 °C was investigated in terms of the change in bio-oil/tar composition after passing through the hot bed of char. The condensed tar compounds formed during the pyrolysis-gasification of biomass were identified quantitatively using GC-MS. Distribution of tar compounds with respect to cracking temperature is presented in Figure 5.1-4. Tar species that were found in the highest concentrations are reported.

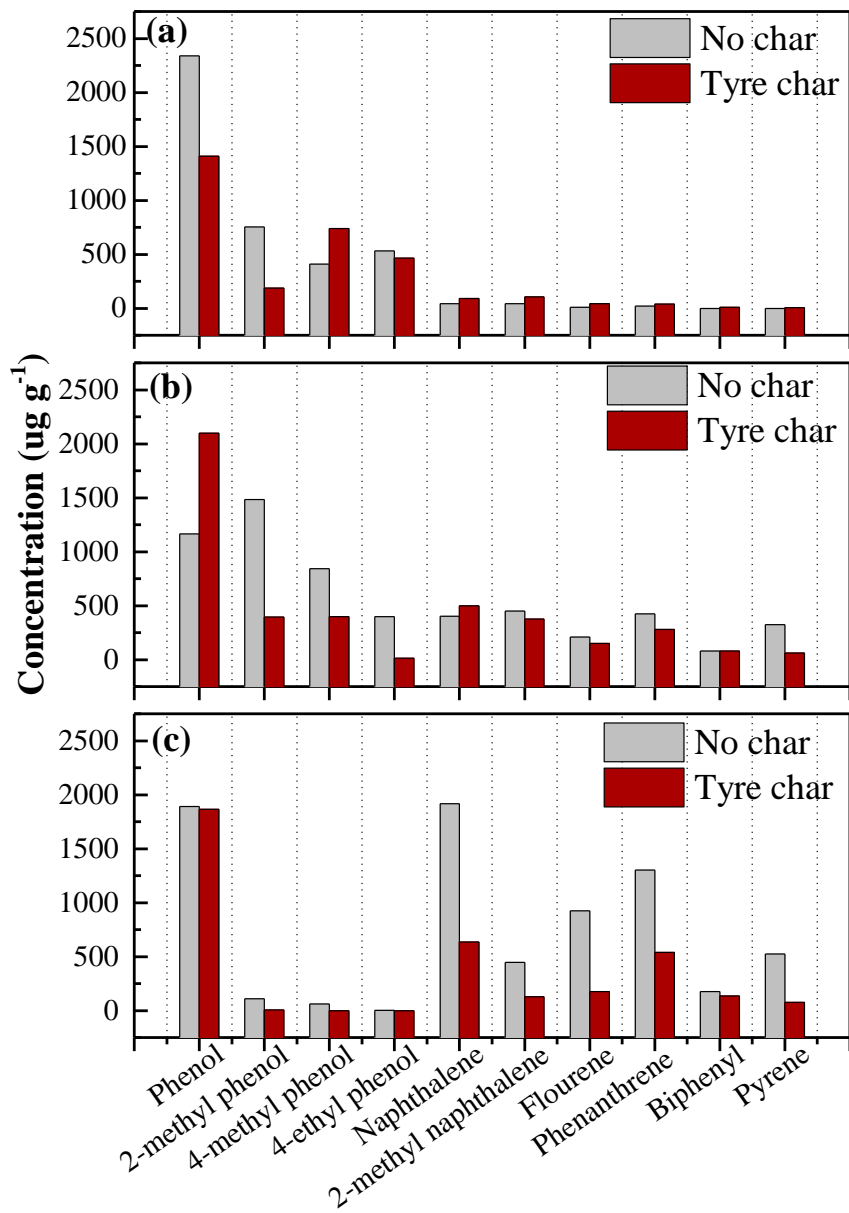


Figure 5.1-4. Distribution of tar compounds with respect to cracking temperature at (a) 600 °C; (b) 700 °C; and (c) 800 °C.

The detected tar species varied with the cracking temperature. The compounds present in the condensed liquid at 600 °C were mainly phenol and alkyl phenols (Figure 5.1-4(a)). The highest yield of phenol (2340  $\mu\text{g g}^{-1}$ ) was reported with no char at 600 °C before it decreased to 1890 ( $\mu\text{g g}^{-1}$ ) at 800°C char temperature. The concentration of phenols decreased with increasing char temperature due to the transition to aromatic hydrocarbons. The PAH compounds could hardly be detected when the cracking temperature was below 700 °C. The major tar compounds identified at 800 °C were

naphthalene, fluorene, phenanthrene and biphenyl. These species have also been reported by others as the main tar compounds during the pyrolysis-gasification of biomass [15]. The catalytic activity of tyre char is noticeable at 800 °C, the addition of tyre char decreased the yields of all the PAH species produced from the pyrolysis-gasification of biomass. However, no change was observed with the phenol concentration. The same observation was reported by Iliopoulou [11], where an MCM-41 catalyst induced the formation of phenols compared to the non-catalytic experiment during the upgrading of the biomass pyrolysis vapours.

Naphthalene is one of the compounds that has been found to be abundant in tar and is often used as a representative tar compound. The yield of naphthalene increased with the increase of temperature from 600 to 800 °C. The highest concentration of naphthalene with both no char and in the presence of tyre char was observed at a temperature of 800 °C. According to some studies [6, 16], various types of catalysts have been tested for naphthalene reduction. For example, in the study by Devi et al. [6], the effectiveness of olivine and dolomite for naphthalene conversion has been examined at a temperature of 800 °C. The tar conversion was found to be 25% and 0% for olivine and dolomite respectively [6]. In this study, at a cracking temperature of 700 °C, naphthalene contributed to 12% of the oil composition in the presence of char compared with 26% of the oil composition without tyre char. It is important to note that at cracking temperature of 700 °C the naphthalene concentration was found to increase slightly with the use of tyre char compared to the experiment without char. This could be due to the decomposition of heavy molecular weight PAHs with 3 & 4 rings producing smaller molecules such as naphthalene. With the increase of temperature to 800 °C, a marked decrease in naphthalene concentration was observed when tyre char was used; the decrease was about 67%. According to Jess [17] the thermal decomposition of naphthalene starts at 1100-1200 °C. However, in this study, the use of tyre char reduced the temperature requirement for naphthalene conversion by reducing the amount by 67% at 800 °C.

The change in tar composition in terms of aromatic rings with the use of tyre char is shown in Figure 5.1-5. Tyre char appears to promote the tar conversion rather than changing the composition.

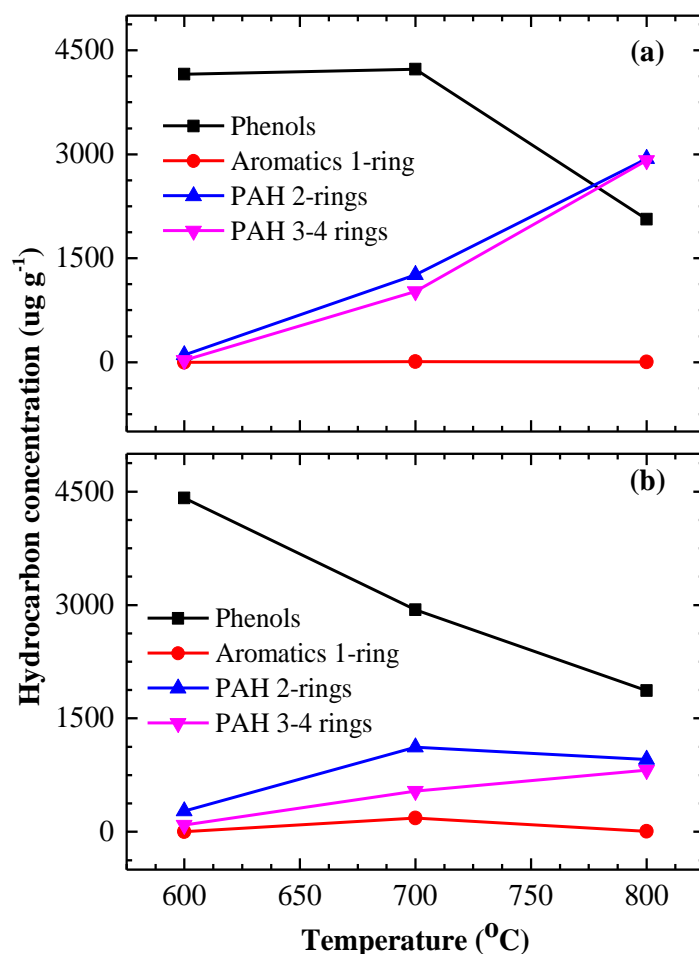


Figure 5.1-5. Tar composition at different char cracking temperatures for (a) without char; (b) with tyre char

The tar compounds were divided into phenols, 1-ring, 2-ring and 3-4 rings PAH. The results show that char cracking temperature plays a significant role in decomposing and changing the bio-oil/tar composition. At the temperature of 600  $^{\circ}\text{C}$ , oxygenated phenolic compounds contribute nearly 100% of the total tar, whereas with increasing cracking temperature to 800  $^{\circ}\text{C}$ , PAHs with 2-4 rings are the dominant compounds.

Phenol is considered as a precursor for naphthalene formation [18]. According to Cypres [19], phenols are stable at a temperature of 700  $^{\circ}\text{C}$ , and at high temperatures, it contributes to tar formation through the reaction mechanism shown in Figure 5.1-5 [18];

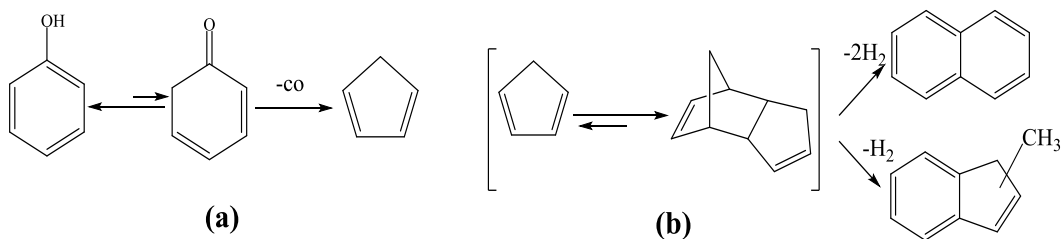


Figure 5.1-6. (a) Pyrolysis of phenol and (b) reaction pathway for the formation of naphthalene and methylindenes [18].

The reaction proceeds with 1,3 hydrogen shift resulting in the formation of 2,4-cyclohexadienone, followed by the elimination of CO (decarbonylation) to form cyclopentadiene (Figure 5.1-6 (a)), which subsequently undergoes a Diels-Alder reaction to form a dimer. The rearrangement of this dimer by the loss of hydrogen results in forming naphthalene (Figure 5.1-6 (b)) [18]. The Diels-Alder reaction is promoted by high reaction temperature [19, 20]. The hydrogen abstraction acetylene addition (HACA) mechanism shown in Figure 5.1-7 is also suggested as another mechanism of PAH formation, which is also promoted at a high reaction temperature [21]. Thus increasing the cracking temperature led to the formation of PAHs.

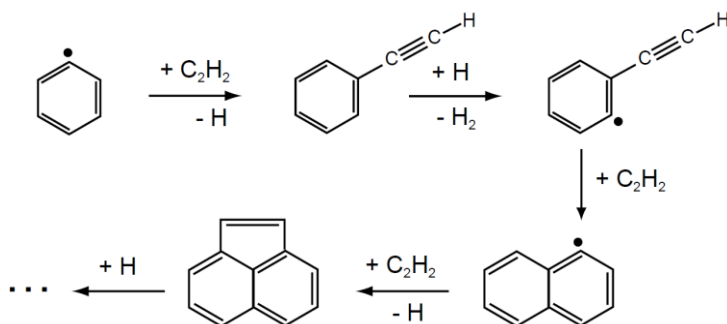


Figure 5.1-7. H<sub>2</sub> abstraction-C<sub>2</sub>H<sub>2</sub>-addition (HACA)

At 700 °C, the main tar compounds were alkyl-substituted PAHs. However, these compounds were shifted to non-substituted PAHs at 800 °C such as naphthalene, phenanthrene and fluorene (Figure 5.1-4). A large decrease was observed in the number of the detected compounds at 800°C. Gilbert et al. [3] observed that the char had a marginal effect on the oil composition at 800 °C and larger molecular PAHs with 2-3 ring compounds were detected. With the use of tyre char, less PAHs were

detected in the condensed tar; the total tar amounts decreased from 8171  $\mu\text{g g}^{-1}$  to 3842  $\mu\text{g g}^{-1}$  at a cracking temperature of 800 °C when char was used. However, the reduction of PAHs was accompanied by an increase of single ring compounds. For example, toluene and styrene were found to be present with the use of tyre char at 700 °C. However, the concentration was not significant. The formation of single ring compounds could be attributed to the catalytic effect of tyre char in decomposing the higher molecular weight hydrocarbons into lighter compounds which then by Diels-Alder reaction resulted in the formation of styrene and toluene.

PAH compounds with 3-4 rings including fluorene, phenanthrene, and pyrene were shown to increase markedly with an increase in the bed temperature to reach the highest concentration at 800 °C and contribute to about 50% of the total tar yield in the absence of char catalyst. Tyre char was effective in reducing these compounds to about 70% compared to the experiment without char.

#### **5.1.4 Size Exclusion Chromatography**

The molecular mass distribution of tar was analysed by size exclusion chromatography. Figure 5.1-8 shows the molecular mass of the derived tar from pyrolysis-gasification of biomass with and without char. The molecular mass distribution from 90 to 240  $\text{g mol}^{-1}$  is reported. The presence of peaks around 88, 93 and 100  $\text{g mol}^{-1}$  might be ascribed to toluene, phenol and styrene respectively. The tar derived from the experimental tests carried out in the absence of char had the highest fraction of high molecular weight compounds in the range of 120-240  $\text{g mol}^{-1}$ . The compounds in this molecular mass range could be due to the presence of PAH compounds such as naphthalene, biphenyl, fluorene, phenanthrene and pyrene as has been identified by GC-MS analysis. As presented in Figure 5.1-8, the high molecular species with masses from 120-240  $\text{g mol}^{-1}$  reduced significantly with the addition of char materials. This is clearly due to cracking of high tar molecular compounds.

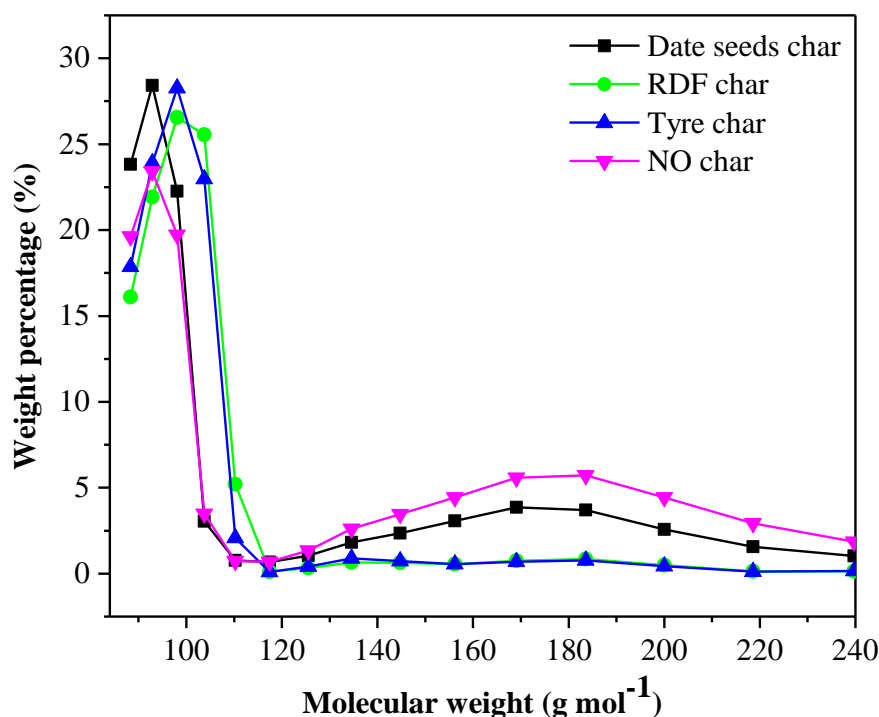


Figure 5.1-8. Size exclusion chromatograms of tar samples

### 5.1.5 Char characterization

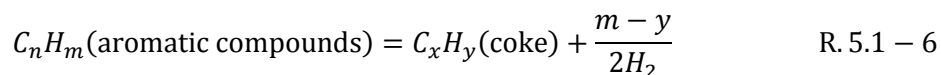
The porous texture of tyre char could have an influence on the tar conversion during pyrolysis/reforming of biomass via enhancing the bio-oil/tar decomposition reactions due to the presence of mesopores in the tyre char. The larger mesopores as opposed to micropores encourages the bio-oil/tar compounds, with their high molecular size, to enter the pores and thereby extend the residence time of tar cracking [22]. According to the literature, an activated carbon with mesoporous texture has been found to enhance the decomposition of heavy molecular compounds into lighter products [23]. The BET surface area and the porous properties of the fresh and used waste derived char samples are shown in Table 5.1-4.

Table 5.1-4. Porous properties of the samples

| <b>Sample</b>    | <b>BET<br/>(m<sup>2</sup> g<sup>-1</sup>)</b> | <b>Micropore volume<br/>(cm<sup>3</sup> g<sup>-1</sup>)</b> | <b>Mesopore volume<br/>(cm<sup>3</sup> g<sup>-1</sup>)</b> |
|------------------|---|---|--|
| Tyre             | 71.657  | 0.090   | 0.561  |
| Used Tyre char   | 63.845  | 0.080   | 0.468  |
| RDF              | 85.273  | 0.068   | 0.126  |
| Used RDF char    | 12.584  | 0.014   | 0.041  |
| Date stones      | 5.191   | 0.006   | 0.004  |
| Used Date stones | 3.975   | 0.008   | 0.004  |

A decrease in the BET surface area was observed for all the char materials after reaction with the biomass pyrolysis gases. The decrease was more obvious for the RDF derived pyrolysis char. The decrease in BET surface area of the tyre derived pyrolysis char was less than that of the biomass date stones. Additionally, there was a 10, 80 and 20% decrease in the measured pore volume of the tyre char, RDF char and date stones char respectively. The decrease in BET surface area of the chars after the char-tar reaction could be attributed to tar deposition onto the carbon surface, followed by condensation and polymerization to form coke. Therefore, chars may lose their catalytic activity with time due to coke accumulation [4]. Boroson et al. [24] also reported a decrease in the surface area of chars due to deposition of tar onto the surface of the char during the cracking of wood pyrolysis tars over a hot bed of biomass char. A similar observation was reported by Zhao et al. [25]. The used char can be simply gasified without the need of regeneration. However, as the biomass moisture could autogenerate steam, char is believed to undergo steam gasification, but there is a possibility that tar vapour could inhibit the char gasification [26, 27]. In a study undertaken by Fushimi et al. [26], a decrease in the reaction rate of char was reported with the introduction of model tar. The hydrogen radical, produced from tar volatiles by breaking of C-H bonds, could chemisorb onto free carbon sites on the char surface and prevent the char gasification. Nevertheless, the metallic species on the char are believed to catalyse the reaction even with the presence of tar volatiles and hydrogen [27].

Hosakai et al. [28] concluded that tar decomposition over char is mainly due to coking (R. 5.1-6) followed by gasification of coke, rather than direct reforming to gaseous species.



Coke/carbon deposition produced from the aromatic compounds formed on the char surface due to the tar decomposition is expected to decrease the porosity of the carbonaceous material. In addition, the accumulation of coke on the surface of the chars may block the available active sites (metal species in the char) thus decreasing the char activity with time [29]. As a consequence, the BET surface area and the pore volumes of the spent char were decreased (Table 5.1-4). Coke formation on the char surface could not be observed during examination of the used char surfaces after reaction using scanning electron microscopy (Figure 5.1-9). The deactivation of char, due to pore blocking, is not considered as a serious problem as the spent char can be used a solid fuel [21] and can be combusted or gasified for energy recovery [28].

The rate of coke deposition and char gasification can be measured from the mass balance of char samples before and after experiment. However, the change in char mass balance was not significant enough to measure the extent of tar adsorption or char gasification. With the presence of steam, coke formation and char gasification are expected to occur simultaneously in which the gaseous products are formed due to these two processes [28]. Both char gasification and coke accumulation do not take place at significant rates; therefore tar cracking is suggested to be due to the catalytic effect of char materials.

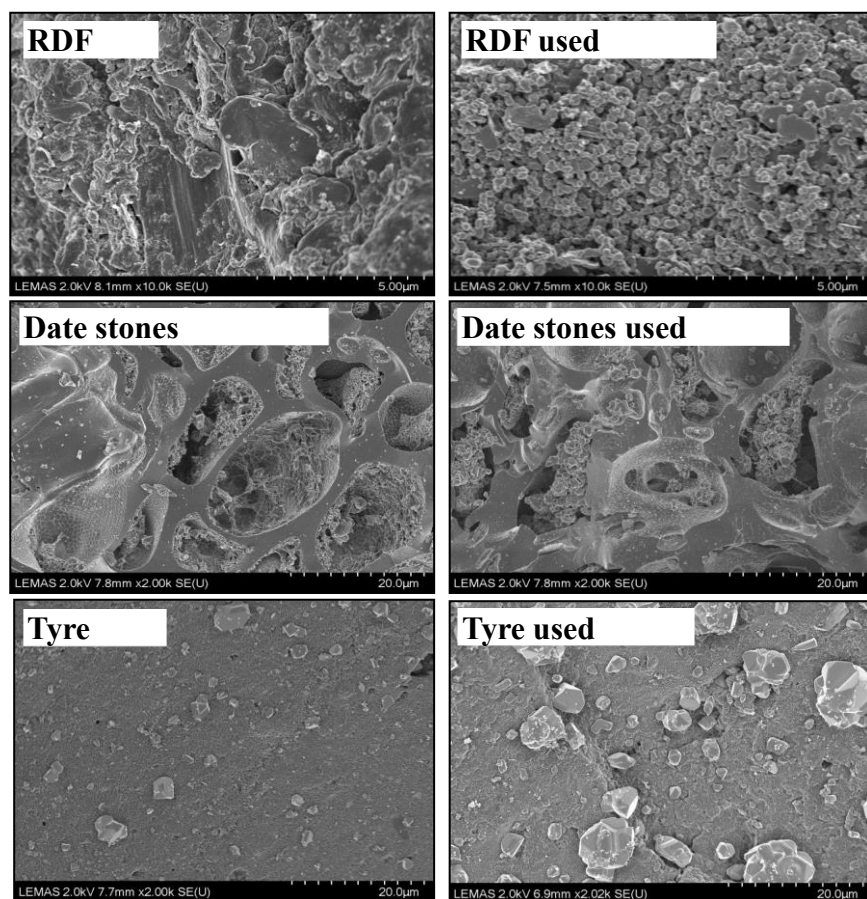


Figure 5.1-9. Scanning electron microscopy (SEM) images of fresh and used char samples.

Figure 5.1-10 shows a simple pathway of a tar cracking mechanism using char. The mechanism of tar cracking over char surface can be simplified as follows; tar molecules adsorb on the active sites, which could be the metals or the oxygen functional groups, and become dissociated into tar fragments and  $H_2$ . Tar radicals could also react with each other through polymerization reactions and form coke which may form new functional groups on the surface of the chars that could also crack at high temperature generating  $H_2$ ,  $CO_2$  and  $CO$  [30].

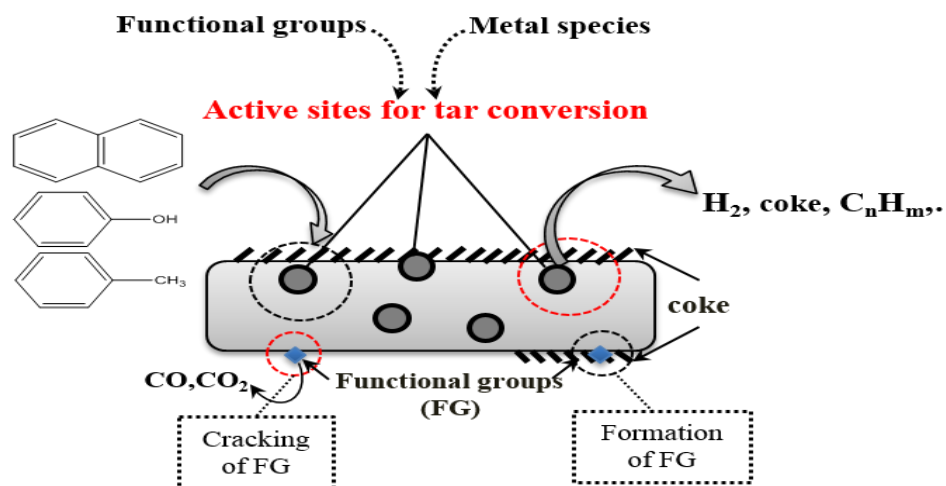


Figure 5.1-10. Tar cracking paths over char materials

### 5.1.6 Influence of the biomass to char ratio

Further experiments were undertaken with the tyre derived pyrolysis char to determine the influence of increasing the mass of char in the second stage hot char reactor in relation to the mass of biomass pyrolysed in the first stage section of the two-stage reactor. Experiments were undertaken at a hot char temperature of 700 °C and biomass to char ratios of 1:1, 1:2 and 1:3. The results in terms of product yield and gas composition are shown in Figure 5.1-11(a) and 5.1-11(b) respectively.

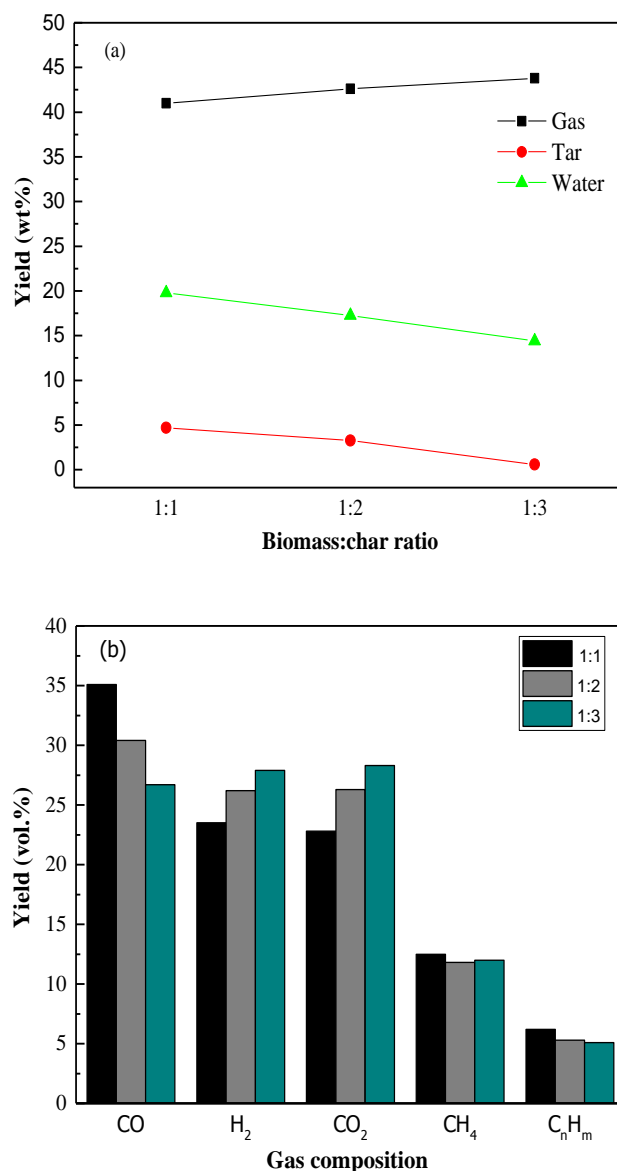


Figure 5.1-11. (a) Product yields and (b) gas composition in relation to biomass: char ratio for the tyre derived pyrolysis char at 700 °C hot char bed temperature.

The results show that as the amount of char was increased in the tar cracking second stage reactor, the yield of condensed bio-oil/tar was significantly reduced from ~25 wt.% to 15 wt.%. In a study carried out by Gilbert et al. [3], the heavy condensable phase was found to be resistant to decomposition with an increase in the amount of char, whereas the light oil fraction showed a decrease with increasing char amount. As the yield of bio-oil/tar decreased, there was a corresponding increase in gas yield as the biomass to char ratio was increased from 1:1 to 1:3. With a higher char amount, the pyrolysis vapour has a longer interaction time in the char bed resulting in cracking

of the tar compounds to gaseous species, particularly H<sub>2</sub> and CO (Figure 5.1-11(b)). With the increase of biomass to char ratio from 1:1 to 1:3, the H<sub>2</sub> concentration increased from 23.5 vol.% to 28 vol.%. Figure 5.1-11 (b) also shows that the CO concentration decreased and the CO<sub>2</sub> concentration increased as the biomass: char ratio was increased, suggesting that autogeneration of steam was producing increased hydrogen and carbon dioxide through the water gas shift reaction. The hydrocarbons also showed a small decrease suggesting reforming of the product hydrocarbon pyrolysis gases.

### **5.1.7 Summary of section 5.1**

Chars produced from the pyrolysis of different waste materials have been used as catalyst for the cracking of biomass derived pyrolysis gases during the pyrolysis-catalytic (char) gasification of biomass. The cracking of biomass derived hydrocarbons by carbonaceous chars was used to simulate the cracking of tar present in gasification syngas. The results showed that the waste derived chars were effective in reducing the condensable bio-oil/tar hydrocarbons with tyre char proving the most effective producing a 70% reduction in bio-oil/tar yield compared to that without char. Analysis of the gaseous compositions indicated that concentrations of H<sub>2</sub> and CO<sub>2</sub> increased with the presence of char due to the catalytic cracking of tars. The results suggest that tar removal by char materials is mainly due to the catalytic conversion and physical adsorption of tar compounds. The performance of chars in this study for tar removal was ordered as tyre char > RDF char > date stones char > no char. Further analysis is needed to investigate the tar conversion combined with char gasification.

## **5.2 Tar model compounds cracking using tyre char**

Section 5.1 examined the use of carbonaceous materials from waste materials for tar conversion. However, tar conversion using carbonaceous materials depends to a high extent on the surface functional groups and the porous texture [31]. Therefore, this section investigates the influence of porous texture and surface chemistry of carbons on tar conversion. Only one type of char was used and the process was carried out using tar model compounds. The effectiveness of tyre char for decomposing of biomass model tar compounds has been carried out in a fixed bed reactor and at a bed temperature of 700 °C. Four model compounds were used including phenol, furfural, toluene and methylnaphthalene. As Naphthalene is one of the main tar components produce during the gasification of biomass, further experiments were carried out with the use of methylnaphthalene as tar model compound. The effect of temperature, reaction time, the porous texture and the acidity of carbon on tar conversion was evaluated.

### **5.2.1 Catalytic activity of tyre char for cracking of tar model compounds**

The effectiveness of tyre char for cracking of model tar compounds at a temperature of 700 °C in terms of aromatic carbon conversion is displayed in Figure 5.2-1. In addition, blank experiments were carried out with each tar model compound, where sand was used as an inert bed material. This was to assess the influence of thermal cracking. The conversion was calculated from the carbon contained in the tar model feed that was converted to gaseous products (CO<sub>2</sub>, CO and CH<sub>4</sub>). Lower carbon conversion was obtained for phenol, toluene and methylnaphthalene. The reactivity of oxygenated compounds seems to be higher than that of non-oxygenated compounds. With both cases (catalytic and thermal cracking), the reactivity of tar compounds followed the order of furfural > phenol > toluene > methylnaphthalene. The results showed that the decomposition rate of the studied model tar compounds was much lower with the use of sand.

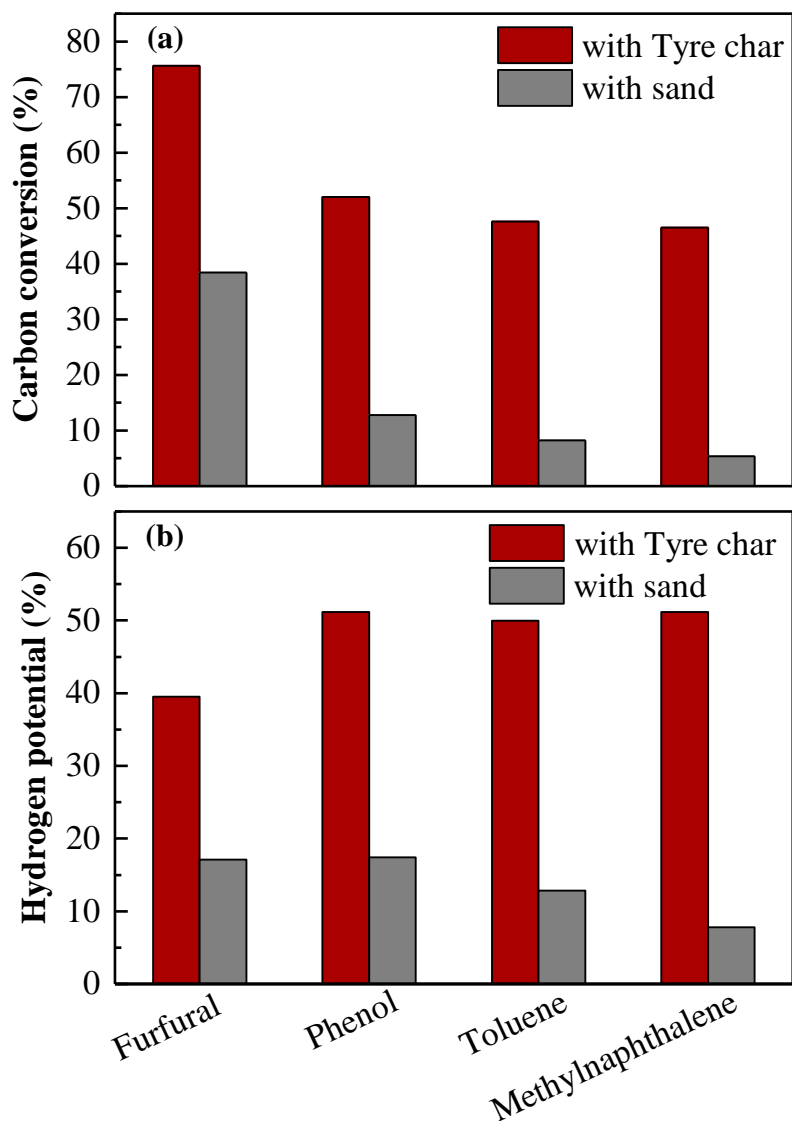


Figure 5.2-1-(a) Carbon conversion; and (b) hydrogen potential of tar model compounds with sand and tyre char.

The highest carbon conversion of (75%) was obtained with furfural and followed by phenol with 54 % carbon conversion. Abu El-Rub et al. [16] showed that commercial biomass char is an effective catalyst for phenol conversion. They achieved 82% conversion with commercial biomass char at a reforming temperature of 800 °C and with a gas residence time of 3 s with the presence of steam. The difference between the results obtained in this work is acceptable as the presence of steam is known to promote the tar cracking process [16]. The toluene conversion obtained in this work (47%) was lower compared with other work, such as that of Lu et al. [32] who reported a 63% toluene conversion at a reaction time of 60 min on sewage sludge char at 750

°C under an inert atmosphere and with a retention time of 0.3 s. However, the toluene conversion reported in this work is in agreement with that reported by Coll et al. [33] over a commercial nickel-based catalyst at 700 °C using steam to carbon ratio of 6.5.

The difference in carbon conversion between toluene and methylnaphthalene was negligible. This result is in agreement with the results obtained by Can et al. [34], where toluene and naphthalene achieved almost similar conversion of about 40% using coconut char at a temperature of 750 °C and with an inlet gas composition of 15 vol.% H<sub>2</sub>O and 8 vol.% H<sub>2</sub>. However, methylnaphthalene seems to be stable and hard to be removed where about 26.9 wt.% of condensed product was obtained. Compared to the results reported in Chapter 5, section 5.1, naphthalene concentration with the presence of tyre char during cracking of biomass tar was a slightly higher than that reported without char, while with the use of naphthalene as tar model compound; tyre char was effective in removing about 46% of naphthalene. Therefore, it may be suggested that the high concentration of naphthalene obtained with the presence of tyre char (section 5.1) at a temperature of 700 °C is due to the fact that the cracking of PAHs with 3 & 4 rings leads to the formation of naphthalene. Figure 5.2-1 (b) displays the hydrogen potential for the studied tar model compounds. The results clearly shows that tyre char promotes the hydrogen yield which was almost similar for the studied tar compounds, with values between 40 and 49%.

The main reactions involved during the catalytic cracking of tar compounds are tar cracking and hydrocarbon reforming. Therefore, the change in the gas composition with/without the use of catalyst is due to these reactions. The gas production increased dramatically with the introduction of tyre char in the second reactor stage in comparison to the experiments carried out with sand. For example, with the use of furfural as tar model compound, the gas yield increased from 39 to 78 wt.% and the hydrogen production was increased from 8 to 18.54 (mmol H<sub>2</sub> g<sup>-1</sup> furfural). The same trend was observed with the other tar model compounds. The gaseous products yield obtained in the catalytic cracking of tar model compounds over tyre char and sand are presented in Figure 5.2-2. The analysis of gaseous products formed during the experiments confirms that cracking reactions were taken place with the use of tyre char.

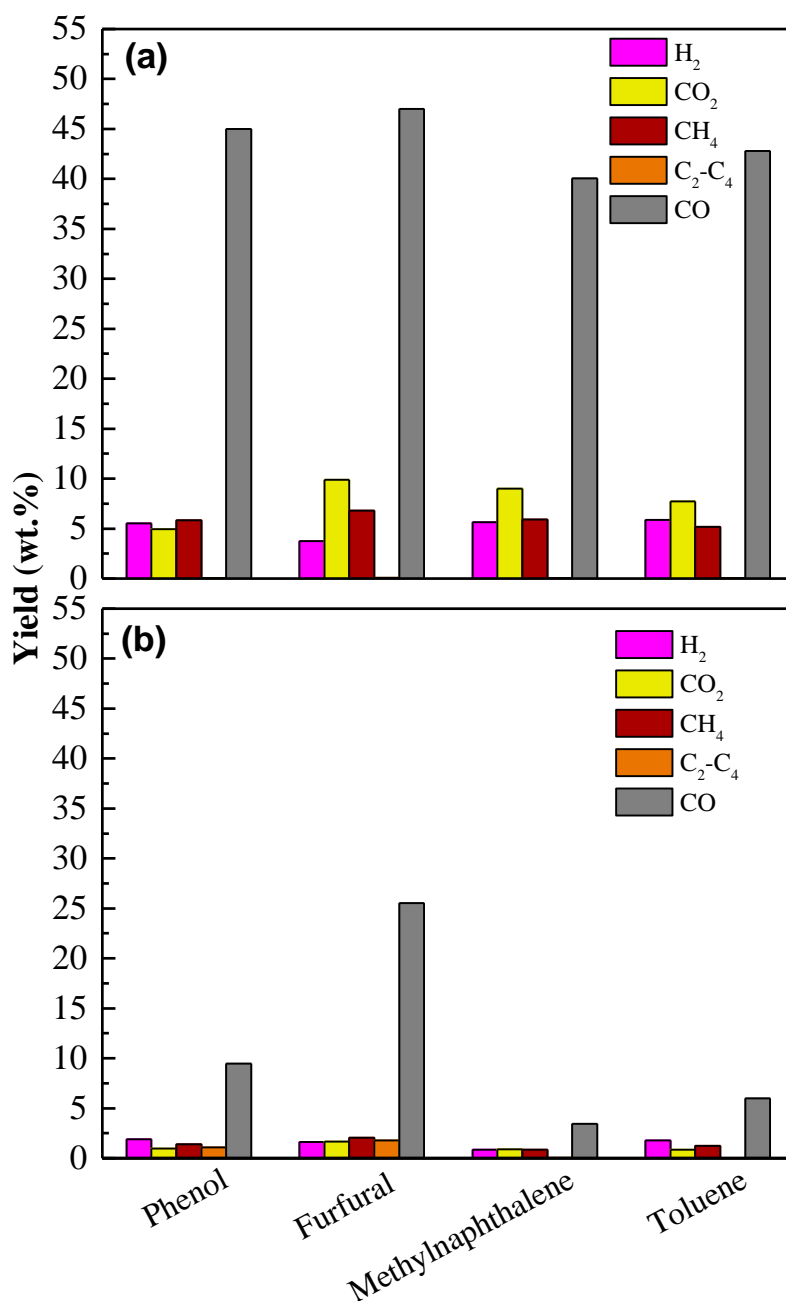


Figure 5.2-2-Influence of tyre char (a); and sand (b) on the gaseous yield (%) from the cracking of tar model compounds.

The major products obtained were CO and CO<sub>2</sub>. A comparison of aromatic compounds with oxygenated hydrocarbons shows that a lower CO yield was obtained with the cracking of aromatic hydrocarbons, which is a consequence of the poorer reactivity of these compounds. The highest CO yield (46 wt.%) was obtained from furfural, whereas the lowest yield was observed for methylnaphthalene (40 wt.%).

The oxygen functional groups on char could interact with tar molecules and enhance the cracking process. Examples of the oxygen functional groups present on carbon surface are displayed in Figure 5.2-3.

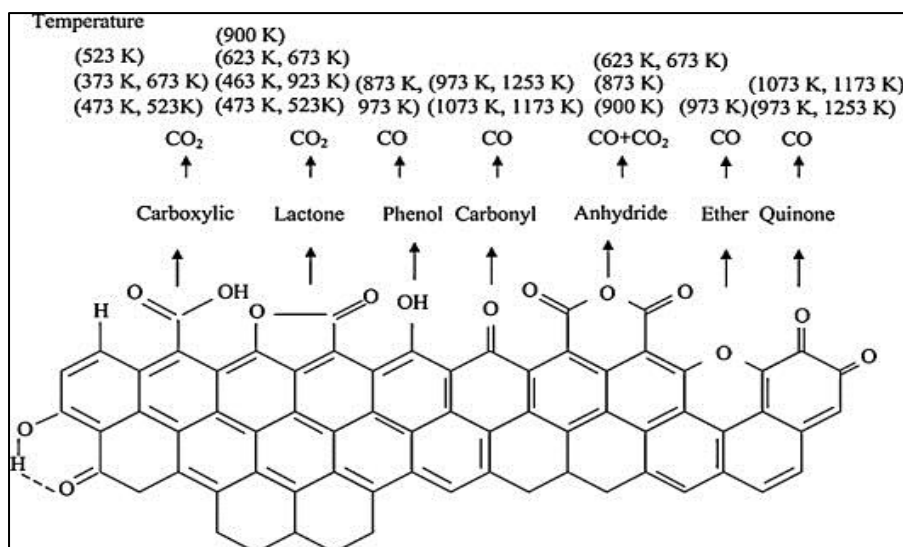


Figure 5.2-3. Oxygen functional groups on activated carbon surface and their decomposition with temperature [35].

In the study by Wang et al. [30], char was found to undergo thermal cracking leading to the production of carbon-containing gases, such as CO and CO<sub>2</sub> [30] which was observed also from the negative mass balance after the experiment. Surface oxygen groups present on the carbon surface are believed to decompose upon heating by releasing CO and CO<sub>2</sub> [36]. However, this has not been observed with the experimental conditions carried out in this research work as high temperature (>700 °C) heat treatment under an inert atmosphere is required to decompose the oxygen functional groups from the carbon surface [35]. In addition, coke could also be produced due to tar cracking. According to Wang et al. [30], the produced coke may react with the oxygen present on the char surface resulting in the formation of carbon-oxygen compounds that could also decompose to CO. However, CO also could be formed from the decomposition of methanol.

As has been reported earlier, many factors might influence the catalytic activity of carbonaceous materials for tar decomposition including the thermal effect, mineral content, surface chemistry and the porous texture. The increase in gas yield and the

change in gas compositions with the use of tyre char suggest that the tar decomposition is mainly due to the catalytic effect of tyre char and not due to the thermal cracking as more gases were produced over tyre char than that with the use of sand. This trend was observed with all the studied tar model compounds. The decrease of the condensed liquid with the use of tyre char could also be due to the adsorption of tar compounds on char surface. Tars are expected to adsorb on the surface of char. As an example of a tar cracking mechanism [30], Figure 5.2-4 shows the reaction pathways of toluene cracking. The reaction starts with the scission of either C-H bond of methyl and generating benzyl and hydroxyl radicals (Path 1) or breaking the C-C bond between methyl and benzene and forming methyl and phenyl radicals (Path 2). The active sites present in char are believed to combine with the formed radicals and facilitate the cracking process. Tar radicals could also react with each other through polymerization reaction and form soot [30].

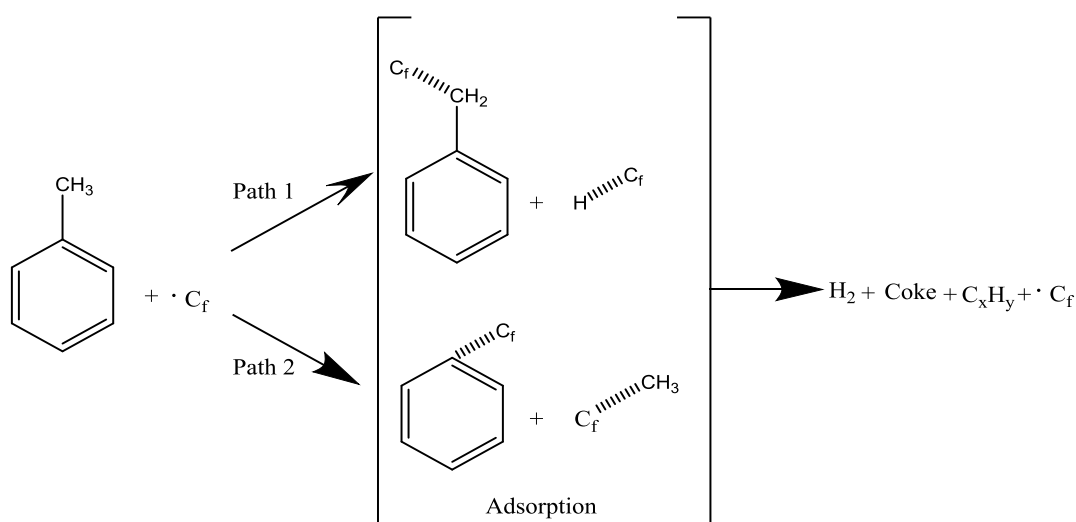


Figure 5.2-4. Reaction pathways of Toluene catalytic cracking [30].

To understand the main role that tyre char plays during the cracking of tar compounds, the fresh and spent tyre chars were examined by TGA-FTIR and the results are shown in Figure 5.2-5. The spent tyre char had some weight loss at a temperature of 900 °C (about 4%), which may be related with the adsorption of heavy tar compounds formed due to the polymerization reaction. However, the difference in weight loss between the fresh and the spent tyre char is not significant suggesting that the decrease of the

liquid content with the use of tyre char is not due to the adsorption mechanism and could be mainly due to cracking of tar compounds on active sites of the char surface into gases. The same conclusion was reported by Jin et al. [37]. The weight loss observed with the spent tyre char at 50 minutes was accompanied with the release of more CO<sub>2</sub> than that with fresh tyre char.

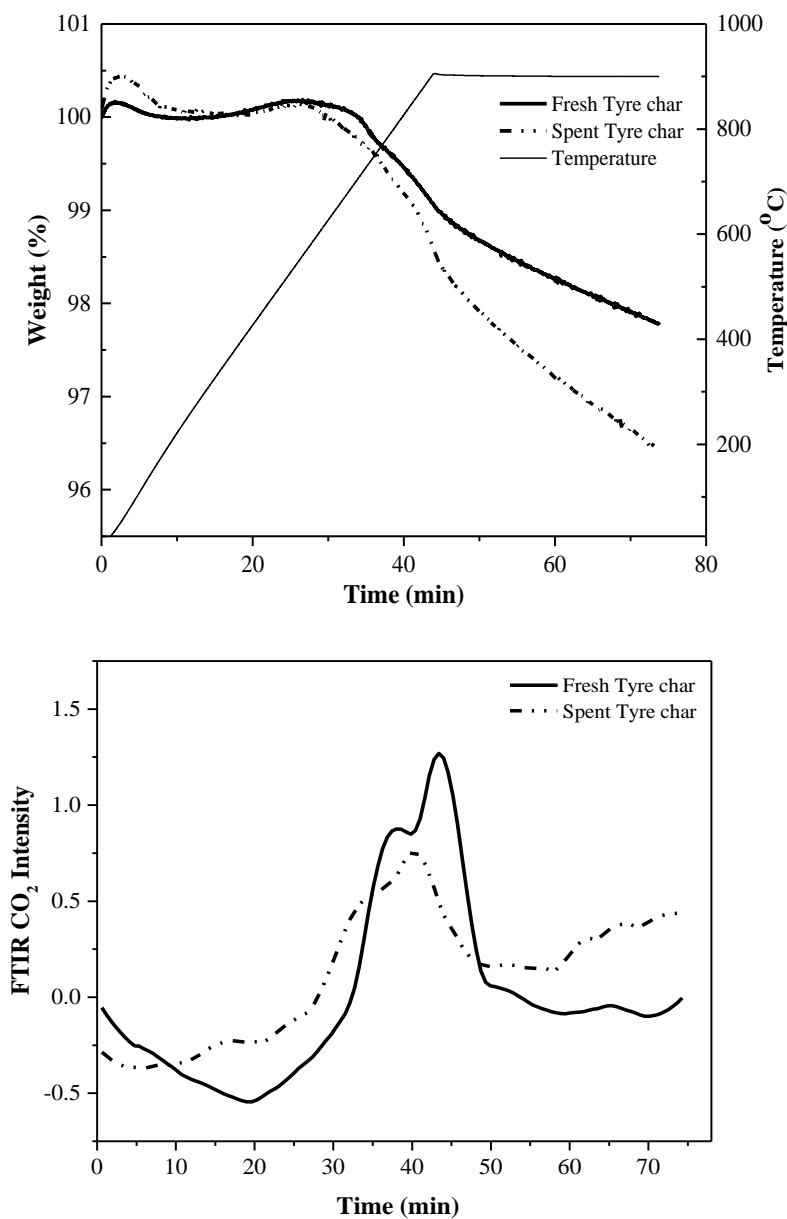


Figure 5.2-5. TGA-FTIR curves of fresh and spent tyre char

### 5.2.2 Parametric study

Naphthalene is one of the main tar components produced during the gasification of biomass [38] and considered as the most representative model of the biomass gasification tar [39, 40]. In addition, as it has been observed in section 5.1, PAHs are the major components at high temperatures  $>700^{\circ}\text{C}$ . The same observation has been reported by others [41, 42]. Therefore, methylnaphthalene was chosen for a further parametric study. According to Han and Kim [43], naphthalene contents in tar is generally above 9%. Don et al. [38] studied the catalytic cracking of methylnaphthalene using various catalysts and concluded that Zeolite and Ni/Mo catalysts were the most effective with a 100 % removal at  $550^{\circ}\text{C}$ . However, the experiments were carried out with the use of 30%  $\text{H}_2$  which is effective in inhibiting coke formation by hydrogenating the aromatic compounds. As a result, only a very small build-up of coke was observed with the used catalysts. In another study reported by Michel et al [39], steam reforming of methylnaphthalene over olivine and olivine supported nickel has been investigated at various temperatures. At  $900^{\circ}\text{C}$ , the methylnaphthalene conversion was about 4% and 31% for olivine and Ni/olivine respectively. The low activity of olivine was attributed to the low BET surface area. Therefore, many factors could influence the tar conversion including the BET, porosity and the reaction atmosphere.

The main aim of this study is to find out the main factors which could influence the tar conversion with the use of tyre char as a catalyst. The methylnaphthalene cracking with tyre char was carried out as a function of reaction time, reaction temperature, porosity and acidity. The effect of varying the reaction temperature was investigated using methylnaphthalene as tar model compound. With the increase of temperature from  $700\text{-}900^{\circ}\text{C}$ , the carbon conversion increased slightly from 46 to 50%. As can be observed in Figure 5.2-6, The condensed liquid gradually decreased, in which at a temperature of  $900^{\circ}\text{C}$  about 5% of the condensed liquid was obtained compared to 25% at  $700^{\circ}\text{C}$ . As a consequence, the gaseous products increased, for example, a high hydrogen yield ( $35\text{ mmol g}^{-1}$ ) was found at a temperature of  $900^{\circ}\text{C}$  compared to  $28\text{ mmol g}^{-1}$  at a temperature of  $700^{\circ}\text{C}$ . Anis et al. [44] found that the amount of condensed products collected during the catalytic treatment of naphthalene at a

temperature of 700 °C, and with the use of dolomite and Y-zeolite, were about 67 and 25 % respectively, which agreed with the result found in this study.

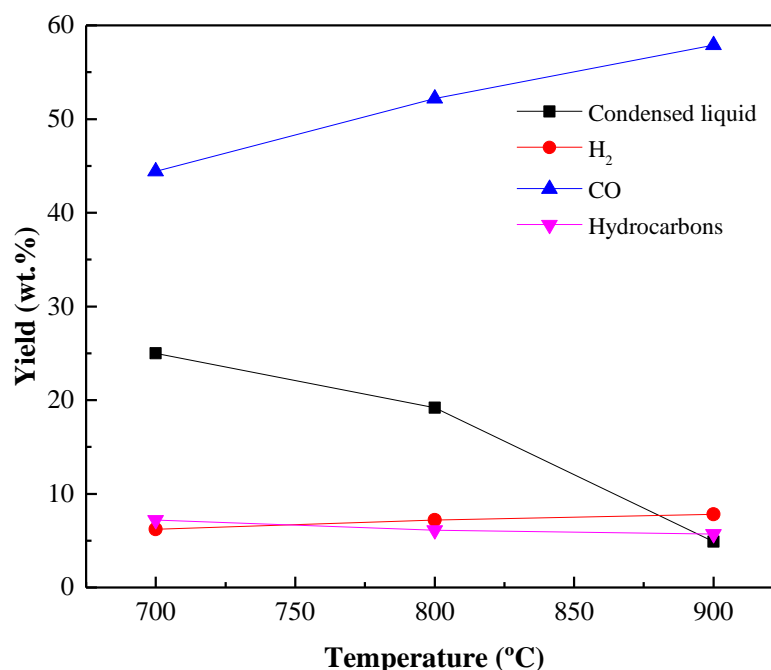


Figure 5.2-6. Products yields of methylnaphthalene cracking over tyre char at different cracking temperatures

According to the study carried out by Anis et al. [44], the thermal treatment of naphthalene showed that it is highly stable at a temperature below 1000 °C and about 70% of the condensed product was obtained at 1050 °C. However, the increase in temperature to 1200 °C led to an increase in the naphthalene removal efficiency and decrease in the condensed product to about 9%. The decrease of condensed liquid at high temperature was associated with the formation of soot which was the highest at this temperature and accounted for 68% of the total obtained product [44]. Further increase of temperature to 900 °C had no major influence on the carbon conversion and the total gas yield. However, the collected liquid product decreased by about 80% compared to that obtained at 700 °C. The results suggest that tar compounds could be trapped on the char surface and accumulate to form coke or soot, without being converted. The analysis of BET surface area agreed with this suggestion, as the BET surface area of the used tyre char at a temperature of 900 °C decreased to 58.8 m<sup>2</sup> g<sup>-1</sup> compared to about 73.4 m<sup>2</sup> g<sup>-1</sup> for the fresh char at 700 °C.

Methylnaphthalene has been found to decompose mostly to naphthalene and accounted for 50% of the total products at a reaction temperature of 900 °C. The first step in the decomposition of methylnaphthalene is the separation of the methyl group from the aromatic ring [45]. Parsland et al. [46] has reported the same trend. However, both Parsland and Leinger et al. [46, 47] reported the formation of low concentrations of other products such as benzene and styrene which has not been observed in this study. This is due to the difference in the reaction atmosphere and the catalysts used. In the study by Parsland et al. [46], the activity of BaNi (1) hexaaluminate catalyst for methylnaphthalene conversion has been investigated with the use of steam as a gasifying agent, while in this study the reaction was carried out in an inert atmosphere. The influence of the presence of H<sub>2</sub>O, CO<sub>2</sub> and H<sub>2</sub> on the naphthalene decomposition using dolomite as a catalyst has been studied by Alden et al [48]. They concluded that both CO<sub>2</sub> and H<sub>2</sub>O promote the cracking process. The de-alkylation of methylnaphthalene resulted in the formation of naphthalene, which can then be catalytically dissociated into radicals of naphthyl and hydrogen due to the cleaving of C-C or C-H bond. With the presence of CO<sub>2</sub> and H<sub>2</sub>O, naphthyl reacts with the oxidative radicals (which formed from CO<sub>2</sub> and H<sub>2</sub>O) resulting in the formation of lower aliphatic and single aromatic compounds. However, in an inert atmosphere, the catalytic decomposition of methylnaphthalene could result only in the formation of naphthalene, which can then produce soot by the polymerization reaction [49].

One of the main things to consider while using a catalyst for tar conversion is maintaining the activity for a long time. The feeding time of methylnaphthalene was extended to 80 min. However, further increase of the feeding period to 80 min, had no influence on the catalytic activity of tyre char for methylnaphthalene decomposition. As illustrated in Figure 5.2-7, the methylnaphthalene conversion was maintained at around 46%

over the studied feeding times. In the study by Hosokai et al. [50], charcoal was reported to exhibit a high naphthalene conversion (96%) at the beginning of the reaction time, and it decreased to about 50% after 45 minutes. The author ascribed this to the coke deposition on the surface of the charcoal which had resulted in a reduction in the BET surface area and pore volume. The stability of biomass char for naphthalene

conversion has also been reported by Zhang et al. [49] in which the char maintained the activity for about 5 h. Hosokai et al. [50] concluded that gaseous species formed with the use of charcoal as a catalyst for naphthalene and benzene cracking is due to the slow thermal cracking of charcoal and coking is the main mechanism for the decomposition of the studied tar compounds.

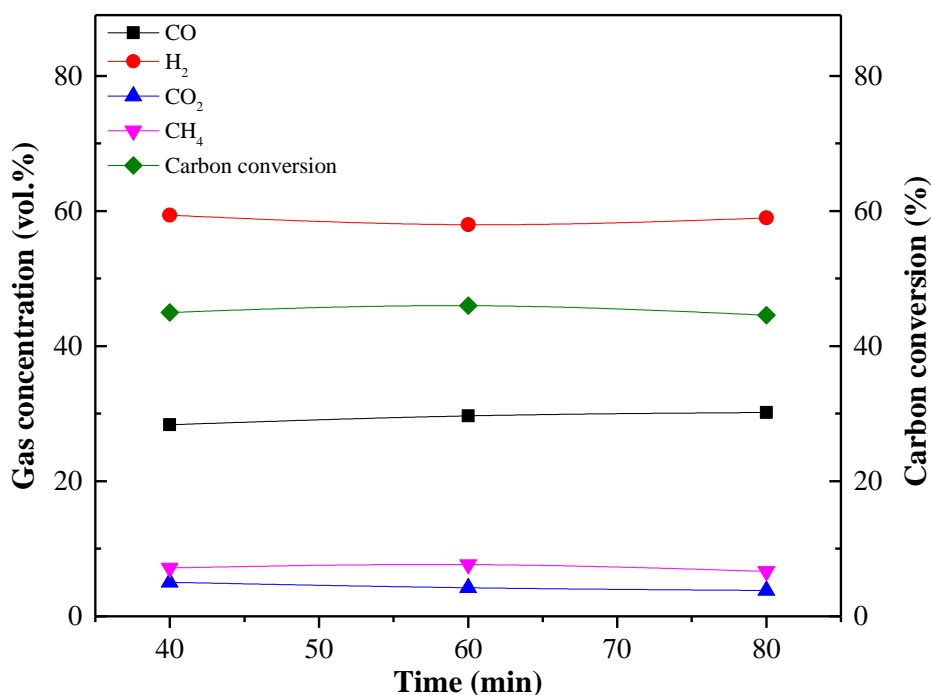


Figure 5.2-7. Influence of reaction time on gaseous compounds and carbon conversion

### 5.2.3 The influence of porosity on methylnaphthalene conversion

To assess the influence of porosity on methyl conversion, two commercial activated carbons with various porous textures were investigated for methylnaphthalene cracking at a temperature of 700 °C. Tyre char is a mesoporous carbon but to eliminate the influence of mineral content of tyre char and to be able to derive the final conclusion about the influence of porosity on methylnaphthalene conversion, a mesoporous activated carbon (AC2) with an ash content of 2 wt.% was used for the comparison along with a microporous activated carbon (AC1). The textural properties of the used samples are displayed in Table 5.2-1.

Table 5.2-1. Influence of carbon porosity on methylnaphthalene conversion, gas yield and hydrogen production

| Sample  | Tyre char | AC1   | AC2   |
|---|-----------|-------|-------|
| BET surface area (m <sup>2</sup> g <sup>-1</sup> )    | 71.7      | 944.1 | 631.0 |
| Mesoporous volume (cm <sup>3</sup> g <sup>-1</sup> )  | 0.561     | 0.304 | 0.687 |
| Microporous volume (cm <sup>3</sup> g <sup>-1</sup> ) | 0.090     | 0.479 | 0.149 |
| Carbon conversion (%)                                 | 46        | 55    | 53    |
| Condensed liquid (wt.%)                               | 24.8      | 11.0  | 20.7  |
| Gas Yield (wt.%)                                      | 61.3      | 73.5  | 71.3  |
| H <sub>2</sub> (mmol g <sup>-1</sup> )                | 28.3      | 33.4  | 20.4  |

There is an obvious difference between tyre char and the used commercial activated carbons in terms of the BET surface area and the well-developed porous texture. The BET surface area of the used commercial carbons was much larger than tyre char. In spite of the large difference in the BET surface area between the tyre char and the commercial activated carbons, the methylnaphthalene removal efficiency of both commercial activated carbons was slightly higher than that with the use of tyre char. Gases evolved during the test indicate an increase in CO, CO<sub>2</sub>, H<sub>2</sub> gas formation with the use of AC1 as shown in Figure 5.2-8. Fuentes-Cano et al. [34] investigated the catalytic activity of various char materials with different porous texture for toluene and naphthalene reforming in an atmosphere of steam and H<sub>2</sub> and concluded that the textural properties of char had no major influence on tar removal. In contrast, Jin et al. [37] reported that the difference in the performance of the studied carbon samples during the upgrading of coal oil is due to the difference in BET surface area. Additionally, the authors concluded that activated carbon had more structural defects than char in which these defects could serve as active sites for cracking of tar compounds. Hosokai et al. [28] investigated the decomposition of tar model compounds using charcoal and observed that coke deposited mainly in the micropores causing the loss of the catalytic activity of char. The mesopore volume of the charcoal remained unaffected. However, in this study, the decrease was found with both micropores and mesopores volumes.

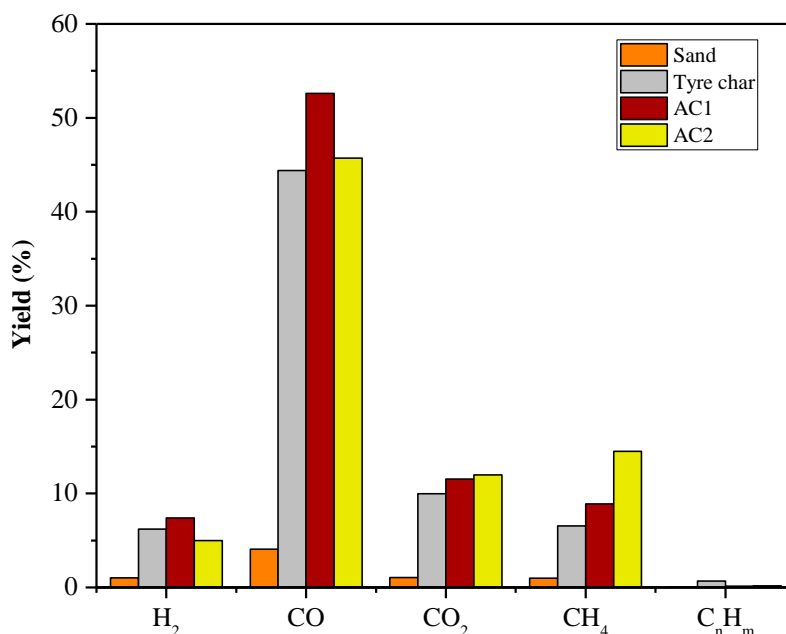


Figure 5.2-8. Influence of carbon porosity on gaseous compounds

The catalytic activity of the inorganic metals for heavy hydrocarbon conversion to light components has been reported by other researchers [37, 51]. Both commercial activated carbons have a well-developed pore structure with high BET surface area, however as it has been found that the difference in the catalytic activity of the used carbons was not significant. This could be related to the effect of the mineral content of tyre char (18 wt.% ash content) which could provide active sites for cracking of methylnaphthalene. The results suggest that the influence of BET surface area of carbon on tar cracking is negligible compared with the mineral content in carbon samples. The results are consistent with the conclusion reported by Li et al [52], in which semi-cokes with a higher amount of mineral content (35 wt.%) had a higher activity in tar cracking than the semi-coke with a well-developed porous structure but had less mineral content (8.3 wt.%). The authors believed that both mineral content and porous texture affects the catalytic activity of the studied semi-cokes for cracking of tar oil. In contrast, Zeng et al. [51] concluded that char with a higher BET surface area exhibited higher catalytic activity for tar removal. Demirbas [53] investigated the catalytic pyrolysis of various biomass samples impregnated with different catalysts and concluded that the maximum hydrogen yield was obtained with the samples impregnated with ZnCl<sub>2</sub>. As shown in Figure 5.2-8, the difference in the H<sub>2</sub> yield produced, as a result of cracking of methylnaphthalene, between the AC1 and tyre char

was only about 1 %. Additionally, the H<sub>2</sub> yield found with tyre char was higher than that with AC2 with a much higher BET surface area which suggests that the influence of mineral matter is more important than the porous texture.

#### 5.2.4 The influence of Acidity on methylnaphthalene conversion

According to Radovic et al. [54], the adsorption efficiency of the carbonaceous material depends to a high extent on the surface chemistry and ash mineral composition. Both Reinoso et al. [55] and Castilla [56] agreed that the effectiveness of activated carbon for the adsorption of organic compounds is mainly determined by the carbon surface chemistry. The nature of surface functional groups can be modified via chemical and physical treatment. The influence of carbon acidity on tar conversion during the pyrolysis-gasification has not been studied before. Al-Rahbi et al. [52] concluded that the higher efficiency of tyre char for tar conversion could be due to the carbon acidity. Buchireddy and his group [57] concluded that zeolite with a higher acidity had a better performance toward naphthalene conversion. One of the ways to form the acidic sites on carbon is to heat the sample in an oxidising environment. Therefore, AC1 was treated with HNO<sub>3</sub> with different molar concentrations. The textural properties of the original and treated activated carbon are displayed in Table 5.2-2. Comparing the treated samples with the starting material (AC1), the physical properties change little after the treatment. The decrease in BET surface area of the oxygenated samples has been reported before [8].

Table 5.2-2. Influence of carbon acidity on methylnaphthalene conversion and hydrogen production.

| Sample  | Untreated<br>AC1 | AC1-<br>1M HNO <sub>3</sub> | AC1-<br>3M HNO <sub>3</sub> | AC1-<br>4M HNO <sub>3</sub> |
|---|------------------|-----------------------------|-----------------------------|-----------------------------|
| BET surface area (m <sup>2</sup> g <sup>-1</sup> )    | 944              | 833                         | 747.79                      | 669.63                      |
| Mesoporous volume (cm <sup>3</sup> g <sup>-1</sup> )  | 0.304            | 0.118                       | 0.116                       | 0.080                       |
| Microporous volume (cm <sup>3</sup> g <sup>-1</sup> ) | 0.479            | 0.451                       | 0.409                       | 0.334                       |
| Acidic groups (mmol g <sup>-1</sup> )                 | 0.695            | 1.19                        | 1.40                        | 1.40                        |
| Carbon conversion (%)                                 | 55               | 57                          | 58                          | 55                          |
| H <sub>2</sub> (mmol g <sup>-1</sup> )                | 33.43            | 30.87                       | 30.4                        | 32                          |

Apparently, from the results presented in Table 5.2-2, the acidic treatment was not effective in enhancing the methylnaphthalene removal efficiency, the carbon conversion of the acid treated activated carbons was not significantly different from the original activated carbon. Additionally, the gas concentration did not change, and it was almost the same with all the tested samples which further show that the treatment had no influence on enhancing the effectiveness of carbon for cracking of tar compounds. This is probably due to the desorption of the oxygen functional groups while heating the char in nitrogen at 700 °C in the second furnace where the reaction has happened and according to Li et al. [58], the oxidised samples released more CO<sub>2</sub> at a temperature of 400 °C. The heat treatment of biochar at a temperature of 750 °C under N<sub>2</sub> for 10 hours has been found to decompose most of the surface oxygenated functional groups [59]. Therefore, the oxygen surface groups due to the acid treatment could be desorbed before the char reacts with the methylnaphthalene. The results are in agreement with those reported by Klinghoffer et al. [8] in which the influence of acidic groups of char have been investigated for methane decomposition at 850 °C and the authors concluded that the acidic functional groups have no influence on the catalytic activity of char. According to the study carried out by Bhandari et al. [60], the acidic activated carbon exhibited lower toluene removal (79%) than the original activated carbon (82%) at a temperature of 700 °C. The authors believed that this could be due to polar properties of the catalysts, formed because of the acidic groups, which can reduce the reactivity of active sites of carbon with toluene. The oxygenated groups are polar while the aromatic ring is non-polar [58]. In contrast, Sechandri and Shamsi [61] concluded that char/dolomite mixture, due to their low BET surface area and surface acidity, had a lower activity for coal tar decomposition than zeolites. The influence of oxygen functional groups on the catalytic activity of char for methane decomposition has been investigated by Klinghoffer et al. [8], and it has been found that the acidic groups desorb at a low temperature.

### **5.2.5 Summary of section 5.2**

The effectiveness of tyre char for decomposing of biomass model tar compounds has been studied in a fixed bed reactor and at a bed temperature of 700 °C. Four model compounds were used including phenol, furfural, toluene and methylnaphthalene to

simulate typical biomass tar compounds produced during biomass gasification. The compounds were fed continuously for 60 min using methanol as a solvent, with a methanol and compound carbon molar ratio of 1. The reactivity of the tar compounds followed the order of furfural > phenol > toluene > methylnaphthalene. High carbon conversion (46-75%) and hydrogen yield (15-28 mmol g<sup>-1</sup>) were obtained in comparison to the non-catalytic experiments. Naphthalene is one of the main tar components produced during the gasification of biomass. Further experiments were carried out with the use of methylnaphthalene as tar model compound in terms of the effect of temperature, reaction time, the porous texture and the acidity of carbon on tar conversion was evaluated with the use of methylnaphthalene as tar model compound. The carbon conversion increased from 46% at 700 °C to 51% at 900 °C. The formation of new by-products as a result of cracking of methylnaphthalene over tyre char was determined using GC-FID. Naphthalene is the main formed compound and accounts for 50 % of the total products at a reaction temperature of 900 °C. The influence of porous texture and surface chemistry on methylnaphthalene conversion was compared using two commercial activated carbons with different porous texture. Neither the surface area nor the surface chemistry of the tested carbons had a role in enhancing the tar decomposition. However, activated carbon with microporous texture had a higher activity than the investigated mesoporous carbons. The waste tyre derived pyrolysis char was shown to be effective in reducing tar compounds produced during biomass gasification.

### **5.3 Steam reforming of biomass tar over sacrificial tyre pyrolysis char for H<sub>2</sub>-rich syngas production**

From section 5.1, it was shown that tyre char had a better catalytic activity for tar cracking than RDF and date stones chars. Therefore, this section investigates the influence of steam addition on hydrogen production and tar reforming using tyre char through a reforming/gasification process using the two stage pyrolysis-reforming reactor which could play a major role in increasing the total gas yield. This process enables the simultaneous reforming of hydrocarbons and steam gasification of char. The study investigates the influence of bed temperature, steam to biomass ratio, reaction time and the effects of tyre ash minerals on syngas quality and hydrogen production. Biomass was used as the feedstock to generate tar/syngas and waste tyre derived pyrolysis char was used as a sacrificial catalyst in a steam reforming process to generate a hydrogen-rich syngas.

#### **5.3.1 Effects of char ash on tar decomposition and hydrogen production**

To examine the influence of ash minerals on tar cracking and increasing the hydrogen yield during the biomass pyrolysis-reforming/gasification process, tyre char was subjected to acid treatment with HCl for the purpose to remove the minerals as described in chapter 3, section 3.1.2. The elemental composition and ash content of the char samples are shown in Table 5.3-1. Tyre char had a high ash content of 18 wt.% and its main metal composition was Zn. The acid treatment was effective for metal removal. After the removal of metals, the carbon content of acid treated char increased while the sulphur and nitrogen contents decreased.

As can be observed in Table 5.3-1, the treatment was effective in removing about 90% of the Zn metal and the total ash content was reduced by ~50%. It has been reported [62] that the ash content of a typical tyre is between 5 and 7 wt.% depending on the type of tyre, comprising mainly additives such as silica and clays, in addition to the additives such as zinc and sulphur. The silica and clay (alumina-silicates) additives would not be removed by the acid treatment process and would account for

the large majority of the 9 wt.% ash content of the demineralised tyre char. It might be expected that the acid treatment process would remove most of the reactive metal from the tyre char, leaving the silica and alumina-silicate filler material.

Table 5.3-1. Ultimate and mineral content of char

|                                 | <b>Original tyre char</b> | <b>Acid treated tyre char</b> |
|---------------------------------|---------------------------|-------------------------------|
| Ash (wt.%)                      | 18.9                      | 9                             |
| <i>Ultimate analysis (wt.%)</i> |                           |                               |
| Carbon                          | 70.06                     | 86.04                         |
| Hydrogen                        | 0.28                      | 0.33                          |
| Nitrogen                        | 0.83                      | 0.37                          |
| Oxygen (by difference)          | 4.78                      | 0.73                          |
| <i>Ash composition (wt.%)</i>   |                           |                               |
| Zn                              | 6.5                       | ND                            |
| K                               | 0.05                      | 0.05                          |
| Ca                              | 0.95                      | ND                            |
| Fe                              | 0.69                      | 0.08                          |
| Si                              | 0.95                      | 1.47                          |

The original and acid-treated tyre chars were used as catalysts for tar cracking during biomass reforming in the presence of steam. With both chars, the influence of bed temperature on the final gaseous compositions was investigated from 700 to 900 °C, at a steam to biomass mass ratio of 3.32 and a reaction time of 60 min. The final temperature of the pyrolysis of the biomass was always 500 °C. The influence of char minerals on total gas yield and gas composition in the presence of steam is shown in Table 5.3-2.

Table 5.3-2. Influence of char minerals on product distribution and gas characterization

|  | Tyre char |       |       | Acid treated tyre char |       |       |
|--|-----------|-------|-------|------------------------|-------|-------|
| Temperature (°C)   | 700       | 800   | 900   | 700                    | 800   | 900   |
| <i>Mass balance based on the biomass sample + water (wt.%)</i> |           |       |       |                        |       |       |
| Gas  | 12.1      | 16.6  | 33.0  | 11.6                   | 15.8  | 26.1  |
| Liquid   | 82.8      | 76.87 | 61.4  | 84.5                   | 79.9  | 69.5  |
| Biomass char   | 5.6       | 5.8   | 5.5   | 5.5                    | 5.9   | 5.5   |
| Mass Balance   | 100.5     | 99.2  | 99.8  | 101.6                  | 101.0 | 97.5  |
| Tyre char recovered (%)  | 100.0     | 91.0  | 82.5  | 101.0                  | 98.0  | 85.5  |
| <i>Mass balance based on the biomass sample (wt.%)</i>         |           |       |       |                        |       |       |
| Gas  | 50.0      | 67.1  | 131.6 | 48.9                   | 63.1  | 106.8 |
| Biomass char   | 23.0      | 23.3  | 22.0  | 22.5                   | 23.5  | 22.5  |
| <i>Gas characterization</i>                                    |           |       |       |                        |       |       |
| HHV (MJ Kg <sup>-1</sup> )                                     | 48.3      | 52.5  | 66.1  | 27.9                   | 44.3  | 63.6  |
| H <sub>2</sub> yield (mmol g <sup>-1</sup> )                   | 8.4       | 12.5  | 39.2  | 2.7                    | 8.6   | 30.5  |
| H <sub>2</sub> +CO (mol mol <sup>-1</sup> )                    | 14.8      | 21.7  | 57.8  | 10.2                   | 20.0  | 52.0  |
| H <sub>2</sub> /CO (mol mol <sup>-1</sup> )                    | 1.31      | 1.37  | 2.11  | 0.37                   | 0.75  | 1.41  |

The reforming and cracking of biomass volatile compounds and the gasification of tyre char produce more gaseous products according to the reactions displayed in Table 5.3-3 [63-65];

Table 5.3-3. Reactions involve during the gasification process

| Reaction type           | Chemical reaction  | Enthalpy $\Delta H$ (KJ mol <sup>-1</sup> ) | Reaction No. |
|-------------------------|--|---|--------------|
| Water gas (primary)     | $C + H_2O \leftrightarrow CO + H_2$                                    | +131  | R 5.3-1      |
| Water gas (secondary)   | $C + 2H_2O \leftrightarrow CO_2 + 2H_2$                                | +76   | R 5.3-2      |
| Boudouard               | $C + CO_2 \leftrightarrow 2CO$   | +172  | R 5.3-3      |
| Hydrogasification       | $C + 2H_2 \leftrightarrow CH_4$  | -74.8                                       | R 5.3-4      |
| Water gas shift         | $CO + H_2O \leftrightarrow CO_2 + H_2$                                 | -41.2                                       | R 5.3-5      |
| Methane steam reforming | $CH_4 + H_2O \leftrightarrow CO + 3H_2$                                | +206  | R 5.3-6      |
| Steam reforming         | $C_nH_m + nH_2O \leftrightarrow nCO + \left(n + \frac{m}{2}\right)H_2$ | -   | R 5.3-7      |

As can be observed from the experimental results presented in Table 5.3-2, with both tyre char samples, total gas yield increased significantly with the increase of temperature to 900 °C, this is due to the reforming of tars (R5.3-7) and the char gasification, as in the second stage the reactions of H<sub>2</sub>O, CO, H<sub>2</sub> and CO<sub>2</sub> with carbon in the tyre char took place [66]. With the use of the original tyre char, the gas yield, hydrogen yield and HHV of the product gas increased from 52.8 to 131.6 (wt.%), 8.4 to 39.2 (mmol g<sup>-1</sup> biomass) and 48.3 to 66.1 (MJ Kg<sup>-1</sup>) respectively as the tyre char temperature was increased from 700 to 900 °C. According to Franco et al. [67], the endothermic char gasification reactions are enhanced at a higher temperature, which can be clearly seen from the decrease of tyre char recovered after reaction at higher reaction temperature (Table 5.3-2). It is worth mentioning that in the experiment with the use of sand and steam at 900 °C, the total gas yield decreased by 56 %, while the liquid product increased by 27 %. Therefore, the increase of gas yield at a higher reforming temperature with the presence of tyre char is mainly due to the catalytic properties of char for reforming of tar and also because of char gasification.

The catalytic effect of the acid treated demineralised tyre char was investigated using the same experimental conditions as with the original tyre char. As presented in Table 5.3-2, the acid treated char exhibited a lower catalytic activity than the original tyre char. For example at a temperature of 900 °C, the total gas yield decreased by ~20 % with the acid treated tyre char compared to the original gas yield at 900 °C. Additionally, the total liquid product was found to be higher with the acid treated tyre char. The results suggest that the ash metals, present in tyre char, play a significant role in enhancing the tar reforming reactions during the biomass pyrolysis-reforming/gasification process. As displayed in Figure 5.3-1, the tyre char temperature had a clear influence on the gaseous species found in the product syngas.

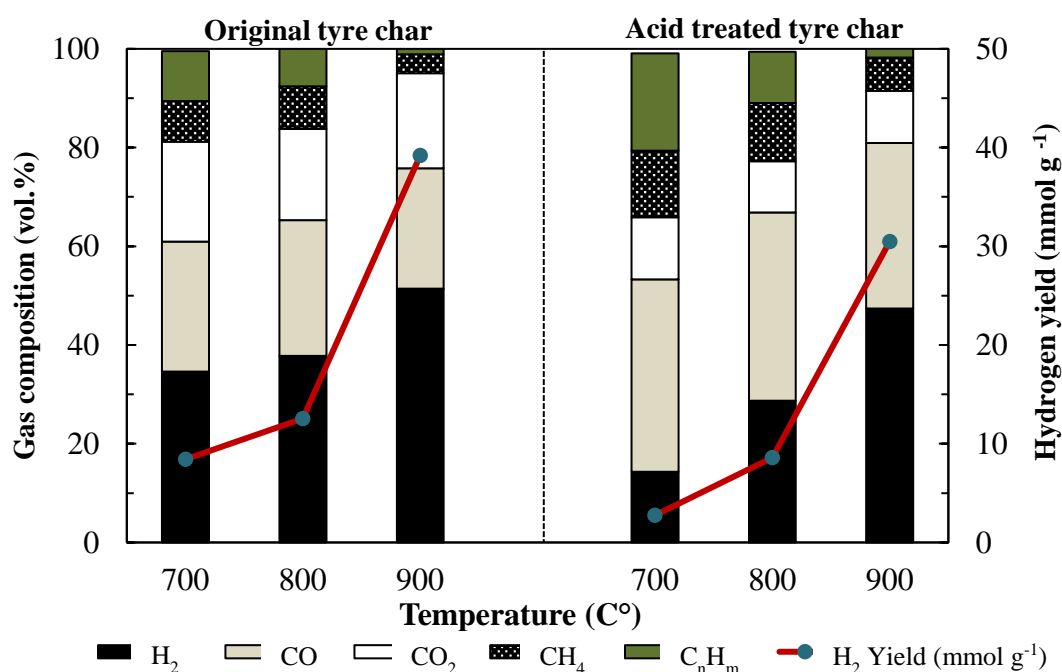


Figure 5.3-1. Gas compositions and hydrogen yield with original and acid treated tyre chars.

The main gaseous compound formed during this process was hydrogen. The hydrogen yield increased with temperature, the maximum hydrogen yield of 39.20 (mmol g<sup>-1</sup>) was obtained at a temperature of 900°C. However, the removal of minerals as a result of acid treatment resulted in a decrease in the hydrogen yield to 30 mmol g<sup>-1</sup>. The decrease in hydrogen yield with the use of acid treated tyre char was also observed at

reaction temperatures of 700 and 800 °C. Ma et al. [68] obtained a hydrogen yield of 83.3 mol/kg from the steam gasification of biochar.

With regards to the gaseous composition formed with the use of original and acid treated tyre char, there is an obvious difference between the results obtained with two types of tyre pyrolysis char, e.g. the hydrogen and CO<sub>2</sub> content were higher with the original tyre char. For example at a temperature of 700°C, the hydrogen content decreased from 34.60 to 14.3 vol.% after the acid treatment of the tyre char. Additionally, the content of CO, CH<sub>4</sub>, C<sub>n</sub>H<sub>m</sub> increased with the use of acid treated tyre char. This suggests that the presence of metals in tyre char had a role in enhancing the steam tar reforming, water-gas shift, hydrocarbon reforming and char gasification reaction. The same observation has been found by Zhang et al. [69].

Table 5-3.2 shows that the H<sub>2</sub>/CO molar ratio decreased sharply with the removal of minerals from the tyre pyrolysis char. The results suggest that the ash metals present in the tyre char promote the water gas shift reaction (R 5.3-5) and the char-steam reactions (R 5.3-1& R 5.3-2). The increase of H<sub>2</sub> concentration with the original tyre char is mainly attributed to the catalytic effect of mineral metals which play a major role in enhancing the catalytic steam reforming and cracking of tar. Additionally, a significant difference was also observed in relation to the hydrocarbon concentration of the product gas with both chars. The same trend was observed by Jiang et al. [70], during the steam gasification of rice straw, in which the hydrogen yield was found to decrease from 10 mmol g<sup>-1</sup> of the original sample to 8.8 mmol g<sup>-1</sup> of acid treated sample. According to Choi et al. [71], the adsorbed tar on the active sites of activated carbon could form coke and with the sequence of thermal and catalytic cracking of tar and coke, hydrogen and light hydrocarbons are produced. The active sites could be the metals; therefore the available active sites on the acid treated tyre char were reduced.

In comparison with the experiments carried out with the use of sand in the second stage catalytic reactor at 900 °C, the concentration of CO decreased with the use of tyre pyrolysis char during the steam reforming of biomass pyrolysis oil, this indicates that the char promotes the CO-shift reaction leading to a high concentration of H<sub>2</sub> and CO<sub>2</sub> [63]. Similar results have been reported by Wang et al. [72]. A significant

decrease in methane concentration was observed. The detected trend in this study agrees with the trend observed by Franco et al. [67]. The influence of gas-char interaction on gaseous composition has been studied by Chen et al. [73]. They concluded that this process had a significant influence on enhancing the hydrogen content from 17 to 37.8 %. According to the reported literature, the water gas shift reaction is promoted at a temperature higher than 700 °C leading to an increase in H<sub>2</sub> and decrease in CO yields [67].

Tyre char promotes the water gas shift reaction at higher temperature leading to a high concentration of H<sub>2</sub>. However, the increase in CO<sub>2</sub> composition is not significant. According to Franco et al [67], other reactions may take place at a temperature higher than 830 °C such as Boudouard reaction which results in consuming the CO<sub>2</sub> concentration and this can be observed from the amount of converted tyre char at 900 °C which was higher than that at 800 °C. Additionally, char steam gasification reactions and methane reforming reaction are enhanced at 900 °C, resulting in an increase in CO content and a decrease in the CH<sub>4</sub> content. The significant increase in H<sub>2</sub> concentration is also due to hydrocarbon cracking and reforming reactions. Wang et al [74] studied the steam reforming of biomass and found that the steam itself had a minor effect on tar reforming without the presence of a char-supported catalyst.

In comparison to the results found with the catalytic cracking, chapter 5 (section 5.1), the addition of an external steam input had a significant influence on changing the syngas composition. For example, at a char bed temperature of 800 °C, an increase of 13% in H<sub>2</sub> and a decrease of 19% and 28% in CO and CH<sub>4</sub> contents respectively was found with the introduction of steam. This is attributed to water gas shift and steam reforming reactions resulting in an increase in H<sub>2</sub>/CO ratio. With steam addition, the H<sub>2</sub>/CO ratio increased to 1.37 compared to a ratio of 0.852 with the absence of steam.

The presented results suggested that tyre ash metal species had a catalytic role in enhancing the hydrogen production. Zhang et al. [69] studied the catalytic conversion of model biomass pyrolytic vapour using biochar and demineralised biochar and reported hydrogen yields of 64 and 59 vol.% respectively. Nanou et al. [75] investigated the influence of ash on enhancing the steam gasification of wood char and

concluded that the addition of ash minerals to the biomass char was effective in enhancing char gasification as the gasification rate of the impregnated char increased by 30% compared to the original char with no minerals. In this study, this can be observed from the decrease in tyre char recovered at the end of the experiment. At all the studied temperatures, the decrease in the original tyre char recovered was more obvious than the acid treated char (Table 5.3-2). This could be due to the presence of metals which could enhance the char gasification. For example at 900 °C, the original and acid treated tyre char yields decreased by 17.5 and 14.5 % respectively.

The catalytic effect of zinc in enhancing the hydrogen yield during biomass gasification has been reported before by other researchers [76]. Gonzalez [76] examined the influence of the presence of  $ZnCl_2$  and dolomite on biomass steam gasification and concluded that at a temperature of 800 °C, the presence of  $ZnCl_2$  had a positive effect in promoting the hydrogen production, compared to dolomite, during biomass gasification in the presence of steam. However, at a temperature of 900 °C, the hydrogen concentration remained almost the same even in the presence of  $ZnCl_2$ . Demirbas [77] compared the catalytic pyrolysis of biomass samples with  $Na_2CO_3$ ,  $K_2CO_3$  and  $ZnCl_2$  and the highest hydrogen yield of 70.3% was obtained from olive husk using 13%  $ZnCl_2$  as a catalyst at 1025K. In contrast, Hamad et al [78] claimed that  $ZnCl_2$  had a negative influence in which the gas yield was found to decrease with the addition of  $ZnCl_2$  to biomass.

The tar compounds found in the condensed liquid were grouped based on the classification system reported by other researchers in which the tar compounds are classified into five classes depending on the number of aromatic rings and the molecular weight [21, 43]. The concentration of the classified tar compounds is shown in Figure 5.3-2.

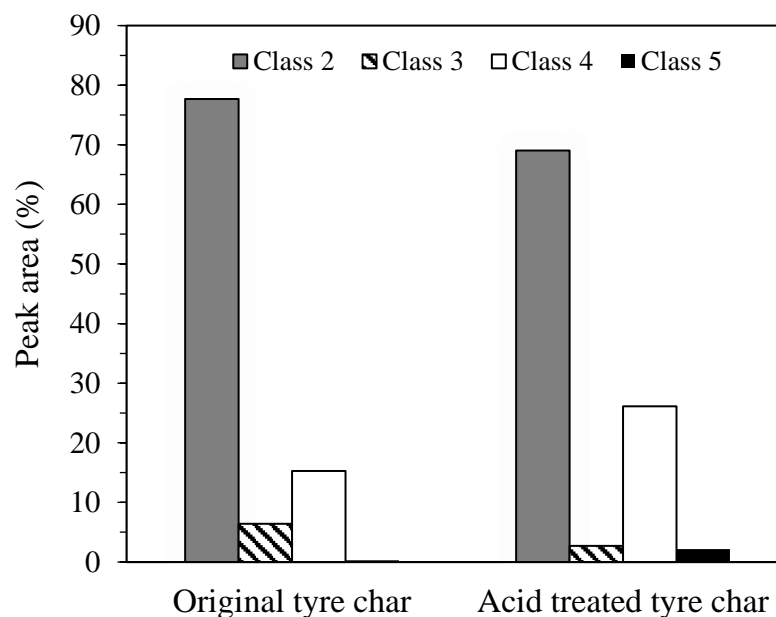


Figure 5.3-2. Concentration of the classified tar compounds in the tar collected from the pyrolysis-reforming/gasification of biomass with tyre char catalyst at 800 °C (Class 2 = heterocyclic compounds e.g. phenols and cresols; class 3 = 1-ring aromatic compounds e.g. ethylbenzene and xylene; Class 4 = 2-3 ring aromatic compounds e.g. naphthalene and phenanthrene; Class 5 = 4-7 ring aromatic compounds e.g. fluoranthene and pyrene).

Class 2 includes tar compounds with heterocyclic compounds such as phenols. Class 3 referred to aromatics with 1-ring such as xylene; while light PAHs, with 2-3 rings, and heavy PAHs were grouped in class 4 and 5 respectively. For the product tars produced using both the original tyre char and the acid-treated tyre char shows that the major tar compounds present came from class 2. The presence of minerals in tyre char seems to promote the cracking of large ring polyaromatic compounds (class 4 & 5) to form light compounds (class 2). Additionally, it can be observed that the concentration of both the light and heavy PAH compounds were increased by 10 and 2 % respectively with the use of acid treated tyre char. In terms of the catalytic activity of the char used in this study, the results show that the original tyre char was more effective in reducing most of the tar compounds than the acid-treated tyre char. Jiang et al. [70], studied the catalytic effects of the inherent alkali and alkaline earth metals on tar decomposition during the steam gasification of biomass via using original biomass and demineralised biomass and reported that the inherent alkali minerals present in biomass char had a significant catalytic effect in enhancing tar reforming, char gasification and water gas shift reactions during the biomass steam gasification

[70]. However, char ash consists of various metal species and the catalytic activity of the metals may not be the same, therefore, Zhang et al [69] carried out another study to investigate the catalytic effects of specific metals on biomass pyrolysis tar cracking, for this purpose biochar was impregnated with different metallic species (K, Ca, Mg, Zn, Fe, Al). It was reported that all the studied metallic elements had a catalytic activity except for Al. The presence of zinc in the tyre ash composition plays a significant catalytic role in enhancing tar reforming reactions. For example, in the study by Oztas and Yürüm [14], coal samples were impregnated with several metals including Zn. The authors observed some catalytic effect of Zn and Ni in decomposing many of the tar compounds.

### **5.3.2 Effect of steam to biomass ratio**

The main aim of the combination of biomass pyrolysis and tar and char gasification in the second stage was to enhance the gas yield and obtain the optimum syngas ratio through shifting the reaction from exothermic to endothermic [79, 80]. Therefore, the influence of steam to biomass (S/B) mass ratio over the range of 1.8-6.0 on hydrogen production and reforming/gasification efficiency was investigated at 900 °C and at a reaction time of 60 min with the use of the original tyre char. According to the reported literature [72, 81], the metal species in char accelerates the dissociation of water into OH\* and O\* intermediates which would then react with the cracked molecular hydrocarbons intermediates, formed during the reforming process, thus promoting the water gas shift reaction and thereby generate hydrogen. Therefore, this process depends on the amount of the dissociated species from water (H\* and OH\*). The hydrogen production yield could be increased by varying the steam to biomass ratio.

The influence of steam to biomass mass ratio on the total gas yield and gas compositions is shown in Figure 5.3-3.

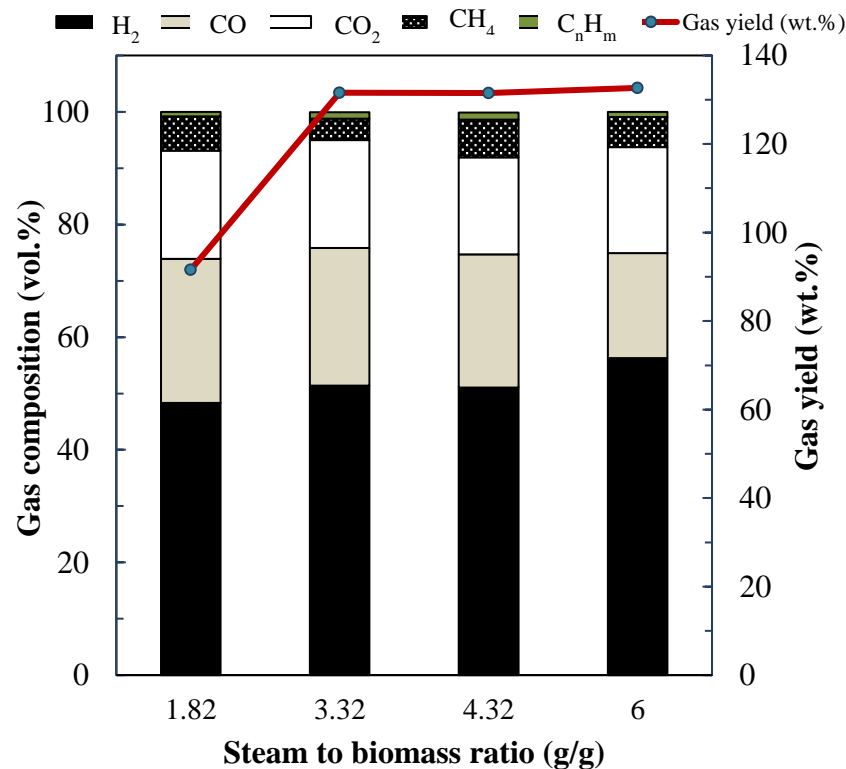


Figure 5.3-3. The influence of steam to biomass (S/B) ratio on gas composition and total gas yield

The increase in steam quantity enhanced the steam reforming of tar and tyre pyrolysis char-steam reactions which results in an increase in the gas yield from 94.82 to 132.6 wt.% (data calculated in relation to the original mass of biomass). The total gas yield increased by ~28% with the increase of steam flow rate (S/B ratio 1.82 to 3.32). At higher S/B mass ratio of 3.32, the effect of steam on gas production was negligible. According to Alipour et al. [82], the high steam to biomass ratio does not always contribute to increase the total gas yield.

As the steam to biomass ratio was increased from 1.8 to 6.0, the hydrogen concentration increased from 47 to 56 vol.% and the CO concentration decreased from 26 vol.% to 19 vol.%. The increase of H<sub>2</sub> and decrease in CO at higher S/B mass ratio is due to the enhanced char steam gasification (R5.3-1) and water gas shift reaction (R5.3-5). However, the increase of H<sub>2</sub> concentration was not significant when the S/B

mass ratio was higher than 3.32. In a study undertaken by Zhang et al. [69], the highest hydrogen yield achieved, during the reforming of bio-oil using biochar, was about 60 vol.% at a steam to model pyrolytic vapour ratio of 4 and a reaction time of 30 min.

Sattar et al. [83] investigated the influence of steam flow rate on the product gases during the gasification of biochar and reported an increase in the hydrogen and CO<sub>2</sub> yields with increasing steam flow rate. However, in this study, both CO and CO<sub>2</sub> yields decreased with an increase in the steam flow rate which could be due to multiple reactions occurring at the same time, such as water gas shift, reforming and char gasification. Yan et al. [64] studied the influence of steam on the gasification of biomass char at a temperature of 850 °C and reported an increase of H<sub>2</sub> yield from 2.15 mol kg<sup>-1</sup> to 57.07 mol kg<sup>-1</sup> with the increase of steam input from 0 to 0.165g min<sup>-1</sup> g<sup>-1</sup> of biomass char.

As observed in Figure 5.3-4, with the increase of S/B mass ratio, the H<sub>2</sub>/CO molar ratio increased while CO/CO<sub>2</sub> decreased which suggests that the water gas shift reaction determines greatly the H<sub>2</sub> production. The same trend was observed by Wei et al. [84]. The H<sub>2</sub>/CO ratio is important in determining the end use of the syngas.

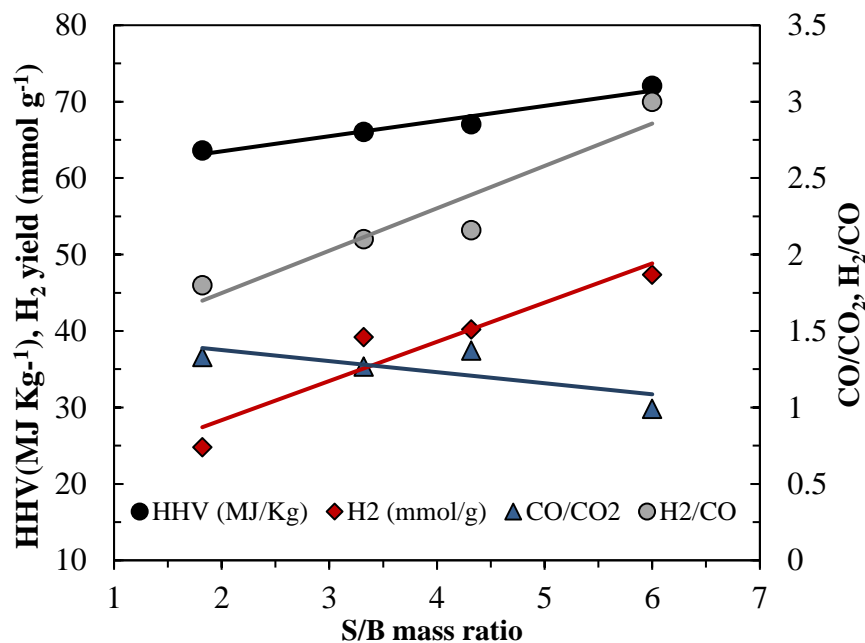


Figure 5.3-4. Effect of steam to biomass ratio on H<sub>2</sub> yield, HHV, H<sub>2</sub>/CO and CO/CO<sub>2</sub>.

The optimum value of  $H_2/CO$  is determined by the required application, for example, the upgrading of syngas for fuel cell applications requires a higher  $H_2/CO$  ratio while a value of 2:1 is needed for Fisher-Tropsch reactions [85]. It is well known that it is costly to produce synthesis gas with a  $H_2/CO$  molar ratio of between 1-2 [86]. In this study, the experiments performed at a steam/biomass ratio of 3.3 and 4.3 produced a syngas ratio of 2 which is more suitable to be used for Fisher-Tropsch synthesis. The HHV increased in the range of the studied S/B ratio to  $72 \text{ MJ Kg}^{-1}$ . Based on the hydrogen concentration and total gas yield, it can be concluded that the optimum steam to biomass ratio for this system is 3.32. Zhang et al. [69] studied the influence of steam on model pyrolytic vapour (2-5 g/g) on the gaseous composition using biochar and concluded that the ratio of 4 was the optimum.

With regards to the tyre char gasification and S/B ratio, the presence of steam enhanced the char conversion as the residual material (reacted tyre char) recovered after the gasification was found to decrease with increasing steam to biomass ratio. The higher S/B mass ratio enhanced the tyre char gasification as the amount of tyre pyrolysis char recovered after the reaction was found to decrease from 90% at a S/B ratio of 1.8 to 73.5% at a S/B ratio of 6.0. Therefore the increase of gas yield at a higher S/B ratio was also due to char gasification as has been mentioned before. High steam to carbon ratio is required to avoid coke accumulation on the surface of the tyre char [87]. However, the decrease was not significant, the increase of steam flow rate by about 70% led to a 20% decrease in the amount of final tyre char recovered. Chen et al [73] reported a 6% decrease in char yield when the S/B ratio was increased from 1 to 4. The char conversion rate can be better enhanced with a long reaction time.

### **5.3.3 Effect of reaction time**

Further experiments were carried out to investigate the influence of reaction time on tyre char gasification at a temperature of  $900 \text{ }^\circ\text{C}$ , to determine whether the char conversion and total gas production could be enhanced by allowing the reaction to proceed for several hours. The variation in gas compositions with reaction time is shown in Figure 5.3-5. With the increase in reaction time, the  $H_2$  concentration remained almost constant and the CO concentration increased. Chaudhari et al. [85],

reported that the hydrogen concentration was also found to remain constant after 1 h reaction time.

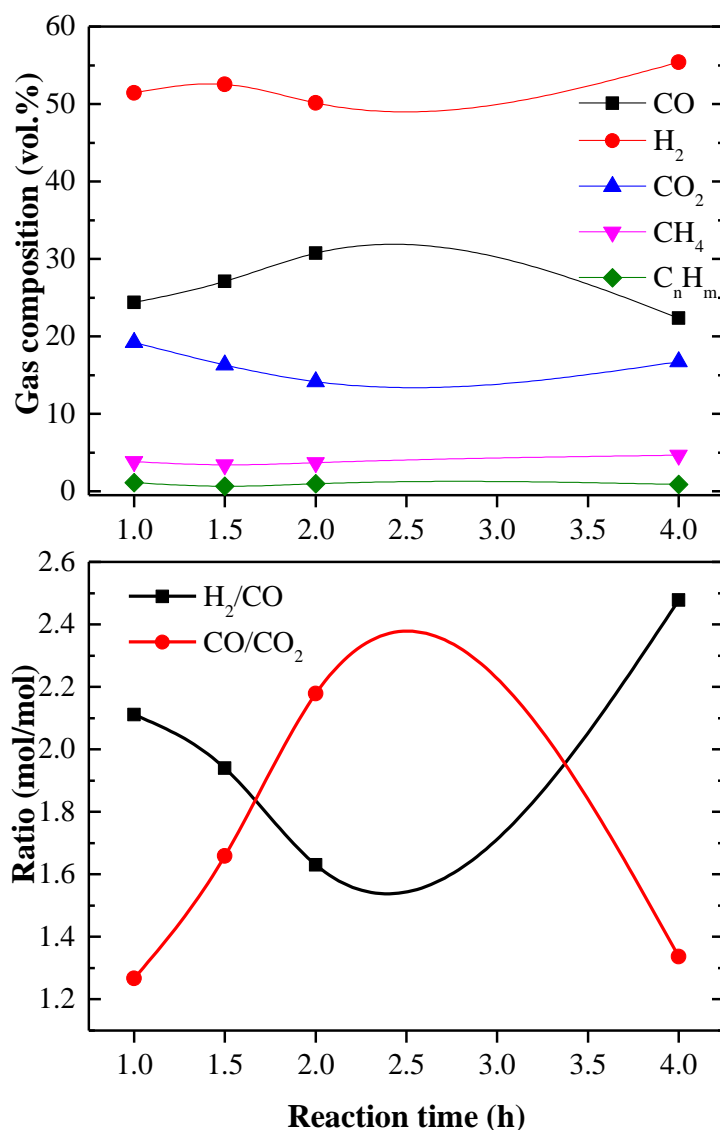


Figure 5.3-5. The influence of reaction time on the product gas compositions

The increase of hydrogen formation during the biomass gasification is mainly due to the reactions of tars and hydrocarbons with char. As can be observed from the gaseous compositions presented in Figure 5.3-5, the hydrogen content remained almost constant with the increase of reaction time from 1 h to 2 h and only a slight increase was observed at a reaction time of 4 h. Additionally, the CO/CO<sub>2</sub> molar ratio increased with time on-stream, while H<sub>2</sub>/CO decreased. These results suggest that the reaction

is complete in 60 min and Boudouard (R 5.3-3) and char reactions with steam (R 5.3-1) are the dominant reactions after 60 min. This agrees with the evolution of CO/CO<sub>2</sub> and H<sub>2</sub>/CO with time. The high H<sub>2</sub>/CO at a reaction time of 60 min is due to the influence of water gas reactions and over the reaction time of 60 min, the char reactions with CO<sub>2</sub> and steam are more important which could explain the increase in CO/CO<sub>2</sub> ratio. However, a decrease in the ratio of CO/CO<sub>2</sub> was observed with the increase in reaction time from 2 h to 4 h; this is due to the gasification of the total fixed carbon, so there was no carbon left in tyre char to react with steam and as a result, CO/CO<sub>2</sub> decreased.

The increase of gas yield with time was found to be correlated with the increase of carbon conversion of tyre char as displayed in Figure 5.3-6.

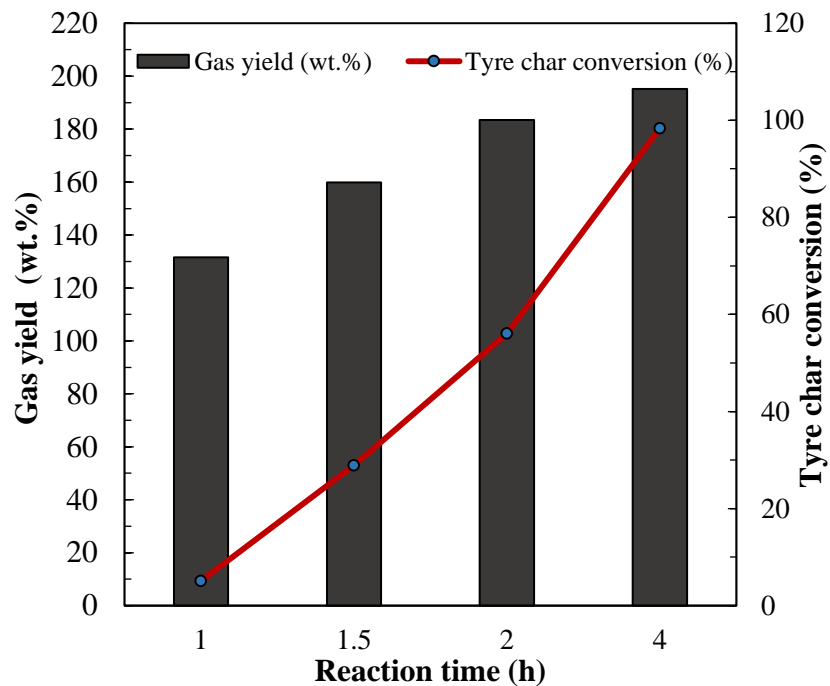


Figure 5.3-6. The influence of reaction time on tyre char conversion and total gas yield

The char conversion was calculated from;

$$C_0 - C / C_0$$

Where  $C_o$  = carbon mass of tyre char before reaction and  $C$  = carbon mass after reaction

For example, tyre char carbon conversion increased by 50% with the increase in reaction time from 1 h to 2 h and the same percentage of increase was observed in the total gas yield which means that the increase in gas yield with time is mainly due to char gasification. For example, the carbon conversion of tyre char increased from 5 to 56% with an increase in reaction time from 1 h to 2 h. Accordingly, the total gas yield increased from 131.55 to 183.40 wt.% (in relation to the original mass of biomass).

As the main aim of this study was to increase the total gas yield through tar reforming and char gasification, the results displayed in Figure 5.3-6 shows that the reaction time had a significant influence on decreasing the amount of tyre char recovered after the reaction. With a reaction time of 4 h, the final tyre char recovered was 6 wt.%, which included carbon and ash, and from Figure 5.3-7, the carbon and ash represent 19.3 and 85 wt.% respectively. The carbon content decreased significantly from 80.6 wt.% after one hour to 19.3 wt.% after 4 hours (Figure 5.3-7).

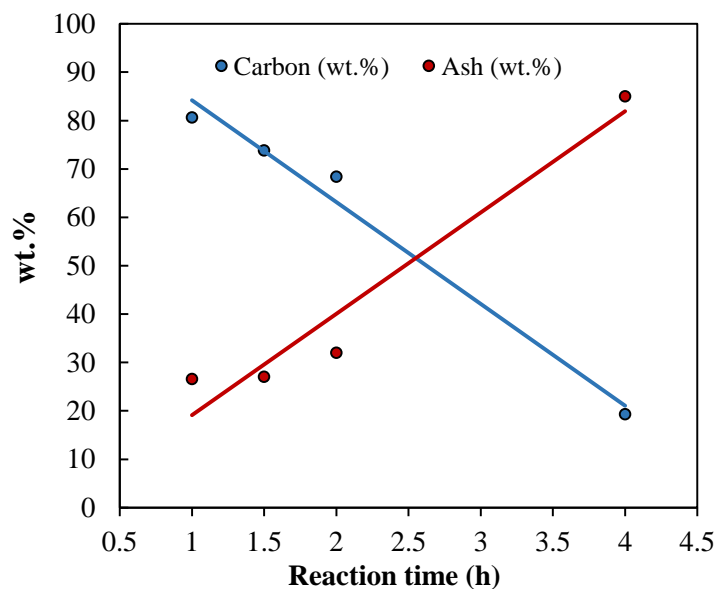


Figure 5.3-7. Carbon and ash content of tyre char from catalytic gasification of biomass at different reaction times

A complete conversion of tyre char was almost achieved with 4 h reaction time. This agrees very well with the results presented in Figure 5.3-6. Char with high ash content can be recycled in construction and cement industries [88].

As tyre char is expected to be gasified with the presence of steam at high gasification temperature, blank experiments of tyre char and steam was carried out where tyre char was gasified at 900 °C for 1 hour (in the absence of biomass in the first pyrolysis stage) with the same experimental conditions as for biomass steam reforming over tyre char. The total gas yield produced from the gasification of tyre char itself was 35.49 wt.% compared to 131.6 wt.% (Table 5.3-2) obtained with biomass tar reforming over tyre char. Therefore, tyre char gasification contributed to about 26% of the total gas yield obtained with biomass tar reforming experiments. Further experiments at 1.5 h, 2 h and 4 h showed that the total gas yield from the steam gasification of the tar (in the absence of biomass) was 55.13 wt.%, 80.36 wt.% and 152.14 wt.% respectively. By comparison with the data in Figure 5.3-6, at 1.5 h the contribution of the tyre char gasification to the total gas yield was 35.5%, after 2 h it was 43.8% and after 4 h the total gas yield contributed by the tyre char gasification was 78.9% of the total gas yield.

In this work, char derived from the pyrolysis of waste tyres has been shown to be effective for the cracking and degradation of gasification tar like compounds during the pyrolysis-catalytic steam reforming of biomass. The metallic mineral content of the tyre pyrolysis chars making a significant contribution to the tar degradation. In addition, the char reacts with the steam to generate hydrogen, and also carbon monoxide, and methane which add to the calorific value of the product syngas. Through the reactions of the tyre char with the steam, the char catalyst for reforming/gasification reactions is consumed or 'sacrificed' as a catalyst.

An overall process concept could be, pyrolysis of waste tyres to recover, valuable tyre pyrolysis oils which have similar properties to a petroleum derived light fuel, steel for recycling into the steel industry, and a product gas with a high calorific value that can be used as process fuel for the tyre pyrolysis process. The product char from tyre pyrolysis may then be used as a catalyst for the cracking/reforming/gasification of tars

from the gasification of biomass to produce as clean syngas, while also contributing to the yield of the biomass syngas through tyre char gasification reactions.

#### **5.3.4 Summary of section 5.3**

In this section, biomass pyrolysis gas and char gasification was investigated to produce hydrogen. The thermal cracking of biomass pyrolysis gases with the presence of steam at a temperature of 900 °C had a small influence on hydrogen production as only 10.94 mmol g<sup>-1</sup> of hydrogen was obtained for the pyrolysis-reforming of biomass with sand. The hydrogen production increased significantly with the use of tyre pyrolysis char in the 2nd stage reforming/gasification reactor to be 39.20 mmol g<sup>-1</sup> biomass due to the simultaneous reactions of tar reforming and char gasification. On the other hand, acid treated tyre pyrolysis char exhibited a lower catalytic activity as the hydrogen production decreased to 30.4 mmol g<sup>-1</sup> biomass at 900 °C. The difference in hydrogen production between the two types of tyre char suggests that the metals in tyre char have a significant catalytic effect in enhancing the water gas shift, tar reforming and char-steam reactions.

The influence of operating conditions including catalytic reforming temperature, steam/biomass (S/B) mass ratio and reaction time were investigated for the purpose of obtaining a high hydrogen production. Among the studied variables, the reforming temperature had the greatest influence on hydrogen production. The results showed that the gas yields and hydrogen production increased with the increase of reforming temperature and S/B ratio due to the enhanced char steam gasification and water gas shift reactions.

## References

1. PARK, J., Y. LEE and C. RYU. Reduction of primary tar vapor from biomass by hot char particles in fixed bed gasification. *Biomass and Bioenergy*, 2016, **90**, pp.114-121.
2. SUN, Q., S. YU, F. WANG and J. WANG. Decomposition and gasification of pyrolysis volatiles from pine wood through a bed of hot char. *Fuel*, 2011, **90**(3), pp.1041-1048.
3. GILBERT, P., C. RYU, V. SHARIFI and J. SWITENBANK. Tar reduction in pyrolysis vapours from biomass over a hot char bed. *Bioresource Technology*, 2009, **100**(23), pp.6045-6051.
4. ABU EL-RUB, Z.Y.K. Biomass char as as in-situ catalyst for tar removal in gasification systems. *University of Twente*, 2008.
5. ABU EL-RUB, Z., E.A. BRAMER and G. BREM. Review of Catalysts for Tar Elimination in Biomass Gasification Processes. *Industrial & Engineering Chemistry Research*, 2004, **43**(22), pp.6911-6919.
6. DEVI, L., K.J. PTASINSKI and F.J.J.G. JANSSEN. Pretreated olivine as tar removal catalyst for biomass gasifiers: investigation using naphthalene as model biomass tar. *Fuel Processing Technology*, 2005, **86**(6), pp.707-730.
7. REN, S., H. LEI, L. WANG, Q. BU, S. CHEN and J. WU. Hydrocarbon and hydrogen-rich syngas production by biomass catalytic pyrolysis and bio-oil upgrading over biochar catalysts. *RSC Advances*, 2014, **4**(21), pp.10731-10737.
8. KLINGHOFFER, N.B., M.J. CASTALDI and A. NZIHOU. Influence of char composition and inorganics on catalytic activity of char from biomass gasification. *Fuel*, 2015, **157**, pp.37-47.
9. FRANZ, M., H.A. ARAFAT and N.G. PINTO. Effect of chemical surface heterogeneity on the adsorption mechanism of dissolved aromatics on activated carbon. *Carbon*, 2000, **38**(13), pp.1807-1819.
10. BECK, J.S., J.C. VARTULI, W.J. ROTH, M.E. LEONOWICZ, C.T. KRESGE, K.D. SCHMITT, C.T.W. CHU, D.H. OLSON, E.W. SHEPPARD, S.B. MCCULLEN, J.B. HIGGINS and J.L. SCHLENKER. A new family of mesoporous molecular sieves prepared with liquid crystal templates. *Journal of the American Chemical Society*, 1992, **114**(27), pp.10834-10843.

11. ILIOPOULOU, E.F., E.V. ANTONAKOU, S.A. KARAKOULIA, I.A. VASALOS, A.A. LAPPAS and K.S. TRIANTAFYLLIDIS. Catalytic conversion of biomass pyrolysis products by mesoporous materials: Effect of steam stability and acidity of Al-MCM-41 catalysts. *Chemical Engineering Journal*, 2007, **134**(1–3), pp.51-57.
12. AL-RAHBI, A.S.S., M.A. NAHIL, C. WU and P.T. WILLIAMS. Waste-derived activated carbons for control of nitrogen oxides. *Proceedings of the Institution of Civil Engineers - Waste and Resource Management*, 2016, **169**(1), pp.30-41.
13. CUNLIFFE, A.M. and P.T. WILLIAMS. Properties of Chars and Activated Carbons Derived from the Pyrolysis of Used Tyres. *Environmental Technology*, 1998, **19**(12), pp.1177-1190.
14. ALTUNTAŞ ÖZTAŞ, N. and Y. YÜRÜM. Effect of Catalysts on the Pyrolysis of Turkish Zonguldak Bituminous Coal. *Energy & Fuels*, 2000, **14**(4), pp.820-827.
15. MICCIO, F., B. PIRIOU, G. RUOPPOLO and R. CHIRONE. Biomass gasification in a catalytic fluidized reactor with beds of different materials. *Chemical Engineering Journal*, 2009, **154**(1–3), pp.369-374.
16. ABU EL-RUB, Z., E.A. BRAMER and G. BREM. Experimental comparison of biomass chars with other catalysts for tar reduction. *Fuel*, 2008, **87**(10–11), pp.2243-2252.
17. JESS, A. Mechanisms and kinetics of thermal reactions of aromatic hydrocarbons from pyrolysis of solid fuels. *Fuel*, 1996, **75**(12), pp.1441-1448.
18. EGSGAARD, H. and E. LARSEN. Thermal transformation of light tar - Specific routes to aromatic aldehydes and PAH. In *Proceedings*. Vol.2. James and James, London. 2001, pp. 1468-1471.
19. CYPRES, R. Aromatic hydrocarbons formation during coal pyrolysis. *Fuel Processing Technology*, 1987, **15**, pp.1-5.
20. WILLIAMS, P.T. and D.T. TAYLOR. Aromatization of tyre pyrolysis oil to yield polycyclic aromatic hydrocarbons. *Fuel*, 1993, **72**(11), pp.1469-1474.
21. MORF, P., P. HASLER and T. NUSSBAUMER. Mechanisms and kinetics of homogeneous secondary reactions of tar from continuous pyrolysis of wood chips. *Fuel*, 2002, **81**(7), pp.843-853.

22. SHEN, Y. and K. YOSHIKAWA. Tar Conversion and Vapor Upgrading via in Situ Catalysis Using Silica-Based Nickel Nanoparticles Embedded in Rice Husk Char for Biomass Pyrolysis/Gasification. *Industrial & Engineering Chemistry Research*, 2014, **53**(27), pp.10929-10942.
23. XU, C., S. HAMILTON and M. GHOSH. Hydro-treatment of Athabasca vacuum tower bottoms in supercritical toluene with microporous activated carbons and metal-carbon composite. *Fuel*, 2009, **88**(11), pp.2097-2105.
24. BOROSON, M.L., J.B. HOWARD, J.P. LONGWELL and W.A. PETERS. Heterogeneous cracking of wood pyrolysis tars over fresh wood char surfaces. *Energy & Fuels*, 1989, **3**(6), pp.735-740.
25. ZHAO, S., Y. LUO, Y. ZHANG and Y. LONG. Experimental investigation of the synergy effect of partial oxidation and bio-char on biomass tar reduction. *Journal of Analytical and Applied Pyrolysis*, 2015, **112**(0), pp.262-269.
26. FUSHIMI, C., T. WADA and A. TSUTSUMI. Inhibition of steam gasification of biomass char by hydrogen and tar. *Biomass and Bioenergy*, 2011, **35**(1), pp.179-185.
27. BAYARSAIKHAN, B., N. SONOYAMA, S. HOSOKAI, T. SHIMADA, J.-I. HAYASHI, C.-Z. LI and T. CHIBA. Inhibition of steam gasification of char by volatiles in a fluidized bed under continuous feeding of a brown coal. *Fuel*, 2006, **85**(3), pp.340-349.
28. HOSOKAI, S., K. KUMABE, M. OHSHITA, K. NORINAGA, C.Z. LI and J.I. HAYASHI. Mechanism of decomposition of aromatics over charcoal and necessary condition for maintaining its activity. *Fuel*, 2008, **87**(13-14), pp.2914-2922.
29. SUEYASU, T., T. OIKE, A. MORI, S. KUDO, K. NORINAGA and J.I. HAYASHI. Simultaneous steam reforming of tar and steam gasification of char from the pyrolysis of potassium-loaded woody biomass. *Energy and Fuels*, 2012, **26**(1), pp.199-208.
30. HUANG, Q., P. LU, B. HU, Y. CHI and J. YAN. Cracking of Model Tar Species from the Gasification of Municipal Solid Waste Using Commercial and Waste-Derived Catalysts. *Energy & Fuels*, 2016, **30**(7), pp.5740-5748.
31. QIAN, K., A. KUMAR, H. ZHANG, D. BELLMER and R. HUHNKE. Recent advances in utilization of biochar. *Renewable and Sustainable Energy Reviews*, 2015, **42**, pp.1055-1064.

32. LU, P., X. QIAN, Q. HUANG, Y. CHI and J. YAN. Catalytic Cracking of Toluene as a Tar Model Compound Using Sewage-Sludge-Derived Char. *Energy & Fuels*, 2016.
33. COLL, R., J. SALVADÓ, X. FARRIOL and D. MONTANÉ. Steam reforming model compounds of biomass gasification tars: conversion at different operating conditions and tendency towards coke formation. *Fuel Processing Technology*, 2001, **74**(1), pp.19-31.
34. FUENTES-CANO, D., A. GÓMEZ-BAREA, S. NILSSON and P. OLLERO. Decomposition kinetics of model tar compounds over chars with different internal structure to model hot tar removal in biomass gasification. *Chemical Engineering Journal*, 2013, **228**, pp.1223-1233.
35. SHAFEEYAN, M.S., W.M.A.W. DAUD, A. HOUSHMAND and A. SHAMIRI. A review on surface modification of activated carbon for carbon dioxide adsorption. *Journal of Analytical and Applied Pyrolysis*, 2010, **89**(2), pp.143-151.
36. FIGUEIREDO, J.L., M.F.R. PEREIRA, M.M.A. FREITAS and J.J.M. ÓRFÃO. Modification of the surface chemistry of activated carbons. *Carbon*, 1999, **37**(9), pp.1379-1389.
37. JIN, L., X. BAI, Y. LI, C. DONG, H. HU and X. LI. In-situ catalytic upgrading of coal pyrolysis tar on carbon-based catalyst in a fixed-bed reactor. *Fuel Processing Technology*.
38. DOU, B., J. GAO, X. SHA and S.W. BAEK. Catalytic cracking of tar component from high-temperature fuel gas. *Applied Thermal Engineering*, 2003, **23**(17), pp.2229-2239.
39. MICHEL, R., A. ŁAMACZ, A. KRZTON, G. DJÉGA-MARIADASSOU, P. BURG, C. COURSON and R. GRUBER. Steam reforming of  $\alpha$ -methylnaphthalene as a model tar compound over olivine and olivine supported nickel. *Fuel*, 2013, **109**, pp.653-660.
40. WANG, T.J., J. CHANG, C.Z. WU, Y. FU and Y. CHEN. The steam reforming of naphthalene over a nickel–dolomite cracking catalyst. *Biomass and Bioenergy*, 2005, **28**(5), pp.508-514.
41. FONT PALMA, C. Modelling of tar formation and evolution for biomass gasification: A review. *Applied Energy*, 2013, **111**, pp.129-141.

42. PUTRO, J.N., F.E. SOETAREDJO, S.-Y. LIN, Y.-H. JU and S. ISMADJI. Pretreatment and conversion of lignocellulose biomass into valuable chemicals. *RSC Advances*, 2016, **6**(52), pp.46834-46852.
43. HAN, J. and H. KIM. The reduction and control technology of tar during biomass gasification/pyrolysis: An overview. *Renewable and Sustainable Energy Reviews*, 2008, **12**(2), pp.397-416.
44. ANIS, S., Z.A. ZAINAL and M.Z.A. BAKAR. Thermocatalytic treatment of biomass tar model compounds via radio frequency. *Bioresource Technology*, 2013, **136**, pp.117-125.
45. TUNÅ, P., F. BAUER, C. HULTEBERG and L. MALEK. Regenerative reverse-flow reactor system for cracking of producer gas tars. *Biomass Conversion and Biorefinery*, 2013, **4**(1), pp.43-51.
46. PARSLAND, C., A.-C. LARSSON, P. BENITO, G. FORNASARI and J. BRANDIN. Nickel-substituted bariumhexaaluminates as novel catalysts in steam reforming of tars. *Fuel Processing Technology*, 2015, **140**, pp.1-11.
47. LEININGER, J.P., F. LORANT, C. MINOT and F. BEHAR. Mechanisms of 1-methylnaphthalene pyrolysis in a batch reactor. *Energy and Fuels*, 2006, **20**(6), pp.2518-2530.
48. ALDÉN, H., E. BJÖRKMAN, M. CARLSSON and L. WALDHEIM. Catalytic Cracking of Naphthalene on Dolomite. In: A.V. BRIDGWATER, ed. *Advances in Thermochemical Biomass Conversion*. Dordrecht: Springer Netherlands, 1993, pp.216-232.
49. ZHANG, Y.-L., Y.-H. LUO, W.-G. WU, S.-H. ZHAO and Y.-F. LONG. Heterogeneous Cracking Reaction of Tar over Biomass Char, Using Naphthalene as Model Biomass Tar. *Energy & Fuels*, 2014, **28**(5), pp.3129-3137.
50. HOSOKAI, S., K. KUMABE, M. OHSHITA, K. NORINAGA, C.-Z. LI and J.-I. HAYASHI. Mechanism of decomposition of aromatics over charcoal and necessary condition for maintaining its activity. *Fuel*, 2008, **87**(13-14), pp.2914-2922.
51. ZENG, X., Y. WANG, J. YU, S. WU, J. HAN, S. XU and G. XU. Gas upgrading in a downdraft fixed-bed reactor downstream of a fluidized-bed coal pyrolyzer. *Energy and Fuels*, 2011, **25**(11), pp.5242-5249.

52. AL-RAHBI, A.S., J.A. ONWUDILI and P.T. WILLIAMS. Thermal decomposition and gasification of biomass pyrolysis gases using a hot bed of waste derived pyrolysis char. *Bioresource Technology*, 2016, **204**, pp.71-79.
53. DEMIRBAŞ, A. Gaseous products from biomass by pyrolysis and gasification: effects of catalyst on hydrogen yield. *Energy Conversion and Management*, 2002, **43**(7), pp.897-909.
54. RADOVIC, L.R., I.F. SILVA, J.I. UME, J.A. MENÉNDEZ, C.A.L.Y. LEON and A.W. SCARONI. An experimental and theoretical study of the adsorption of aromatics possessing electron-withdrawing and electron-donating functional groups by chemically modified activated carbons. *Carbon*, 1997, **35**(9), pp.1339-1348.
55. RODRÍGUEZ-REINOSO, F. The role of carbon materials in heterogeneous catalysis. *Carbon*, 1998, **36**(3), pp.159-175.
56. MORENO-CASTILLA, C. Adsorption of organic molecules from aqueous solutions on carbon materials. *Carbon*, 2004, **42**(1), pp.83-94.
57. BUCHIREDDY, P.R., R.M. BRICKA, J. RODRIGUEZ and W. HOLMES. Biomass gasification: catalytic removal of tars over zeolites and nickel supported zeolites. *Energy & Fuels*, 2010, **24**(4), pp.2707-2715.
58. LI, B., Z. LEI and Z. HUANG. Surface-Treated Activated Carbon for Removal of Aromatic Compounds from Water. *Chemical Engineering & Technology*, 2009, **32**(5), pp.763-770.
59. YIP, K., M. XU, C.-Z. LI, S.P. JIANG and H. WU. Biochar as a fuel: 3. Mechanistic understanding on biochar thermal annealing at mild temperatures and its effect on biochar reactivity. *Energy & Fuels*, 2010, **25**(1), pp.406-414.
60. BHANDARI, P.N., A. KUMAR, D.D. BELLMER and R.L. HUHNEKE. Synthesis and evaluation of biochar-derived catalysts for removal of toluene (model tar) from biomass-generated producer gas. *Renewable Energy*, 2014, **66**, pp.346-353.
61. SESHADRI, K.S. and A. SHAMSI. Effects of temperature, pressure, and carrier gas on the cracking of coal tar over a char-dolomite mixture and calcined dolomite in a fixed-bed reactor. *Industrial and Engineering Chemistry Research*, 1998, **37**(10), pp.3830-3837.
62. EVANS A, E.R. *The composition of a tyre: Typical components*. Banbury Oxford, UK, 2006.

63. MA, Z., S.-P. ZHANG, D.-Y. XIE and Y.-J. YAN. A novel integrated process for hydrogen production from biomass. *International Journal of Hydrogen Energy*, 2014, **39**(3), pp.1274-1279.
64. YAN, F., S.-Y. LUO, Z.-Q. HU, B. XIAO and G. CHENG. Hydrogen-rich gas production by steam gasification of char from biomass fast pyrolysis in a fixed-bed reactor: Influence of temperature and steam on hydrogen yield and syngas composition. *Bioresource Technology*, 2010, **101**(14), pp.5633-5637.
65. RUIZ, J.A., M.C. JUÁREZ, M.P. MORALES, P. MUÑOZ and M.A. MENDÍVIL. Biomass gasification for electricity generation: Review of current technology barriers. *Renewable and Sustainable Energy Reviews*, 2013, **18**, pp.174-183.
66. LUO, S., B. XIAO, Z. HU, S. LIU, X. GUO and M. HE. Hydrogen-rich gas from catalytic steam gasification of biomass in a fixed bed reactor: Influence of temperature and steam on gasification performance. *International Journal of Hydrogen Energy*, 2009, **34**(5), pp.2191-2194.
67. FRANCO, C., F. PINTO, I. GULYURTLU and I. CABRITA. The study of reactions influencing the biomass steam gasification process☆. *Fuel*, 2003, **82**(7), pp.835-842.
68. MA, Z., S. ZHANG, D. XIE, Y. YAN and Z. REN. Hydrogen Production from Bio-Char via Steam Gasification in a Fluidized-Bed Reactor. *Chemical Engineering & Technology*, 2013, **36**(9), pp.1599-1602.
69. ZHANG, S.-P., Z.-Q. CHEN, Q.-J. CAI and D. DING. The integrated process for hydrogen production from biomass: Study on the catalytic conversion behavior of pyrolytic vapor in gas–solid simultaneous gasification process. *International Journal of Hydrogen Energy*.
70. JIANG, L., S. HU, Y. WANG, S. SU, L. SUN, B. XU, L. HE and J. XIANG. Catalytic effects of inherent alkali and alkaline earth metallic species on steam gasification of biomass. *International Journal of Hydrogen Energy*, 2015, **40**(45), pp.15460-15469.
71. CHOI, Y.-K., M.-H. CHO and J.-S. KIM. Steam/oxygen gasification of dried sewage sludge in a two-stage gasifier: Effects of the steam to fuel ratio and ash of the activated carbon on the production of hydrogen and tar removal. *Energy*, 2015, **91**, pp.160-167.
72. WANG, Y.-G., J.-L. SUN, H.-Y. ZHANG, Z.-D. CHEN, X.-C. LIN, S. ZHANG, W.-B. GONG and M.-H. FAN. In Situ Catalyzing Gas Conversion

Using Char as a Catalyst/Support during Brown Coal Gasification. *Energy & Fuels*, 2015, **29**(3), pp.1590-1596.

73. CHEN, Z., S. ZHANG, Z. CHEN and D. DING. An integrated process for hydrogen-rich gas production from cotton stalks: The simultaneous gasification of pyrolysis gases and char in an entrained flow bed reactor. *Bioresource Technology*, 2015, **198**, pp.586-592.
74. WANG, D., W. YUAN and W. JI. Char and char-supported nickel catalysts for secondary syngas cleanup and conditioning. *Applied Energy*, 2011, **88**(5), pp.1656-1663.
75. NANOU, P., H.E. GUTIÉRREZ MURILLO, W.P.M. VAN SWAAIJ, G. VAN ROSSUM and S.R.A. KERSTEN. Intrinsic reactivity of biomass-derived char under steam gasification conditions-potential of wood ash as catalyst. *Chemical Engineering Journal*, 2013, **217**, pp.289-299.
76. GONZÁLEZ, J.F., S. ROMÁN, D. BRAGADO and M. CALDERÓN. Investigation on the reactions influencing biomass air and air/steam gasification for hydrogen production. *Fuel Processing Technology*, 2008, **89**(8), pp.764-772.
77. DEMIRBAŞ, A. Yields of hydrogen-rich gaseous products via pyrolysis from selected biomass samples. *Fuel*, 2001, **80**(13), pp.1885-1891.
78. HAMAD, M.A., A.M. RADWAN, D.A. HEGGO and T. MOUSTAFA. Hydrogen rich gas production from catalytic gasification of biomass. *Renewable Energy*, 2016, **85**, pp.1290-1300.
79. CHEN, G., J. ANDRIES, Z. LUO and H. SPLIETHOFF. Biomass pyrolysis/gasification for product gas production: the overall investigation of parametric effects. *Energy Conversion and Management*, 2003, **44**(11), pp.1875-1884.
80. ZHAO, B., X. ZHANG, L. SUN, G. MENG, L. CHEN and Y. XIAOLU. Hydrogen production from biomass combining pyrolysis and the secondary decomposition. *International Journal of Hydrogen Energy*, 2010, **35**(7), pp.2606-2611.
81. WANG, S., X. LI, F. ZHANG, Q. CAI, Y. WANG and Z. LUO. Bio-oil catalytic reforming without steam addition: Application to hydrogen production and studies on its mechanism. *International Journal of Hydrogen Energy*, 2013, **38**(36), pp.16038-16047.

82. ALIPOUR MOGHADAM, R., S. YUSUP, W. AZLINA, S. NEHZATI and A. TAVASOLI. Investigation on syngas production via biomass conversion through the integration of pyrolysis and air–steam gasification processes. *Energy Conversion and Management*, 2014, **87**, pp.670-675.
83. SATTAR, A., G.A. LEEKE, A. HORNING and J. WOOD. Steam gasification of rapeseed, wood, sewage sludge and miscanthus biochars for the production of a hydrogen-rich syngas. *Biomass and Bioenergy*, 2014, **69**, pp.276-286.
84. WEI, L., S. XU, L. ZHANG, C. LIU, H. ZHU and S. LIU. Steam gasification of biomass for hydrogen-rich gas in a free-fall reactor. *International Journal of Hydrogen Energy*, 2007, **32**(1), pp.24-31.
85. CHAUDHARI, S.T., S.K. BEJ, N.N. BAKHSHI and A.K. DALAI. Steam Gasification of Biomass-Derived Char for the Production of Carbon Monoxide-Rich Synthesis Gas. *Energy & Fuels*, 2001, **15**(3), pp.736-742.
86. WENDER, I. Reactions of synthesis gas. *Fuel Processing Technology*, 1996, **48**(3), pp.189-297.
87. HOSOKAI, S., K. NORINAGA, T. KIMURA, M. NAKANO, C.Z. LI and J.I. HAYASHI. Reforming of volatiles from the biomass pyrolysis over charcoal in a sequence of coke deposition and steam gasification of coke. *Energy and Fuels*, 2011, **25**(11), pp.5387-5393.
88. HE, M., Z. HU, B. XIAO, J. LI, X. GUO, S. LUO, F. YANG, Y. FENG, G. YANG and S. LIU. Hydrogen-rich gas from catalytic steam gasification of municipal solid waste (MSW): Influence of catalyst and temperature on yield and product composition. *International Journal of Hydrogen Energy*, 2009, **34**(1), pp.195-203.

## CHAPTER 6. CONCLUSIONS AND FUTURE WORK

---

An interesting environmental and sustainable concept is to convert waste materials to carbonaceous materials which are then used in pollution control applications. This thesis is aimed to investigate the potential low-cost waste-derived feedstocks to produce valuable carbonaceous materials for (i) nitric oxide control or (ii) tar conversion. To achieve this goal, waste tyre, refused derived fuel (RDF), and date stones were selected as raw waste materials to prepare the carbonaceous materials.

(i) The presence of nitrogen oxides ( $\text{NO}_x$ ) in industrial flue gases is problematic since emissions of  $\text{NO}_x$  produce acid rain and ozone formation. The  $\text{NO}$  removal performance of the activated carbons, derived from the steam activation of the tyre, RDF and date stones at  $900\text{ }^\circ\text{C}$  has been investigated using a fixed bed reactor at low temperatures ( $25\text{-}100\text{ }^\circ\text{C}$ ) and compared with several commercial activated carbons. Moreover, the influence of chemical activation of the waste tyre on porosity and subsequent  $\text{NO}$  removal has been studied.

(ii) One of the most promising biomass conversion processes is gasification in which the complex biomass hydrocarbons are thermally degraded into useful gaseous species, mainly hydrogen, carbon dioxide and carbon monoxide. However, tar formation in syngas is a serious problem. One of the most efficient techniques for tar removal is catalytic steam reforming in which tar compounds can be converted into useful gases. To cope with the challenges associated with deactivation of commercial catalysts because of coking or sulphur poisoning, char as a by-product obtained by the pyrolysis of organic matter is cheap and easily replaceable. In this work, the effectiveness of waste derived chars for tar decomposition has been investigated using a two stage fixed bed reactor. The influence of cracking temperature, char amount, porosity, oxygen functional groups, steam and ash minerals on tar decomposition and hydrogen production has been studied.

The overall conclusions of this research are summarised as follows:

## **6.1 Waste derived activated carbons for NO removal**

### **6.1.1 Nitrogen oxide removal using commercial and waste-derived physically activated carbons**

Activated carbons were synthesised from waste materials and investigated for their efficiency for the removal of NO at a low temperature of 50 °C. The wastes used were waste biomass (date stones), processed municipal solid waste in the form of refuse derived fuel and waste tyres. Activated carbons were prepared through carbonisation of the waste feedstock followed by subsequent physical activation with steam. Date stones were shown to be a more suitable precursor for the formation of a highly porous activated carbon with a high BET surface area. This was ascribed to the low ash content (4 wt.%) contained within the date stones feedstock compared to that found with tyre (7 wt.%) and RDF (11 wt.%). Chemical characterization of the waste raw materials revealed a high concentration of Zn and Ca with tyre and RDF respectively. The presence of high amounts of alkaline species in the RDF was reflected by the high basicity of the RDF derived activated carbon.

The NO sorption capacity of the waste-derived activated carbons was compared with several commercial activated carbons which exhibited a very well developed porous texture. The waste-derived activated carbons had NO adsorption efficiencies, which were between 50% and 70% of those achieved for the commercial activated carbons. Date stones activated carbon exhibited the highest NO removal efficiency of 40%, while RDF and tyre achieved 23 and 21%, conversion of 800 ppm NO, respectively. It was also shown that the nitrogen oxide adsorption uptake depends on the porous structure, particularly the presence of micropores in the activated carbon, but to a lesser extent on the surface area and acid–base surface groups on the carbon surface.

The NO/activated carbon reaction at low temperature was enhanced by the presence of oxygen. Based on the overall analysis of NO adsorption on activated carbon in the presence of oxygen, the nature of the NO adsorbed species formed on the activated carbon surface after NO adsorption were suggested to be in the form of  $-\text{NO}_2$  and  $-\text{NO}_3$ , which indicates that the adsorbed NO is oxidized in the presence of oxygen.

NO adsorption by the waste derived activated carbons appeared to be due to physical adsorption (Vander Waals forces) of nitric oxide on carbon surface as a significant decrease of carbon adsorption capacity was observed with the increase of adsorption temperature to 100 °C.

### **6.1.2 Activated carbons from chemical activation of waste tyres for low temperature NO control**

To further investigate the role of carbon porosity on NO adsorption, tyre chars were chemically activated with KOH, K<sub>2</sub>CO<sub>3</sub>, NaOH and Na<sub>2</sub>CO<sub>3</sub>. These chemical activating agents were chosen for the purpose to develop the porous texture of waste tyre derived activated carbon. The product activated carbons were then examined for their ability to adsorb NO at low temperature (25 °C).

Pyrolysis of tyre followed by chemical activation, in particular with KOH, resulted in the formation of activated carbons with a greater extent of porosity in comparison with the physically activated carbons. The highest BET surface area of 621 m<sup>2</sup> g<sup>-1</sup> was achieved with the chemical activation of tyre char with KOH at an activation temperature of 900 °C and KOH to char ratio of 3:1. The influence of chemical activation parameters on the porosity development of the resultant tyre activated carbons revealed that both the chemical activation temperature and the type of chemical agent had a more pronounced influence on the porous texture development compared to the other investigated parameters.

Both BET surface area and micropore volume were maximised with the activation temperature of 900 °C and with the use of KOH as the activating agent. As a result, activated carbon prepared through this preparation route exhibited the highest NO removal efficiency at 75% compared to 40% with the physically activated waste tyre at the adsorption temperature of 25 °C and with NO inlet concentration of 400 ppm and oxygen concentration of 10%. The waste tyre derived activated carbons prepared using K<sub>2</sub>CO<sub>3</sub>, NaOH and Na<sub>2</sub>CO<sub>3</sub> alkali-activating agents appeared to have little influence on NO removal from the flue gases. From the experimental investigation and characterization of the series of prepared chemically activated waste tyre, the

adsorption ability of waste tyre depends on to a great extent on the procedure of activation and the porous properties, in particular, the micropore volume. As a result, this study showed that the chemically activated tyre derived activated carbon is a promising sorbent for NO capture at low temperature.

## **6.2 Tar decomposition using waste derived pyrolysis chars**

### **6.2.1 Thermal decomposition and cracking of biomass pyrolysis gases using a hot bed of waste derived pyrolysis chars**

Chars produced from the pyrolysis of different waste materials have been investigated for their use as a catalyst for the catalytic cracking of biomass pyrolysis gases during the two-stage pyrolysis-gasification of biomass. Wood pellets were pyrolysed in a fixed bed reactor at 500 °C and the resultant pyrolysis vapours were then passed to a second stage reactor to undergo secondary cracking reactions over the waste derived pyrolysis chars at temperatures from 600 °C to 800 °C. The chars were produced from the pyrolysis of waste tyres, refused derived fuel and biomass in the form of date stones. The results showed that the hydrocarbon tar yields decreased significantly with all the char materials used in comparison to the non-char catalytic experiments.

Higher cracking temperature was favourable for tar decomposition. For example, at a cracking temperature of 800 °C, the total product hydrocarbon tar yield decreased by 70% with tyre char, 50% with RDF char and 9% with biomass date stones char compared to that without char. Analysis of the tar composition showed that the content of oxygenated compounds decreased and polycyclic aromatic hydrocarbons increased in the product tar at higher char temperatures. In addition, Bio-oil/tar with 2-4 aromatic ring could significantly be transformed into smaller gas species with increased concentrations of most noticeably hydrogen in the gas yield. For instance, at a cracking temperature of 800 °C, the hydrogen concentration increased markedly from 19.6 vol.% with no char to 25, 29 and 34 vol.% with the use of a hot bed of date stones, tyre, and RDF chars respectively in the second stage.

The tar composition from the biomass pyrolysis/cracking at a cracking temperature 800 °C was dominated by polycyclic aromatic species of naphthalenes, fluorene and

phenanthrene. Different amounts of these tar species were obtained from the biomass pyrolysis-cracking process with the three types of char materials. The results showed that tyre char was the most effective waste derived char for the reduction of hydrocarbon tar compounds from 8171  $\mu\text{g g}^{-1}$  with no char to 3842  $\mu\text{g g}^{-1}$ . The high catalytic activity of char was ascribed to the catalytic effect of ash minerals, which could act as the active sites for tar cracking.

Analysing the spent char materials after the reaction with the biomass pyrolysis volatiles showed a decrease in the BET surface area, which may suggest the coke formation due to the deposition of tar species on the char surface.

### **6.2.2 Catalytic activity of tyre char for cracking of tar model compounds**

To overcome the complexity of real biomass tar, the effectiveness of tyre char for cracking of tar model compounds was carried out at a cracking temperature of 700 °C. The use of tyre char for cracking of tar model species showed a high activity, producing a carbon conversion (46-75%) and hydrogen yield (15-28 mmol  $\text{g}^{-1}$ ), which was far higher than that of cracking with sand (blank). Methylnaphthalene was the most refractory one among the studied tar compounds, whereas furfural presented the highest reactivity. With all the studied tar species, the total gas yield was found to increase markedly with the presence of tyre char compared to thermal cracking with sand.

Additionally, the influence of porosity of carbonaceous materials on methylnaphthalene cracking was studied. The catalytic activity of tyre char was compared to two different commercial activated carbons with varied porous texture. However, with the significant difference in the porous texture and the BET surface area of the tested carbonaceous materials, the difference in methylnaphthalene conversion over the commercial activated carbons and tyre char was negligible, indicating the marginal effect of the BET surface area. The tyre mineral content may contribute to the sorption effect, as tyre char with a higher mineral content (18 wt.%) had almost a similar catalytic activity to the commercial activated carbons with a developed porous texture but lesser mineral content.

Furthermore, the role of surface oxygen functionalities on contributing to the catalytic activity of carbonaceous materials was investigated via the oxidation of the commercial activated carbon with nitric acid. The acid treatment was successful in increasing the total acidic groups on the activated carbon. However, the catalytic activity of the treated samples for methylnaphthalene conversion was similar to the original activated carbon, suggesting that the oxygen functional groups have no catalytic role in enhancing the char catalytic activity for tar cracking.

### **6.2.3 Steam reforming of biomass tar over sacrificial tyre pyrolysis char for H<sub>2</sub>-rich syngas production**

The simultaneous reforming and gasification of pyrolysis gases and char was investigated for H<sub>2</sub>-rich syngas production and tar reduction during the gasification-reforming of biomass using a two stage fixed bed reactor. The catalytic role of ash minerals on tar decomposition using tyre char was studied. The char was demineralized via treatment with hydrochloric acid. The biomass sample was pyrolysed under nitrogen at a pyrolysis temperature of 500 °C, the evolved pyrolysis volatiles were passed to a second stage with steam, and the gases were reformed in the presence of tyre char as a catalyst. The influence of catalyst bed temperature, steam to biomass ratio, reaction time and tyre ash metals were investigated.

The influence of the catalytic activity of tyre ash minerals on the composition of syngas and tar decomposition during the steam reforming of biomass was significant as the removal of minerals led to a decrease in the H<sub>2</sub> yield. The results demonstrated that when the reforming temperature increased from 700 to 900 °C, the hydrogen yield increased from 8.4 to 39.2 mmol g<sup>-1</sup> with the original tyre char and from 2.7 to 30.5 mmol g<sup>-1</sup> with the acid treated tyre char. In addition, the use of demineralized tyre char caused a marked decrease in total gas yield and an increase of the condensed liquid fraction with all the investigated reforming temperatures. Moreover, the H<sub>2</sub>/CO molar ratio decreased significantly with minerals removal from 1.31 with the original tyre char to reach only 0.37 with the acid treated char at a reforming temperature of 700 °C. The results obtained confirm that the high activity of tyre char for tar decomposition during the biomass-reforming process is mainly due to the catalytic

role of metals present in tyre char. The presence of ash metals played a significant role in enhancing the water-gas shift, char gasification, steam tar reforming, and hydrocarbon reforming reactions. The catalytic activity of tyre char was described by the presence of a quite high percentage of Zn of 6.5 wt.% that had a positive influence in enhancing the tar reforming reactions and thereby promoting the hydrogen production during the biomass gasification.

Raising the steam injection rate and reforming temperature led to increased hydrogen production as steam reforming and char gasification reactions were enhanced. Over the ranges of operating conditions examined, the maximum hydrogen content reached 56 vol.%, and the ratio of H<sub>2</sub>/CO varied between 1.3 to 2. The presence of steam promoted char conversion, however, increasing the steam to biomass ratio from 3.32 to 4.32 g g<sup>-1</sup> did not influence the char conversion, and the obtained H<sub>2</sub> yield was almost the same at ~51 vol.%. Therefore, tyre char can be used as an effective catalyst for cracking/reforming of heavy hydrocarbons from the biomass gasification, and could also contribute to the total syngas yield through char gasification.

## **6.3 Future work**

### **6.3.1 Waste derived activated carbons for NO removal**

- Further work could be carried out to investigate the effectiveness of waste derived activated carbons for NO removal in the presence of simulated flue gas containing N<sub>2</sub>, CO, O<sub>2</sub>, NO, and H<sub>2</sub>O. This would provide information about the influence of other gaseous species on nitric oxide removal.
- Waste derived activated carbons could be tested for the simultaneous SO<sub>x</sub>/NO removal. This would enable investigation of the sorption capacity of waste derived activated carbons for multi-pollutants.
- Investigate the regeneration and the re-usability of the spent waste derived activated carbons for nitric oxide removal by heating the used carbons in a furnace at 600 °C under an inert atmosphere.
- Further work could be carried out on surface chemistry modification (nitrogen content) to improve the carbon sorption efficiency. In addition, explanation of

the effect of different types of carbon functional groups including nitrogen and oxygen groups on NO adsorption needs further investigations which would also help to gain information on the role of acidic and basic groups. This could be done by using TGA combined with MS, TPD or X-ray Photoelectron Spectroscopy (XPS)

### **6.3.2 Tar decomposition using waste derived pyrolysis chars**

- The waste-derived pyrolysis chars were shown to reduce the tar content as well as increase the hydrogen yield. However, the catalytic activity of biomass char was not high. Further work could be done on char preparation in order to enhance the catalytic activity. The char preparation conditions such as pyrolysis temperature and heating rate may influence the char properties and consequently the catalytic activity. In addition, metal additions to char could be investigated.
- Further research could be carried out to further understand the tar reduction mechanism over a char bed, for example, the origin of active sites that simulate the cracking process.
- This research work has shown that tar conversion over a hot bed of char is promising, however, the effect of char particle size and gas velocity on the tar outlet concentration should be further investigated. In addition, long-term stability of char for tar cracking could be carried out to quantify the catalytic deactivation of char samples. The deactivation behaviour of char materials could be investigated by leading tar model, for example, methylnaphthalene, for 20-400 min through a hot bed of char material.
- Examine the evolution of sulphur-containing gases while using tyre char which contains sulphur. This could be carried out downstream of the reactor using a scrubber to trap the sulphur species such as SO<sub>2</sub> and H<sub>2</sub>S.